Robust Pareto – Optimum Routing of Ships utilizing Deterministic and Ensemble Weather Forecasts

vorgelegt von
Diplom-Ingenieur
Jörn Hinnenthal
aus Berlin

von der Fakultät V – Verkehrs- und Maschinensysteme
der Technischen Universität Berlin
zur Erlangung des akademischen Grades

Doktor der Ingenieurwissenschaften
– Dr.-Ing. –

genehmigte Dissertation

Promotionsausschuss:

Vorsitzender:	Prof. Dr.-Ing. Jürgen Siegmann
Berichter:	Prof. Dr.-Ing. Günther F. Clauss
Berichter:	Prof. Dr.-Ing. Apostolos D. Papanikolaou

Tag der wissenschaftlichen Aussprache: 18.12.2007

Berlin 2008
D 83

Acknowledgement

Inspired by my participation as student assistant in the European research project SEAROUTES, I decided to continue the research into ship route optimization that I already started within my diploma thesis. In this regard I owe my deepest gratitude to my promoters Dr.-Ing. Stefan Harries and Prof. Dr.-Ing. Lothar Birk, who encouraged me to become scientific assistant and to continue with this work up to a doctoral thesis.

I want to express my gratitude to my promoter and supervisor Prof. Dr.-Ing. Günther Clauss for his encouragement to publish scientific results, for the outstanding composition of guidance and freedom, and for generous support whenever I asked for. I also want to express my gratitude to my second supervisor Prof. Dr.-Ing. Apostolos Papanikolaou for his instantaneous agreement to contribute in the doctoral committee, and I only regret that I didn't involve him much earlier into this work. Also many thanks to the chairman of the doctoral committee Prof. Dr.-Ing. Jürgen Siegmann for supporting a fast and frictionless procedure.

Special thanks I owe to my former colleagues Claus Abt, Dr.-Ing. Justus Heimann, and Henning Winter for reliable support and many fruitful discussions. The same applies to my present, esteemed, and embosomed colleagues Felix Fliege, Gonzalo Tampier Brockhaus and Dr.-Ing. Uwe Boettner who built for a long time the core of the workgroup at Technische Universität Berlin for me, the fundament for the efficiency and the pleasure within my work. Further on I would like to thank all my colleagues that I not mentioned by name, because they not directly contributed to this work, I got a lot of support in other projects and found wonderful companions.

Sincere thanks are given to Dr. Øvind Saetra whom I met within the SEAROUTES project, who provided me with exquisite weather forecasts, and who inspired me to apply ensemble forecasts for the routing problem. Sincere thanks are also given to Thor Marquardt, chief officer at Hapag Lloyd, for his valuable support and consultancy regarding navigation and operation of ships and basic conditions of maritime transport, and to Dr. Masaru Tsujimoto from the National Maritime Research Institute in Tokyo, who became an esteemed colleague during his time in Berlin and who inspired me a lot within our lively discussions on routing. Special thanks also to Gabriele Schmitz for her excellent high-speed proofreading.

Finally and most of all I would like to express my gratitude to Nicole Reimer, my beloved wife, who encourages me and believes in me and our partnership, also in times that are everything else than mellifluous.

Jörn Hinnenthal – Berlin, March 2008

Abstract

Sophisticated routing of ships is increasingly recognized as an important contribution to safe, reliable, and economic ship operation. The more reliable weather forecasts and performance simulation of ships in a seaway become, the better they serve to identify the best possible route in terms of criteria like: *ETA* (estimated time of arrival), fuel consumption, safety (of ship, crew, passengers. and cargo), and comfort. This establishes a multi-objective, non-linear, and constrained optimization problem in which a suitable compromise is to be found between opposing targets.

For its solution a new optimization approach to select the most advantageous route on the basis of hydrodynamic simulation and sophisticated weather forecast is posed. Transfer functions are employed to assess the operating behavior of a ship in waves. Probabilistic ensemble forecasts, provided by the European Centre for Medium-Range Weather Forecasts ECMWF, are applied to account for the stochastic behavior of weather. The routes in adverse weather conditions are established as perturbations of a parent route in calm weather, which is assumed to be the concatenated great circles between waypoints. Utilizing a B-spline technique, the number of free variables for describing both the course and the velocity profile is kept low. For solving the multi-objective, non-linear, and constrained optimization problem the commercial package modeFRONTIER is successfully applied. In order to balance opposing criteria and to value the performance of optimized routes an approach suggested by the Italian economist Vilfredo PARETO is adopted. A multi-objective genetic algorithm turns out to be a suitable optimization method to identify PARETO optimum routes for a sustainable support of a conscious decision-making process.

An elaborated example is given for an intercontinental container service, employing the Panmax container vessel CMS HANNOVER EXPRESS, between Europe and North America. Different weather situations for the North Atlantic are taken into account. Sensitivity studies are applied to validate the set-up and to conduct plausibility tests. The robustness of optimized routes against weather changes, time loss, fuel consumption, accelerations, slamming, and parametric rolling are taken into account.

Kurzdarstellung

Zur Gewährleistung eines sicheren, zuverlässigen und wirtschaftlichen Schiffsbetriebes kommen zunehmend Routing-Systeme zur Anwendung. Um sichere Aussagen über die Reisedauer, den Brennstoffverbrauch, Sicherheit oder auch den Komfort an Bord treffen zu können, spielen die Zuverlässigkeit von Wettervorhersagen und die der Simulation der Seegangseigenschaften des Schiffes eine große Rolle. Dieses führt letztlich zu einem nicht-linearen Optimierungsproblem mit mehreren, oftmals antagonistischen Gütekriterien. Der Lösungsraum ist zudem durch Nebenbedingungen beschränkt.
Zur Lösung dieser Aufgabe wird ein neu entwickelter Ansatz vorgestellt. Auf Basis von Bewegungssimulationen des Schiffes im Seegang und detaillierten Seegangsprognosen werden optimale Kurse und zugehörige Geschwindigkeitsprofile eines Schiffes identifiziert. Das Betriebsverhalten des Schiffes im Seegang wird dabei mit Hilfe von Übertragungsfunktionen und Seegangsspektren bestimmt. Zunächst kommen deterministische Seegangsvorhersagen zum Einsatz; später werden diese durch Ensemble-Vorhersagen erweitert, um das stochastische Verhalten möglicher Wetterentwicklungen abzubilden. Die Seegangsprognosen werden vom European Centre for Medium-Range Weather Forecasts ECMWF zur Verfügung gestellt.
Zur Beschreibung von Routenvarianten wird eine Perturbationsmethode verwendet. Sie basiert auf der Darstellung des Kurses und eines zugehörigen Geschwindigkeitsprofils durch B-Splines. Für die Lösung der Optimierungsaufgabe kommt die generische Optimierungs-Software modeFRONTIER zum Einsatz. Zur Bewertung optimierter Routen unter dem Aspekt sich widersprechender Gütekriterien, wird ein von dem italienischen Ökonomen Vilfredo PARETO vorgeschlagenes Konzept verwendet. Ein heuristisches Suchverfahren, der Genetische Algorithmus für mehrere Gütekriterien, zeigt gute Ergebnisse bei der Suche nach PARETO optimalen Routen, die zur Unterstützung der Routenplanung herangezogen werden können.
Die neu entwickelte Optimierungsmethode wird am Beispiel eines Containerservices mit der CMS HANNOVER EXPRESS im Nord Atlantik erläutert. Die Auswirkungen verschiedener Wetterszenarien auf ein Optimierungsergebnis werden dargestellt. Empfindlichkeits- und Variationsstudien dienen der Validierung und zur Plausibilitätskontrolle.

Content

List of Figures

List of Tables

Nomenclature

Units which are dependent on the particular assignment of a symbol are referred to as [dep.].

latin symbols and abbreviation	name	unit or value
a	index	[-]
a, i, j, m, n	control variable	[-]
a	parameter of a harmonic or random process	[dep.]
ã	amplitude of a harmonic function	[dep.]
$a_{1/3}$	significant wave amplitude	[m]
A_e/A_0	propeller blade area ratio	[-]
A_m	midship cross-sectional area	[m^2]
A_m	midship cross-sectional area coefficient	[-]
AP, APP	aft perpendicular	-
a_{rms}	root mean square of the wave amplitude	[m]
B	breadth of a ship	[m]
C	peak enhancement function of a power spectrum	[-]
C_B	block coefficient	[-]
COG	center of gravity	-
C_P	pressure coefficient	[-]
C_parameter	parameter used as constraint	[dep.]
C_{WP}	water plane area coefficient	[-]
D	propeller diameter	[m]
dep.	unit depends on the appropriate symbol or abbreviation	-
df, DF	deterministic forecast	-
DIST	sailed distance in nautical miles	[nm]
DOE	design of experiment	-
D_P	draft at point P	[m]
E	threshold exceedings	[times/h]
ef, EF	ensemble forecast	-
ETA	estimated time of arrival, here a synonym for the duration of a journey	[h]
ETA_{min}-*DF*	time minimum route based on a deterministic forecast	-
ETA_{min}-*EF*	time minimum route based on an ensemble forecast	-
ETA_{min}-*EF#*	time minimum route based on ensemble forecast no. #	-
ETA_{min}-*MF*	time minimum route based on a mean ensemble forecast	-
f	frequency	[1/s]
FP, FPP	forward perpendicular	-
g	gravity constant	9.807 m/s^2
g	inequality constraint	[dep.]
GA	genetic algorithm	-
GM_T	transverse metacentric height	[m]

GT	gross tonnage	[m^3]
h	equality constraint	[dep.]
$H_{1/3}$, $h_{1/3}$	significant wave height / double wave amplitude	[m]
H_{crit}, h_{crit}	critical wave height	[m]
H_{rms}	root mean square of the wave height	[m]
J	propeller advance ratio	[-]
J	term within the peak enhancement function of a power spectrum	[-]
k	form factor	[-]
k	wave number, $2\pi/\lambda$	[rad/m]
K_{QS}	torque coefficient	[-]
K_{TS}	thrust coefficient	[-]
k_{xx}	radius of inertia for the roll motion	[m]
lat	latitude	[deg]
lon	longitude	[deg]
LCB	longitudinal center of buoyancy	-
LCF	longitudinal center of flotation	-
LPP, L_{PP}	length between perpendiculars	[m]
L_{wave}	wave length	[m]
L_{WL}	length of water line	[m]
M_{33}	potential mass coefficient of the heave motion, non-dimensionalized with ρA_m	[-]
mf, MF	mean ensemble forecast	-
m_{nS}	n^{th} order moment of the motion power spectrum	[$(m/s^{n/2})^2$, $(rad/s^{n/2})^2$]
$m_{n\zeta}$	n^{th} order moment of the wave power spectrum	[$(m/s^{n/2})^2$, $(rad/s^{n/2})^2$]
$m_{0\dot{S}}$	0^{th} order moment of velocity power spectrum	[$(m/s)^2$, $(rad/s)^2$]
$m_{0\ddot{S}}$	0^{th} order moment of acceleration power spectrum	[$(m/s^2)^2$, $(rad/s^2)^2$]
MCR	maximum continuous rating of a main engine	[MW at rpm]
MOGA	multi objective genetic algorithm	-
MSI	motion sickness incidence	[%]
n	number of revolutions of a propeller	[1/s]
N_{33}	potential damping coefficient of the heave motion, non-dimensionalized with ρA_m sqrt(2g/B)	[-]
nef	number of ensemble forecasts	[-]
nph	number of times per hour	[1/h]
nph@ap	number of events per hour suspicious for parametric rolling at AP	[1/h]
nph@cog	number of events per hour suspicious for parametric rolling at COG	[1/h]
nph@fp	number of events per hour suspicious for parametric rolling at FP	[1/h]
nph4hcrit	number of wave height exceedings suspicious for parametric rolling	[1/h]
Obj	objective function	[dep.]
O_parameter	parameter used as objective	[dep.]
p	probability density distribution	[-]
P	parameter vector	[dep.]

P	probability	[-, %]
p_{cr}	critical pressure	[kN/m^2]
P/D	pitch-diameter ratio of a propeller	[-]
PR	parametric rolling	-
P_S	shaft power	[kW]
r	lever vector, the vertical distance from center of gravity to a considered point	[m]
r_{AW} / ζ_a^2	response function of the added resistance in waves, normalized mean value of added resistance in regular waves	[kN / m^2]
R_A	air resistance	[kN]
R_{ADD}	additional resistance	[kN]
RAO	response amplitude operator, squared transfer function	[-]
R_{APP}	resistance of appendages	[kN]
R_{AW}, RAW	added resistance due to waves	[kN]
R_B	additional resistance due to the bulbous bow	[kN]
RF	response function for the added resistance due to waves	[kN/m^2]
R_F	frictional resistance	[kN]
RMS	root mean square value	[dep.]
rpm	rounds per minute, propeller revolutions	[1/min]
R_T	calm water resistance	[kN]
RTD	retarded time of departure	[h]
R_V	viscous resistance	[kN]
$R_{\zeta\zeta}(\tau)$	autocorrelation function regarding the stochastic parameter ζ	[m^2]
s_a	ship response amplitude, a = 1 – 6	[m, rad]
$s_{a1/3}$	significant amplitude of the ship response	[m, rad]
s_a / ζ_a	transfer function	[m/m, rad/m]
$scale$	maximum orthogonal perturbation in percent of the parent route length	[-]
$sfoc$	specific fuel oil consumption	[g/kWh]
$SMCR$	specified maximum continuous rating of a main engine	[MW at rpm]
$slprob$	slamming probability	[%]
s_P	vector of translatory motion at point P	[m]
s_{P3rel}	relative vertical motion between a point P and water surface	[m]
$spef$	specific fuel consumption	[t/h]
s_R	rotation vector of the center of gravity	[rad]
s_T	translation vector of the center of gravity	[m]
S	vector of spatial shift parameter	[-]
$SIMPLEX$	downhill Simplex-algorithm according Nelder and Mead	-
$S_S(\omega)$	power spectrum of the ship response	[dep.]
$S_{SP}(\omega)$	power spectrum of the ship response at point P	[dep.]
$S_\zeta(\omega)$	power spectrum of swell	[m^2/(rad/s)]
$S_{\zeta\zeta}(\omega)$	autospectrum regarding the stochastic parameter ζ	[m^2/(rad/s)]
t	thrust coefficient	[-]
t	time	[h]

T	draft of a ship	[m]
T	time period, e.g. sample period of recorded wave elevation	[s]
T_0	mean zero-up-crossing wave period	[s]
T_{0S}	mean zero-up-crossing period of the ship motion	[s]
T_1	mean wave period	[s]
T_e	natural period of the roll motion	[s]
T_{enc}	wave encounter period	[s]
T_p	peak period of the power spectrum	[s]
T_{pitch}	pitch period of the ship motion	[s]
U	wind speed at 19m above the sea level	[m/s]
v_{cr}	critical velocity	[m/s]
v_{max}	maximum for the velocity perturbation	[kn]
v_{min}	minimum for the velocity perturbation	[kn]
V	vector of velocity shift parameter	[-]
V_S	ship speed	[m/s]
w	wake fraction	[-]
x, y, z	variable	[-]
$xacc$	significant amplitude of acceleration, x-direction	[m/s^2]
X	vector of decision variables	[dep.]
$yacc$	significant amplitude of acceleration, y-direction	[m/s^2]
$zacc$	significant amplitude of acceleration, z-direction	[m/s^2]
Z	number of propeller blades	[-]

greek symbols	**name**	**unit or value**
α	course angle	[deg]
α	Phillips constant, used within power spectra	0.0081
β	decay parameter, used within power spectra	0.74
β	incident wave angle of swell	[deg]
ε	phase shift	[rad]
γ	shape parameter, used within power spectra	[-]
γ	wave encounter angle	[deg]
η_{0s}	open water efficiency	[-]
η_P	relative rotative efficiency	[-]
η_S	shaft efficiency	0.99
λ	wave length	[m]
ρ	density of sea water	1025 kg/m^3
σ^2	variance of a stochastic process	[dep.]
σ_a	standard deviation of the wave amplitude	[m]
σ_ζ	standard deviation of the wave surface displacement	[m]
τ	time lag, variable of the autocorrelation function	[s]
ω	frequency	[rad/s]

ω_0	zero-up-crossing frequency	[rad/s]
ω_e	wave encounter frequency	[rad/s]
ω_p	peak- or modal frequency	[rad/s]
ζ	wave elevation, wave surface displacement	[m]
ζ_α	wave amplitude	[m]
$\zeta_{rel\ crit}$	critical relative wave amplitude	[m]
ζ_{rms}	root mean square of the wave surface displacement	[m]

1 Introduction to weather routing of ships

During the last years ship monitoring, routing assistance, and decision support became important topics for safe and reliable sea transport. Decision support systems for a route optimization regarding weather and sea state are important tools to improve the reliability of sea trade within a transport chain or to increase comfort and safety of crew and passengers.
Generally an optimum route complies with the desired time of arrival at minimum fuel consumption and maximum safety. Permissible and reasonable loads on the ship, the cargo, and the crew are not allowed to exceed. This establishes a multi-objective, non-linear, and constrained optimization problem in which a suitable compromise is to be found between opposing targets.

Following the casual statistics of IMO (2000) for ships of 100GT and above, there were 533 registered serious and very serious casualties at sea, 64 thereof in heavy weather. These comprise 145 total losses, 38 thereof in heavy weather. Even 3 years later in 2003, the number of severe casualties amount to 150, all in all 109 total losses of ships greater than 100GT were registered, thereof 40 in heavy weather. The most affected ships are general cargo ships, accounting for nearly 20% of the world merchant fleet, but suffering over 40% of the total losses. However, total loss is only one aspect in the consequences of heavy weather, structural damages and the loss of cargo are some other. E.g. Container ships: in comparison to general cargo ships they seem to be much more safe regarding the danger of total loss. In a way container ships possess of an unmeant safety device, their stability increases in consequence of loosing on-deck container when roll angles or transverse accelerations exceed a critical limit. In 1998, the M/V APL CHINA gained notoriety and became the most famous victim of the Pacific typhoon BABS. Sole the loss of cargo amounted for more than 100M US$. 406 containers were lost and more than 1000 damaged. The ship was able to reach the harbor on its own.

Fig. 1: APL China on arrival in the Port of Seattle (by courtesy of R. Ahern, Los Angeles, CA)

Besides loss and damage of cargo and ship, each casualty bears the risk and sometimes results in damage to persons and loss of life. Therefore each accident poses the question if it could have been avoided. It is a concern of ship design, maintenance, operation, and prudent seamanship. Notwithstanding the commercial pressures imposed by shipping schedules, it is the master's sole discretion to take whatever action he/she sees appropriate to maintain the safety of the crew, vessel, and cargo. Driving the vessel too hard may result in damage to the cargo or to the vessel itself. Being overcautious annoys the charterer. In this context, situation awareness regarding oncoming weather condition and the expected impact on the ship is of greatest importance for a route planning. It is a ship's master who finally has to face this challenge and who solely is responsible for route decisions and for the safety of crew, ship, and cargo.

As rough weather condition are often not avoidable, it is of greatest importance for a master to have reliable weather data available on board to reduce the risk of accidents excited by the sea condition. Additionally, as the average temperature currently rises, extreme weather conditions may become more probable.

To support the decision making when planning a journey various services and systems are available. They reach from guidance by meteorologists to on-board decision support systems. Nevertheless, an improvement of currently available decision support systems is desirable, e.g. to increase the reliability of weather forecasts and the prediction of consequences or to enable optimization procedures to handle more than one objective target simultaneously. The latter one would support a master to easily decide, if he/she wants to put the focus of a route optimization on an arrival on schedule, on fuel savings, on the avoidance of weather conditions that may become hazardous, or on any combination of these criteria.

The aim of this work, therefore, is to suggest a novel approach to the optimization of ship routes in adverse weather and to investigate its merits, without claiming completeness of the model. It will be shown, however, that an extension of the optimization scheme is rather straightforward, allowing the quick incorporation of further analyses. Finally, posing and solving a route optimization problem as a multi objective and constraint optimization task supports conscious decision making, also in complex situations, where various objective targets have to be balanced.

The following overview on scientific work and routing services serve to give an impression of the current state of the art. It is not intended to mention all available publications and services but to illustrate the diversity of routing services and current development in research.

1.1 State of the art in applied research

Design and operation of sea trade frequently uses modern optimization and simulation methods. They are employed in tasks like fleet planning, fleet sizing and scheduling, the integration of the sea transport into a supply chain, acceleration of loading- and unloading operations, and improvements of the production line. Further they support to solve particular design tasks, e.g. for the optimization of a hull shape or the reduction of steel weight. Here optimization applied within decision support systems for weather routing purposes is considered. The term routing itself is used with different meanings. CHRISTIANSEN et al. (2004) give a comprehensive overview on optimization in sea trade. They define routing as the assignment of sequences of ports to be visited by the ships. Ship weather routing as addressed here is called environmental routing.

With regard to the considered period of time environmental or weather routing can be:

- short term routing, regarding the current sea condition and its consequences for the next minutes up to hours, to give advice of suited countermeasures,
- medium term routing, regarding the sea condition predicted by forecasts, to provide recommendation of favorable routes for a particular voyage,
- long term routing, regarding long-term weather statistics, e.g. applied for fleet planning.

In the following simply routing will be addressed, this implies weather- or environmental routing applying medium range weather forecasts, i.e. medium term routing is considered here.

The awareness of current and oncoming weather and sea conditions, at all times, are of greatest importance for the route planning and navigation of a ship's master. Formerly this knowledge was derived solely by direct observations on-board a ship and by the individual knowledge of a master about characteristic weather conditions in a particular sea area. Later on, this was supported by means of statistical evaluation of long-term observations. Ever since the invention of radio technology, it is possible to supply a ship during the whole journey with weather forecasts and supplementary weather observations from other ships. Since the sixties of the last century, ship officers are able to use routing advises from weather routing departments of meteorological institutes, where the prediction of the ship reaction in wind and waves is based on the officers experience with the considered ship or similar ships.

JOURNÉE and MEIJERS (1980) discuss the influence of natural speed loss, defined by rough sea resistance and maximum load of the main engine, and voluntary speed loss, to prevent severe motions, shipping green water, slamming, or propeller racing. In the second part of their publication, the influence of routing on the fractions of operational costs is shown. The biggest influence can be expected on the fuel and lubrication oil consumption. The breakdown of operation costs by MEIJERS is illustrated in Fig. 2. A program to assess the speed loss in a seaway is applied to the evaluation of different routes. Therein the ship performance is assessed by means of a seakeeping method based on strip theory. For a given weather condition advantages of a route decision are discussed. Costs for damage of cargo and ship are neglected, as they are hardly known.

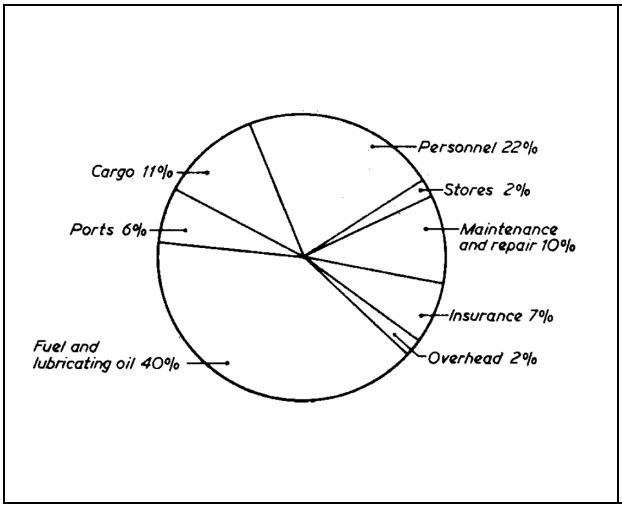

Fig. 2: Breakdown of operational costs
(MEIJERS, 1980)

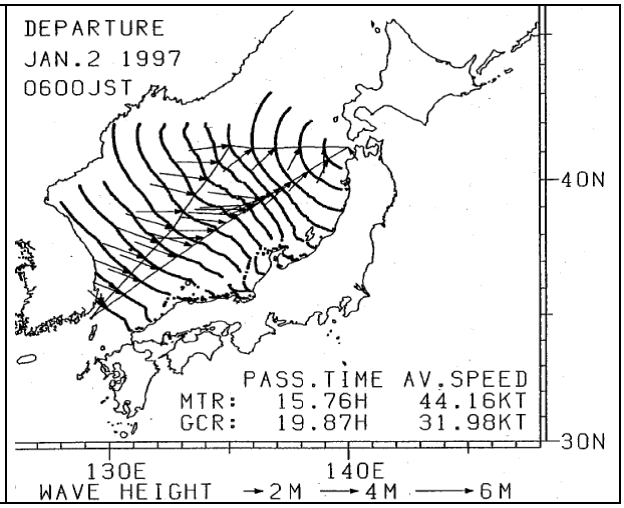

Fig. 3: Isochrone method
(HAGIWARA et al. 1999)

HAGIWARA et al. (1999) present route optimizations on a 50kn high-speed catamaran for the Sea of Japan. They use an optimization algorithm, the isochrone method, to find the time minimum route for sea conditions described by currents and wave forecasts. This method, illustrated by Fig. 3, repeatedly computes an isochrone, i.e. the attainable time front that describes the outer boundary reachable from the departure point after a certain time. The assessment of the ship performance at sea is achieved by sea trials with a smaller ship. Minimum fuel routes for a given time of arrival are accomplished by adjusting the speed of the time minimum route.

In the nineties, a group of Dutch researchers and companies created an expert system, the Ship Performance Optimization System SPOS (SPAANS and STOTER, 2000). Already in 2000 they could look back to their experience with 75 installations of this system. SPOS consciously is an on-board routing system. It should combine the forecast of meteorologists about the oncoming weather with the experience of the master about the ship, who finally is responsible for navigational planning. Initially the system used the isopone method by HAGIWARA and SPAANS (1987), an extension of the isochrone method. An isopone is the plane of equal fuel consumption that defines the outer boundary of the attainable region in a three-dimensional space, i.e. position and time. But finally the isochrone method is applied, because this method is less complex and easier to comprehend. The main reason for this decision is the higher acceptance of the isochrone method by the navigational staff. SPOS supplies a graphical user interface to display geographic- and weather data. Up to 5 routes can be generated and balanced against each other, the great circle route, rhumb line, time minimum route, and two user defined routes. The ship performance is supplied by a numerical model, which has to be calibrated according to a particular ship by the crew. Comparisons between ship operation with and without SPOS show that the time of operating in bad weather can be reduced to a quarter.

To control the stochastic behavior of weather, i.e. the uncertainty of the weather forecast, in route optimization TREBY (2002) suggests the application of ensemble forecasts instead of their deterministic counterparts. An ensemble is a set of forecasts with an equal probability for the point in time where the forecast starts. At later time steps the probability is adjusted according to the concordance of observed weather and the prediction of each member of the ensemble forecast. TREBY applies a dynamic programming algorithm, originally developed by BELLMAN[1], to detect the fastest course of a yacht in a racing competition. (Further information on the ensemble forecast system is given in section 3.3)

The EU 5th framework research project SEAROUTES (2003) bundles the whole knowledge on ship routing. To describe the project at best is to look for the full title:

“SEAROUTES – Advanced Decision Support for Shiprouting based on Full-scale Shipspecific Responses as well as Improved Sea and Weather Forecasts including Synoptic, High Precision and Realtime Satellite Data”.

One of the most important topics in routing is to obtain reliable forecast data. The best code is useless if the upcoming weather condition is not known sufficiently. Therefore the project addresses possible and necessary improvements of forecasts extensively. SEAROUTES establishes a decision support system SEAROUTES DSS for the optimization of ship routes based on medium range weather forecasts. The assessment of the seakeeping behavior of a particular ship is performed by strip theory- or panel methods. Comparisons of both methods and different codes also with model trials are conducted. State-of-the-art technology for analysis and forecasting of sea states is applied to get most accurate and reliable wave and weather forecasts to simulate the ship performance on a particular route. For the route optimization BELLMANs dynamic programming is used. It is a graph algorithm starting from an initial guess, e.g. the great circle route. From this initial route an orthogonal grid is build. Fig. 4 serves to illustrate this method.

[1] Richard Ernest Bellman, applied mathematician and theoretical physicist, 1920-1984, USA

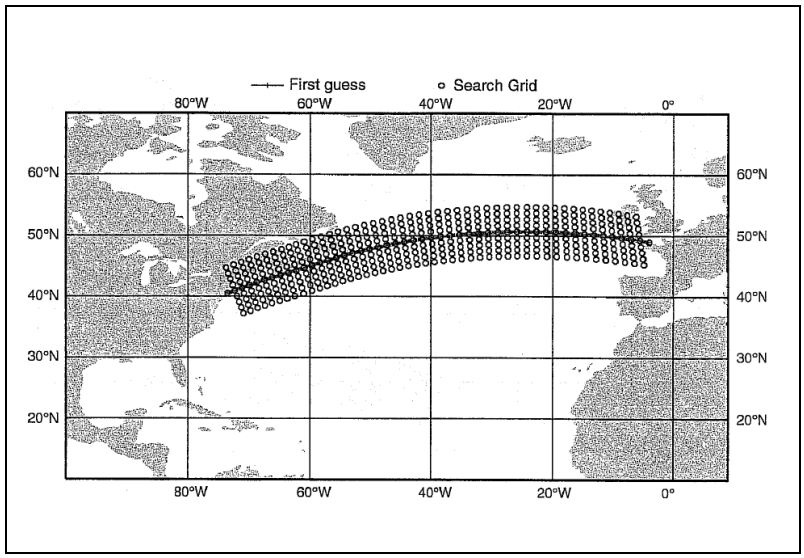

Fig. 4: Grid for BELLMANs dynamic programming, North Atlantic route (by courtesy of ECMWF)

The Figure represents the first guess route and the adjunctive search grid. This grid is evaluated step by step from the origin towards the destination of the route. For example, starting at the most eastern point of Fig. 4, all routes to the next column of grid points are evaluated. For this first step a cost function is calculated. According to this cost function, a preset number of best routes to this column are stored and taken as initial courses to the next column of grid points. Again the cost function for all the combinations of courses is calculated, values are integrated for the whole routes from the origin to the considered column of the search grid. Again a number of best routes so far are stored and the step to the next column is executed. This procedure continues until the destination point is reached. If finally a better route than the initial guess is found, the same procedure starts with this improved route as first guess. If no further improvement is possible, the first iteration loop is done and a second iteration on a refined grid starts. The initial mesh size is 1-2°, it will be refined during the optimization. The most important advantage of the BELLMAN method, compared to gradient based methods, is its ability to transcend relative optimum solutions. The method is known to be very fast, but it is single objective and the cost function is often not conceivable. A more comprehensive description of the method, applied to routing, is given by HOFFSCHILDT et al. (1999).

"The benefits of any ship routing system, however good the model is, will always depend on the quality of the forecasted weather parameters that are used to force the system", SAETRA (2004). Therefore, a measure for the certainty of a forecast is desirable. SAETRA applies ensemble forecasts, produced by the ensemble prediction system EPS of the European Centre for Medium-Range Weather Forecasts ECMWF, to give an estimate of probable forecast errors. He shows that the spread of the significant wave height in the ensemble forecast can be related to the spread of routes optimized within its forecast members. Fig. 5 represents a typical optimization result. The solid blue line represents the optimum route within the high-resolution deterministic forecast. It is overlaid with error bars. The boxes represent the 10 and 90 percentiles for the spread of ship routes, i.e. 80% of all routes can be found inside these boxes. The whiskers on the error bars show the position of the outliers. In that way probable deviations from the initially identified optimum route are visualized. A big error bar represents a high probability of weather changes and vice versa. A high probability of weather changes implies a high probability of necessary route adaptations during the journey and low reliability for initially predicted fuel consumption and time of arrival.

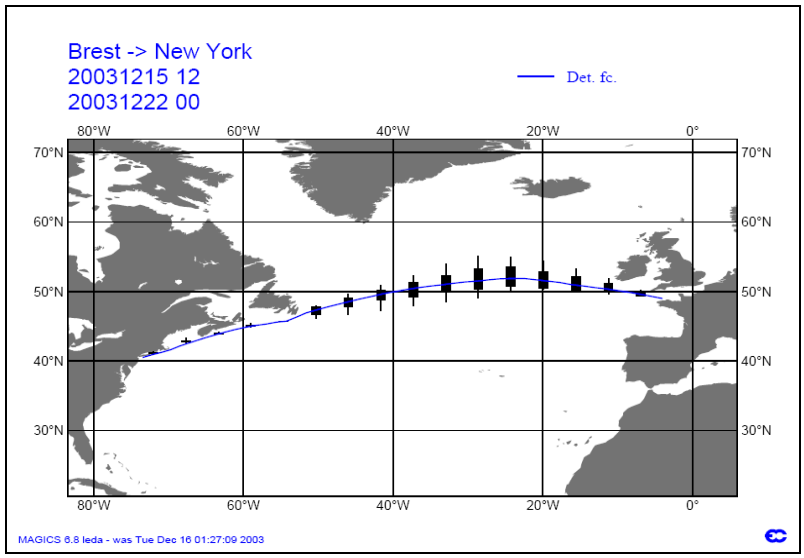

Fig. 5: Ensemble ship routing (by courtesy of ECMWF)

Parallel to the developments in Europe, the Japanese National Maritime Research Institute NMRI developed a navigation system called WAN, Weather Adaptive Navigation, TSUJIMOTO and TANIZAWA (2006). The system uses the augmented LAGRANGE[2] multiplier method in order to handle objectives and constraints during the optimization. In that way optimum routes possess minimum fuel consumption for an arrival on schedule and e.g. restricted vertical acceleration at the forward perpendicular. TSUJIMOTO and TANIZAWA show that dependent on the objective of the optimization, i.e. whether the objective is the minimization of traveling time or the minimization of fuel consumption, a ship encounters harsh or calmer sea conditions. The common preconception that ships with routing systems always encounter higher waves cannot hold. For a Panmax container vessel on a transpacific route they fond fuel savings up to 26% compared to the great circle route at maximum attainable speed.

Beside these developments on ship route optimization, other, related projects address on monitoring and short-term prediction for hazardous situations.

PAPANIKOLAOU et al. (2000) put their focus in a direction that may be described as an initial en-route monitoring or short term decision support. They establish a Seakeeping Information Booklet SIB, to be understood as an upgraded stability booklet that describes the "safe operational envelope" due to speed, heading, and wave condition for different types of bulk carriers. Motivated by the loss of MV DERBYSHIRE in 1980 the considered ship responses include bending moments. Apparently, hull strength becomes a parameter for navigational decisions.

As a supplement to the criteria for intact stability of ships specified in IMO (1988), resolution A.749(18), the Maritime Safety Committee approved a "guidance to the master to avoid dangerous situations in following and quartering seas", IMO (1995). This became necessary as basic stability criteria turned out to be insufficient for a safe ship operation in adverse sea conditions.

[2] Joseph Louis Lagrange, comte de l'Empire , 1736-1813, mathematician and astronomer, Italy

The guidelines give recommendations to prevent capsize and heavy roll motion due to:

- surf-riding and broaching-to,
- reduction of intact stability caused by riding on the wave crest at midship,
- synchronous and parametric roll motion,
- and combinations of further various dangerous phenomena.

Meanwhile these guidelines are extended and supersede by the "revised guidance to the master for avoiding dangerous situations in adverse weather and sea conditions", IMO (2007). As before, it is designed to accommodate all types of merchant ships. Therefore the Maritime Safety Committee explicitly recommends tailor-made software, which takes into account characteristics of an individual ship.
The guidelines are restricted to preventive measures for extreme roll motion and capsize, hazards and risks in adverse weather like e.g. slamming, longitudinal and torsional stresses, or collision and stranding are not considered. In this regard the decision-making that takes into account all possible risks becomes a quite complex task. For this reason the demand for a supporting tool that identifies suited countermeasures in any hazardous situation further increases.

In October 2002, the classification society GERMANISCHER LLOYD (2002) installed a Shipboard Routing Assistance System SRAS on-board of a post-Panmax container vessel of the Greek shipping company COSTAMARE. The OCTOPUS software of AMARCON B.V. builds the framework of SRAS. It serves as control unit for a wave- and a hull response monitoring system, contains tools for route planning and evaluation regarding to weather data and to resulting ship responses, and provides the graphical user interface for SRAS. The system assesses the surrounding wave field and the probability of particular ship responses in half-hourly intervals. It reports to the master if the probability of these responses exceeds predefined threshold values. In the initial setup warnings are given for the slamming probability and for accelerations at the bow, meanwhile the assessment of parametric rolling is included, RATHJE and BEIERSDORF (2004).

During the last years Technische Universität Berlin contributed in several scientific projects addressing ship stability in irregular seas, CLAUSS et al. (2003) and CRAMER et al. (2004). Even if the focus is put on the improvement of ship design, an important result from the operational point of view are tailor-made data bases for particular ships, e.g. represented by polar plots that enable a master to identify dangerous wave conditions and give advice, how to avoid them at the best. Current projects, like LaSSe – Lasten auf Schiffe im Seegang, directly address this topic. They serve to establish an on-board system that provides a short-term prediction of the pressure field at the outer hull regarding the approaching waves measured by a wave monitoring system. In this way, it is possible to predict the load on the ship and ship motions a few minutes before they occur; hazardous events that could not be predicted by any forecast will be identified, instantaneous countermeasures can be executed, q.v. CLAUSS (2008).

The EU 6th framework research project ADOPT (2005) currently develops a risk-based decision support system for ship operation in rough seas. The **ADOPT DSS – Advanced Decision Support System For Ship Design, Operation, And Training** accounts for environmental, hydrodynamic, structural and operational factors that influence the decision making on-board a ship. Based on measurements and acquisition of all relevant data the system displays the current and also short, and medium term predictions of operating conditions. Further on the system conducts an evaluation by means of simulations and risk-based safety assessment techniques, accounts for the uncertainty of related information and for consequences of navigational measures. By this means guidance for a conscious decision making in terms of safe and economic navigation is given.

From different points of view it is useful to combine a forecast based route decision support system with a short-range wave monitoring system, if this is already installed on-board. As regards content, both systems can use similar methods and databases for the assessment of the ship motion in a seaway. Integrated bridge design demands for the reduction of devices. Last but not least, it is favorable for the route decision support to access data of the wave monitoring system. In that way the reliability of a forecast can be checked on-site.

1.2 Routing services

A characteristic difference of services for routing is whether the system or support comes from ashore or if there is an installation on-board a ship. In the first case it can be simply a forecast for weather and waves, or the service comprises advises from meteorologists and experienced masters based on their personal knowledge or acquired by automated optimization methods. Sometimes the service includes vessel tracing to enable the shipping company to watch the current positions and operating conditions of their ships.
The latter case consists of any on-board installed routing system, in most cases, a software running on a PC to display defined routes and resulting ship responses according to a weather- and wave forecast. It often comprises optimization functionality for the automated detection of favorable routes. In some cases the on-board system is integrated into a monitoring environment, i.e. an integrated system of a processing framework and measurement devices, e.g. to measure the surrounding wave field or sensors for loads and accelerations. A fully integrated system therefore includes medium term and short-term response prediction, i.e. response prediction based on forecasts and measured wave fields. In that way it provides support for navigation and maneuvering based on predicted and measured ship responses. Generally these systems also perform voyage data recording. Tab. 1 gives an overview on some available routing systems and services. It serves to illustrate their diversity and is an arbitrary selection. Therefore it does not aim to give a complete overview on routing system or service providers.

Tab. 1: Exemplary compilation of routing service or decision support systems

service provider	service / system	weather forecast	route planning	route optimization	warning system	ship monitoring	data recording	vessel tracking
Aerospace and Marine International (USA)	Weather 3000, internet service, maps displaying fleet and weather information	X					X	X
Applied Weather Technology (USA)	BonVoyage System, on-board system	X	X					
Deutscher Wetterdienst (Germany)	MetMaster, MetFerry, ashore routing systems, advice on demand		X	X				
Euronav (UK)	seaPro, on-board system, software or fully integrated bridge system	X	X				X	
Finish Meteorological Institute (Finland)	weather and routing advice from ashore for the Baltic sea	X	X					
Fleetweather (USA)	meteorological consultancy from ashore	X	X					X
Force Technology (Denmark)	SeaSense, real-time on-board decision support system managing wave-induced structural loads and ship motions				X	X	X	
Germanischer Lloyd, Amarcon B.V. (Germany, Netherlands)	Shipboard Routing Assistance System SRAS	X	X		X	X	X	
Meteo Consult (Netherlands)	SPOS, on-board routing system	X	X	X			X	
Metworks Ltd. (UK)	meteorological consultancy from ashore	X	X					
Norwegian met office, C-Map (Norway, Italy)	C-Star, on-board system	X	X					
Oceanweather INC., Ocean Systems INC. (USA)	Vessel Optimization and Safety System, VOSS, on-board system	X	X	X	X			
Swedish met and hydrology institute (Sweden)	Seaware Routing ™, Seaware Routing Plus ™ and Seaware EnRoute Live ™, on-board systems, and support ashore	X	X		X	X	X	
US Navy (USA)	STARS, on-board system	X	X	X		X		
Weather News International, Oceanwaves (USA, Japan)	Voyage planning system VPS and ORION, combination of ashore and on-board routing and optimization software	X	X	X				
Weather Routing Inc. (USA)	routing advice from ashore and Dolphin navigation program combined with a web-based interactive site	X	X					
Transas (UK)	Ship Guard SSAS, on-board system, software or integrated to bridge system	X	X			X	X	X

If at all automated route optimization methods are applied, all these systems and services operate single objective. That means, the optimization follows the ambition to improve a route in one matter, e.g. to find the route with the earliest estimated time of arrival *ETA* or to find the route with the lowest fuel consumption for a given *ETA*. However, in the latter example the objective function already becomes unhandy. To handle arrival on schedule and

lowest fuel consumption simultaneously, a delay has to be penalized and weighted against the fuel consumption. In that way, it is a combination of at least two objectives in one objective function. This is necessary for the applied optimization algorithms but unfavorable for a conscious decision support of a master. For this purpose a separate handling and assessment of the applied objectives would be better, i.e. compared to a single objective method, a multi-objective approach would be favorable.

1.3 A new approach to route optimization

So far, it appears that a route optimization procedure should be able to operate multi objective. Furthermore it has to consider a large amount of parameters that have an influence on a ship route decision:

- There are environmental parameters like restrictions in the navigable water, swell, wind waves, wind, currents, and drift ice. Most of these parameters are brought into the decision making by forecasts. Obviously an assessment of the reliability of the forecasts is desirable.
- Ship-sided parameters like ship size, hull shape, and the load condition, have a direct influence the ship characteristics in waves. The available main engine power forces a reduction of speed in higher waves, structural conditions may be regarded, too.
- Operational parameters cover the whole range of situations that might cause harm to the ship, the cargo, to passengers, or crew. For a reliable sea transport, situations that bear the risk of capsizing by parametric rolling, surf riding, or stability loss in following waves have to be prevented. Just as well, operational conditions that enable overcritical slamming, propeller racing, large amounts of green water on deck, and extreme accelerations should be avoided. Normally on-site countermeasures like course changes or speed reduction are employed to avoid damage of the ship or cargo or to guarantee the well-being of passengers and crew.

Dependent on a particular service the main aspect of a route decision is variable. Cruise liners may put focus on the well-being of passengers, a container service looks for safety of cargo and for being on schedule. Both are interested in reducing operating costs, mainly fuel- and lube oil consumption. Furthermore the global load on the ship structure becomes more and more deciding for a route decision, too.
This study establishes a new approach to route optimization. It is multi-objective and therefore optimization results are easy to overview. The method is able to produce meaningful results, e.g. to identify fuel minimum routes even if an arrival on schedule is impossible due to severe weather conditions. For the set-up two objectives are considered. They are fuel consumption representing operational costs and estimated time of arrival *ETA*. Later on the approach will be extended, considering the sensitivity of optimized routes to probable weather changes. Regarding the environmental conditions, it is decided to put the focus on swell as being the crucial factor for the ship motion in waves. For the time being, wind, wind waves, and currents are left out of consideration. The load on the main engine is observed to guarantee that the operational conditions agree to the main engine characteristic. Initially the operational parameters, as posed in the SEAROUTES project, are adopted, i.e. thresholds for slamming probability and accelerations on the bridge. These parameters, defining the “safe operational envelope”, are extended at a later point of this study. The presented optimizations belong to a westbound Atlantic crossing of the HAPAG LLOYD Panmax container vessel CMS HANNOVER EXPRESS. This ship is used for the set-up of the route optimization process since she is well known from the SEAROUTES project.

Fig. 6: CMS HANNOVER EXPRESS (by courtesy of Hapag Lloyd)

It is the purpose of this work to document the set-up and to make a feasibility study for this new approach to ship route optimization, not to develop turnkey ready software. As a start, chapter 2 introduces some basic principles and terms of optimization that are important for the understanding of the applied optimization procedures. Chapter 3 illustrates navigational aspects, i.e. route planning: determination of course and ship speed and its numerical representation. Furthermore the applied forecasts and the numerical modeling of swell is shown. Following, the fundamentals and the set-up of the mathematical model of the ship in waves are presented in chapter 4. The modeling of two extensions, namely for motion sickness incidence and parametric rolling, and some numerical recipes are given here, too. Chapter 5 continues with the set-up of the optimization procedure and shows the implementation of the numerical ship into a generic optimization environment. In chapter 6, the capability of the route optimization approach is assessed by means of different sensitivity studies. Finally a summary of this work and some aspects for further research are given in chapter 7.

2 Basic principles and terms of optimization

Before transforming the routing problem into an optimization task, it is necessary to introduce some basic terms and methods of optimization. The principle of optimization itself is very old. It is a matter of opinion, if optimization exists since the beginning of life on earth or since the beginning of humankind. However, since humans are aware about their capability to decide, optimization is a conscious behavior.
In a mathematical definition, the term optimization refers to the study of problems in which a real function is to be maximized or minimized by systematically choosing the values of variables from within an allowed set and by means of acceptable computational resources. The first optimization technique, which is known as steepest descent, goes back to GAUSS[3]. Since that time, reams of optimization algorithms have been developed, generic ones as well as ones that are tailor-made for a particular problem.
The problem statement in modern engineering technology bases on optimization tasks initially posed within the field of operations research. These became solvable due to the progress in computer technology. In this respect the modern age of numerical optimization began in the middle of the last century. Since that time the progress in optimization is closely related to the progress in computational capability and additional applied methods, e.g. simulation tools for computational fluid dynamics. Parallel to the developments in other fields of engineering, optimization in maritime design and operation stepwise improved to solve assignments of increasing complexity. Based on the research studies at the University of Michigan, see e.g. BENFORD (1965), NOWACKI et al. (1970) optimized main dimensions of a tanker to achieve minimum required freight rates. Numerous projects of applied research at Technische Universität Berlin represent the progress in optimization with regard to ship and offshore design since the seventies of the last century; e.g. NOWACKI and LESSENICH (1976) optimized main dimensions of a tanker, bulk carrier and a general cargo ship with regard to the required freight rates, HARRIES (1998) established a comprehensive method for parametric design and hull form optimization regarding ship resistance coupling computer aided design, methods for computational fluid dynamics, and optimization, BIRK and CLAUSS (2001) applied optimization techniques to a parametric hull form variation of offshore structures to minimize downtime.
For a continuative introduction to optimization and a comprehensive overview on optimization methods the study of BIRK and HARRIES (2003) is recommended, in particular because it is devoted to the optimization in marine design.

The least common denominator of al assignments in optimization is to minimize or maximize an **objective function**. Therefore the minimum requirements to state a problem as an optimization task, is to transform it into one objective function:

$$O = f\left(\overline{X}, \overline{P}\right), \tag{2.1}$$

i.e. a closed mathematical description of the problem in that way that the minimum (maximum) of this function represents the desired optimum. Then, optimization is the process of finding the set of **decision variables** $\overline{X}$ for a set of given **parameters** $\overline{P}$ that represent the minimum (maximum) of the objective function. Objective functions can be linear, uni- or multi-modal. In the first case the optimum (minimum or maximum) is mostly achieved at a boundary of the decision variables. Unimodal functions contain one single optimum, whereas multi-modal functions can afford suboptimal minima or maxima or more than one absolute

[3] Carl Friedrich Gauß, mathematician, astronomer, geodesist and physicist, 1777 – 1855, Germany

extremum of the same magnitude, named **local optima**. If there is one optimum that exceeds all the others, it is called **global optimum**. Certainly, it is the challenge of an optimization to prove that there is a global optimum and to identify it.
If the solution of the problem is subject to one or more boundary conditions it is called **constrained**. In principle two different types of **constraints**, equality- and inequality constraints, exist:

$$h_i\left(\overline{X}, \overline{P}\right) = 0, \quad i = 1,...,N, \tag{2.2}$$

$$g_j\left(\overline{X}, \overline{P}\right) \geq 0, \quad j = 1,...,M, \tag{2.3}$$

A set of decision variables that **violates** these constraints, i.e. one or more constraints obtain $h_i \neq 0$ or $g_j < 0$, is called **infeasible**. The constraints that cause infeasibility are also referred to as **active** constraints. If no violation of constraints exists, these constraints are **inactive**. Sometimes it is favorable to have the possibility to switch constraints on or off. In this case they are referred to as **enabled** or **deactivated**. An enabled constraint can be active or inactive, a deactivated constraint has no influence on the optimization.
In general, the decision variables represent a particular **design** of the subject matter that is to be optimized. The term decision variables, therefore, is the equivalent to **design variables**. The set of all designs that can be built by the set of permissible permutations of the design variables is called **design space**. In case of active constraints it is subdivided into **areas of feasible designs** and **areas of infeasible designs**. Furthermore constraints can generate local and global optima although the objective function is linear or unimodal.
If more than one objective function is addressed, the optimization is called **multi-objective**. In doing so, it is possible that two or more objectives represent a certain contradiction and the design space is bordered by a set of solutions for which an improvement in one objective can only be realized by impairing another objective. Such a border is called **PARETO**[4] **frontier** and the designs of this set are **PARETO optimal** designs, i.e. there is no design that is the best with regard to all objectives.

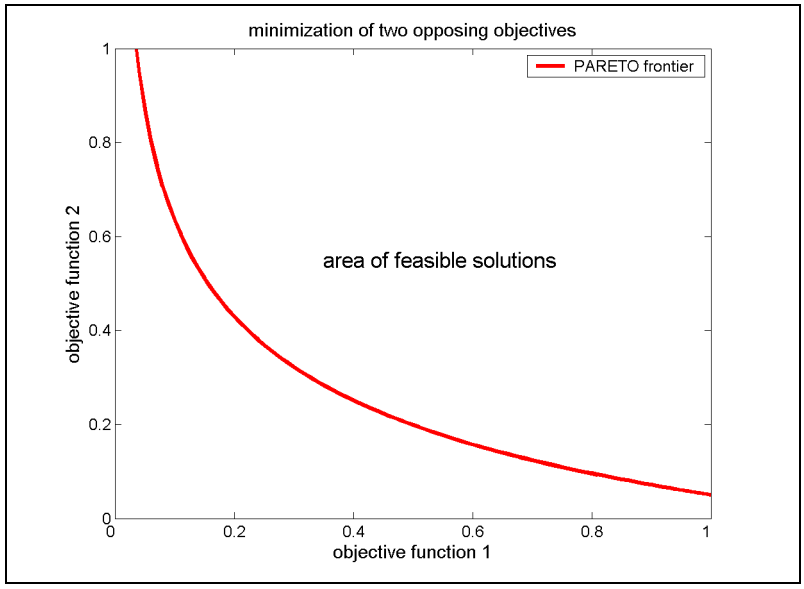

Fig. 7: PARETO frontier and area of feasible solutions

Fig. 7 serves to illustrate an optimization aiming a minimization of two opposing objective functions. The solid line marks the PARETO frontier.

[4] Vilfredo Pareto, engineer ,economist and sociologist ,1848-1923, Italy

All designs that are represented by function values on the left side and below this frontier are infeasible. Designs represented by function values above and right from the frontier are not necessarily feasible, but feasible designs can only be found in this area. The designs that mark the PARETO frontier, or designs that are at least close to these, represent optimum solutions. Dependent on the weighting of the objectives, it is now possible to consciously select a particular solution. Methods of multi-criteria decision-making can follow up but are consciously ignored within this study.
Related to the optimization task, it is necessary to find a suited optimization algorithm. Generally they can be divided into two types: **deterministic** and **stochastic algorithms**. To step forward towards the optimum, deterministic methods use e.g. function values, gradients, and higher derivations to define a new set of design variable. These algorithms are fast but tend to stick to local optima. Stochastic methods always produce a portion of their designs by a random process. Thus they are able to "jump" trough the solution space. This enables them to avoid premature convergence at local optima. In return, an optimization mostly takes more time.
In the following, two algorithms will be discussed more detailed as they are applied within this study on route optimization. They are a SIMPLEX algorithm representing a deterministic method and a genetic algorithm GA, a stochastic method. Both methods require a number of initial designs that depends on the dimension of the solution space. $\overline{X} \in \Re^n$ yields a *n*-dimensional solution space.

2.1 SIMPLEX algorithm

The SIMPLEX method by NELDER and MEAD (1965) is a commonly used, nonlinear optimization algorithm for optimizing an unconstraint objective function in an n-dimensional space. The algorithm works in principle as follows:

1. It requires $n+1$ initial designs or starting points, i.e. for a 2-dimensional problem they build a triangle, a tetrahedron for 3-dimensional, and a polytope (simplex) with $n+1$ vertices for n-dimensional problems.
2. The objective function is evaluated for all $n+1$ points. If one of the designs is good enough the algorithm stops.
3. Otherwise the worst point is deleted and replaced by a new one. In this way a new polytope is built.
4. Continue the loop with step (2).

The core of the algorithm is the strategy in step (3) to build the new simplex:

a) Reflect the worst point about the centroid of all others.
b) If this point is now better than all the others, expand the step in the same direction.
c) If it is simply better than before, continue with step (2).
d) However, if the point gets worse in either case, shrink the simplex e.g. to half size around the best point and continue at step (2).

The algorithm terminates if the attainable improvement at successive optimization loops falls below a preset convergence limit. Meanwhile the SIMPLEX method is widely extended, e.g. to preserve an equable shape of the simplex or even some random capabilities are adopted to overcome the convergence at local optima. For the discussion on the convergence properties

see LAGARIAS et al. (1988). Although it is not formally proved for more than $n = 2$, the SIMPLEX algorithm is widely used in high dimensional optimization problems.

2.2 Genetic algorithms, GA and MOGA

"The systematic utilization of stochastic events is one of the recipes of success of evolution", SCHÖNEBURG et al. (1994). It is a process of searching mainly based on three principles: **mutation**, **recombination**, and **selection**. By inspiration of the biological archetype, two types of evolutionary algorithms have been built independently, one is called evolutionary strategy ES by RECHENBERG (1973) and the other one genetic algorithms GA by HOLLAND (1975). In the beginning ES and GA were rather different, e.g. ES used a real-valued coding and a variation of the genotype was solely done by recombination whereas GA used binary-valued coding and a lot of effort was put to various mutation schemes. But even more, it was a philosophical dispute; ES supporters aimed to develop a strong optimization tool for engineering problems; GA supporters wanted to improve the understanding of natural adaptation processes and to design artificial systems having properties similar to natural systems. The genetic algorithms nowadays often are a merging of both strategies (as is known, some who are deeply involved in the matter would strictly disagree). Nevertheless, the ability to overcome local optima by applying stochastic schemes unifies both algorithms. For the initial set-up to solve the route optimization problem, it is decided to apply a multi-objective genetic algorithm MOGA of the generic optimization environment modeFRONTIER by ES.TEC.O (1999). In the following, the focus is put on the genetic algorithm. Surely any other stochastic method may work, too.
The basic idea of a genetic algorithm is as follows: the genetic pool of a given population potentially contains the solution, or a better solution, to a given adaptive problem. This solution is not "active" because the genetic combination on which it relies is split between several subjects. Only the association of different genomes can lead to the solution. HOLLAND's method is especially effective because it does not only consider mutation (mutations improve very seldom the algorithms), it also utilizes genetic recombination (crossover). This recombination, the crossover of partial solutions, greatly improves the capability of the algorithm to approach and eventually find the optimum, EMMECHE (1994). In fact, the desired solution may happen not to be present inside a given genetic pool, even a large one. If so, mutations allow the generation of new genetic configurations that widen the gene pool and improve the chances to find the optimal solution. Mutation diversifies the genetic pool and prevents premature convergence, whereas selection affects a harmonization. To obtain a satisfying performance of the algorithm it is necessary to align the associated mechanisms for mutation, selection, and recombination accurately. As genetic algorithms are based on heuristics, no general convergence is proved.
The principle steps of a genetic algorithm are as follows:

1. Encode the problem in a binary string, i.e. transform the free variables that describe a possible solution design (**phenotype**) into a suited binary representation (**genotype**).
2. Randomly generate a set of initial designs, the first **generation** or **start population**. This one includes the **genetic pool** representing a group of possible designs.
3. Evaluate the **fitness** value for each design, i.e. a ranking of the designs. Mostly the value of the objective function relative to the one of the other designs is used. In case of a multi-objective optimization it is deciding if a design is a member of the PARETO frontier or if it is closed to it.
4. Select the designs that will mate according to their share in the population global fitness. The probability to be taken into consideration to create descendants is

dependant on the fitness. The consideration of the best designs within the next generation is only ensured if **elitism** is applied.

5. The designs that fail the selection are deleted. All others are used to fill up the population again. As a general rule, the number of designs in each generation remains the same. The **reproduction** to build new designs is performed by crossover and mutation mechanisms, i.e. a permutation and random variation of the binary strings that represent the free variable.
6. Start again from point (3) if no convergence limit or the number of maximum generations is reached.

The potential to produce design variants directly depends on the number of designs per generation. But as the mechanism that brings forward the process towards better solutions (step 4 and 5) is accessed only once per generation, a large number of designs decelerates the propagation towards a better solution. In a sense, the setup of a genetic algorithm is an optimization process itself.
To illustrate the mode of operation and the performance of a SIMPLEX an a GA, both methods are applied to maximize the following bivariate test function, available as the *peaks* function within MATLAB (2002):

$$z = 3\,(1-x)^2 \cdot \exp\left(-x^2 - (y+1)^2\right) - 10\left(-x/5 - x^3 - y^5\right) \cdot \exp\left(-x^2 - y^2\right) - 1/3\ \exp\left(-(x+1)^2 - y^2\right). \quad (2.4)$$

Fig. 8 represents a perspective and a contour plot of equation (2.4), a function with three humps and two hollows.

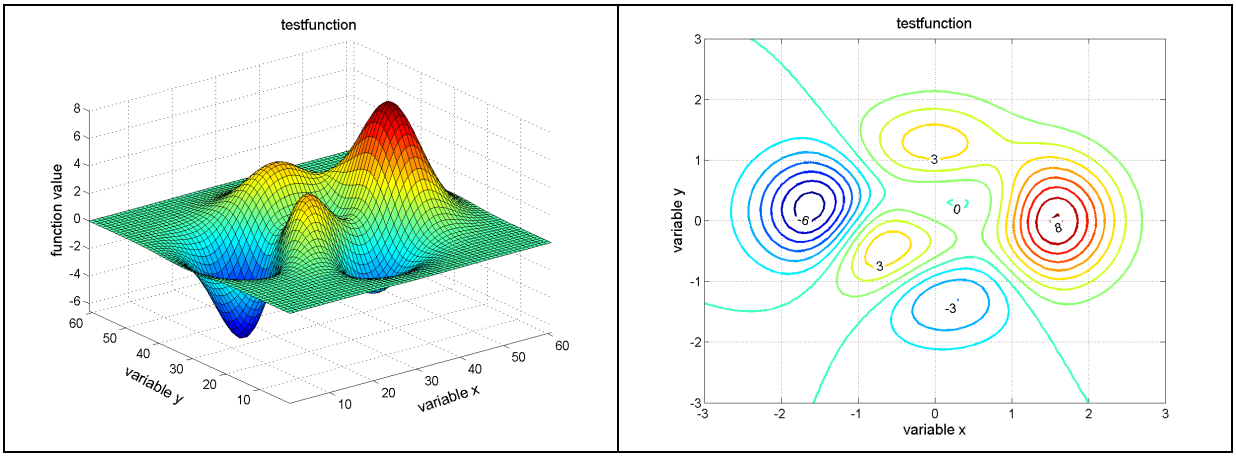

Fig. 8: Test function, perspective and contour plot

Both algorithms used the same start designs represented by square dots at the lower left edge of the contour plots in Fig. 9. Because the SIMPLEX requires only three starting points whereas the GA needs at least four, the first optimization step of the SIMPLEX is used as the fourth starting point for the GA. Both methods are supposed to find the maximum value of the test function at $x = 1.6$ and $y = 0.0$.

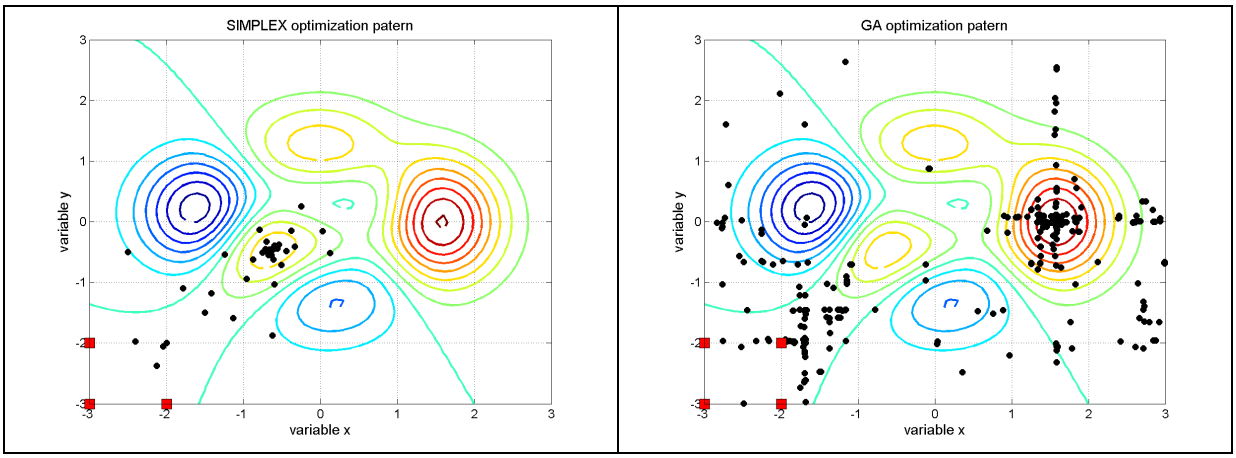

Fig. 9: SIMPLEX and GA search pattern

Obviously the SIMPLEX converges directly towards the nearest local maximum. The maximum is crossed slightly but not far enough to detect the humps behind. The optimization stops due to an achieved convergence limit. The GA indeed is able to detect the global optimum. Admittedly it needs much more designs to reach it. It mostly preserves the orthogonal characteristic given by the start designs. Fig. 10 illustrates the convergence process of both optimization methods. The SIMPLEX, represented by red asterisks, quickly propagates towards the nearest local optimum. It needs only 80 designs to converge. Normally nothing is known about the function to be optimized, therefore it is only proved that a local optimum is found. However, the GA needs some time "to come out of the corner.“ For a GA the start population is chosen unfavorable. It has to increase the gene pool, to spread out and become more moveable by mutating and recombining the initial designs. At design number 415 it reaches the global optimum.

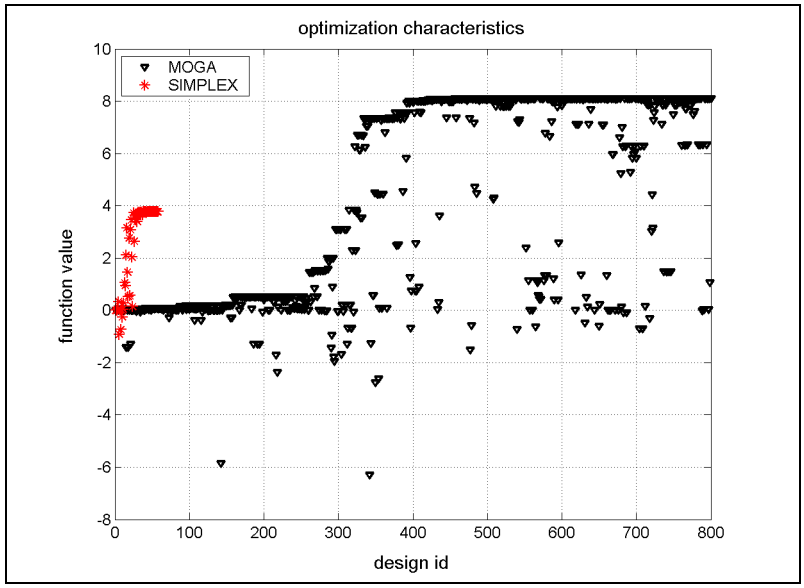

Fig. 10: Optimization characteristics

As there is no guarantee that really the global optimum is found, it is recommended to continue the optimization to support at least the assumption that the optimization succeeded. In this case, the price for reaching the global optimum is the tenfold number of required designs. Nevertheless, it shows the ability of a GA to prevent a premature convergence and not to stick to local optima. It is interesting to see that both, local maxima are apparently

ignored by the GA. If there has been a very slim maximum, it probably would have been overlooked. Finally, there is no guarantee, it is a trade-off between computational effort, and strategies to improve the global convergence, e.g. test various start designs or make variations of the parameters that control the algorithm.
In spite of all difficulties connected to optimization, without these methods a route optimization problem as attended here would become intractable. Therefore it is very impressive to realize the number of possible designs that are considered. In section 5.1 it is shown that at least 17 free variables are required for the applied routing example. Assuming that each variable can take 20 discrete values (essentially it is much more), the number of possible design variants would be:

$$discrete\ steps^{number\ of\ free\ variables} = number\ of\ possible\ designs\,, \qquad (2.5)$$

which results to $20^{17} = 1.3 \cdot 10^{22}$ designs. If one design evaluation requires 2.5s (it is currently the time required for the assessment of the ship behavior at 60 points of a single route) the evaluation of all possible designs would take 10^{12} millennia. The present version of the route optimization runs 20 000 designs and requires at most 14h. Of course this is too much, but is has to be borne in mind: the calculations are conducted on a simple 2.8GHz personal computer. There have been no efforts with regard to the programming language to optimize the run-time, and the GA is not adapted to the route optimization problem. In most cases it requires 3000 to 5000 designs to identify the PARETO frontier, all further designs are used to prove the result. It is therefore accepted to be a reliable and efficient method to optimize ship routes.

3 Modeling of ship route and environmental conditions

This chapter introduces the applied methods to generate a ship route, section 3.1, and to describe the corresponding weather conditions, sections 3.2 and 3.3. The used definitions of angles and directions are illustrated in Fig. 11:

- The course angle α describes the forward direction of the ship. It is 0° for a ship sailing in northern direction, increasing towards East, i.e. 90° means sailing towards East.
- The incident wave angle γ describes the direction of swell. It is 0° for wave crests propagating from North to South, increasing towards East, i.e. 90° means that wave crests propagate from East to West.
- The wave encounter angle β describes the direction of approaching waves relative to the sailing direction of the ship. It is 0° for following waves and 180° for heading waves. Encounter angle of 90° represent beam seas from either starboard or portside.
- Locations on-board the ship are given in a ship-bound coordinate system with positive x-direction ahead, y-direction to portside, and z-direction upward. The origin of this coordinate system is at the center of gravity of the ship.
- All routes and maps are represented on a Cartesian coordinate grid, ordinate and abscissa depict degrees of latitude and longitude, respectively.

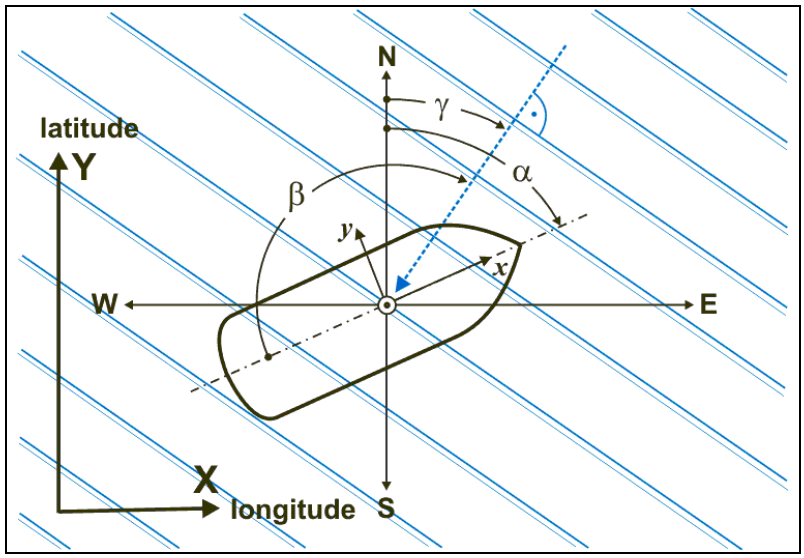

Fig. 11: Definition of angles and directions

3.1 Route description and perturbation

The schedule of the example container service, used for the set-up of the route optimization, is given in Fig. 12. It depicts the stations of the round trip and the durations of each step of the journey, e.g. the trip from Southampton to New York takes 8 days.

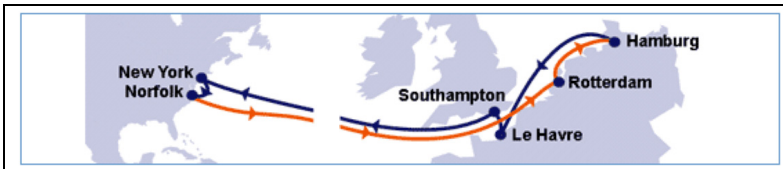

North America to Europe →

From / To	Rotterdam	Hamburg	Le Havre	Southampton
New York	13	15	17	18
Norfolk	11	13	15	16

Europe to North America →

From / To	New York	Norfolk
Rotterdam	13	15
Hamburg	11	13
Le Havre	9	11
Southampton	8	10

Fig. 12: Atlantic Express / ATX (North Atlantic)
(source: www.hapag-lloyd.com)

The route optimization focuses on the open water part of the journey. Pilot time and estuary traveling are deliberately left out of the investigation as they admit only small variations. For that reason the route optimization starts at the western end of the English Channel (5°W, 49°N) and ends in the estuary of New York (70°W, 41°N). It spans a distance of roughly 3000nm. Sailed at 23kn it would take 130h, approximately 5.5 days. Compared to the schedule of Fig. 12, the journey from Southampton to New York comprises 2.5 days pilot time and 5.5 days at open water. Only for the open water part, the ship route is varied in time and space. Thus, the route optimizations presented here necessitate a time period of less than 130h for the optimized part of the journey to arrive on schedule.
Necessary parameters to describe the route are longitude, latitude, course angle, and speed as time-dependent values. For a discrete route description, as applied here, these parameters have to be given in a sufficient resolution that ensures that all necessary environmental properties are included. Further parameters that are regarded for the decision support are derived according to this description, e.g. the significant wave height or the fuel consumption.
To design both, the spatial and the temporal pattern of a route in terms of free variable, the course and the velocity profile are expressed as B-splines. An initial course and an appropriate velocity profile, referred to as parent route, are given in advance. Perturbations of the parent route in time and space are realized by superposing GREVILLE[5]-spaced shift splines to the parent splines. The solid line in Fig. 13 shows the course spline of the parent route for a westbound North Atlantic crossing. The route follows the great circle from Bishops Rock to the region south of Newfoundland. Afterwards it continues rhumb line to New York. The dashed lines represent the maximum northern and southern perturbations. For the investigations presented here, the maximum allowed perturbation is set to 10% of the arc length of the parent route to either starboard or portside direction. The northern perturbation is constricted to avoid land collision at Newfoundland and at Southern Ireland. Alternatively a validation of a route in terms of geographical feasibility is performed during the optimization process. A variable representing a later departure is introduced to model a waiting of the ship for better sea conditions.

[5] Thomas Nall Eden Greville, mathematician, 1910 – 1998, University of Wisconsin, USA

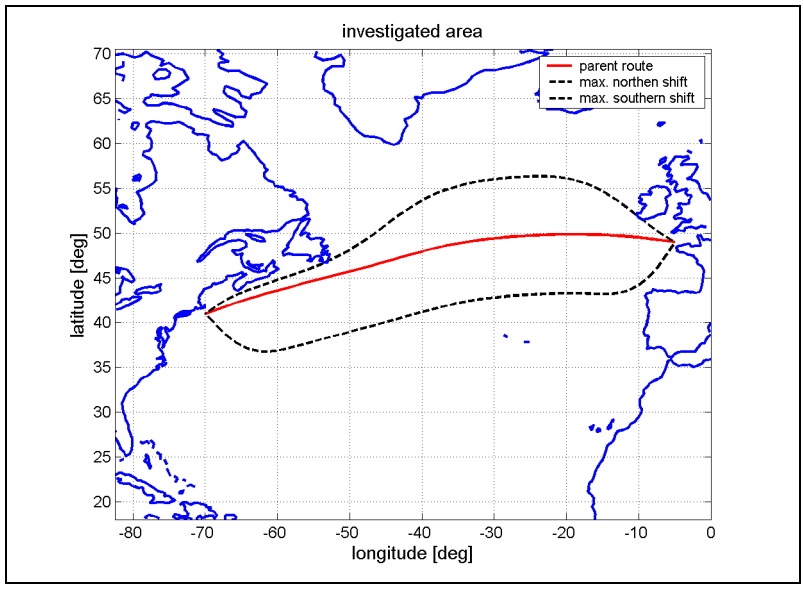

Fig. 13: Parent route and maximum perturbations

Fig. 14 presents shift splines and example routes as realized with seven parameters for the spatial shift. The horizontal positions of the shift spline vertices are computed according to the method of GREVILLE-abscissa. The vertical offsets are taken as the free variables of the optimization task.
The variation of the velocity profile is accomplished in the same way. Here the parent spline straightens up and represents a ship speed of 24kn. The perturbation is performed by superposing a shift spline in order to define a reduction of the design speed.

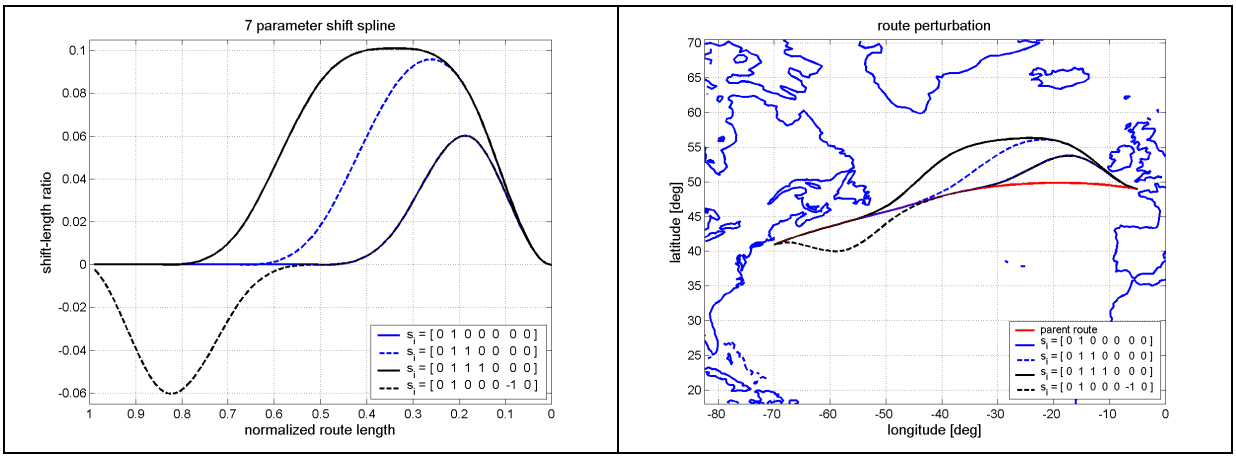

Fig. 14: Shift spline and perturbed parent route

Applying the GREVILLE-abscissa provides a harmonization of the variability of the splines that are used for the course- and the velocity profile perturbation. The method couples the step size of the control variables to the arc length of the splines. E.g. all splines are parameterized from 0 to 1. A control variable of 0.5 represents a point in the middle of the splines. This means, the number of passed vertices and of vertices lying ahead is the same. That is why the variability of the spline segments also is the same. This is maintained for each value of the control variable. Thus the variability of passed and remaining spline segments for the course and the velocity profile is the same. A detailed description of the applied spline technique is given in FARIN (2001).

Tab. 2 summarizes free variables and constants as used for the route perturbation.

Tab. 2: Free variables and constants of the route perturbation

type	name	content
free variables	$\boldsymbol{S} = [s_1 - s_n]$	vector of spatial shift parameter
	$\boldsymbol{V} = [v_1 - v_n]$	vector of velocity shift parameter
	RTD	retarded time of departure
constants	*scale*	maximum orthogonal perturbation in percent of the parent route length
	vmin	minimum for the velocity perturbation
	vmax	level of the parent velocity spline and maximum for the velocity perturbation

Former investigations concerning the number of free variables showed that at least nine variables for the description of the velocity profile and seven variables to describe the course are necessary to obtain a sufficient temporal and spatial resolution of the route that correlates to the wave pattern as well as to the geographical conditions in the North Atlantic, cp. HINNENTHAL and SAETRA (2005).

3.2 Deterministic weather forecast and parametric wave model

Meteorological institutes like the European Centre for Medium-Range Weather Forecasts operate global and associated local climatologic models. These are initialized and tuned with atmospheric and environmental data, measured by satellites, meteorological stations ashore and at sea, or special devices for particular measurements like wave buoys allocated over the whole globe. Dependent on required accuracy and computational effort, these models make use of a more or less dense numerical grid for which they calculate a wide range of climatologic data. These data are used to produce e.g. weather- or wave forecasts.
In principle, the ECMWF provides three different types of deterministic sea state forecasts. Therein wave data for a particular position and time are available as:

- Directional spectra, representing the energy distribution of swell and wind sea depending on frequency and directional distribution,
- Integrated directional spectra, representing the energy distribution depending on the frequency for a prevailing direction (referred to in the following as ECMWF-1D), or
- Wave parameter derived from ECMWF-1D; significant wave height $H_{1/3}$, peak period T_p and prevailing direction β. For practical purposes, e.g. when evaluation ship responses, these parameters are used in combination with standard spectra like the JONSWAP spectrum and the modified PIERSON-MOSKOWITZ spectrum, respectively.

For the work presented here, three different weather scenario illustrated in Tab. 3 are applied. They describe a calm weather condition, a rough sea state, and an intermediate condition. The data cover the North Atlantic from 0.0°- 82.5°W and 18.0°- 70.5°N. They are given on a grid of 1.5° an in time steps of 12h. Actually, these data are re-analysis data from the data archive of ECMWF. Anyhow, they are used as deterministic forecasts for the set-up and within most investigations of this study.

Tab. 3: Maximum wave heights of considered weather scenarios

sea condition	date	maximum $H_{1/3}$ [m]	corresponding T_p [s]
calm	6.6. – 16.6.2001	5.4	10.2
medium	1.1. – 11.1.2003	12.0	15.4
rough	20.1. – 30.1.2002	15.0	14.9

For practical purposes only the parametric description, i.e. significant wave height $H_{1/3}$, peak period T_p and wave angle β, is used. This is necessary to keep the computation time and the amount of data in a reasonable magnitude. Anyhow, for the computation of the ship motion in waves as applied here, a representation of the sea condition by means of a wave energy spectrum is needed. Various parametric representations are available. They all refer to a form given by PIERSON and MOSKOWITZ (1964), see e.g. CLAUSS et al. (1988 / 1994) and HASSELMANN et al. (1975):

$$S_\zeta(\omega) = \alpha g^2 \omega^{-5} \exp\left\{-\beta\left(\frac{\omega_0}{\omega}\right)^4\right\} \quad \text{for } \omega > 0 \,. \tag{3.1}$$

With:
$\alpha = 0.0081$, and $\beta = 0.74$,
$\omega_0 = g/U$, and $U =$ wind speed 19.5m above the sea level,
the original form of the PIERSON-MOSKOWITZ spectrum is obtained.

The parameter α and β are fixed for closest fit to measured data of developed wind sea for the North Atlantic. The transformation of (3.1) to the commonly used two-parameter form is shown by CLAUSS et al. (1994).

$$S_\zeta(\omega) = 4\pi^3 \frac{H_{\frac{1}{3}}^{\,2}}{T_0^{\,4}} \cdot \omega^{-5} \exp\left\{-16 \frac{\pi^3}{T_0^{\,4}} \cdot \omega^{-4}\right\} \tag{3.2}$$

represents the PIERSON-MOSKOWITZ spectrum for the parameters significant wave height $H_{1/3}$ and zero up crossing period T_0. Following the relation:

$$H_{\frac{1}{3}} = 0.99771 \cdot \alpha \cdot g \cdot T_0^{\,2} \,, \tag{3.3}$$

equation (3.2) is identical to (3.1). Meanwhile, this form is applied for independent values of $H_{1/3}$ and T_0 resulting in a modification of the spectra. For that reason, it is called modified PIERSON-MOSKOWITZ spectrum.

$$S_\zeta(\omega) = 5.57\pi^3 \frac{H_{\frac{1}{3}}^{\,2}}{T_1^{\,4}} \cdot \omega^{-5} \exp\left\{-22.28 \frac{\pi^3}{T_1^{\,4}} \cdot \omega^{-4}\right\}, \tag{3.4}$$

represents the PIERSON-MOSKOWITZ spectrum for the parameters significant wave height $H_{1/3}$ and mean period T_1, also known as BRETSCHNEIDER spectrum, BRETSCHNEIDER (1957), or ITTC two-parameter spectrum. To apply equation (3.2) or (3.4) to the wave data given by ECMWF, the relation $T_0 = 0.711 \cdot T_p$ or $T_1 = 0.772 \cdot T_p$ can be used, JOURNÉE (2000).

Within the Joint North Sea Wave Project in 1968 - 1969, extensive wave measurements in the North Sea were carried out. It was found out that multiplying (3.4) with a peak enhancement function is most suitable to describe the measured spectra. Equation (3.5) represents the JONSWAP formulation given by LLOYD (1998):

$$S_\zeta(\omega) = 5.57\pi^3 \frac{H_{\frac{1}{3}}^{\,2}}{T_1^4}\cdot\omega^{-5}\,\exp\left\{-22.28\,\frac{\pi^3}{T_1^4}\cdot\omega^{-4}\right\}\cdot 0.658\cdot C\,, \qquad (3.5)$$

where $0.658\cdot C$ is the peak enhancement function,

with $C = 3.3^J$ and $J = \exp\left\{-\left(\frac{\omega/\omega_p - 1.0}{\gamma\sqrt{2}}\right)^2\right\}$,

$\omega_p = 2\pi/T_p$ is the frequency of the spectral peak or modal frequency,

and a parameter γ with $\gamma = 0.07$ for $\omega < \omega_p$, and $\gamma = 0.09$ for $\omega > \omega_p$, to scale the peak width at frequencies above and below the modal frequency. According to JOURNÉE (2000) the relation $T_1 = 0.834\cdot T_p$ can be used to provide the mean period used within equation (3.5).

In 1978 the JONSWAP spectrum was advised, by the 15th ITTC, for coastal waters with limited fetch. For a given significant wave height and wave period both spectra, JONSWAP and PIERSON-MOSKOWITZ, have the same area under the spectral curve and therefore they represent the same amount of wave energy. Thus, for underdeveloped wind sea both formulations are admissible. It will be illustrated in section 6.2 (cp. Fig. 56 on page 74) that the ECMWF-1D often lies, so to speak, "in between" the PIERSON-MOSKOWITZ and the JONSWAP spectrum. Standard practice for the North Atlantic is the application of a PIERSON-MOSKOWITZ spectrum.

3.3 Ensemble weather forecast

The deterministic forecast represents one likely development of the sea state but gives no information about the probability of its occurrence. In contrast, the operational ensemble prediction system EPS generates a set of 50 forecasts. The data format, i.e. grid and time resolution, are the same like in deterministic forecasts. These ensemble members have an almost equal probability of occurrence. They are generated by a superposition of small perturbations to the operational analysis before launching the forecast calculation. The method is based on the assumption that the forecast calculation is able to properly predict the weather development, if it is based on a proper data set of the current weather situation. In this view the error of the forecast is caused by errors in the measurement of the current weather situation, and the perturbations of the start data are related to this error in the measurements.

The ensemble spread measures the "differences" between the ensemble members, or the differences between particular parameters given by the forecasts. It is related to the forecast uncertainty. Small spread indicates low forecast uncertainty, and vice versa. Generally the uncertainty increases while going further into the forecast, BIDLOT et al. (2002). Ensemble forecasts are used to assess the amount of possible weather changes for the operation of ships and offshore devices. Here they will be applied to evaluate the robustness of optimized ship routes against weather changes.

Fig. 15 shows significant wave heights predicted for one particular ship route. The Figure serves to illustrate the differences between deterministic- (re-analysis) and ensemble forecast. Furthermore a mean ensemble forecast is shown. This one can be used instead of a deterministic forecast to get a more likely estimate of the weather development but it is to exercise with caution. The building of a mean value attenuates the time correlation of the data and therefore a mean forecast undervalues the sea condition when maximum values show a distinct time shift.

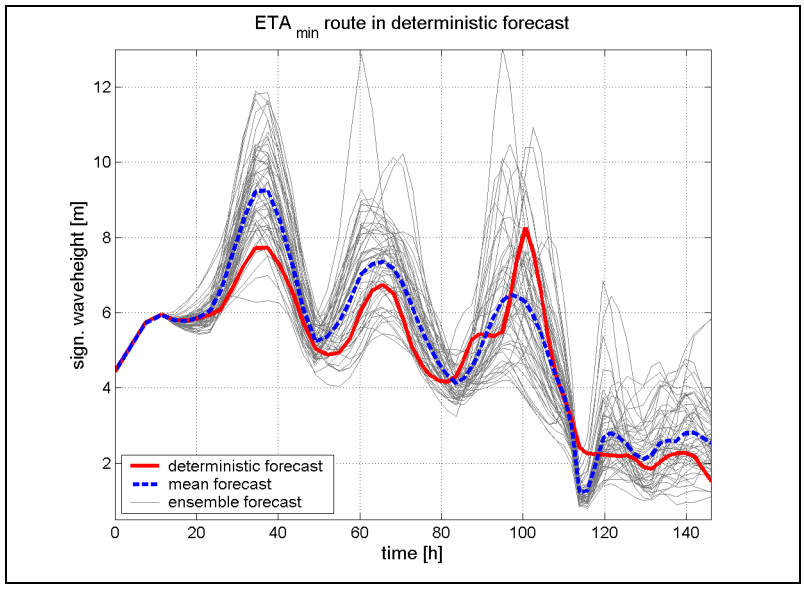

Fig. 15: Ship route in different forecasts

The route in Fig. 15 takes 143 hours. During this time three areas of adverse weather will be crossed. It can be seen that the spread in the predicted wave height increases with an increasing forecast horizon. In other words, the accuracy of the forecast decreases while it is progressing in time. But also, and this is much more harmful for ship routing, the spread increases in adverse weather situations. Commonly used as a rule of thumb, it is said that deterministic forecasts are reliable within a three days horizon. This obviously is not the case in the situation depicted in Fig. 15. Here the ensemble forecast demands on caution when approaching the first extreme wave field approximately 30 hours after departure.

4 Assessment of ships responses in waves

It is expected that route optimization at harsh sea conditions is strongly affected by a restricted operability of the ship. For this reason all factors that can cause harm to the ship, the cargo, to passengers, or to the crew should be considered to support safe ship operation:

- regarding the absolute motion of the ship there are extreme accelerations in longitudinal, transverse, and vertical direction and different mechanisms of extreme roll motion that cause large roll angle or accelerations, e.g. resonant rolling, parametric rolling, stability loss in following waves, surf riding and broaching, as well as capsize,
- regarding the relative motion between ship and water surface there are propeller racing, slamming, or large amounts of green water on deck,
- regarding operational parameters there are structural loads and main engine load due to the increasing ship resistance in waves.

Here only a choice of parameters is considered just to investigate the functioning of the suggested new routing approach, they are slamming, vertical accelerations on the bridge and main engine load. Because an optimization requires numerous calculations of the ship responses in an actual sea state, a fast method is needed to describe the ship in waves. In this case the statistical evaluation method, using transfer functions provided by strip-theory and wave spectra, is applied. This serves to estimate the ship responses for a particular route and corresponding weather conditions.
Initially this chapter introduces the application of transfer functions and summarizes the basic equations of this method, as far as they are applied for this route optimization approach. Following, the conversion into a "response database" for the ship motion is shown. This step is favorable to accelerate the calculation of ship responses during the route evaluation. The chapter continues with a critical view on the applied methods and closes by introducing two approaches that are not common in classic strip-theory. These address motion sickness incidence and parametric rolling.

4.1 Ship motion and transfer function

In general, the response or output signal of a linear system is calculated from the product of an input signal and a response function. In this case the input signal is a spectrum of an irregular sea state, the response function is the squared transfer function of the ship motion, and the output signal represents a ship motion spectrum.

$$S_s(\omega) = \left| \frac{s_a}{\zeta_a} \right|^2 \cdot S_\zeta(\omega) \qquad (4.1)$$

The input signal is the energy density spectrum of a particular sea state $S_\zeta(\omega)$, in short the wave spectrum. It can be derived by means of a FOURIER[6] analysis of a measured sea state. In this way, irregular long crested waves are represented as a superposition of harmonic waves of frequency ω, amplitude ζ_a, and with a random phase shift. The spectrum contains information about the amount of energy of a sea state and about the distribution of energy over the frequency range of the spectrum. It can be used to calculate e.g. the significant wave height $H_{1/3}$, peak period T_P, and other characteristic values of a sea state.

[6] Jean Baptiste Joseph Fourier, mathematician and physicist, 1768 – 1830, France

$S_s(\omega)$ is the energy density spectrum of the ship motion, in short the response spectrum. Like the wave spectrum, it does not contain any information about the phase relation of the harmonic components, i.e. there is no information about the motion in time. Also the response spectrum will be evaluated statistically. For example the significant amplitudes of the motions in the six degrees of freedom (the interest is mainly on heave-, roll- and pitch motion) and characteristic periods (e.g. mean zero-up-crossing periods) can be determined.

The transfer function $|s_a/\zeta_a|$ represents the relation of amplitudes of the ship motion s_a and the exciting harmonic wave component ζ_a. It is dependent on the frequency of excitation. For each degree of freedom of the ship motion, a transfer function can be calculated. Three translatory degrees of freedom are considered: surge, sway, and heave (index a = 1,2,3) and three rotational degrees of freedom: roll, pitch, and yaw (index a = 4,5,6). $|s_{3a}/\zeta_a|$ e.g. is the transfer function of the heave motion. In ship hydrodynamics a squared transfer function is commonly denoted as response amplitude operator *RAO*.
In the strict sense a transfer function consists of magnitude and phase, i.e. for each frequency of the input signal a magnification factor and a phase shift of the response is given. Generally transfer functions are computed for the center of gravity motion. As long as the ship is regarded as a rigid body they are valid to describe rotary motions at all positions on-board a ship. However, the transfer functions for the translatory motion of the centre of gravity are only valid for this particular point. For all other positions on-board a ship the transfer functions of rotary- and translatory motions have to be superimposed taking into account the frequency dependent phase angle. This e.g. is done for the calculation of transfer functions for the vertical motion on the bridge. The statistical evaluation of ship motions regards only the magnitude of the transfer function, i.e. the amplitude characteristics is employed whereas the frequency characteristic is discarded because the phase relation of the wave spectrum is not known.
In principle, the response characteristic is assumed to be linear, i.e. regarding a harmonic excitation:

- a doubled amplitude of the exciting wave results in a doubled amplitude of the ship response,
- and the frequencies of the input and the output signal are the same.

The first condition is only partly fulfilled. As long as restoring- and mass forces are dominant the system behaves linear. When viscous effects arise the system appears increasingly non linear. This applies to motions in the region of natural frequencies and in particular to roll motions. Fig. 16 serves to illustrate the effect of non-linear damping coefficients; it shows transfer functions for the roll motion at beam seas. In the natural frequency region the magnitude of the ship response is governed by viscous damping. Because damping coefficients depend not only on the height and frequency of exciting waves but also on the ship motion itself, they have to be calculated iteratively. Higher waves cause larger ship motion in connection with increasing damping coefficients, which finally reduces the magnitude of the transfer function. During the calculation of a transfer function, linearized terms are used to consider viscous effects. The linearization is done for a mean expected wave height (variation from 1 to 7m in Fig. 16). In that way motions excited by higher waves are overestimated because damping effects are underestimated. This can be considered as a little safety factor in the determination of resonant roll motions. Motions like parametric rolling, surf riding and broaching are even more difficult to assess, as they are highly non-linear. Furthermore, within generic seakeeping codes based on strip theory these motions are decoupled from the exciting forces.

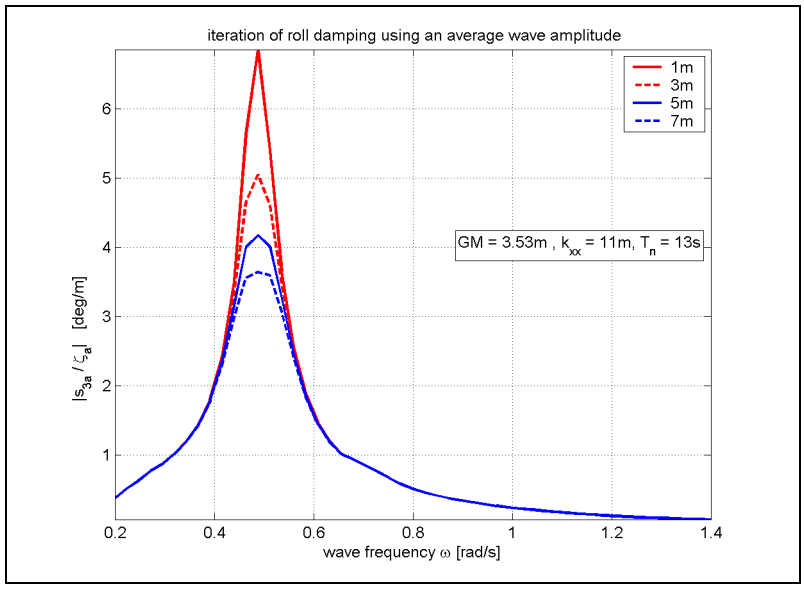

Fig. 16: Transfer functions for the roll motion
$\beta = 90°$, $V_s = 23$kn

For the calculation of transfer functions the desktop-program SEAWAY is utilized, JOURNÉE (2001). SEAWAY is a strip-theory code, bases on potential theory, and operates in the frequency domain. It solves a three-dimensional problem by integrating two-dimensional solutions (strips) over the ship length. In principle the ship is assumed to be a slender body at zero-speed, i.e. fluid flow velocities in the transverse direction are much greater than in the longitudinal direction. SEAWAY provides two different methods to account for forward speed effects referred to as ordinary- and modified strip theory. Furthermore the program offers different semi-empirical methods to account for the influence of viscous damping on the roll motion. A comprehensive overview on the program and all implemented features is given by JOURNÉE and ADEGEEST (2003). Fig. 17 shows the frame representation of the CMS HANNOVER EXPRESS, as it is used by SEAWAY.

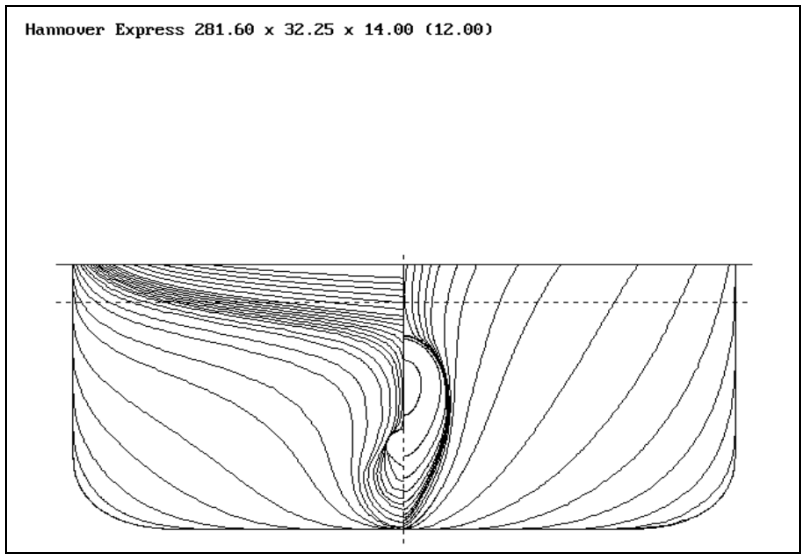

Fig. 17: Sections CMS HANNOVER EXPRESS

Besides transfer functions for the center of gravity motions for all six degrees of freedom and transfer functions for the motions of selected points, absolute and relative to the free surface,

two different methods are available to determine response functions for the added resistance due to waves. The methods are the radiated energy method according to GERRITSMA and BEUKELMANN (1972) and the integrated pressure method according to BOESE (1970). The numerical results initially used within the route optimization procedure are:

- The transfer functions of the translatory motions on the bridge. They are used to calculate the significant amplitudes of lateral and vertical accelerations on the bridge (loading on the crew by means of accelerations).
- The transfer functions of the motion at a point "10% of *LPP* behind *FP*", relative to the free surface are used to calculate the slamming probability.
- The response functions for the added resistance due to waves are used within the calculation of the fuel consumption (preferably according to the integrated pressure method of BOESE which displays a smother distribution over the wave frequency ω than its radiated energy counterpart).

Fig. 18 shows some transfer function and response functions for the added resistance due to waves. From left to right they are: transfer functions for the vertical motion on the bridge, transfer functions for the relative vertical motion at the bow, and response functions for the added resistance due to waves. They are given for a wave encounter angle of 180° (head sea) and for ship speeds of 13, 18, and 23kn. The figure serves to illustrate the principle shape of transfer functions and response functions.

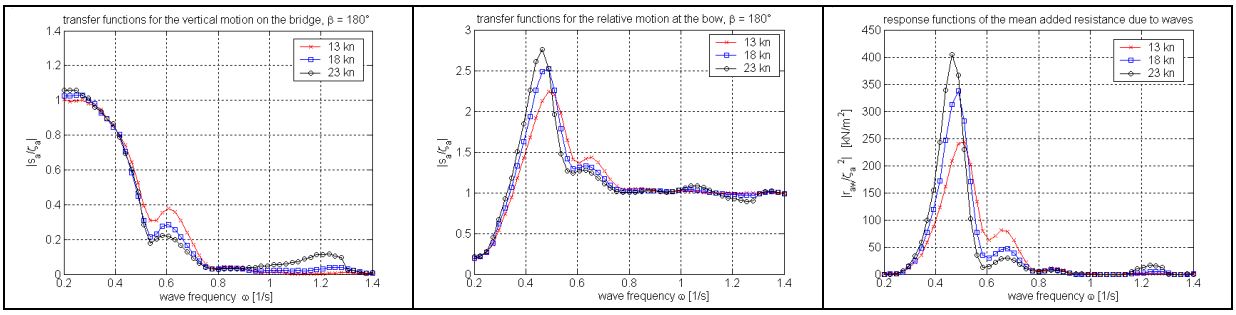

Fig. 18: Representative transfer functions and response functions for the added resistance in waves

It is decided to employ a basic but representative model of the ship in waves, as the focus is put on the capability of the route optimization approach. Because roll motions are strongly depend on viscous effects it is more complex to integrate them to the model compared to other modes, e.g. vertical acceleration. A first step can be to apply the appropriate transfer function with reference to the exciting wave height, cp. Fig. 16. But for the time being it is decided to take the prediction of natural roll motions out of consideration. However, a method to account for situations that are suspicious for parametric rolling is suggested in section 4.9.
Regarding the added resistance in waves, there exist meanwhile more sophisticated methods based on direct pressure integration over the instantaneous wetted surface, taking into account second order wave drift forces, see e.g. JOURNÉE and MASSIE (2001) These are not applied here, simply because they are not offered by the employed strip theory code. Furthermore the employed methods provide satisfactory results as wind forces and current are left out of consideration yet.
It will be a task of future work to identify suited and fast methods to predict all ship characteristics that are relevant for a routing decision support.
The employed mathematical model and procedures to describe ship responses in waves are presented in the following sections.

4.2 Statistical evaluation of the ship motion in irregular waves

For the description of the sea state a wave spectrum according to PIERSON and MOSKOWITZ (1964) is used. It describes the distribution of wave energy over harmonic frequency components and is given as a function of the significant wave height $H_{1/3}$ and the average zero crossing period T_0. Directional parameters are neglected. Therefore the spectrum describes long crested waves, swell, encountering from one prevailing direction:

$$S_\zeta(\omega) = \frac{124.03 \cdot H_{\frac{1}{3}}^{\ 2}}{T_0^{\ 4}} \cdot \omega^{-5} \cdot \exp\left\{\frac{-496.1}{T_0^{\ 4}} \cdot \omega^{-4}\right\}. \tag{4.2}$$

The evaluation of the ship motion uses the 0th and higher order moments of the response spectrum of the ship. It is the product of the squared transfer function with the wave spectrum. However, the encounter frequencies of the harmonic components of a wave spectrum are modified due to the ship speed and the wave encounter angle:

$$\omega_e = \omega - k\, V_s \cos\beta. \tag{4.3}$$

Since the statistical evaluation uses the response spectrum for the encounter frequency, the wave spectrum has to be transformed from the wave frequency- to the encounter frequency representation:

$$S_s(\omega_e) = \left|\frac{s_a}{\zeta_a}\right|^2 \cdot S_\zeta(\omega_e). \tag{4.4}$$

Claiming for an equivalent amount of energy in the frequency bands $\Delta\omega$ and $\Delta\omega_e$ results in the equation:

$$S_\zeta(\omega_e) \cdot d\omega_e = S_\zeta(\omega) \cdot d\omega. \tag{4.5}$$

From equation (4.5) follows equation (4.6) that can be used for the transformation of the wave spectrum to its encounter frequency representation:

$$S_\zeta(\omega_e) = \frac{S_\zeta(\omega)}{\frac{d\omega_e}{d\omega}}. \tag{4.6}$$

Applying the response spectrum obtained by equation (4.4), the nth order moment of the response spectrum is calculated by:

$$m_{ns} = \int_0^\infty S_s(\omega_e) \cdot \omega_e^{\ n}\, d\omega_e. \tag{4.7}$$

The transformation of the wave spectrum is unproblematic in head- and quartering seas. In contrast, the denominator of equation (4.6) shows a zero point for encounter angle of less than 90°. This results in singularities in the integrand of equation (4.7). Fig. 19 illustrates the zero-gradient for following waves. At a wave frequency of approximately ω = 0.4 the gradient $d\omega_e / d\omega$ becomes zero.

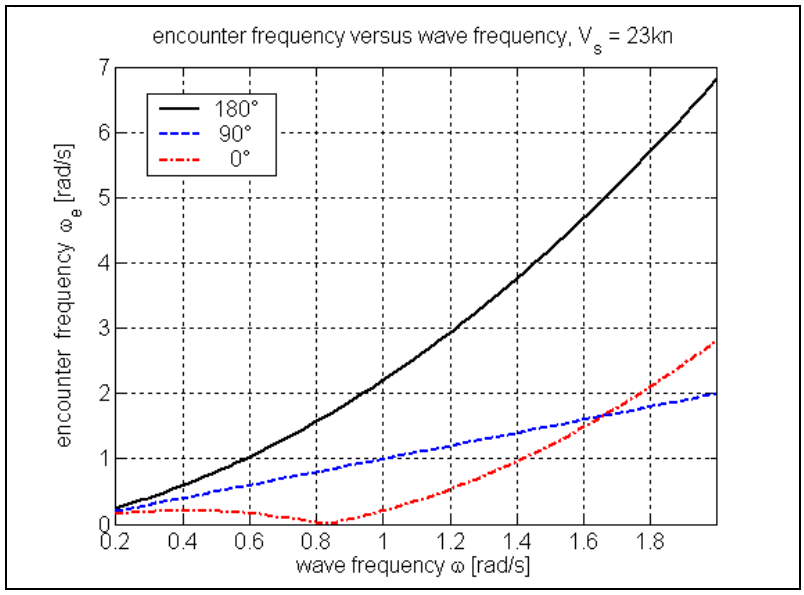

Fig. 19: Encounter frequency versus wave frequency

But equations (4.6) and (4.7) also show the validity of the following equation to determine the n[th] order moments of the response spectrum:

$$m_{ns} = \int_0^\infty S_s(\omega_e) \cdot \omega_e{}^n \, d\omega_e = \int_0^\infty S_s(\omega) \cdot \omega_e{}^n \, d\omega, \qquad (4.8)$$

with equations (4.1) and (4.4) for the calculation of response spectra.

In this way the integration over the wave frequency avoids singularities in the integrand.

The linearity of the applied method is used within the determination of significant amplitudes of velocities and accelerations. Wave- and response spectra are considered as a superposition of harmonic components. For that reason, the calculation of a velocity- and acceleration response spectra is not necessary. The 0[th] moment of the velocity response spectrum equals the 2[nd] moment of the motion response spectrum:

$$m_{0\dot{S}} = m_{2S}. \qquad (4.9)$$

And the 0[th] moment of the acceleration response spectrum is equals to the 4[th] moment of the motion response spectrum:

$$m_{0\ddot{S}} = m_{4S}. \qquad (4.10)$$

A detailed derivation of equations (4.9) and (4.10) is given in Appendix 1.
Finally the calculation of the ship motion is achieved by means of a statistical evaluation of these moments. The significant double amplitude of the ship motion is:

$$2\, s_{a\frac{1}{3}} = 4 \cdot \sqrt{m_{0S}}. \qquad (4.11)$$

And the mean zero-up-crossing period of the motion is:

$$T_{0S} = 2\pi \sqrt{\frac{m_{0S}}{m_{0\dot{S}}}} = 2\pi \sqrt{\frac{m_{0S}}{m_{2S}}}. \qquad (4.12)$$

4.3 Acceleration on the bridge

Generally transfer functions are related to the center of gravity motion. To investigate the ship motion at another point, the transfer function for this point has to be built. Since the ship is regarded as a rigid body, the transfer functions for the rotatory motions are unaffected. The translatory motions of a particular point on-board the ship are described by a superposition of rotatory- and translatory center of gravity motions, considering the lever to this point and the angular phase shift of the considered motions.
As motions are regarded to be small, this can be done in the following way:
The vector of the translatory motion at a point P is built by adding the vector of the translatory center of gravity motion and the cross product of the vector of the rotatory center of gravity motion and the appropriate lever-vector:

$$\bar{s}_P = \bar{s}_T + \bar{s}_R \times \bar{r}, \tag{4.13}$$

with:

$\bar{s}_P = (s_{P1}, s_{P2}, s_{P3})^T$ the vector of the translatory motion of point P,

$\bar{s}_T = (s_1, s_2, s_3)^T$ the vector of the translatory center of gravity motion,

$\bar{s}_R = (s_4, s_5, s_6)^T$ the vector of the rotatory center of gravity motion and

$\bar{r} = (x_P, y_P, z_P)$ the lever-vector from *COG* to P.

Each element of the motion vectors contains a phase term $e^{i\varepsilon_j}$ that has to be considered within the superposition, cp. JOURNÉE (2000):

$$s_j = s_{ja} \cdot e^{i\varepsilon_j} \cdot e^{i\omega_e t} \text{ with: } j = (1,...,6). \tag{4.14}$$

In this way the strip-theory code SEAWAY calculates transfer functions for arbitrary points on-board a ship. Here a point on the bridge, 61m in front of the aft perpendicular, and 44m above the keel line, is considered. These transfer functions are used to derive the response spectra for the motions in x-, y-, and z-direction:

$$S_{sP}(\omega) = \left| \frac{s_{Pa}}{\zeta_a} \right|^2 \cdot S_\zeta(\omega). \tag{4.15}$$

Actually the 4th order moments according to equation (4.10) are used to calculate the significant amplitudes of acceleration for these motions:

$$\ddot{s}_{Pa1/3} = 2 \cdot \sqrt{m_{4SP}}. \tag{4.16}$$

When optimizing a ship route, the occurring accelerations on the bridge have to stay within a defined limit. For the time being, thresholds imposed within the European project SEAROUTES (2003) are used. Thus, the maximum allowed significant amplitude of acceleration on the bridge in the lateral directions is $0.2g$, in vertical direction $0.15g$ ($g = 9.807\text{m/s}^2$). These constraints are imposed to ensure the well-being of the crew.

4.4 Slamming

Slamming is defined as the coincidence of two events: according to OCHI it is the emergence of the bow, 10% of the ship length *LPP* behind the forward perpendicular *FP* and its subsequent dunking above a critical velocity. In JOURNÉE (2000) the critical velocity is given by:

$$\dot{s}_{cr} = 0.0928 \cdot \sqrt{g \cdot L_{pp}} \,. \tag{4.17}$$

Both, the emergence of the bow and the velocity of its dunking, depend on the relative motion between ship and free water surface. That means, the transfer function of the relative motion for the considered point 10% of *LPP* behind *FP* at the keel line has to be calculated.
The relative vertical motion between ship and wave at a point P (x_P, y_P) and with a wave encounter angle β is:

$$s_{P3\,rel} = s_{P3} - \zeta_a \cdot e^{i(k(x_P \cos\beta + y_P \sin\beta))} \,. \tag{4.18}$$

This equation is used within SEAWAY to deduce the transfer function of the relative motion:

$$\frac{s_{P3\,rel}}{\zeta_a} = \frac{s_{P3}}{\zeta_a} - e^{i(k(x_P \cos\beta + y_P \sin\beta))} \,. \tag{4.19}$$

In addition the amplitudes of the relative motion $s_{P3\,rel}$ are adjusted by allowances for static- and dynamic swell up, i.e. allowances that account for the deflection of the water surface caused by the forward speed and the oscillating motion of the ship. Within SEAWAY these allowances are calculated from empirical formulae based on model experiments given by TASAKI, cp. JOURNÉE (2000).

Transfer functions, according to equation (4.19), and wave spectrum are used to calculate the response spectrum of the relative motion:

$$S_{sP\,rel}(\omega) = \left| \frac{s_{P3\,rel}}{\zeta_a} \right|^2 \cdot S_\zeta(\omega) \,. \tag{4.20}$$

Actually the 0th and 2nd order moments of the response spectrum are needed.
Since the ship motion represents a narrow banded GAUSSian process (narrow banded: the number of maxima is equal to the number of zero-up crossing events), the response spectra of the relative motion and of the relative velocity can be represented by a RAYLEIGH[7] distribution. Generally, the RAYLEIGH probability density distribution is:

$$p_{Rayleigh} = \frac{s_{P\,rel}}{\sigma^2} \cdot \exp\left\{ \frac{-s_{P\,rel}^{\,2}}{2\,\sigma^2} \right\} . \tag{4.21}$$

Here the variance of the process σ^2 is the 0th moment of the response spectrum considering the relative motion and the 2nd moment for the velocity, respectively. The probability of an emergence of the bow is the probability for a relative motion that exceeds the draft D_P at 10% *LPP* behind *FP*:

$$P\left\{ s_{P\,a\,rel} > D_P \right\} = \exp\left\{ \frac{-D_P^{\,2}}{2\,m_{0\,S\,P\,rel}} \right\} . \tag{4.22}$$

[7] John William Strutt, 3rd Baron Rayleigh, physicist, 1842 – 1919, England

The probability for a re-entrance velocity that is higher than the critical velocity is calculated by:

$$P\left\{\dot{s}_{P\,a\,rel} > \dot{s}_{cr}\right\} = \exp\left\{\frac{-\dot{s}_{cr}^{\,2}}{2\,m_{2\,S\,P\,rel}}\right\}. \tag{4.23}$$

Presuming statistical independence of these events, the probability of slamming is calculated from:

$$P\left\{slam\right\} = \exp\left\{\frac{-D_p^{\,2}}{2\,m_{0\,SP\,rel}} + \frac{-\dot{s}_{cr}^{\,2}}{2\,m_{2\,S\,P\,rel}}\right\}. \tag{4.24}$$

With a zero-up-crossing period of the relative motion:

$$T_{0\,S\,P\,rel} = 2\pi\sqrt{\frac{m_{0\,S\,P\,rel}}{m_{2\,S\,P\,rel}}}, \tag{4.25}$$

the number of slams per hour is calculated from:

$$N\left[slams/hour\right] = \frac{3600}{T_{0\,S\,P\,rel}} \cdot P\left\{slam\right\}. \tag{4.26}$$

The maximum allowed slamming probability within the route optimization is set to 3%. This threshold as well is taken from the SEAROUTES project.

4.5 Fuel consumption and load to the main engine

In the following the method for the calculation of the fuel consumption during a journey is described. It is adapted to the equipment and the hydrodynamic characteristics of CMS HANNOVER EXPRESS, who is used for the set-up of the route optimization procedure, and considers the design load condition given in SAMSUNG (1991). Since no shaft generator is installed, the considered power demand is restricted to the demand for propulsion. Fuel demand of auxiliary engines is neglected yet.
Thus the operation point of the main engine, i.e. the machine power P_S at a particular rate of revolution *rpm*, depends on the over-all resistance and the ship speed. For a ship speed required within the optimization process, it is necessary to control if the operation point is permitted. Finally the specific fuel consumption for this operation point is determined.

4.5.1 Determination of the over-all resistance

The over-all resistance R_{total} is regarded as the sum of calm water resistance R_T and mean added resistance due to waves R_{AW}:

$$R_{total} = R_T + R_{AW} \,. \tag{4.27}$$

According to the hypothesis of FROUDE[8], the calm water resistance consists of:

$$R_T = R_V + R_W + R_{ADD} \,, \tag{4.28}$$

or rather, following the method of HOLTROPP and MENNEN (1984), that is applied here:

$$R_T = (1+k)\, R_F + R_W + R_{APP} + R_A + R_B \,. \tag{4.29}$$

The components are:

R_V viscous resistance = $(1+k)\, R_F$,
k form factor,
R_F frictional resistance,
R_W wave resistance,
R_{ADD} additional resistances = $R_{APP}+R_A+R_B$,
R_{APP} resistance of appendages (bilge keel, rudder),
R_A roughness allowance and still air resistance, and
R_B resistance due to the bulbous bow.

Additional the applied method provides the thrust deduction fraction t, the wake fraction w and the relative rotative efficiency η_r, cp. also HOLTROP (1978). The following figure represents the composite of the calm water resistance.

[8] William Froude, engineer, hydrodynamicist, and naval architect, 1818 – 1879, England

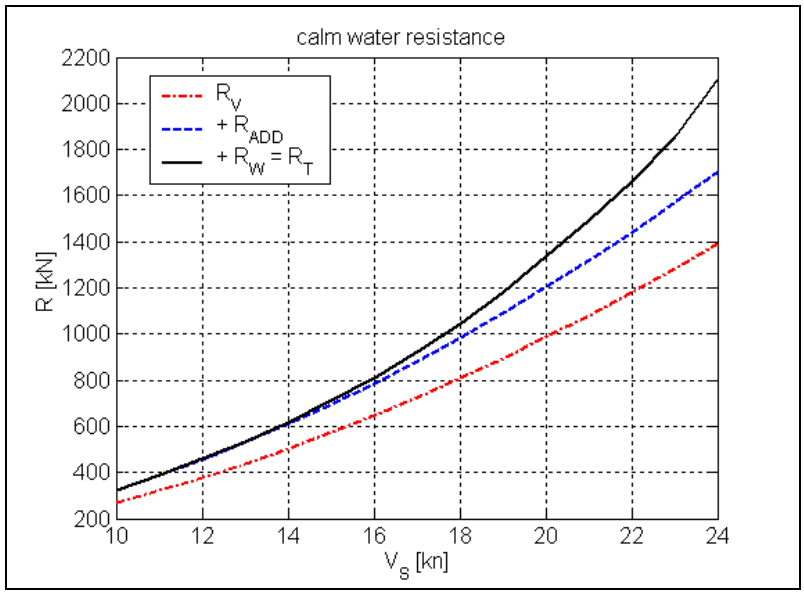

Fig. 20: Calm water resistance

Response functions for the added resistance are applied to determine the added resistance due to waves. SEAWAY provides two different methods to calculate these response functions. The method of BOESE (1970) integrates the oscillating pressure on the wetted surface. GERRITSMA and BEUKELMANN (1972) determine the added resistance by means of the radiated wave energy. Fig. 21 represents response functions for both methods. The left side depicts response functions for the method of BOESE, the right side those of GERRITSMA and BEUKELMANN, respectively.

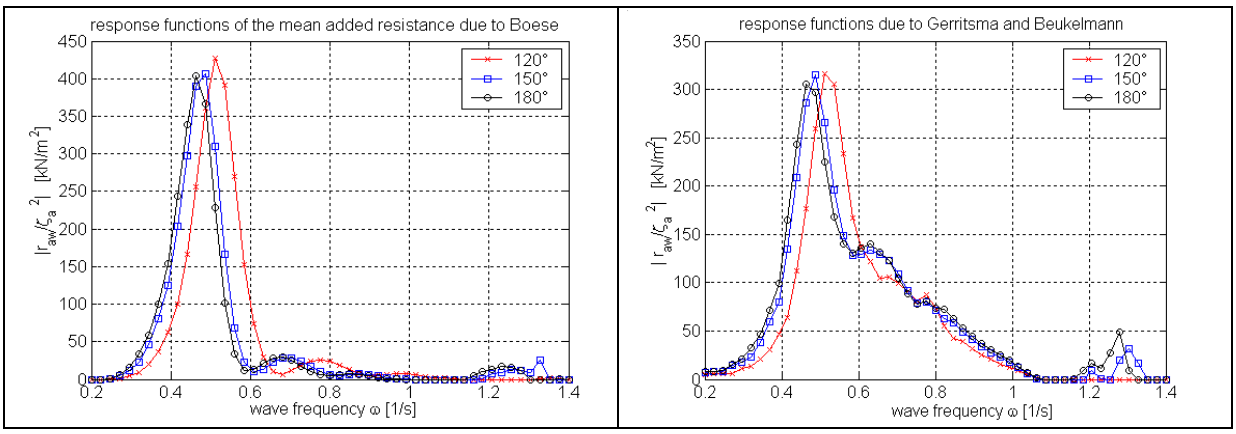

Fig. 21: Response functions for the added resistance due to waves

The shape of the response functions in the area of $\omega = 1.2$ to 1.4 results from a numerical imperfection of the method used within strip-theory to calculate potential mass- and damping coefficients, commonly known as irregular frequencies[9]. Thus, for the determination of the added resistance, the functions according to BOESE are preferred. The quality of the numerical results is better, i.e. less affected by numerical irregularities.

[9] Irregular frequencies are caused by singularities in the GREEN's function. They occur during the determination of hydrodynamic coefficients. Because they are strongly dependent on the frame shape and the frequency of a motion, they are difficult to avoid, cp. JOURNÉE and ADEGEEST (2003). For further information see Appendix 2.
George Green, mathematician and physicist, 1793 – 1841, England

The mean added resistance in waves is determined from:

$$R_{AW} = 2 \cdot \int_0^{\infty} \frac{r_{AW}}{\zeta_a^{\,2}} \cdot S_\zeta(\omega)\, d\omega\,, \qquad (4.30)$$

with: $\frac{r_{AW}}{\zeta_a^{\,2}}$ the response function for the added resistance due to waves.

Fig. 22 serves to illustrate the mean added resistance as a function of the ship speed for a significant wave height of 7m and a peak period of 14s in head sea. At a ship speed of 15kn the mean added resistance amounts to the same magnitude like the calm water resistance. Even if it decreases at a higher ship speed, the total resistance at this sea state assumedly increases the capacity of the main engine. This will be checked within the determination of the engine operating point.

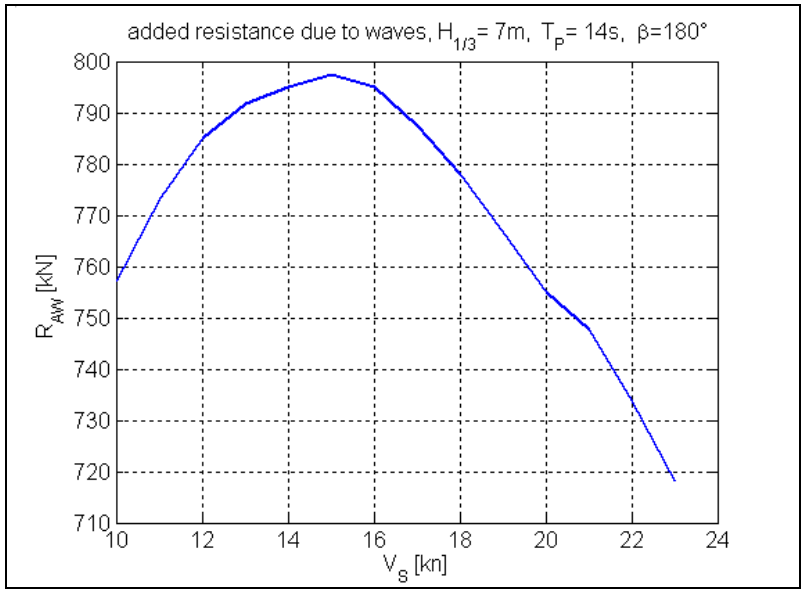

Fig. 22: Added resistance due to waves

4.5.2 Propeller characteristics and operation point

The "full scale HANNOVER EXPRESS" propeller characteristic is derived from the propeller characteristic of a similar model scale propeller given by YASAKI (1962).

Tab. 4: Propeller data

propeller data	HANNOVER EXPRESS	model propeller
diameter *D*	8.25m	0.25m
number of blades *Z*	6	6
slope ratio *P/D*	1.036	1
area ratio A_e/A_0	0.795	0.7

The full-scale propeller characteristics are provided by applying corrections for the REYNOLDS[10]-number and roughness to the model propeller data, according to ITTC (1978). Fig. 23 shows the propeller characteristic that is used for the CMS HANNOVER EXPRESS.

[10] Osborne Reynolds, physicist, engineer and mathematician, 1842 – 1912, England

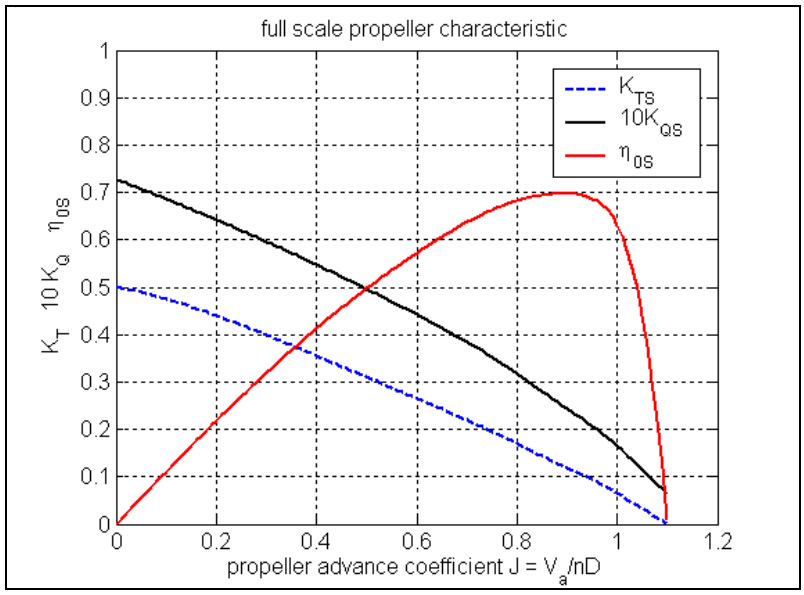

Fig. 23: Full-scale propeller characteristic

Thrust, torque, and propeller advance velocity are represented dimensionless:

$$J = \frac{V_A}{n \cdot D}, \tag{4.31}$$

$$K_{TS} = \frac{T}{\rho n^2 D^4}, \tag{4.32}$$

$$K_{QS} = \frac{Q}{\rho n^2 D^5}, \tag{4.33}$$

with:

J	advance ratio,
K_{TS}	thrust coefficient,
K_{QS}	torque coefficient,
V_A	advance speed,
n	revolution frequency of the propeller,
D	propeller diameter,
ρ	density of sea water, and
η_{0S}	open water efficiency, $K_{TS} \cdot J / 2\pi \cdot K_{QS}$.

The determination of the operating point of the propeller is accomplished according to thrust identity. Therefore the ratio K_{TS}/J^2 has to be built:

$$\frac{K_{TS}}{J^2} = \frac{R_{total}}{(1-t)(1-w)^2 V_s^2 D^2 \rho}. \tag{4.34}$$

Following, equation (4.34) is multiplied by J^2 and depicted in the propeller characteristic. The intersection with the curve for K_{TS} represents the operating point of the propeller. Fig. 24 illustrates the determination for two different ship speeds, 10kn and 23kn, at a sea state of 6m significant wave height, 12s peak period, and in head waves.

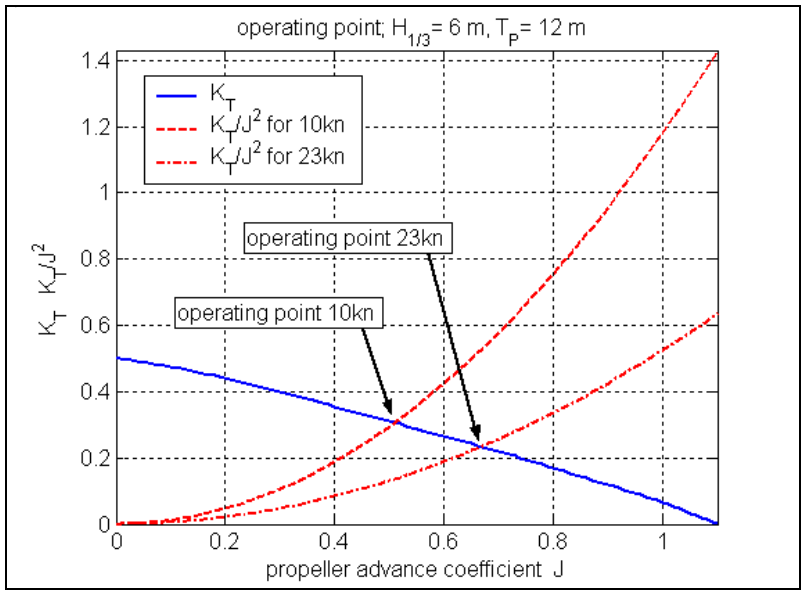

Fig. 24: Determination of the operating point

By means of the operating point of the propeller, the required power and rate of revolution of the main engine are determined from:

$$n = \frac{V_s \cdot (1-w)}{J \cdot D}, \tag{4.35}$$

$$P_S = \frac{2\pi\, n^3 D^5 K_{QS}}{\eta_s \eta_R}, \tag{4.36}$$

with:

P_S shaft power,
η_S shaft efficiency (0.99),
η_R relative rotative efficiency.

4.5.3 Feasibility of the operation point of the main engine

Since the ship velocity is a given value within the optimization, it has to be controlled if the operating point of the main engine is in accordance with the main engine characteristic, MAN B&W (2000). Fig. 25 represents the normalized main engine characteristic. It shows the permitted operation area for the main engine of CMS HANNOVER EXPRESS, a 9K90MC. This area is bordered by 4 lines:

- a boundary line for engine overload caused by the limited ability of the turbo chargers to compress air ($\sim n^2$),
- a boundary line for the maximum allowable mean effective pressure ($\sim n$),
- a boundary line for the nominal power (*MCR*, ~constant), and
- a boundary line for the maximum rate of revolution at *MCR*. At most 5% above the nominal rate of revolution.

Former two lines specify the available power for an operation point below the nominal rate of revolution. They are used as the characteristic of the control unit of the main engine.

Additional the curve for the power demand of the propeller under nominal operating conditions (~ n^3) and the specified *MCR* point are shown (*SMCR*, maximum rating for continuous operation required by the yard or the owner).

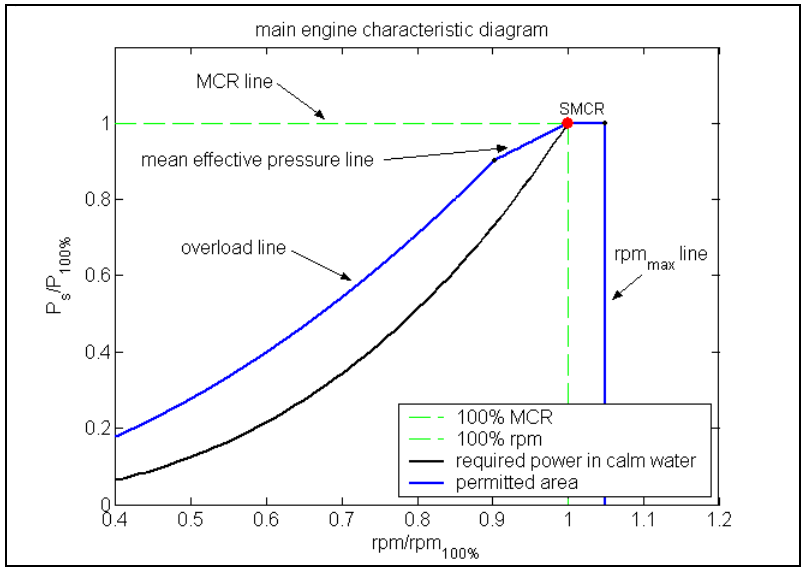

Fig. 25: Main engine characteristic

The lower limit of the main engine operability is not explicitly modeled. Since the ship uses a fixed pitch propeller and the ship speed is bounded below by the perturbation of the velocity profile at 10kn, it is not possible to derate the main engine. Furthermore the masters individual preferences in operating the main engine, e.g. to avoid soot, can be modeled by increasing the minimum allowed ship speed. For the time being these aspects are neglected, as for the purpose of this study a quiet simple main engine model is absolutely sufficient.

4.5.4 Specific fuel consumption

Fig. 26 shows the specific fuel oil consumption *sfoc* according to MAN B&W (2000).

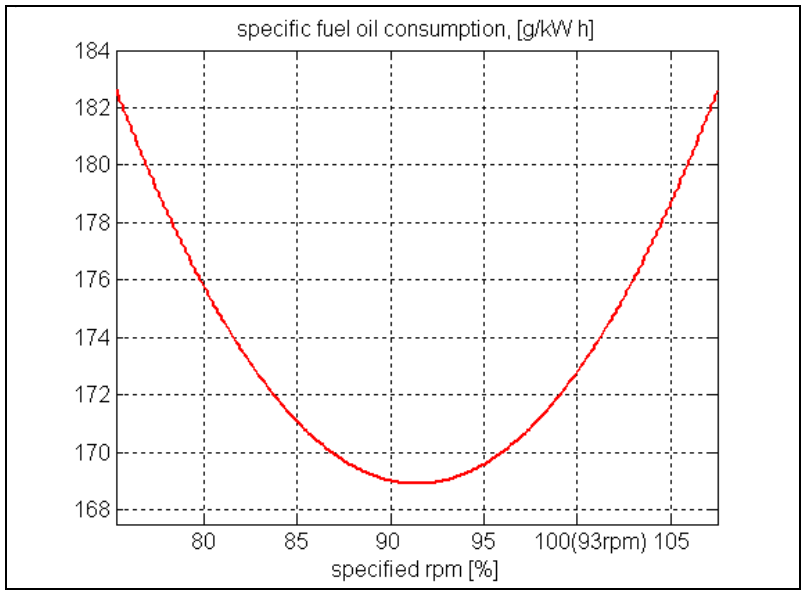

Fig. 26: Specific fuel oil consumption, *sfoc*

It is dependent on the rate of revolution of the main engine. The specific fuel consumption *spef* follows from:

$$spef\left[\frac{t}{h}\right] = sfoc\left[\frac{g}{kWh}\right] \cdot P_S\,[kW]\,\frac{1t}{1000000g}. \tag{4.37}$$

The over-all fuel consumption for a whole journey is calculated from:

$$overall\ \ fuel\ consumption\,[t] = \sum_{departure}^{arrival} spef \cdot \Delta t\,[h], \tag{4.38}$$

with: Δt: required time for a route segment.

The over-all fuel consumption of a journey is one objective of the route optimization. Lubrication oil and fuel consumption of the auxiliary engines are not considered. To keep things simple, the consumption of lubrication oil is regarded to be proportional to the fuel oil consumption of the main engine, therefore savings by route optimization are proportional to fuel savings as well. The fuel consumption of the auxiliary engines is time dependent. Faster routes will be the more fuel saving ones. Actually this type of fuel consumption is not known exactly, e.g. it would be necessary to have the number of reefer container on-board. An extension of the model is straightforward but nonetheless omitted as it is not necessary for this study.

4.6 Practical calculation of ship responses

To accelerate the optimization process, the determination of ship responses due to waves on a particular route is pre-processed as far as possible. Since the equations to determine the moments of the response spectra (4.8 – 4.11) are linear in terms of the squared significant wave height,

$$m_i = H_{\frac{1}{3}}^{\ 2} \cdot \overline{m_i}, \tag{4.39}$$

it is reasonable to calculate a ship response due to a significant wave height $H_{1/3}$ of 1m and to scale it afterwards with the actual wave height. Fig. 27 shows PIERSON-MOSKOWITZ spectra for $H_{1/3}$ = 1m.

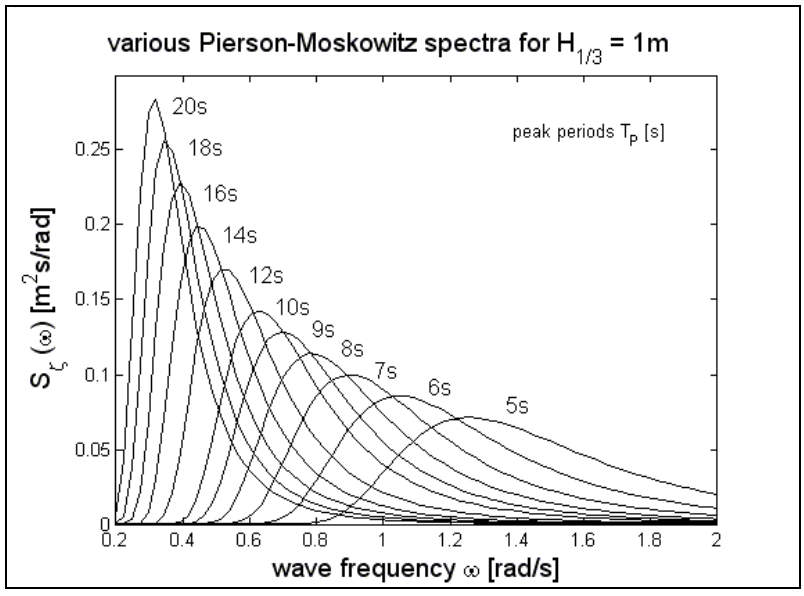

Fig. 27: PIERSON-MOSKOWITZ spectra for $H_{1/3}$ = 1m

All of the spectra are equal in terms of m_0, the area under the curve, i.e. they contain the same amount of wave energy. Whereas the peak is more pronounced when peak periods T_p increase or simply "the longer the waves get". These spectra are used to calculate a "ship response data base". Therein the ship responses for $H_{1/3}$ = 1m and peak periods T_P in steps of 1s are stored. The actual ship responses are calculated by interpolations for T_P, encounter angle β, and ship velocity V_S and by scaling the appropriate values with the appearing wave height.
Applying the moments of the response spectra according to a significant wave height $H_{1/3}$ of 1m, acceleration, slamming probability, and added resistance due to waves are accounted by:

$$\ddot{s}_{pa1/3} = \frac{2 \cdot H_{\frac{1}{3}} \cdot \sqrt{\overline{m}_{4s_p}}}{9.807} \quad [g] \,, \tag{4.40}$$

$$P\{slam\} = \exp\left[-\frac{1}{2\, H_{\frac{1}{3}}} \cdot \left\{ \frac{D_p^{\,2}}{\overline{m}_{0s\,prel}} + \frac{\dot{s}_{cr}^{\,2}}{\overline{m}_{2s\,prel}} \right\} \right] \cdot 100 \quad [\%], \tag{4.41}$$

$$R_{AW} = \frac{H_{\frac{1}{3}}^{\,2} \cdot \overline{R}_{AW}}{1000} \quad [kN]. \tag{4.42}$$

Additional they are transformed to the units of the threshold values used within the route optimization.
Furthermore, the ship responses can be depicted as functions of the significant wave height $H_{1/3}$ and the peak period T_p. Fig. 28 – Fig. 34 serve to illustrate the dependency of the ship response on these two crucial factors for selected operating conditions. The figures cover a range of T_p = 0 – 30s and $H_{1/3}$ = 1 – 15m. Furthermore a borderline, the wave-breaking limit, for a maximum significant wave height $H_{1/3\,max}$ is given. Here the physically maximum wave height H_{max} is assumed to be 1/10 of the wave length and to be approximately the double of the significant wave height $H_{1/3}$. The area of interest is on the left side of the borderline.

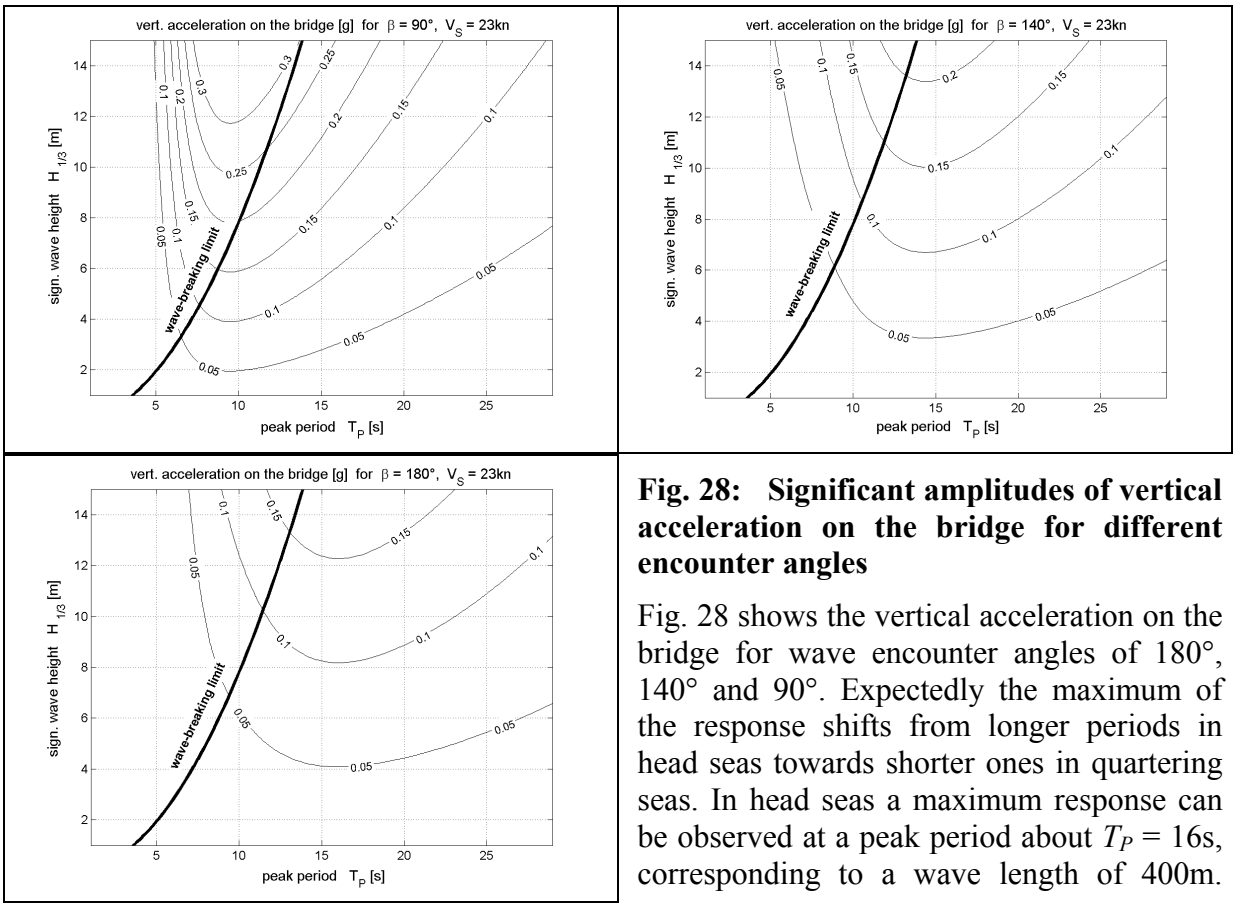

Fig. 28: Significant amplitudes of vertical acceleration on the bridge for different encounter angles

Fig. 28 shows the vertical acceleration on the bridge for wave encounter angles of 180°, 140° and 90°. Expectedly the maximum of the response shifts from longer periods in head seas towards shorter ones in quartering seas. In head seas a maximum response can be observed at a peak period about T_P = 16s, corresponding to a wave length of 400m.

Having in mind the ship length LPP = 281m and the natural period of the pitch motion of 8.2s, this seems quite plausible. For quartering seas the maximum shifts towards a peak period T_P = 8.5s, the natural frequency of the heave motion. The influence of the encounter angle is relatively small at longer waves (T_P > 14s), whereas in shorter waves (T_P < 14s) a significant increase of the ship response can be observed when taking course towards quartering seas.
Fig. 29 represents the vertical acceleration on the bridge in head seas for a ship speed of 16 and 23kn, the design speed. Obviously only a distinct reduction of the ship speed is suited to clearly reduce accelerations. The little shift of the maximum responses from T_p = 16s to 15s is caused by the reduction of the wave encounter frequency due to the reduced ship speed.

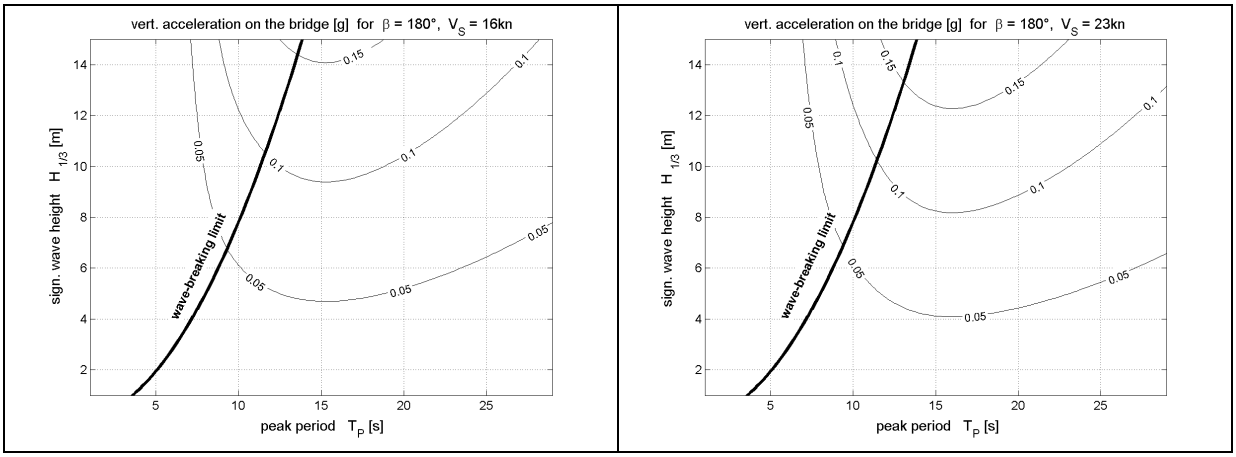

Fig. 29: Significant amplitudes of vertical acceleration on the bridge for different ship speeds

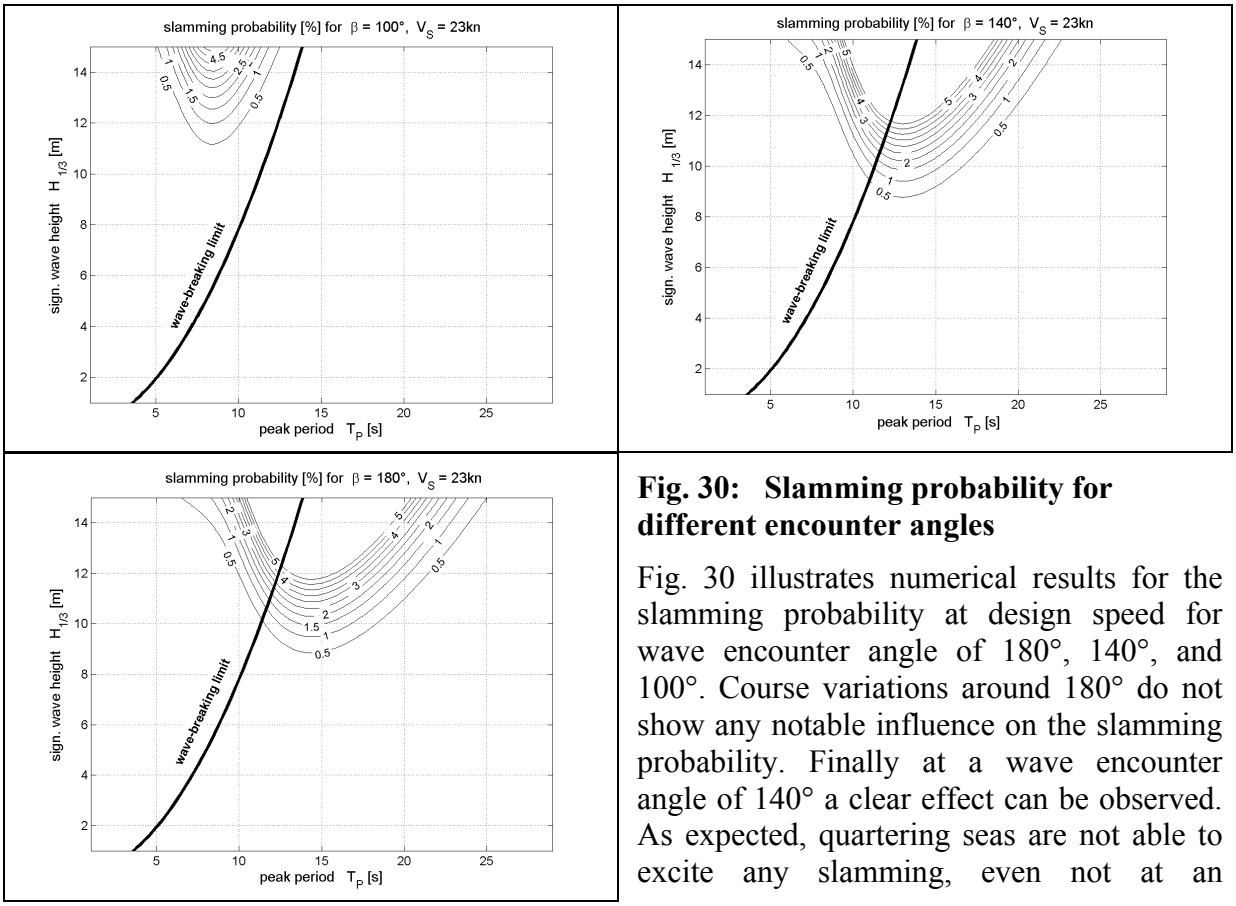

Fig. 30: Slamming probability for different encounter angles

Fig. 30 illustrates numerical results for the slamming probability at design speed for wave encounter angle of 180°, 140°, and 100°. Course variations around 180° do not show any notable influence on the slamming probability. Finally at a wave encounter angle of 140° a clear effect can be observed. As expected, quartering seas are not able to excite any slamming, even not at an

encounter angle of 100° where we have still a ship response according to the transfer function, but physically no exciting waves are possible. Nevertheless, in contrast to the accelerations on the bridge, the slamming probability can be reduced by changing course to more quartering seas.
Similar to the responses for the acceleration on the bridge presented in Fig. 29 there is a distinct reduction of the ship speed necessary to clearly reduce the slamming probability.

The mean added resistance due to waves R_{AW} for head sea conditions at design speed is presented in Fig. 31. It shows maximum values for a peak period T_p = 15s. This corresponds to a wave length of 350m, about 70m more than the ship length. Supported by Fig. 21 it can be seen that the added resistance is less affected by changes of the wave encounter angle and increases when speed is reduced (compare Fig. 22). Surely the decrease in the calm water resistance overcompensates the increase of the added resistance due to waves at lower speed.

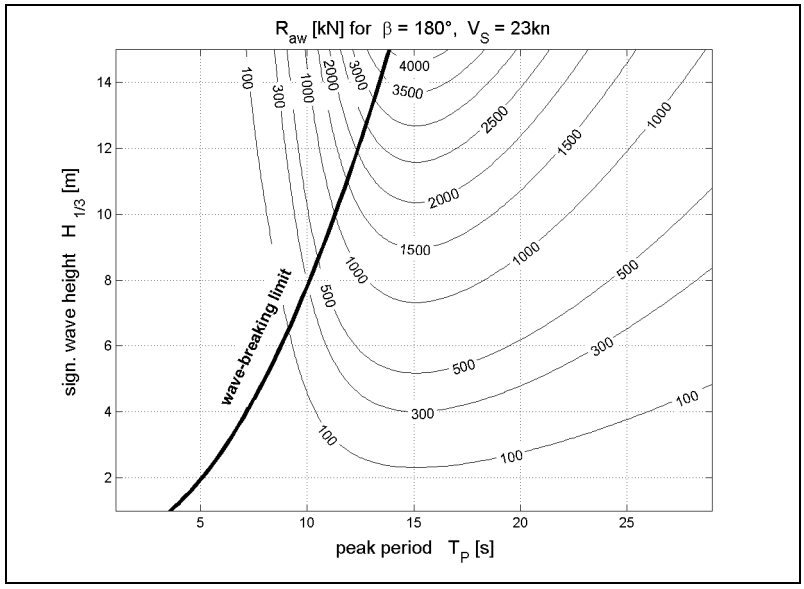

Fig. 31: Added resistance due to waves

Further on Fig. 32 presents the required brake power of the main engine at 22kn and at design speed of 23kn. The line for 41MW marks the maximum continuous rating of the main engine (*MCR*) and cannot be exceeded.

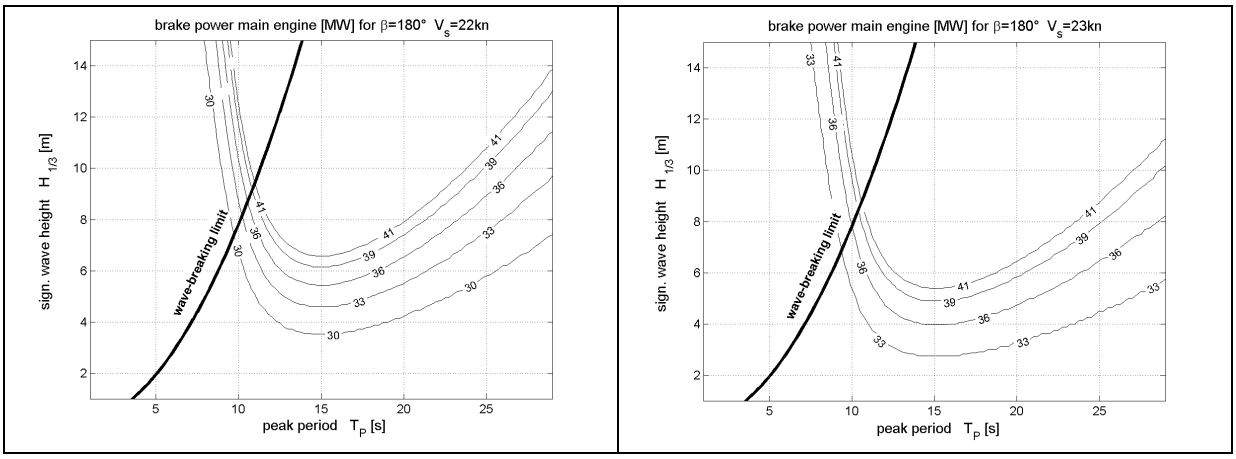

Fig. 32: Brake power at reduced and design speed

Fig. 33 illustrates the specific fuel oil consumption for these two ship speeds.

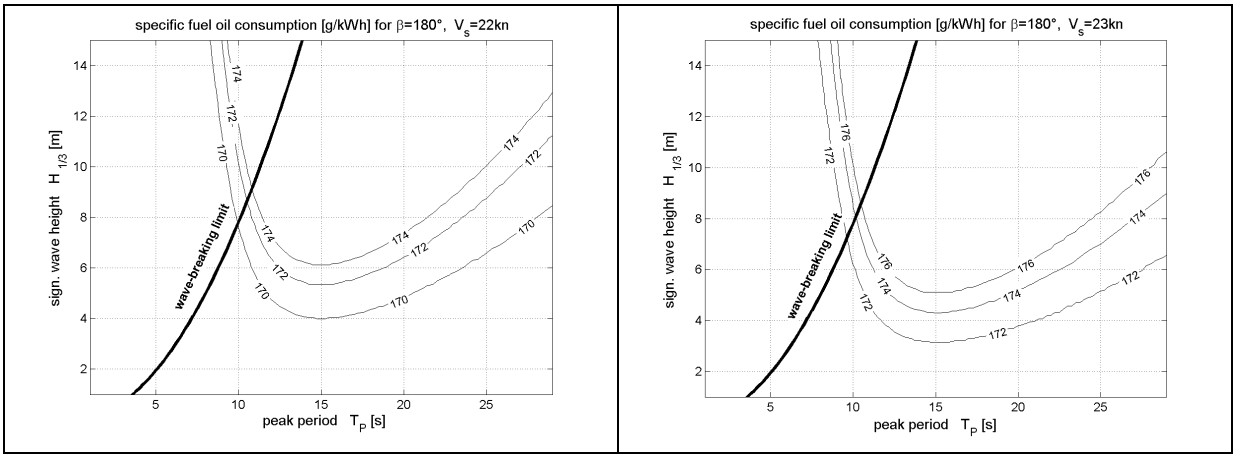

Fig. 33: Specific fuel oil consumption at reduced and design speed

Finally Fig. 34 shows the specific fuel consumption according to these operating conditions. The trembling shape of the lines is caused by the discretization of the propeller model, established as a good compromise between accuracy and computational effort.

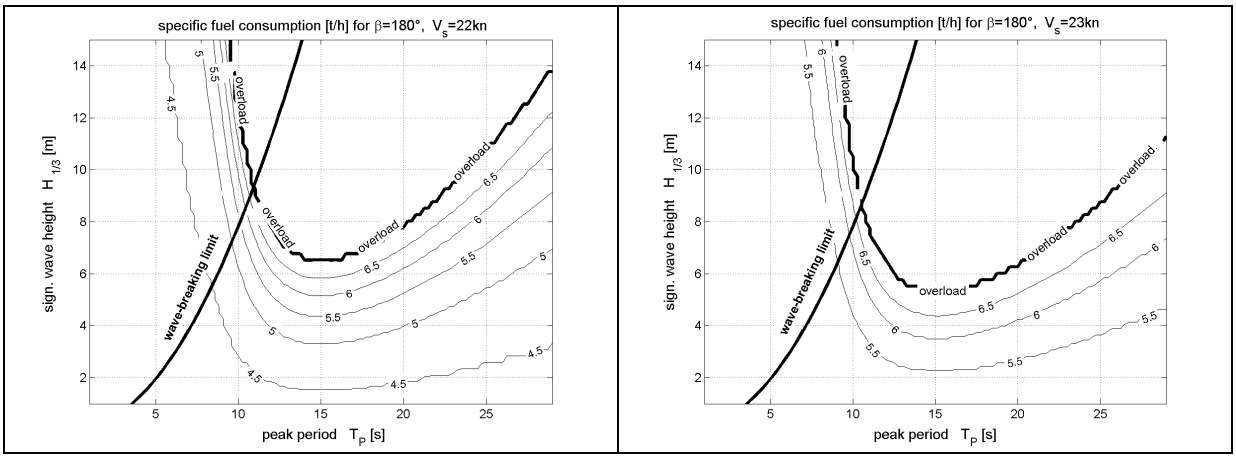

Fig. 34: Specific fuel consumption at reduced and design speed

4.7 Avoiding irregular frequencies

Irregular frequencies are a well-known numerical disturbance during the determination of hydrodynamic coefficients e.g. used within strip-theory methods. If no access to the source code of the program is given, they are hardly to avoid, cp. Appendix 2. In that case they can be identified by a plausibility check, and anyhow the numerical result can be emended. Fig. 35 shows a response amplitude operator for the vertical motion on the bridge. The left part of the figure shows the transfer function like calculated by the strip-theory program. Physically there is no reason for the peak at a wave frequency 1.3, just as the shape of the transfer function between ω = 1.0 – 1.3 can be doubted. Assuming that the ship response at frequencies above ω = 1 (corresponding wave length 60m) cannot be higher than the one at ω = 0.8 (corresponding wave length 100m, the natural frequencies of the heave motion lies at ω = 0.74 and for the pitch motion at ω = 0.76) it is reasonable to smooth this transfer function by setting the ship responses to zero for ω > 1.

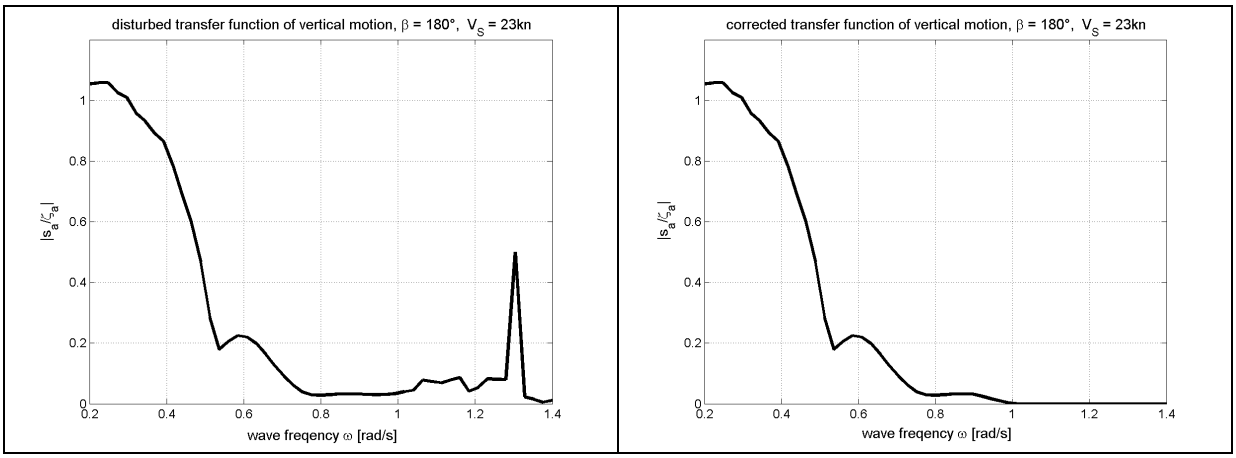

Fig. 35: Transfer function before and after smoothing

Fig. 36 shows resulting ship responses like presented in section 4.6. Again the left part represents the calculation using the disturbed transfer function, the right part the smoothed transfer function respectively. The extreme amplification of responses, in particular in shorter waves, is caused by 4th order moments used when calculating the significant amplitudes of acceleration.

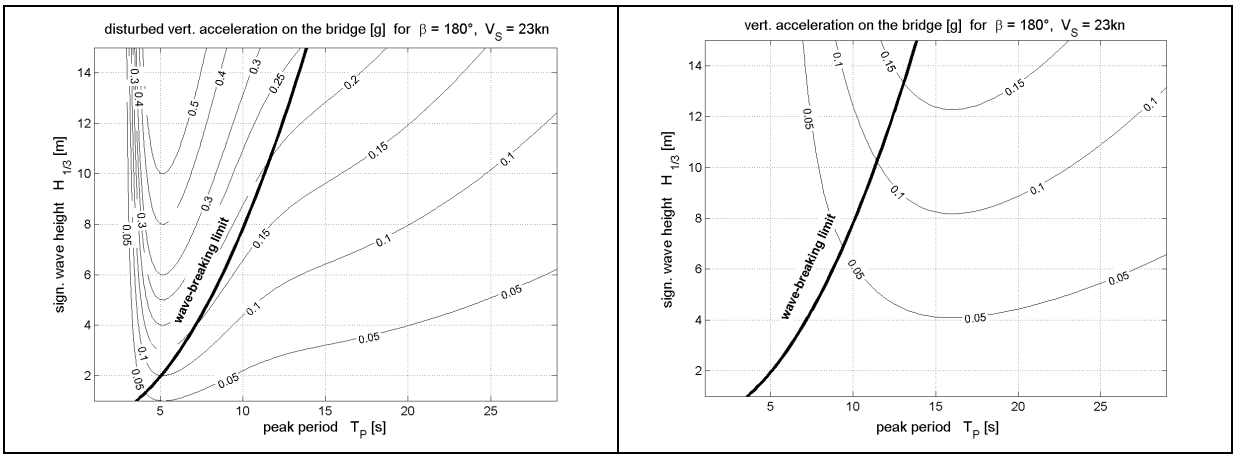

Fig. 36: Ship responses, disturbed by irregular frequencies (left) and corrected(right)

A similar post processing is applied to all transfer functions before calculating the "response data base" whenever it is necessary.

4.8 Add-on for motion sickness incidence

Beside the recommendation given within the SEAROUTES project, the Institute of Naval Medicine gives a threshold value for a maximum vertical acceleration, PINGREE (1988). If no data for the frequency of excitation and its duration are available, a value of 1.75m/s^2 *RMS* (root mean square) is suggested as the approximate level at which disturbances may occur to tasks such as writing, control operation, etc.
The *RMS* of a harmonic function $\boldsymbol{a}$ with the amplitude $\tilde{a}$ is defined as:

$$RMS = \sqrt{\frac{1}{T}\int_0^T a^2 dt} = \sqrt{\frac{1}{2\pi}\int_0^{2\pi} (\tilde{a}\sin(\phi))^2 d\phi} = 0.707 \cdot \tilde{a} \,. \tag{4.43}$$

The definition of *RMS* can also be applied to a stochastic process ***a*,** and in this case it equals m_0, the square root of the area under curve of the motion spectrum that describes this process, i.e. the square root of the variance σ^2 of the stochastic process:

$$RMS = \sqrt{\frac{1}{T}\int_0^T a^2 dt} = \sqrt{m_0} = \sigma \,. \tag{4.44}$$

The investigations on motion sickness are generally conducted with harmonic excitation. Since stochastic motions of the same *RMS* as their harmonic counterpart show much higher amplitudes, an equivalent harmonic excitation is built by using the significant amplitude of the ship response. Being $a_{1/3} = 2\sqrt{m_0}$, the significant amplitude of the ship response, the equivalent *RMS* according to KRAPPINGER (1983) is calculated by:

$$RMS = 1.414 \cdot \sqrt{m_0} = 0.707 \cdot a_{1/3} \,. \tag{4.45}$$

Therefore the threshold value given within SEAROUTES of 0.15*g* for the significant vertical acceleration equals 1.0m/s^2 *RMS*. Recommendations applying $a_{1/10}$, the mean value of the one-tenth highest amplitudes, would result in 1.3m/s^2 *RMS*.

Because of these discrepancies of the threshold values and the fact that thresholds represent only a rough description of the effect of vertical accelerations on the crew, a refined method is desirable. That is why the concept of motion sickness incidence *MSI* as given in ISO 2631 is introduced to route optimization. The *MSI* gives the percentage of people that suffer from severe discomfort dependent on the *RMS* of acceleration, the frequency, and the duration of the excitation (in the following simply *RMS* is used for *RMS* of acceleration). The investigations of KRAPPINGER (1983) provide a mean value applied as threshold where kinetosis appears. It is dependent on the frequency of excitation and acts on the assumption that log(*RMS*) is GAUSSian distributed:

$$\mu = 0.87 + 4.36\log(f) + 2.73\log(f)^2 \,, \tag{4.46}$$

with:

μ: mean value applied as threshold where kinetosis appears,
f: frequency of excitation.

E.g. 10^{μ} is the *RMS* value at frequency f for a 2h exposure where 50% of the crew suffers from motion sickness. The variance of log(*RMS*) is independent on the frequency, i.e. $\sigma^2 = 0.221$. So that the distribution function becomes:

$$F\left[\log(RMS)\right] = \frac{1}{\sqrt{2\pi}\cdot\sigma}\int_{-\infty}^{\log(RMS)} \exp\left[\frac{-(\log(RMS)-\mu)^2}{2\,\sigma^2}\right] d\left(\log(RMS)\right). \tag{4.47}$$

Expressed in percent this distribution function is known as $MSI = 100 \cdot F\left[\log(RMS)\right]$.

For durations of exposure different from 2h an equivalent *RMS* for a 2h exposure is calculated according ISO 2631, assuming that $RMS^2 \cdot t = const.$:

$$RMS(t = 2h) = \sqrt{\frac{RMS(t)^2 \cdot t}{2}} \,. \tag{4.48}$$

Fig. 37 shows isolines for 10% *MSI* as a function of frequency and duration of exposure.

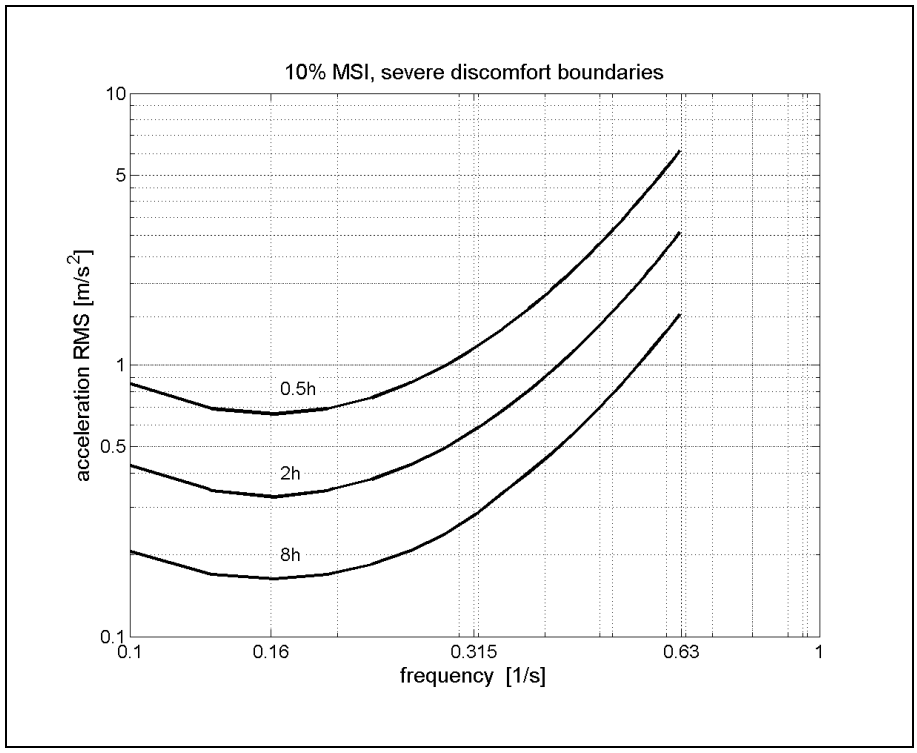

Fig. 37: 10% *MSI* isolines

The left diagram of Fig. 38 depicts the isolines of *MSI* for a 4h exposure at 180° wave encounter angle and 23kn ship speed. The right diagram is the counterpart for the significant vertical acceleration. Obviously the concept of applying a threshold value to the vertical acceleration underestimates the load on the crew. Furthermore the application of *MSI* is more meaningful to assess the consequence of vertical acceleration as it includes the frequency and the duration of the exposure.

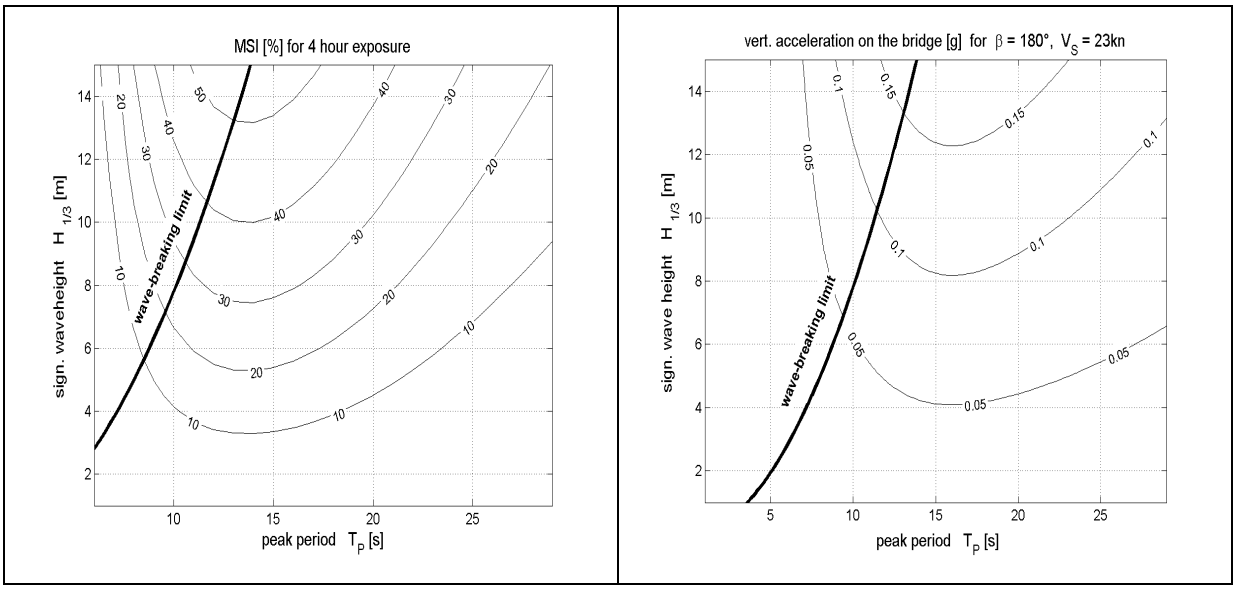

Fig. 38: *MSI* and significant amplitudes of vertical acceleration on the bridge

4.9 Add-on for parametric rolling

Auto-parametrically excited roll motion, or shortly parametric rolling, was initially classified as a cock-and-bull story of seafarers to excuse ship accidents caused by human failure. Nowadays the mechanism that generates these extreme roll motions is known and the ship-wave parameter constellation that affords parametric rolling is identified. Actually strip-theory and transfer functions, as applied here for a route optimization, are not capable to predict parametric rolling or a probability of such an event. However, it should be possible to identify situations that are suspicious for parametric rolling. Therefore this investigation puts its focus on the impact on an optimization result, if such situations are avoided. To set up a routine to identify situations that are susceptible to parametric rolling two contributions to the discussion at the 13th SNAME ad hoc panel, SHIN et al. (2005) and KRUEGER et al. (2006), have been combined. Both are presented below as far as they are used here. Actually both approaches step much further, as they claim to be able to predict extreme roll motions or capsizing in rough seas. In the following they are simply referred to as SHIN and KRUEGER approach.

4.9.1 Introduction of criteria from the Shin approach

SHIN et al. (2005) point out that dependent on the relation between angle, length, and period of the encountering waves on one hand and pitch and natural roll period on the other hand, certain relations of these parameter are suspicious for parametric rolling.
Considering a ship in heading or following waves, there seem to be no external forces that may induce roll motion. But this motion phenomenon depicts the difference between mathematical model and real life. Even long crested waves are superimposed by wave components with directions that are different from the prevailing direction. Wind load is a further factor, so that at least a bit of roll motion is always induced and present. As long as damping forces exceed exciting forces the amplitudes of this roll motion do not attract attention. During parametric rolling the frequency of exciting forces matches the natural roll frequency or a multiple of it. As damping forces are relatively low, the amplitudes of the roll motion increase dramatically. A further amplification of the process is caused by means of oscillating restoring forces due to a periodically changing metacentric height GM_T. Changes in the shape of the water line provide maximum uplifting forces during a ship sails in a wave trough, whereas minima of GM_T occur while a ship sails on a crest. In particular modern container vessel and other ships with pronounced bow flare and extreme stern overhang are affected.

A typical mechanism is as follows:
Assuming a ship is sailing in head sea, the wave length matches approximately L_{PP} and the ship is pitching down its bow into an approaching wave with a little heel angle to starboard. In this situation the restoring forces for the roll motion are high, and if the wave is high enough it takes the ship by its bow flare, raises the bow, and powerfully rolls the ship to portside direction. The ship reaches the upright position during the wave crest passes the midship region. Now as restoring forces are small the ship rolls unresisted onward to portside. Again it pitches down the bow into the next wave crest, but with a much higher heel angle than on the starboard side before. If this process has started and matches the natural roll period of the ship only instantaneous course changes can avoid further increasing of roll amplitudes and finally, the loss of cargo or a capsizing of the ship. Reducing speed is an adequate countermeasure if sea states that may become critical are detected early enough. Because this course of motion typically takes two pitch periods associated with one roll period it is commonly called the

2:1 type of parametric rolling. A more or less symmetric roll motion, i.e. large roll angles to starboard and port side, characterizes this type. Another kind of parametric rolling is the 1:1 type. In this case one roll period is associated to one pitch period. An asymmetric roll motion, i.e. large roll angles to starboard or port side, characterizes the 1:1 type. Dependent on the ratio of oscillating restoring- and oscillating exciting forces the 1:1 or the 2:1 type of parametric rolling is met. In this regard the ship size, ship speed, wave direction (i.e. head or following seas), and the metacentric height GM_T are deciding parameters. SHIN et al. (2005) do not explicitly addressed the 1:1 type, even if their numerical model is able to predict it. According to SHIN the following parameters are characteristic for parametric rolling:

- Heading or following sea.
- The wave length matches approximately the ship length.
- The time for one roll period takes two pitch periods and matches approximately the natural roll period.
- A required wave height brings about exciting forces that exceed the damping forces.

Regarding a route optimization, the first two parameters can directly be obtained from weather forecast data and the course angle of the ship. Wave direction and course angle provide the wave encounter angle and the wave length according LEWIS (1998, Vol. III) is:

$$L_{wave} = \frac{g}{2\pi} T_P \cdot T_0 . \qquad (4.49)$$

The third parameter, the natural roll period, is strongly affected by the wave height and the wave period. Fig. 39 shows the metacentric height GM_T for the CMS HANNOVER EXPRESS in a STOKES-III[11] wave of 7.5m wave height and 283m wave length, approximately the ship length. Associated natural roll periods are assessed by the formula for the natural period at calm water

$$T_e = \frac{2\,\pi\,k_{xx}}{\sqrt{g\,GM_T}} , \qquad (4.50)$$

with the radius of inertia k_{xx} of 12.4m. This figure simply should illustrate the strong effect of waves on the stability and the roll motion characteristics of the ship. The phase, given at the abscissa, represents the shift of the wave crests. Phase = 0 or 1 means wave crests at *FP* and *AP*. Phase = 0.5 represents a wave crest amidships.

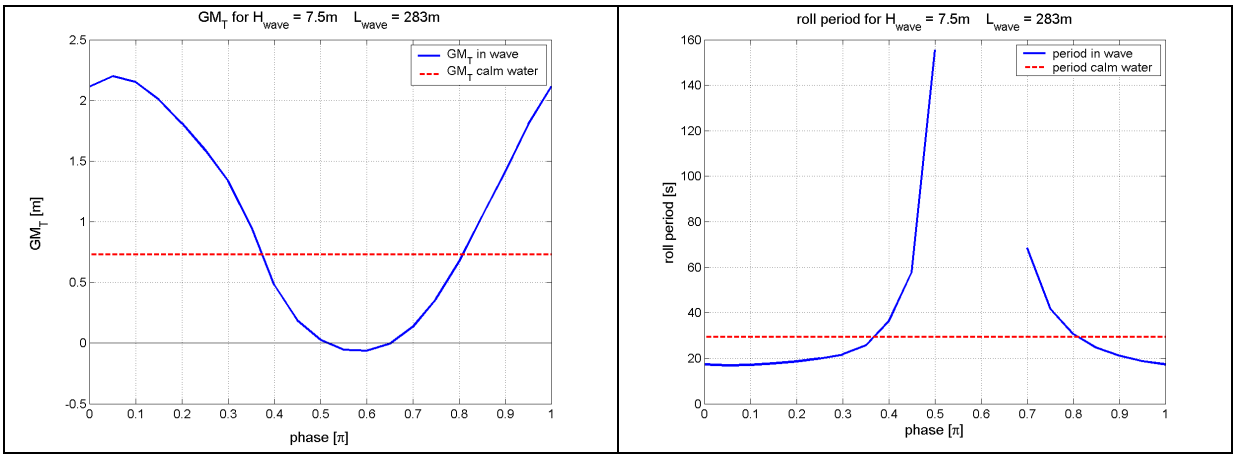

Fig. 39: GM_T and roll period

[11] George Gabriel Stokes, mathematician and physicist, 1819 – 1903, Great Britain

In this position of the wave GM_T becomes even negative which causes the gap in the curve of the roll period on the right side, an indicator for vanishing upright stability.

At low wave heights the effects on the calm water natural roll frequency may be negligible. While in a parametric rolling situation, where the wave length matches the ship length, the modification of the natural roll frequency is dependent on the wave height. Are waves high enough, the "natural frequency" becomes almost the wave encounter frequency.
SHIN detects situations that are susceptible for parametric rolling by transforming differential roll equation to the MATHIEU[12] equation and identifies bounded and unbounded solutions. However, this method is too extensive in computing time to include it to a route optimization where thousands of weather situations have to be evaluated. But latter two parameters, the natural frequency and the required wave height, can be condensed into one, an overcritical wave height. For this purpose, the approach suggested by KRUEGER is used.

4.9.2 Additional criteria provided by the Krueger approach

KRUEGER et al. (2006) carry out capsize simulations for various ship types and load conditions. At this, roll angle of more than 50° are ranked as a capsize event. They conclude that "the energy introduced into any specific hull form in a sea state may be expressed by the alteration of the areas below the righting levers at trough and crest condition" and "that the most important phenomena leading to large rolling angles can be directly accessed by linking the righting lever changes between crest and trough condition to the minimum stillwater stability requirements". The method for the stability assessment proposed by KRUEGER does not distinguish between capsizing due to e.g. stability loss in following seas or due to parametric rolling (both 1:1 and 2:1 type). It is posed to assess a required safety level for ships in a group of probable sea states. Here the method is used to assess a critical wave height. Higher waves characterize a sea state that becomes suspicious for parametric rolling.
For this purpose the alteration of the lever curves for a design load condition at $GM_T = 0.73$m are studied. Fig. 40 shows two investigated cases. They are lever curves for calm water, trough- and crest condition at a wave length of 283m and 5m or rather 10m wave height. The figures nicely illustrate the increase in the alteration at higher waves. The shape of the calm water lever curve is strongly dependent on the metacentric height GM_T, whereas the alterations of the lever curve are affected by the wave height and the hull shape.

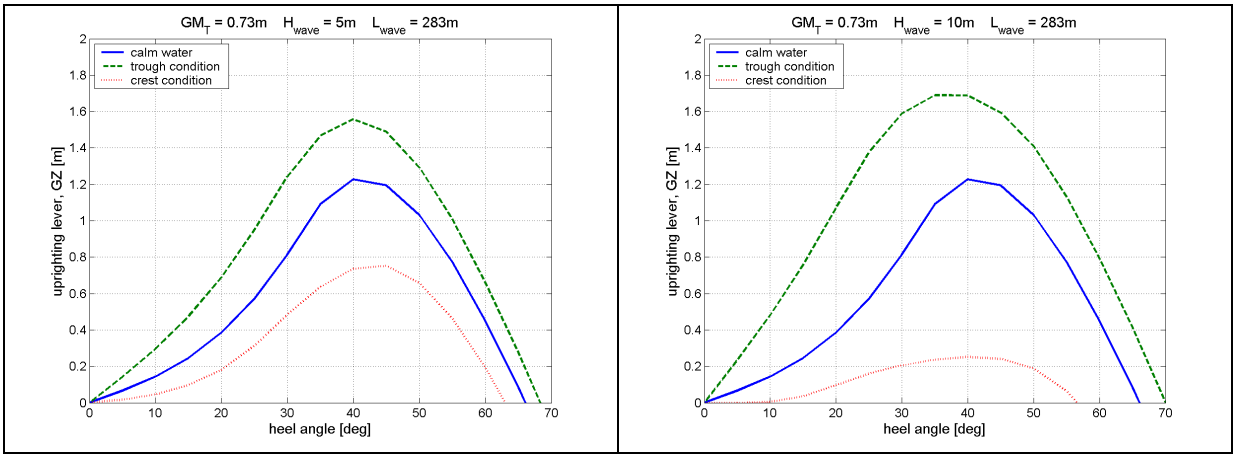

Fig. 40: Lever curves for calm water, trough and crest condition

[12] Émile Léonard Mathieu, mathematician, 1835 – 1890, France

Although the approach does not distinguish between capsizing due to stability loss in a wave crest and due to parametric rolling conditions, and although capsize is the final result, i.e. severe parametric rolling may also occur without capsizing, this approach can be used to assess a threshold value for a critical wave height.
KRUEGER et al. use a capsize index a_k to decide whether a ship can be operated safely in a given sea state or not. Within this index they use the following capsize probability based on their simulations and applicable to all ships:

$$a = 1 - \sqrt{s40 \cdot sh\max}\,, \tag{4.51}$$

i.e. $a = 1$ represents 100% capsize probability and $a = 0$ is 0% respectively.
The factors under the root are as follow:

$$s40 = \begin{cases} \dfrac{a40/a40_{diff}}{k1} & if \quad 0 \le a40/a40_{diff} \le k1 \\ 0 & if \quad a40/a40_{diff} < 0 \\ 1 & if \quad a40/a40_{diff} > k1 \end{cases}$$

$$sh\max = \begin{cases} \dfrac{h\max/h\max_{diff}}{k2} & if \quad 0 \le h\max/h\max_{diff} \le k2 \\ 0 & if \quad h\max/h\max_{diff} < 0 \\ 1 & if \quad h\max/h\max_{diff} > k2 \end{cases}$$

With $a40$ being the area from 0 - 40deg under the lever curve at limiting stability conditions and $a40_{diff}$ the difference of the areas of the lever curves at the current load condition. With $h\max$ and $h\max_{diff}$ the same is put for the maximum uplifting levers. According to the recommendation of KRUEGER the factors *k1* and *k2* are set to 0.7.
The left side of Fig. 41 shows the lever curves for GM_T = 0.73m (design load condition, calm water, crest and trough condition) and for GM_T = 0.37m (minimum or limiting stability condition according to IMO resolution A.749(18), code on intact stability). On the right side the capsize probability dependent on the wave height is shown. The wave length is held constant and matches approximately the ship length.

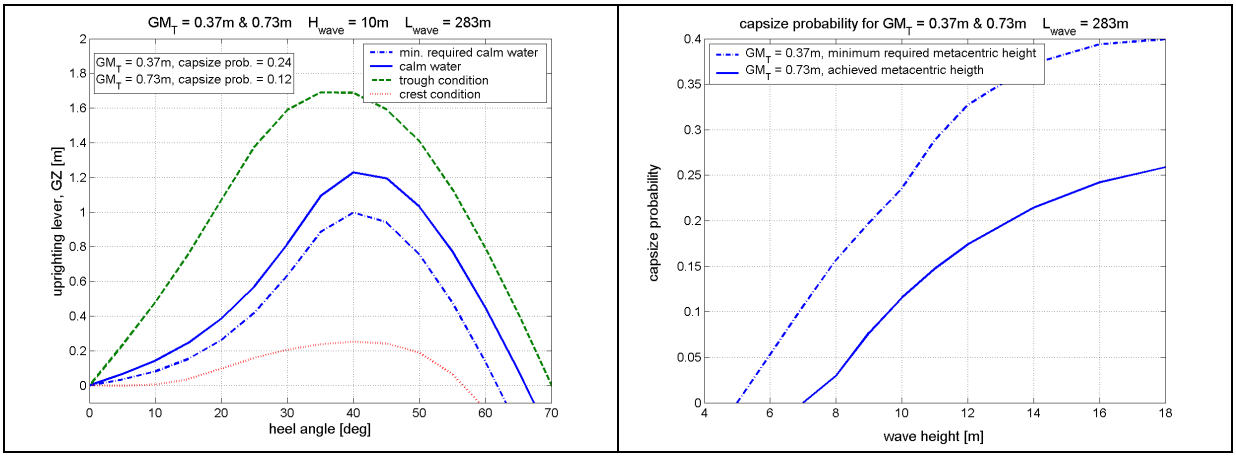

Fig. 41: Lever curves and capsize probability

For 10m wave height the capsize probability for a ship sailing at limiting stability conditions is about 24%. For the design load condition considered here the capsize probability decreases to 12%, i.e. the increased metacentric height of GM_T = 0.73m already enhances safety as regards the capsize probability.

The diagram on the right side of Fig. 41 is used to set a threshold value h_{crit} for the wave height. For example: parametric rolling needs a group of consecutive waves showing an overcritical wave height. That is why an event that causes a capsize probability of, reasonably assumed, 12% should be tolerated only once per hour. This implies a threshold $h_{crit} = 10\,m$. Assessing the wave height to be the double wave amplitude $h = 2\,\zeta_a$ leads to the probability that a critical amplitude is exceeded by:

$$P\left(\zeta_a > \tfrac{1}{2}\,h_{crit}\right) = \exp\left(\frac{-\left(\tfrac{1}{2}\,h_{crit}\right)^2}{2\,m_o}\right). \qquad (4.52)$$

Considering the relation of significant wave height and 0th moment of the wave spectrum:

$$h_{1/3} = 4\,\sqrt{m_0}\,, \qquad (4.53)$$

the probability of exceeding a critical wave height becomes:

$$P\left(h > h_{crit}\right) = \exp\left(\frac{-2\,h_{crit}^{\,2}}{h_{1/3}^{\,2}}\right). \qquad (4.54)$$

The number of times per hour the wave height exceeds the critical wave height is calculated by:

$$E\left[number\ per\ hour\right] = \frac{3600}{T_{enc}}\exp\left\{\frac{-2\,h_{crit}^{\,2}}{h_{1/3}^{\,2}}\right\}. \qquad (4.55)$$

For the time being the value E is set to "1", i.e. a threshold of maximum one exceeding per hour is required. Therefore the tolerated probability P calculated according to equation (4.54) also depends on the encounter period T_{enc} given in equation (4.55), i.e. the tolerated probability is dependent on the ship speed and the wave encounter angle, cp. equation (4.3).

Tab. 5 gives an example for the HANNOVER EXPRESS at design load condition, GM_T = 0.73m. The critical wave height h_{crit} is set to 10m, related to a capsize probability of 12%, according to Fig. 41. A joint capsize probability can be calculated from the probability calculated according to equation (4.54) multiplied with the probability of 12%.

Tab. 5, Joint capsize probability for T_P = 16.5s, V_s = 23kn, h_{crit} = 10m, head- and following seas

encounter angle	180°, head waves	0°, following waves
encounter period T_{enc}	10.0s	46.6s
probability for waves above h_{crit}	0.0028	0.013
capsize probability	0.12	0.12
joint capsize probability	$3.3 * 10^{-4}$	$1.6 * 10^{-3}$

The following section describes the assembly of the approaches and the set-up of the procedure to assess parametric rolling within route optimization.

4.9.3 Combination of the approaches

Fig. 42 to Fig. 45 serve to illustrate the set-up of the parametric-rolling-module used within the route optimization. They show calculations for CMS HANNOVER EXPRESS at head seas and 23kn ship speed. The natural roll period in calm water is 29s, GM_T is 0.73m, design load condition. The wave peak period T_P has been varied from 2s to 29s. The significant wave height $H_{1/3}$ has been set to a fortieth of the appropriate wave length calculated by equation (4.49). The left diagram of Fig. 42 shows the wave length and significant wave height versus the peak period. They are used as an input parameter for this exemplary variation study. The right diagram shows the corresponding pitch period of the ship and the encounter period of the waves. At a peak period of 16.5s the zero-up-crossing-pitch period matches the wave-encounter period. The corresponding wave length is 290m, the significant wave height is about 10m. Apparently the area around T_P = 16s is suspicious for parametric rolling because the parameter constellation mentioned in section 4.9.1 is fulfilled.

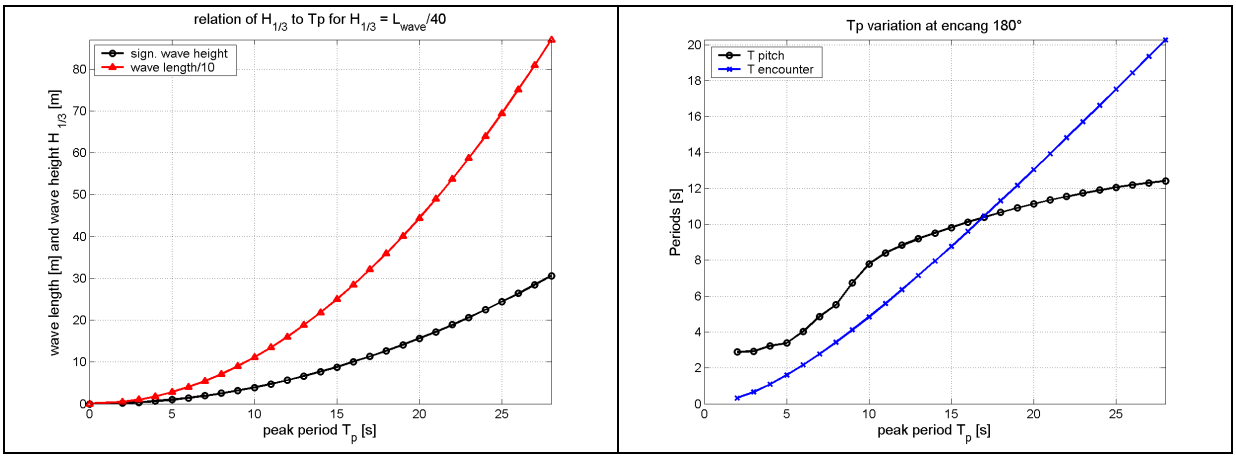

Fig. 42: Variation of the wave peak period

Fig. 43 depicts the ship response at *FP*, *COG*, and *AP*. Absolute motions and also vertical motions relative to the wave surface are shown. As expected, motions increase with increasing wave height and wave period. The higher amplitudes at the forward perpendicular are caused by a center of the waterline area lying abaft, as typical for these ships (in calm water the center of the waterline area is approximately 10 m behind of the center of gravity). The magnitudes of the motions appear credible.

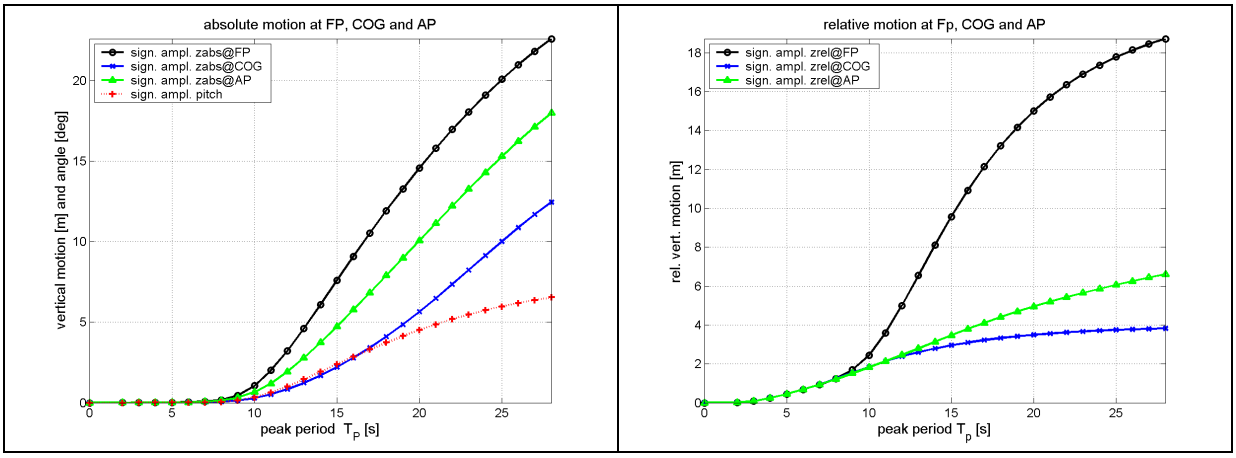

Fig. 43: Absolute and relative motion at *FP*, *COG*, and *AP*

The previous section describes how to set up a threshold value for the wave height. As a start position for further investigations it is put to h_{crit} = 10m, representing a capsize probability of 12%. Such an event will be tolerated only once per hour.
Another attempt, aiming to increase the influence of the pitch motion, uses the relative displacement between ship and free surface at *FP*, *COG*, and *AP*. Instead of a maximum tolerable wave height h_{crit} a threshold for maximum relative motion $\zeta_{rel\ crit}$ is posed. Similar to equation (4.55), the number of times this threshold will be exceeded is calculated by:

$$E\left[number\ per\ hour\right] = \frac{3600}{T_{enc}} \exp\left\{\frac{-\zeta_{rel\ crit}^{\ 2}}{2\ m_{0\ s\ rel}}\right\}. \qquad (4.56)$$

As aforementioned for equation (4.55) the value *E* is set to "1", i.e. here too a threshold of maximum one exceeding per hour is required.
If no ship motion is regarded a wave height of 10m causes approximately a relative displacement of 5m at *FP*, *COG* or *AP*. The consideration of the hull shape (cp. Fig. 44) suggests that a wave elevation at the stern may have a higher impact on the ship as the stern overhang is reached more quickly. The bow shows steeper angles of entrance in the vertical direction. For this reason a moderate adaptation of $\zeta_{rel\ crit}$ seems reliable.

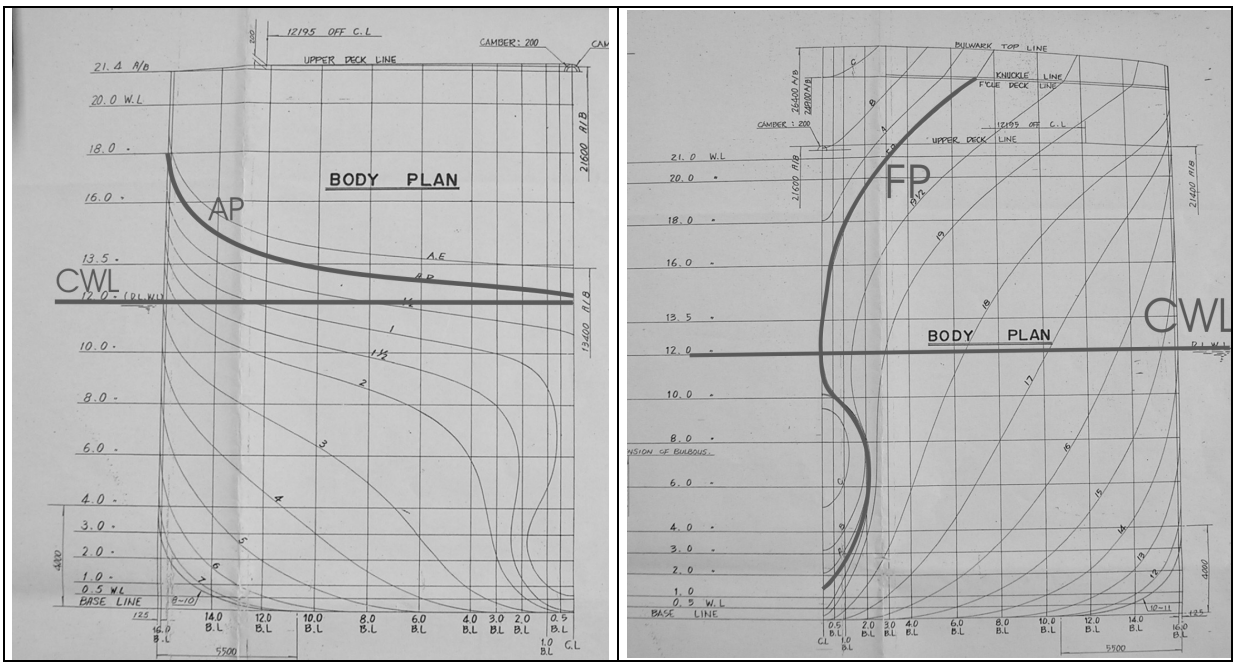

Fig. 44: Ship lines at *FP* and *AP*

For the time being the tolerable relative motion between ship and water surface $\zeta_{rel\ crit}$ is arbitrarily set to:

- 6m for *FP*
- 5m for *COG*
- 4m for *AP*

According to equation (4.55) or (4.56) the exceeding of a threshold value E is calculated if:

- the wave length is in the range of the ship length,
  for a start $0.75 \cdot L_{pp} < L_{wave} < L_{pp} \cdot 1.5$ is used,
- the wave encounter angle β approaches head or following sea,
  for a start a range of $\beta + 5° < 180°$ or $\beta - 5° < 0°$ is used,
- the encounter period T_{enc} matches the pitch period T_{pitch}
  for a start $(T_{enc} - T_{pitch}) < T_{pitch} \cdot 0.1$ is used,

otherwise E is set to zero.
Maxima of exciting forces are detected by comparing encounter- and pitch periods (third bullet point). The natural roll period is not considered, as it is strongly dependent on the wave height. In this way the method is able to identify wave conditions that can excite both, the 1:1 or the 2:1 type of parametric rolling. The ranges, so far, are arbitrarily set and need further investigation and validation by model tests or numerical simulation, e.g. following IMO (2007) the range for the wave encounter angle β has surely to be increased. For the time being they are used for the route optimization as aforementioned to apply and investigate the proposed add-on.
In the way described above, sea states and ship responses are evaluated during the route optimization. Parameter constellations that are suspicious for parametric rolling are recognized and assessed by the frequency of exceeding thresholds for the absolute and the relative wave height at *FP*, *COG*, or *AP*, respectively. The left part of Fig. 45 shows the exceeding E for the variation presented in Fig. 42. In the right part, these functions are shaped considering critical parameter constellations, i.e. E is evaluated only if wave length, pitch- and wave period, and encounter angle indicate that parametric rolling is probable. Although the threshold for the significant amplitude at *FP* is increased, the most events where the threshold value is crossed happen at *FP*.

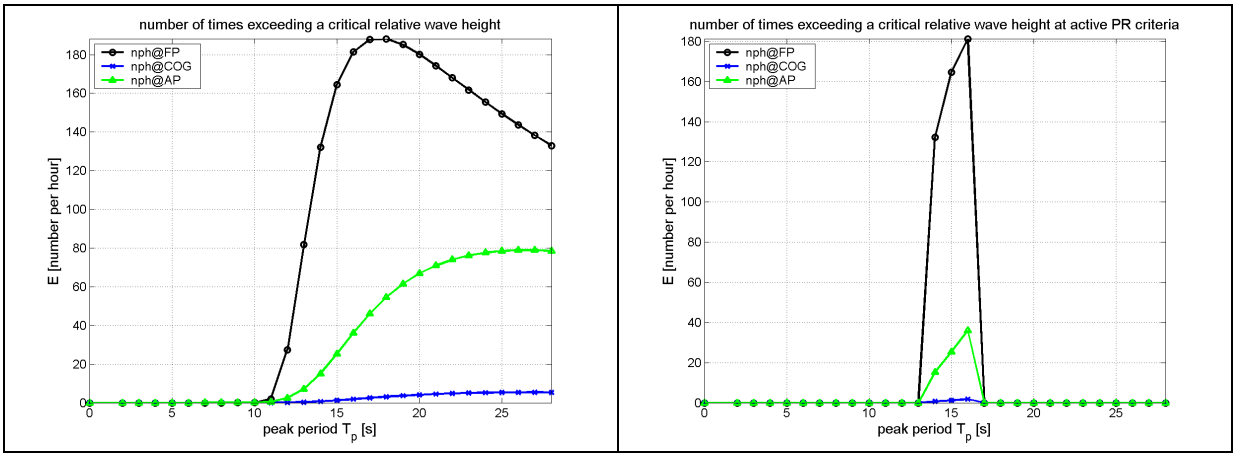

Fig. 45: Threshold exceeding generally and for parametric rolling conditions

Section 6.5 introduces first investigations upon the developed parametric-rolling-module in a route optimization. Furthermore comparative studies on the utilization of h_{crit} and $\zeta_{rel\ crit}$ for the calculation of E are presented.

It is very important to line out that the above developed add-on should be a first step to identify sea states and courses that are suspicious to parametric rolling. It does not cover all the possible situations that are able to cause capsize or extreme roll motions. For this purpose e.g. a much larger range of wave encounter angle has to be considered.

4.10 Considered ship responses

Tab. 6 summarizes the characteristics of CMS HANNOVER EXPRESS considered in this study. Besides these criteria, the table gives information about the focused locations on the ship and the name of the parameter within the mathematical model. Additionally it is specified if these parameters are sensitive to variations of the ship speed V_S, the peak period of the encountering waves T_P, or the encounter angle β. Cells of Tab. 6 that are left blank display that there is no pronounced sensitivity. Values or ranges of values display that there are peaks or areas of extreme responses. All parameters show sensitivity within at least two of the variations. As a start, all of them appear to be crucial for a route optimization.

Tab. 6: Considered ship attributes and summary of ranges of extreme responses

criteria	at / of	parameter name	V_s [kn]	T_p [s]	β [deg]
accelerations	bridge	*xacc*	18 / 24	9.5	150 / 170
	bridge	*yacc*	-	12.0	110
	bridge	*zacc*	-	10.0	100
motion sickness	bridge	*MSI*	-	10.0	100
slamming probability	10% behind *FP*	*slprob*	24	13.0	130 - 180
parametric rolling	*FP*	*nph@fp*	24	14.0 -16.0	175 - 180
naming convention is	*COG*	*nph@cog*	-	15.0 -16.0	175 - 180
given in section 6.5.1	*AP*	*nph@ap*	10	12.0 –13.0	175 - 180
on page 91	wave heights	*nph4hcrit*	-	-	175 - 180
added resistance	ship	*Raw*	14 - 16	13.0 - 15.0	130 - 180

5 A multi objective, stochastic approach for the route optimization

The first section of chapter 5 explains the setup of the route optimization procedure. Following, section 5.2 addresses the optimization method. Here the application of deterministic and stochastic optimization methods is discussed. The final section 5.3 focuses on the amount of probable fuel saving for achievable estimated times of arrival.

5.1 Optimization setup

Tab. 7 illustrates parameters being used for an initial setup of the route optimization. The first letter of a free variable ***s*** or ***v*** shows if it refers to a spatial or a velocity perturbation of the route. Constraints are marked by a capital ***C*** followed by the threshold they refer to. Objectives start with capital ***O*** followed by the parameter to be optimized. Constraints for acceleration on the bridge and slamming use thresholds that are used within the SEAROUTES project. Later on, during the course of the sensitivity studies presented in chapter 6, further constraints for parametric rolling and motion sickness incidence will be included. Finally a third objective to minimize the risk of unfavorable weather changes will be established.
Three types of free variables are applied: shift variable for the spatial shape of the route, shift variable for the shape of the velocity profile during the journey, and a variable that performs a delayed departure. Four constraints are imposed for lateral and vertical accelerations and for the slamming probability. Three additional constraints are needed to control the feasibility of a route variant in terms of main engine operability, time range of available weather data, and land collision. Finally, two objectives are applied, for the estimated time of arrival *ETA*[13] and for the fuel consumption, both of them are to be minimized, and furthermore *ETA* has to match the schedule.

Tab. 7: Parameter of the optimization setup

parameter	name	value	utilization
free variable	*s1* to *s7*	-1.0 to 1.0	spatial route perturbation
	v1 to *v9*	0 to 1.0	velocity profile perturbation
	RTD	0 to 12	later departure
constraint	*C_xacc*	0.2 *g*	upper limit for lateral acceleration
	C_yacc	0.2 *g*	upper limit for lateral acceleration
	C_zacc	0.15 *g*	upper limit for vertical acceleration
	C_slprob	3%	upper limit for slamming probability
	C_spef	dep.	operability of main engine, etc.
	C_fuel	dep.	over all fuel consumption
	C_eta	dep.	time range of available weather data
objective	*O_eta*	---	arrival on schedule
	O_fuel	---	minimum fuel consumption

[13] In the strict sense, the duration of a journey and not *ETA* is minimized. However, all route optimizations start at the time t = 0h and aim to optimize the time that is needed to arrive at a destination point. For this reason *ETA* is used as a synonym for the duration of a journey.

In principle it is possible to simply use the estimated time of arrival *ETA* and the fuel consumption *FUEL* as objectives. But it turned out that tailored objective functions are able to control, speed up, and improve the optimization result:

$$Objective\ ETA = \left(ETA - set\ value\ ETA - \Delta t\right)^2, \tag{5.1}$$

$$Objective\ FUEL = weight \cdot \left(FUEL - FUEL \cdot \frac{ETA}{set\ value\ ETA - \Delta t} \right)^2. \tag{5.2}$$

Equations (5.1) and (5.2) show the objectives, applied in most of the presented optimizations. Equation (5.1) uses the squared difference between *ETA* and a set value, representing an arrival on schedule. The objective function considering the fuel consumption (5.2) includes a term containing *ETA* as well. In this way slow routes are forced to save more fuel, whereas the fuel saving of faster routes is not handled as strictly. The time deduction Δt is used to obtain objective function values that still can be minimized, even if an arrival on schedule is reached. The weight in equation (5.2) serves to provide values of equal magnitude for both objective functions. In the terminology of evolutionism this modeling of objective functions denotes an increasing selective pressure in favor of faster route designs. It is a common technique to control the optimization process by modifying the fitness function instead of applying the original objective. This method should not be mistaken for the application of utility functions in multi-criteria decision-making. Utility functions are a combination of objectives and assigned weights to emphasize single objectives. This is deliberately not applied here, as it should be the conscious decision of a master which route he/she takes from a set of feasible routes and which objective is considered to be more important than another.

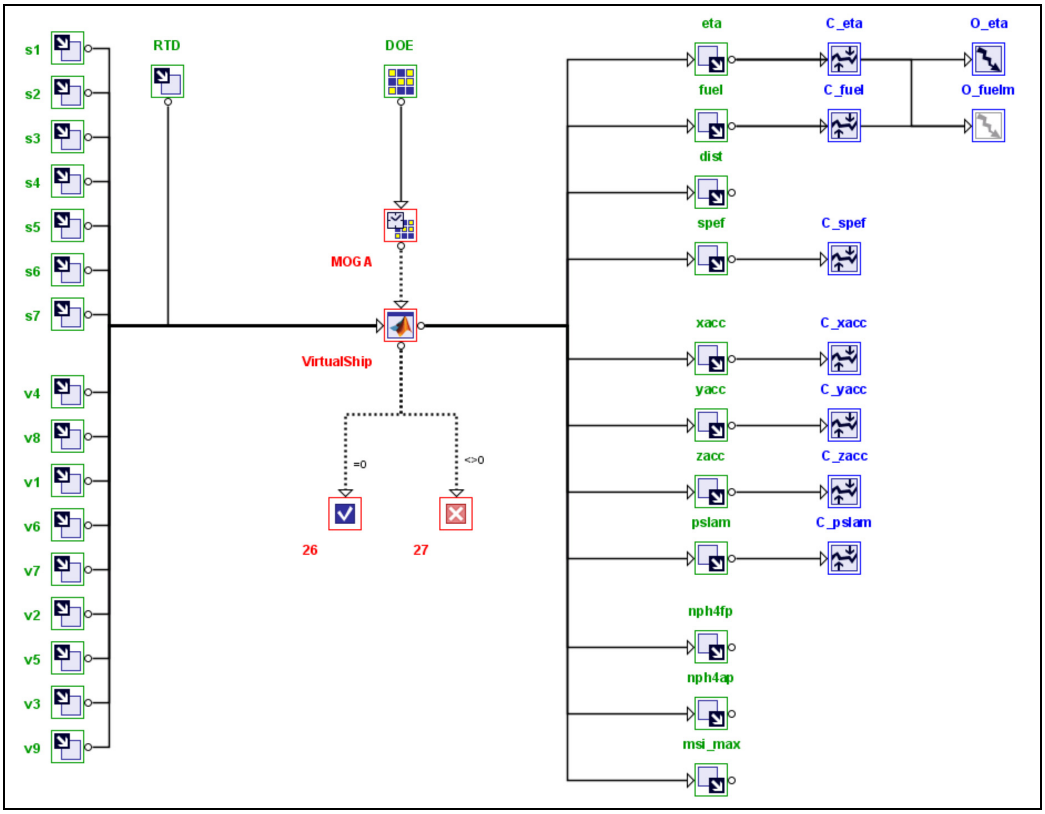

Fig. 46: modeFRONTIER process flow chart

For the optimization task the generic optimization software modeFRONTIER of ES.TEC.O s.r.l. (1999) is utilized. Fig. 46 shows the flow chart of modeFRONTIER as it is used for the setup of the route optimization. Following the process flow, the diagram can be read from left to right. Solid lines represent the data flow, dotted lines the process flow during the optimization. With the nodes on the left side free variables are defined as input parameters. These are transferred to a node that performs the generation and evaluation of a route variant, called ***VirtualShip***. The result is given to output parameter nodes and can now be passed over to nodes that perform the evaluation in terms of constraints and objectives.
In the middle of the figure four other nodes can be seen. The *DOE* (design of experiment) is needed to provide initial start designs for the optimization. The node below serves to select the optimization method and settings like the number of loops or convergence parameter.
The two nodes below contain modules for the process control to decide whether a simulation is successful or not.

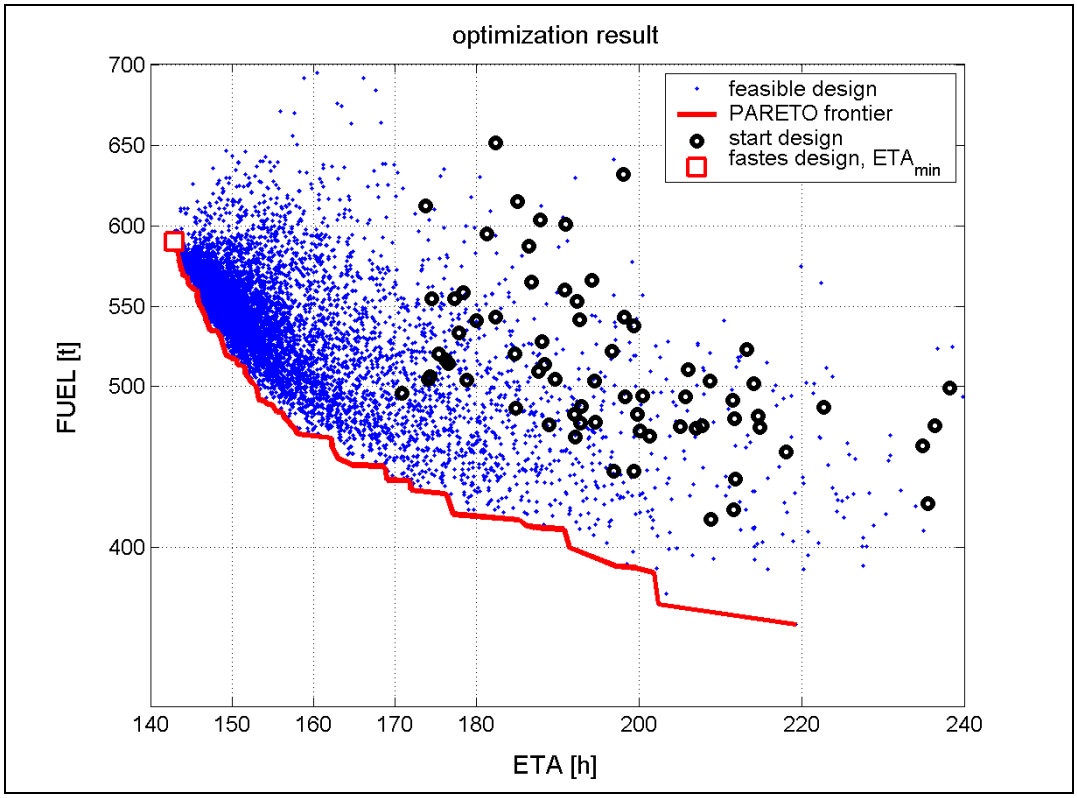

Fig. 47: Feasible route designs and PARETO frontier

Fig. 47 shows a result of a multi-objective route optimization at rough sea conditions (20. – 30.01.2002). Each dot represents a feasible route that can be taken into account for a route decision considering *ETA* and *FUEL*. Infeasible solutions are not depicted.
The bold black circles represent the initially given designs, the set of feasible solutions to start the optimization. This set has to be produced in advance of the optimization, for example by a random search method.
A bold line, the PARETO frontier, borders the solution space. It is built by the set of solutions for which a single objective cannot be further improved without deteriorating any other objective. All feasible routes lie above and to the right of the PARETO frontier. Those variants that are closest to the frontier display low passage time for reasonably low fuel consumption. Apparently it is impossible to decrease *ETA* below certain limits without impairing *FUEL*.

Fig. 48 shows the fastest variant of these routes (*ETA* 143h, *FUEL* 594t). Furthermore the wave data of the deterministic forecast are depicted. The wave fields in the figure mostly propagate from west to east. The contour lines represent the current significant wave height during the crossing. The route and the actual position of the ship (a dot at the end of the bold black line) are drawn, too.

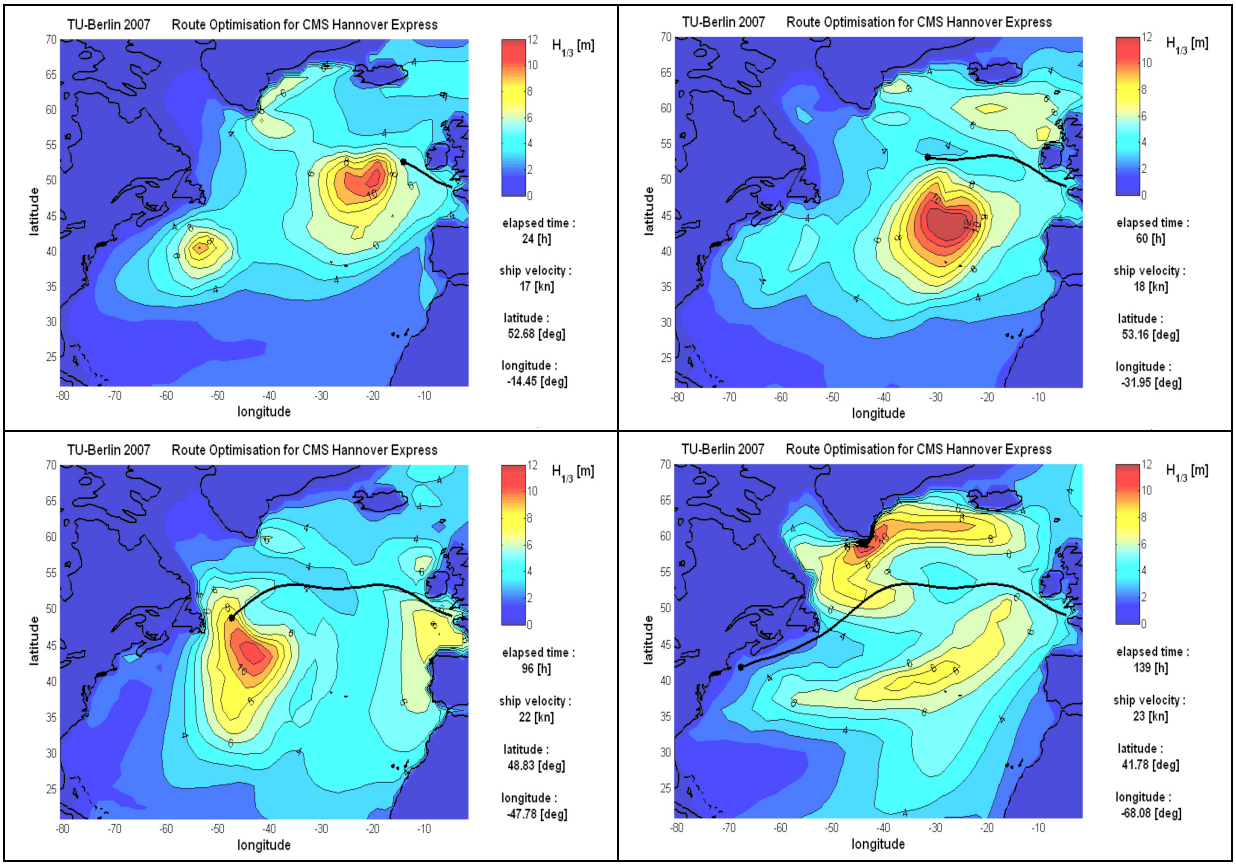

Fig. 48: Optimized westbound North Atlantic crossing

Four stations of the journey are depicted:

- Upper left picture: 24h after departure a strong wave field passes the ship, it turns towards North before reaching the ship.
- Upper right picture: A second wave field is surrounded northerly during the third day.
- Lower left picture: The protuberance of a third wave field towards Northwest at the end of the fourth day causes extreme load to the ship and the crew, however, constraints are not violated.
- Lower right picture: Finally the ship reaches the shallow and calm water in front of New York.

5.2 Simplex versus Genetic Algorithm

For the choice of an appropriate optimization method various aspects are to be taken into account:

- The optimizer should be able to handle more than one objective function. Although it is commonly used to combine different objectives into one objective function, these approaches generally produce intricate objective functions.
- The shape of the solution space and the one of the objective function is crucial for the decision about applying a deterministic or a stochastic optimization method. Deterministic methods are mostly sufficient for unimodal objective functions, whereas multi-modal functions require methods that provide heuristic or stochastic attributes. The introduction of constraints may change the characteristic of an objective function. Within the presented ship routing, constraints distort a unimodal objective function to one with local and global optima. Furthermore the spatial-temporal dependency, between free variables describing the course and the velocity profile, causes a shift of the range where free variables produce feasible solutions or even builds islands of feasible combinations of free variables.
- Finally the optimizer should be able to produce the solution within reasonable time expenditure.

The last aspect is not attended yet as it is the requirement of a final implementation. The runtime improvements realized within the MATLAB routines that model the virtual ship are mentioned in section 4.6.

In this section the focus is put on the qualitative aspects, in particular the one mentioned in the second bullet point. For this purpose different optimization methods with enabled and deactivated constraints are applied. The results for two representative investigations are given below:

Fig. 49 shows four different optimization results. Two optimizations are conducted with a SIMPLEX (representative for deterministic methods), and two apply a multi-objective genetic algorithm MOGA (representative for stochastic methods). For SIMPLEX all investigated route designs are depicted. The only requirement for SIMPLEX is to identify the minimum *ETA* routes regardless of fuel consumption. For the MOGA optimizations only the PARETO frontiers are shown. All feasible designs above and right from the PARETO frontier are not depicted. The solid line is built by the PARETO optimum route designs where only the basic constraints for main engine operability are enabled (the gray shaded ones in Tab. 7). The dotted line marks the PARETO designs when also vertical accelerations are constrained. By applying this constraint the minimum attainable *ETA* increases about 20h. Dots and triangles mark the route designs that are investigated during corresponding SIMPLEX optimizations. All optimizations start with relatively slow routes, i.e. at the right side of Fig. 49. Identifying faster variants generally involves increasing fuel consumption. Optimizations applying SIMPLEX perform 10 times faster than MOGA, but obviously they are not able to find the assumed global optimum.

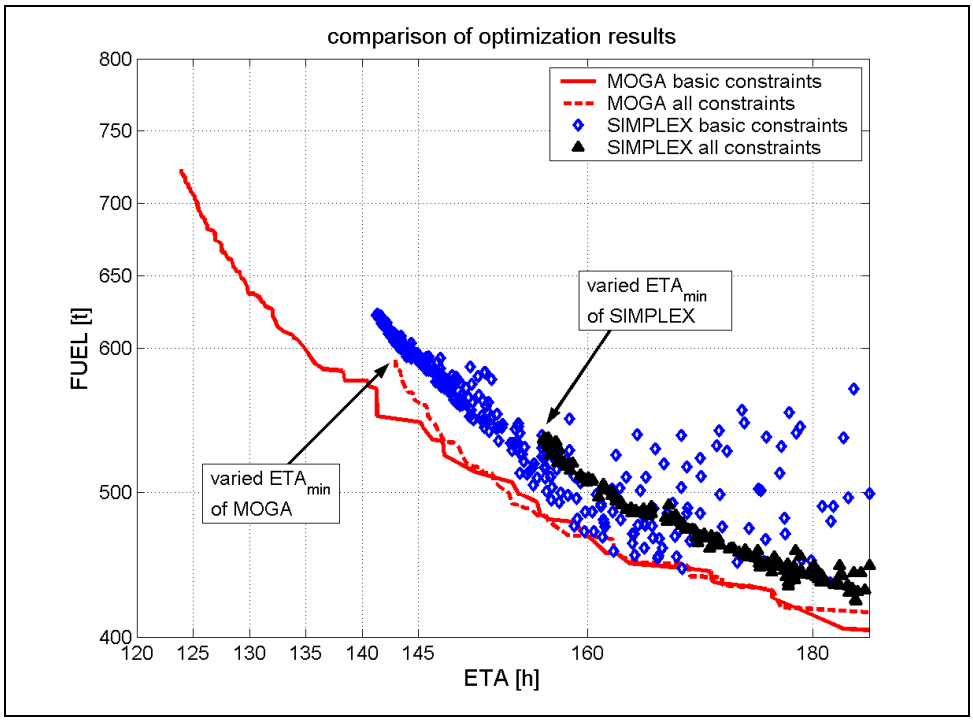

Fig. 49: MOGA and SIMPLEX optimization results

Fig. 50 is taken from investigations considering a separate variation of individual free variables. In this case the two time minimum routes pointed out in Fig. 49 are considered. These investigations serve to enlighten the differences in the optimization results of both optimization methods:

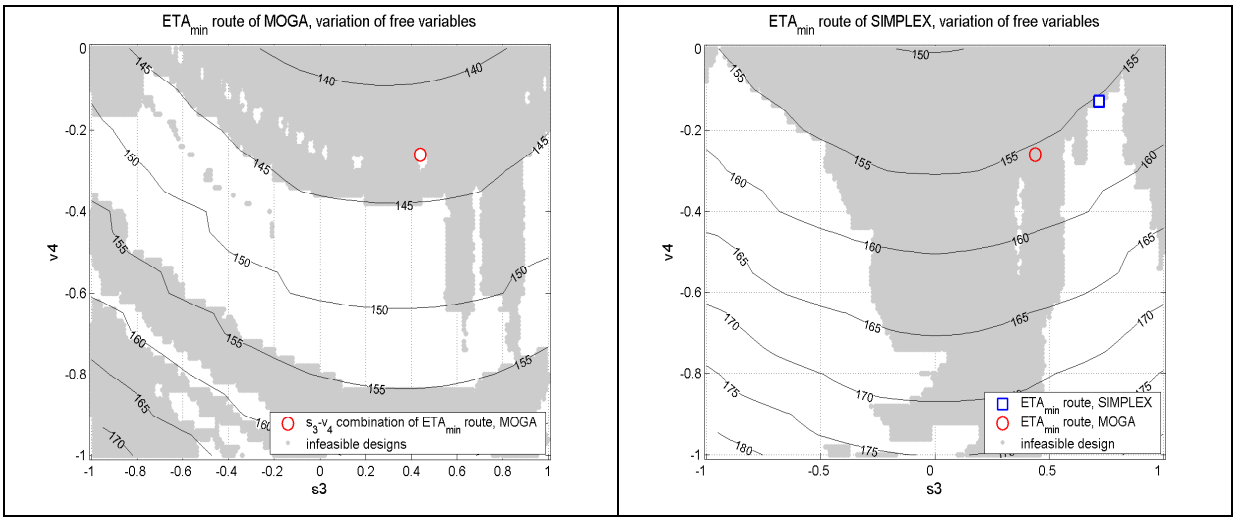

Fig. 50: Variation of free variables

The figure depicts a variation of the variables s_3 and v_4, describing course and velocity profile of a route segment at the middle of the journey. The left part of the figure is a variation of the time minimum route found by MOGA, on the right hand side the one for the time minimum route of the SIMPLEX, respectively. The s_3-v_4-combinations of the time minimum routes are marked by a red circle for the MOGA and a blue square for the SIMPLEX optimization. The contours represent *ETA* due to the variation of s_3 and v_4. Infeasible combinations of free variables are shaded gray. Obviously both varied routes represent an optimum, i.e. the time

minimum route that is feasible regarding these two free variables. An improvement is only possible by violating one or more constraints. Considering the SIMPLEX investigation at the right side of Fig. 50, the combination of free variables for the time minimum route, found by the MOGA optimization, produces an infeasible design. This means that variables are dependent among each other, and being feasible or not depends on the combination of all variables. Certainly Fig. 50 is a very malicious example for the characteristic of the objective function and its limitation due to active constraints. But it nicely shows the extraordinary dynamic behavior of the solution space that is after all responsible for the malfunction of the SIMPLEX. It shows that the optimizer must be able to produce solutions that jump through the solution space to overcome borders built by active constraints or to detect islands of feasible combinations of variables. Furthermore this variation gives advice for necessary investigations regarding the quality of an optimization result. An optimization result that allows wider variations of free variable is more favorable than the one that immediately turns infeasible. In this context also the severity of a constraint violation is of interest. Investigations considering these aspects are given in the chapter 6.

Based on the presented considerations, it is decided to apply the MOGA as the primary optimization method in the following. Certainly any other stochastic optimization method can be adopted as well. Deterministic methods are applied only to control whether a local refinement is possible.

5.3 Potential fuel savings by route optimization

Besides increasing the safety and reliability of ship operation and detecting the range of attainable times of arrival *ETA*, fuel saving is a major target of route optimization. Two different optimizations serve to assess the amount of possible fuel or time saving by applying route optimization. The results are illustrated in Fig. 51 and Fig. 52:

- The first optimization uses unbound course and velocity profiles, i.e. the parameters for the course and velocity perturbation s_i and v_i are used as free variables. The optimization serves to assess the maximum of possible fuel- or time savings. The optimization result is represented by a PARETO frontier in Fig. 51 (solid line). For this optimization achievable improvements become a trade-off between (i) fuel savings by avoiding bad weather and (ii) additional fuel consumption because the circumnavigation of bad weather areas causes longer routes. The achievable *ETA* and the fuel consumption depend on both, the variation of the ship speed and the variation of the sailed route.
- The second optimization is conducted with a fixed course, the unperturbed parent route, i.e. only the parameters of the velocity perturbation v_i are used as free variables. This represents a strategy of ship operation where a fixed course is sailed and the speed is reduced according to the weather conditions. The dashed line in Fig. 51 represents the resulting PARETO frontier. In this case *ETA* and the fuel consumption, depend only on the perturbation of the velocity profile.

Fig. 52 depicts three routes, courses, velocity profiles, and the respective specific fuel oil consumption, selected from the PARETO optimum routes pointed out in Fig. 51:

- route 1: fastest attainable route achieved by variation of both, course and ship speed,
- route 2: PARETO optimum route achieved by variation of both, course and ship speed with the same *ETA* like route 3,
- route 3: fastest attainable route achieved only by variation the ship speed.

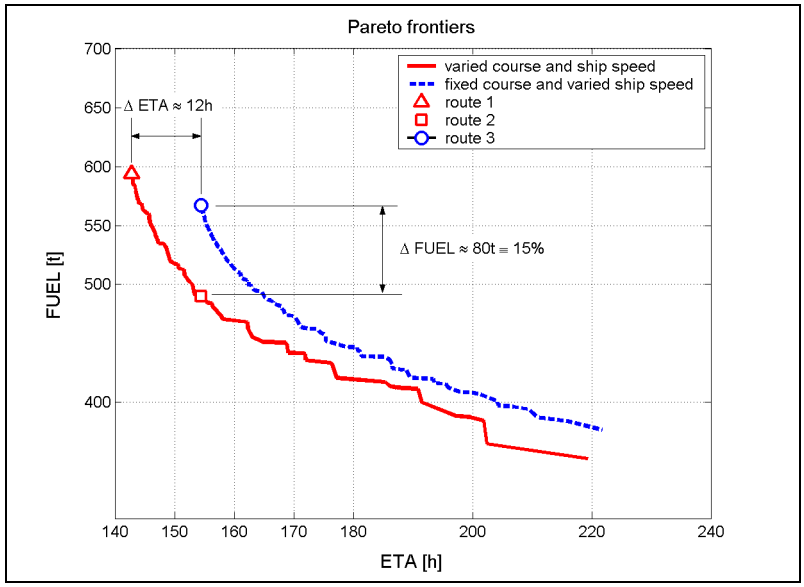

Fig. 51: PARETO frontiers for optimizations with fixed and with unbound course

The left side of Fig. 52 shows the courses of routes 1, 2, and 3. The right side depicts the respective ship speed and the specific fuel oil consumption during the journey for route 2 and 3, the routes with an *ETA* of 155h.

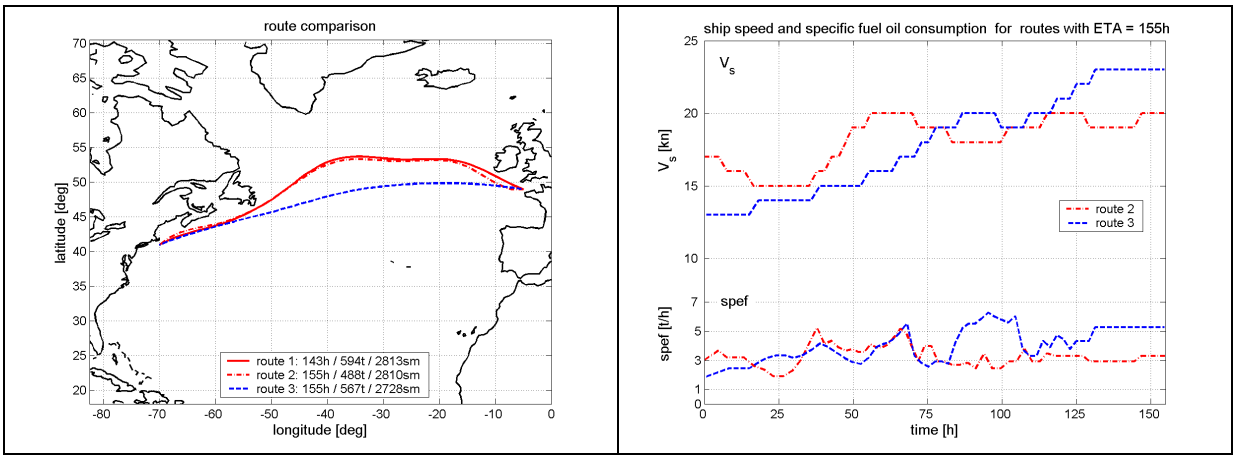

Fig. 52: Courses, velocity profiles, and specific fuel consumption for optimizations with fixed and with unbound course

The numeric values for *ETA*, fuel consumption, and distance of the compared routes are given in Tab. 8.

Tab. 8: Route comparison to assess the potential fuel saving

route	*ETA*	fuel consumption	average ship speed	distance	free variables
no.	[h]	[t]	[kn]	[nm]	[-]
1	143	594	19.7	2813	**s** and **v**
2	155	488	18.1	2810	**s** and **v**
3	155	567	17.6	2728	only **v**

It turns out that the spatial perturbation improves the optimization result. For the same time of arrival (route 2 and 3) fuel savings of roughly 15% are possible. On the other hand it becomes possible to arrive 12h earlier although the route takes a longer course (route 1).
Comparing the routes of Fig. 52 supports the opinion that an optimum route is a combination of an optimum course and an optimum velocity profile. Due to the longer distance of route 2 the ship has to sail faster (see the averaged ship speed given in Tab. 8). During the first half of the journey route 2 shows higher speed than route 3, however the specific fuel oil consumption is comparable to the one of route 3. This is achieved by circumnavigating bad weather and a resulting reduced added resistance due to waves. In the second half of the journey route 3 has to speed up to meet *ETA*, consequently the fuel consumption increases. For route 2 is admissible to maintain speed and the fuel consumption clearly falls below the one of route 3.

Under rough weather conditions, here the optimization uses the forecast of a rough weather condition in January 2002, the optimum course doesn't necessarily follow the shortest track. Furthermore, Fig. 48 and Fig. 52 illustrate the complexity of decision making in navigation. It is evident that the benefit from route optimization increases in adverse weather situations. For calm sea conditions the decision-making becomes easier. The additional resistance due to waves diminishes and maximum fuel saving is achieved by sailing the shortest route as slow as possible, i.e. below a certain sea state there is no need for route optimization. For example at the medium weather conditions (January 2003) that are investigated within this study, the attainable fuel saving reduces to 3%. In contrast to the optimization within the rough weather scenario, this reduction of the fuel consumption is mainly achieved by reducing the sailed distance. The influence of the weather condition on route optimization will be further addressed in section 6.1.

6 Validations and extensions

The previous chapters present the setup of the route optimization procedure as a combination of simulation and optimization techniques. Following, the reliability and capability of this approach is analyzed. This is achieved by means of **sensitivity analysis** and **plausibility controls**. General conditions, e.g. the applied weather forecast, are changed to observe if the resulting optimization output is plausible and therefore reliable. On the other hand, these studies serve to get an idea of the influence of various deciding parameters on a ship route optimization result. Here parameter variations serve to assess the sensitivity of the approach to changes of e.g. external conditions or parameters like threshold values and to particular constraints. Thus the investigations also provide insight to the capability of the optimization. In this way a first validation of the ship route optimization approach is achieved. The following investigations will be presented in this chapter:

- Section 6.1 shows optimization results for a calm, a medium, and a rough weather scenario. This investigation serves to get a first plausibility control of the optimization results. As expected, the fastest route at calm sea conditions is the shortest course sailed at maximum speed. Also at medium sea condition the fastest route takes the shortest course, however, the ship speed has to be reduced temporarily. Within the rough weather scenario the fastest route doesn't follow the shortest course. Optimum ship speed and optimum fuel consumption are achieved by circumnavigation of storm areas. In doing so, a compromise between additional fuel consumption due to a longer course and fuel saving by reducing the additional resistance due to waves is found. On the one hand the ship speed is reduced due to operational requirements (posed thresholds, permitted engine load), on the other hand it represents a tactical measure to reduce the fuel consumption (await a storm area to pass by).
  It turns out that the rough weather case is the most challenging case for a route optimization. In this case an arrival on schedule seems impossible. During the optimization numerous route variants are ranked as infeasible due to violated constraints, and optimum routes show considerable deviations from the shortest course. Therefore the following sections focus exclusively on the rough sea condition.

- Section 6.2 concentrates on the wave forecast and the modeling of swell by means of wave spectra. The section focuses on the influence of different descriptions of long crested waves on the optimization result, namely the spectra according to JONSWAP and PIERSON-MOSKOWITZ.
  Comparisons of 1D-spectra of the European Centre for Medium Range Weather Forecast ECMWF and corresponding PIERSON-MOSKOWITZ spectra show remarkable differences in the distribution of wave energy over the frequency. The area under the spectral curves, i.e. the total amount of wave energy, is the same. During a review of wave data it is observed that the JONSWAP and PIERSON-MOSKOWITZ spectra represent so to speak edge cases of the 1D-ECMWF spectrum. In some cases the energy distribution of the 1D-ECMWF spectrum resembles more the one of the JONSWAP spectrum, sometimes it is more similar to the distribution of a PIERSON-MOSKOWITZ spectrum. In the vicinity of storm areas the curve of the 1D-ECMWF spectrum appears to lie in between the one of the JONSWAP and the one of the PIERSON-MOSKOWITZ spectrum. Especially these areas are of interest for ship routing as they are barely navigable.
  The comparison of optimization results shows only small differences of the PARETO frontiers for fast routes. At lower speed the frontiers are congruent. The number of

constraints for the slamming probability and engine overload that are violated increases when a JONSWAP spectrum is applied. Comparisons of representative transfer functions support this observation, both, spectra and transfer functions show maxima in the same frequency range.
However, the optimization result is governed by another constraint, the one for vertical acceleration on the bridge. This constraint shows no sensitivity regarding the applied spectrum.
Based on these investigations it is decided to apply a PIERSON-MOSKOWITZ spectrum in the following, as it is the standard spectrum for the North-Atlantic. Certainly slamming and engine overload are not always of minor importance for a route decision. For this reason the introduction of shape parameters, e.g. similar to the parameters of the JONSWAP formulation (equation 3.5), can improve the quality of the forecast data that are used within the route optimization. These parameters can be provided as a supplement to the weather data, i.e. the forecast would exist of data for the significant wave height, wave period, wave angle, and three to four shape parameters.

- Section 6.3 focuses on the geometric description of the hull shape and its influence to predicted ship responses and to optimization results. This is done to give an answer to the open question on how accurate a particular hull shape has to be modeled for the determination of ship responses within routing. For this purpose the seakeeping characteristics of two further ships, scaled to Panmax-size and combined with the calm water resistance and the engine characteristics of the HANNOVER EXPRESS, are used for a route optimization in the rough weather scenario.
  The optimizations show differences in the PARETO frontiers, in the courses, and in particular in the velocity profiles of optimized routes. Advantages and disadvantages of a particular hull shape result from the contributions of all considered seakeeping criteria, i.e. optimality cannot be reduced to the contribution of a single criteria. Even if the influence on the seakeeping behavior of the hull shape above the water line is neglected by strip theory, it appears recommended to use a geometric description of the ship hull that is as accurate as possible.

- Section 6.4 discusses the consequences of constraint- and threshold variations on the optimization result. During the investigations so far, it is observed that the optimization results for the rough sea scenario are strongly governed by constraints. In particular the threshold for admissible vertical acceleration on the bridge shows a strong influence on the shape of a PARETO frontier. The definition of reasonable threshold values turns out to be one of the major tasks for the set-up of a route optimization procedure. Here the variations serve to confirm or, if necessary, to adjust the originally applied thresholds.
  As expected, the variations of the threshold for the significant amplitude of vertical acceleration on the bridge show a considerable influence on the optimization result. It has to be decided if this threshold is set too tight. Comparisons with optimization results applying a second evaluation method for vertical accelerations, namely the motion sickness incidence *MSI*, advise against an increasing of the threshold for significant amplitudes of vertical acceleration (currently 0.15*g*).
  Regarding the threshold for the slamming probability, variations of threshold values within a reasonable range have no influence on the PARETO frontier. The concept of evaluating the slamming probability may need revision.

Following variations and combinations of thresholds for vertical acceleration and slamming support the observations that:

- Admissible variations of the constraint regarding the slamming probability do not affect the shape of the PARETO frontier, however, they influence the optimization process.
- The constraint for vertical acceleration is dominant in any case.
- The fastest routes taken from optimizations with varied threshold values only differ in 1h regarding the time of arrival and 3% regarding the fuel consumption, although they show distinct differences regarding their courses, i.e. the effect on the PARETO frontier is small. A cautious interpretation is: Even if the routing-problem is characterized by high complexity, it seems to be of "good nature", i.e. deviations from an optimum course do not totally disturb the merit of an optimized route.

- Section 6.5 discusses an extension of the optimization approach with a further constraint, namely for parametric rolling.
  Parametrically exited roll motion poses a serious threat to a safe operation of ships. In particular ships with large bow flare and stern overhang, like container ships, are affected. The motion sequence of parametric rolling is not comparable to the one of resonant rolling. Therefore this phenomenon requires a separate treatment. Here the model posed in section 4.9 is tested and discussed with regard to its influence on a route optimization result.
  The applied thresholds for the absolute wave height and the relative wave height at the center of gravity, the fore-, and the aft perpendicular can be adjusted reasonably among each other. The developed extension serves to avoid wave conditions that are suspicious for parametric rolling, a prediction however is not possible. Regarding the fact that differences in the weather development become even more probable the more a forecast reaches into the future and that already relative small waves are able to excite parametric rolling, it appears recommended to support the officer on watch by means of a monitoring- and warning system.

- Section 6.6 addresses the robustness of an optimization result regarding the uncertainty of a weather prediction. For this purpose a criterion representing the robustness of an optimized route to probable weather changes is established. It is used as constraint as well as objective function for the optimization.
  A mean-ensemble forecast provides only information of restricted usability regarding the robustness of a route. Whereas the ensemble forecast (the set of 50 forecasts with an equal probability of occurrence) provides meaningful results concerning the expected practicability of an optimized route. An optimization with simultaneous consideration of three objectives, accounting for the time of arrival, the fuel consumption, and for robustness, provides excellent results. Two extremely robust PARETO-optimum routes that match the schedule are identified. They differ distinctly from the time minimum route optimized within the deterministic forecast that is too slow to match the schedule. A recalculation in analyzed weather points out that these routes are only affected by minor and furthermore bearable violations of the constraint for vertical acceleration. Therefore they appear to be feasible.
  The results of this investigation emphasize the importance of reasonably appointed thresholds. A constraint that is set too tight can exclude an optimization result that probably turns out to be feasible and favorable later on, i.e. the range of permissible solutions is narrowed unnecessarily.

From these optimizations follows a categorization of constraints:

- Hard constraints, e.g. engine overload, this constraint should be set tight to keep a power reserve.
- Soft constraints, e.g. for vertical accelerations on the bridge; if minor exceedings are permitted this constraint can be set less tight to avoid that favorable route variants are discarded ab initio.

To compare single routes of different optimization results mostly time minimum routes are used. Naturally all PARETO designs, and therefore also routes of different optimizations that match the same *ETA*, can be used for comparisons. Actually a route that complies with the schedule may be favorable to one that is faster but consumes more fuel. Nevertheless, for two reasons it is decided to use time minimum routes for comparisons:

- In the applied rough weather case it turns out that an arrival on schedule is hardly possible. In this case the time minimum route becomes interesting because it represents the earliest possible arrival.
- From the optimization point of view, it is desirable to completely fill out the entire solution space, i.e. to detect all feasible solutions. Generally optimizations start at slow route designs and successively approach faster designs. In most cases it becomes more difficult to build feasible routes the faster they get. Therefore, when addressing the capability of an optimization set-up, it is meaningful to compare the time minimum routes.

6.1 Various weather conditions

The first and simplest test case for a routing tool is a route optimization in a calm weather scenario. In this case, when no constraints are active, the fastest ship route can only be the shortest route at maximum speed. Furthermore it should be a PARETO design. Within the following investigations three different weather conditions are used. Tab. 9 illustrates the considered wave forecasts. A calm weather condition during summer 2001, medium and rough sea conditions are taken from winter 2003 and 2002, respectively. Maximum occurring significant wave heights and corresponding peak periods are mentioned to give an idea of the weather conditions. These data refer to the first 5 days of the forecasts. The last four columns of Tab. 9 depict the attained time minimum *ETA*s, the averaged ship speed during the journey, the corresponding fuel consumption, and distances. These routes are found by a single optimization applying a MOGA. At calm and medium wave conditions the fastest routes are also the shortest ones. At medium sea condition the fastest route requires 3 hours more than at calm sea condition. Here temporary speed reductions are necessary to avoid active constraints and main engine overload. The fuel saving due to reduced speed and additional consumption due to added resistance in waves almost balance. At rough sea condition the shortest route is not the fastest anymore. Due to the wave conditions the ship speed has to be reduced significantly and therefore an arrival on schedule is impossible (this requires an ETA_{min} of approximately 130h). On the other hand, the fuel saving due to the reduced speed exceeds the additional consumption due to the added resistance. Anyhow, this is no cause for delay and main engine maintenance arise.

Tab. 9: Applied forecasts and optimization results

sea condition	period	$H_{1/3\ max}$ [m]	at T_p [s]	ETA_{min} [h]	mean V_s [kn]	*FUEL* [t]	*DIST* [nm]
calm	6.6. – 16.6.2001	5.4	10.2	114	23.8	694	2716
medium	1.1. – 11.1.2003	12.0	15.4	117	23.2	704	2716
rough	20.1. – 30.1.2002	15.0	14.9	143	19.7	585	2811

Fig. 53 depicts the optimization results for the three forecasts. The diagrams on top are fuel consumption *FUEL* vs. estimated time of arrival *ETA* and distance *DIST* vs. *ETA* for the calm weather condition. In the middle, the same diagrams are shown for the medium wave condition. The diagrams for the rough sea condition are below.
Each blue dot represents a feasible route variant. The red dots mark feasible PARETO optimum routes. Within the calm sea- and the medium sea case the optimization identifies the shortest possible connection (2716nm) to be the fastest, and further more a PARETO optimum route. Slower PARETO optimum routes do not necessarily take the shortest track. Here the trade-off between (i) increasing fuel consumption due to additional resistance in waves and a longer distance and (ii) fuel saving due to speed reduction is crucial. Taking 2728nm, the route at medium sea that matches schedule is still quite near to the shortest track. Within the rough sea condition, no feasible routes are identified on the shortest track. This does not mean that there aren't any feasible routes, but they are not considered because they are too time-consuming.

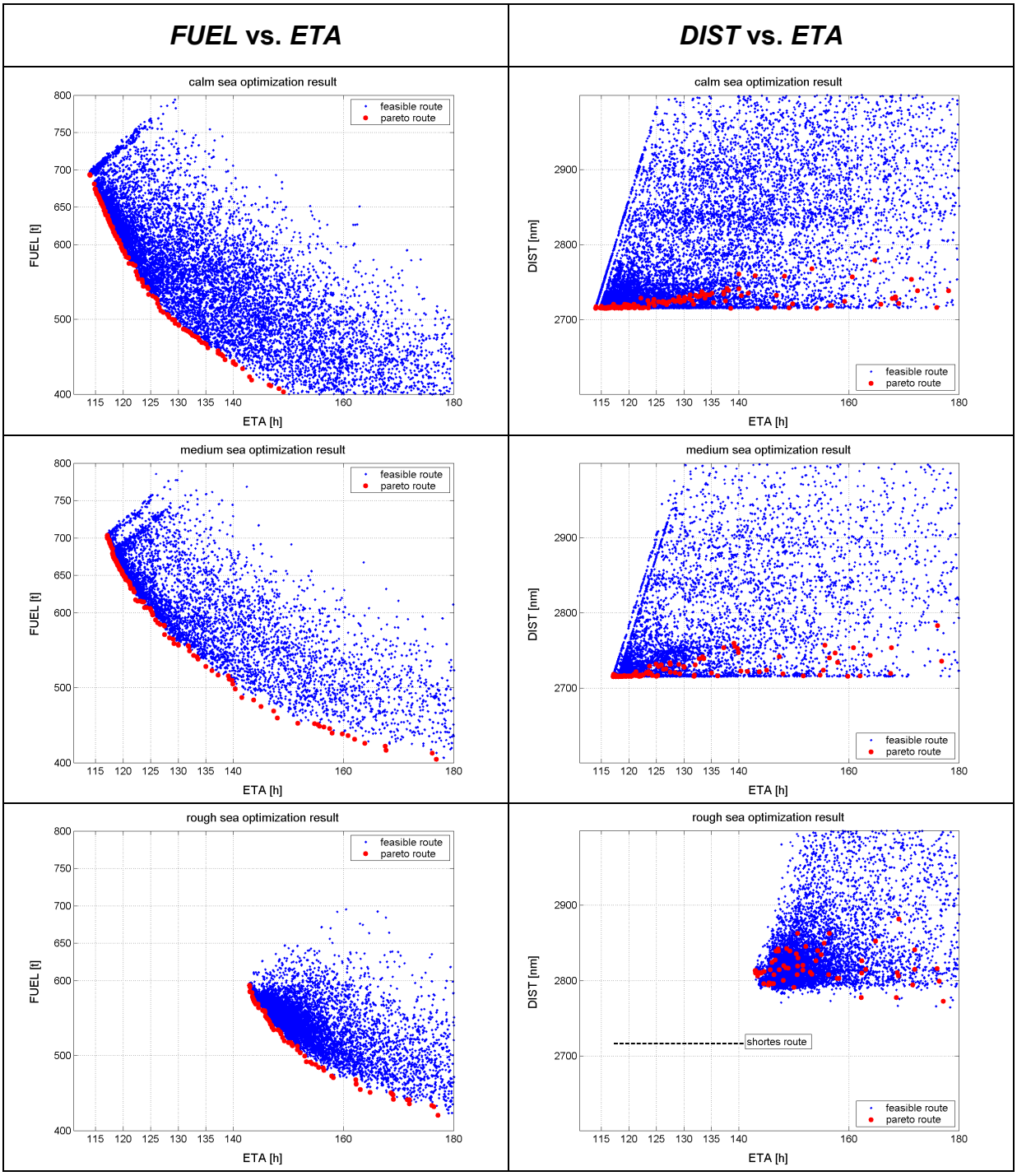

Fig. 53: Optimization results at different wave conditions

Fig. 54 compares the PARETO frontiers for the three weather conditions. It illustrates the remarkable influence of the weather condition on the fuel consumption. At calm and medium sea condition an arrival on schedule is possible, i.e. there are available routes of *ETA* = 130h. But for the medium sea condition the fuel consumption increases about 15%.

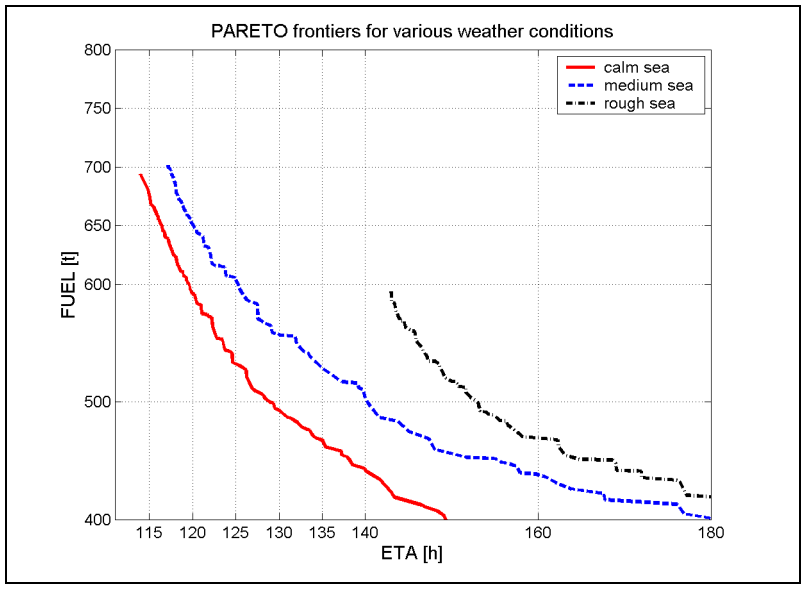

Fig. 54: PARETO frontiers for calm, medium and rough sea

Fig. 55 shows the fastest routes for each weather condition. It clearly shows that in this case the fastest route at rough sea condition is not the shortest one. Altogether the optimization provided the expected result: as far as no constraints are active the shortest route is also the fastest one. But the shortest route is not always necessarily a PARETO optimum route.

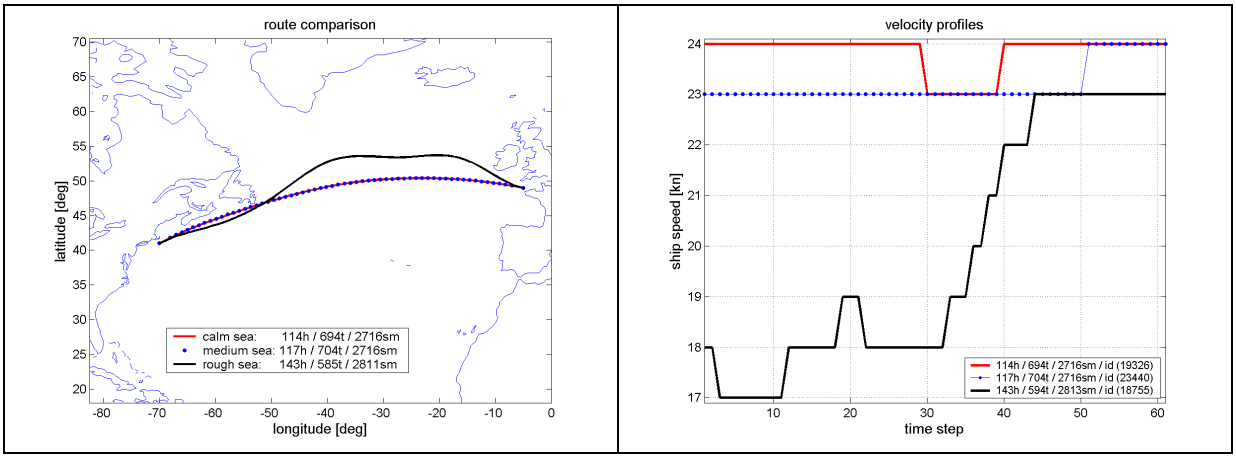

Fig. 55: Fastest routes for different wave conditions

Fig. 55 also illustrates a further characteristic of the optimization applying a multi objective genetic algorithm MOGA. Between Newfoundland and New York the fastest rough sea route doesn't follow the shortest track, as both other routes do. But there are no extreme wave conditions that prohibit taking the shortest way, neither in the rough weather case. Furthermore it is no restriction of the applied B-spline modeling technique, like a southern overshoot due to the northern perturbation in advance. This disfigurement is caused by the applied optimization method, the MOGA. Taking the shortest track between Newfoundland and New York yields an improvement of 0.5 hours in *ETA*, i.e. the attainable improvement is relatively small. Applying elitism during the optimization ensures that the fastest variants are taken over to the next generation. Nevertheless, the probability to be considered for recombination, mutation, and crossover depends on the fitness relative to other members of the generation. Therefore, when having flat shaped optima like here, an improvement of the optimization result becomes less probable the more the optimum is reached.

It has to be kept in mind, that the applied MOGA is not at all adapted to the route optimization problem. Fore sure this is an important task for further research.

The optimizations at various weather conditions show that the rough weather case is the most challenging case for a route optimization. For this reason all following investigations focus exclusively on the rough sea condition.

6.2 Wave spectra variation

Considering the applied wave data of ECMWF, peak periods of 13 – 15s (ω = 0.4 – 0.5 rad/s) are typical in the vicinity of rough weather in the North Atlantic. Therefore the wave spectra represented in Fig. 56 are typical for a sea state that can be found in rough weather areas. The figure shows an ECMWF-1D spectrum compared to a JONSWAP and a PIERSON-MOSKOWITZ spectrum built by the appropriate wave parameter $H_{1/3}$ and T_p. Obviously the spectral distribution of wave energy strongly depends on the applied spectra. With a peak periods T_p of 13.5s, they show a mean wave length of about 300m that is approximately the length of the considered ship. It is assumed that the application of different spectra causes differences in the predicted ship motion. Consequently a route optimization result should be affected as well, especially when it is governed by constraints.

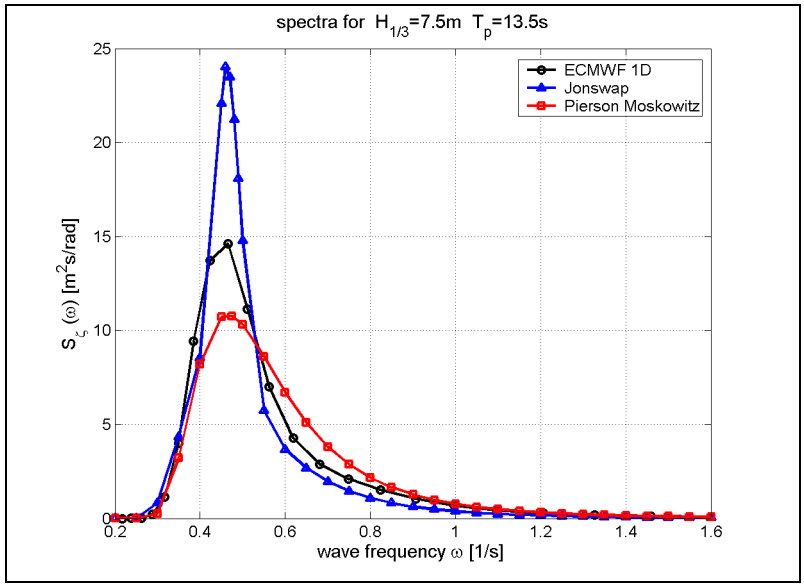

Fig. 56: Typical storm spectra for the North Atlantic, PIERSON-MOSKOWITZ, JONSWAP and ECMWF-1D spectrum

To analyze this phenomenon, two comparative optimizations are conducted. Both use the deterministic rough-weather forecast. In one case the wave parameter are associated with a JONSWAP spectrum, in the other case a PIERSON-MOSKOWITZ spectrum is applied. The application of the rough weather forecast ensures that the optimization result is governed by constraints. Fig. 57 depicts the PARETO designs for these optimizations. In the range of *ETA* from 148 – 159 h no remarkable difference in the PARETO frontiers is found. However, below 147h the frontiers separate and the application of the PIERSON-MOSKOWITZ spectrum provides more feasible designs down to 143h. To prove that this is not just a defect of the optimization, all designs evaluated during the MOGA optimization applying the PIERSON-MOSKOWITZ spectrum are recalculated applying a JONSWAP spectrum.

The recalculation approves the former optimizations as shown in Fig. 57[14].

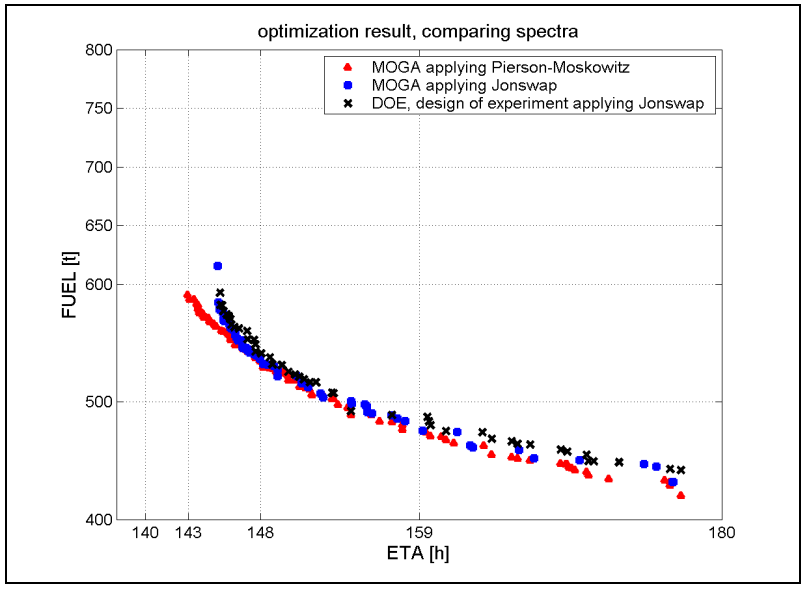

Fig. 57: Optimization result applying a PIERSON-MOSKOWITZ and JONSWAP spectrum

To investigate the reason for the differences in the optimization results, the focus is put on the active constraints. Tab. 10 gives maximum, minimum, and mean values for significant amplitudes of vertical accelerations on the bridge and for slamming probability regarding the optimizations shown in Fig. 57. Below the number of routes, thereof infeasible routes and the number of active constraints, absolute and as percentage of all routes are given. *C_zacc* for example denotes the constraint for vertical acceleration on the bridge. Remarkable differences are found for the constraints that control the maximum acceptable slamming probability *C_slprob* and the specific fuel oil consumption *C_spef*; the latter becomes active in case of main engine overload.

Tab. 10: Comparison of JONSWAP and PIERSON-MOSKOWITZ spectra

		JONSWAP			PIERSON - MOSKOWITZ		
		min	mean	max	min	mean	max
***zacc* [m/s²]**		0.09	0.16	0.27	0.09	0.16	0.25
***slprob* [%]**		0	0.44	7.8	0	0.2	5.3
number of	**routes**	18964 (100%)			18925 (100%)		
	infeasible	11483 (61%)			10682 (56%)		
	active *C_zacc*	10409 (55%)			10361 (55%)		
	active *C_slprob*	**529 (3%)**			**229 (1%)**		
	active *C_spef*	**3725 (20%)**			**1544 (8%)**		

To verify this evaluation 33000 randomly produced designs presented in Tab. 11 are investigated (for a sufficient coverage of the design space the variables *RTD* and v_9 are set constant. 15 free variables are remaining: $2^{15} = 32768 \rightarrow 33000$ designs. This means that for each free variable, there are at least two design variants that differ in only one variable).

[14] Recalculated designs are called *DOE*, design of experiment. This terminology is borrowed from the generic optimization tool modeFRONTIER. Here a simple evaluation of designs without using any optimization technique is termed *DOE*.

Tab. 11: Recalculation comparing JONSWAP and PIERSON-MOSKOWITZ spectra

	JONSWAP	PIERSON - MOSKOWITZ
number of designs	33000 (100%)	
thereof infeasible	30861 (94%)	28297 (86%)
active *C_zacc*	29090 (88%)	25877 (78%)
active *C_slprob*	7538 (23%)	1326 (4%)
active *C_spef*	20790 (63%)	14077 (43%)

It shows that JONSWAP spectrum produces 8% more infeasible routes. Here even an increase of infeasible routes due to bridge acceleration is found. But while *C_zacc* is active on routes of the whole solution space, the other two constraints affect mostly fast and fuel consuming routes. It is obvious that fast routes are more vulnerable to main engine overload. Due to the ship speed the calm water resistance is relatively high and only a limited sea margin is possible. Further on, regarding active constraints, Fig. 58 and Fig. 59 show representative transfer functions and response functions for the added resistance due to waves for a wave encounter angle of 180°.

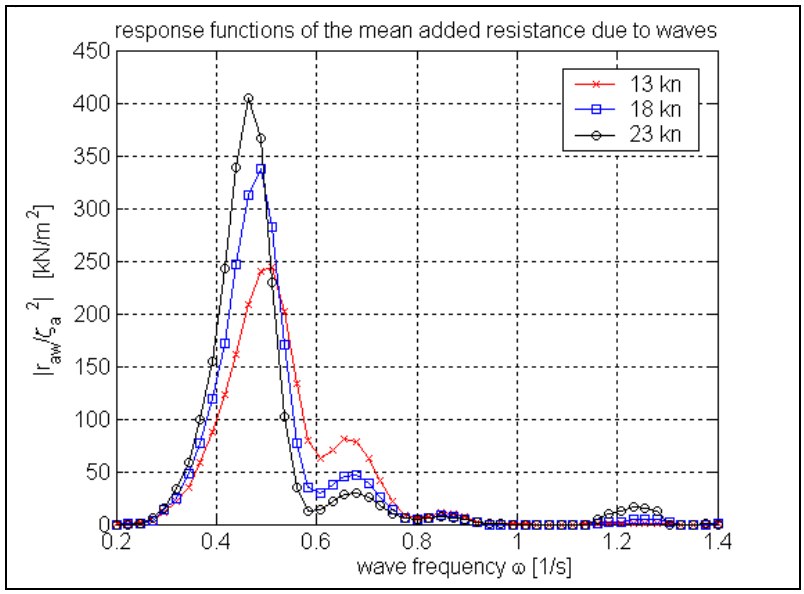

Fig. 58: Representative response functions for different ship speeds (enlarged diagram of Fig. 18)

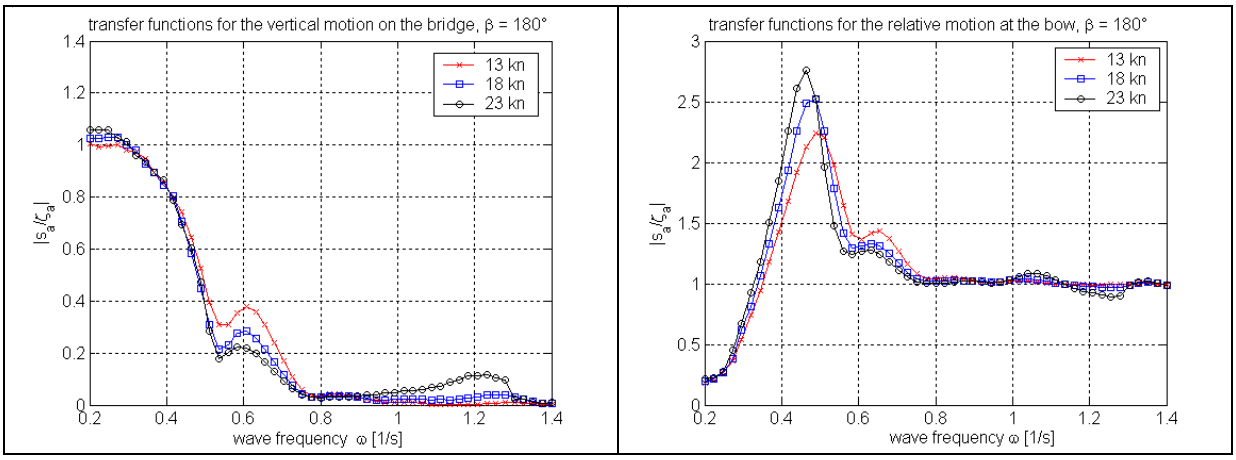

Fig. 59: Representative transfer functions for the vertical motion on the bridge and for the relative motion between water surface and bow (enlarged diagrams of Fig. 18)

The response functions for the added resistance show a pronounced peak in the frequency range where maximum wave energy can be found in a typical rough weather scenario, visible in Fig. 56. The magnitude of the peak is speed dependent but shows nearly no sensitivity within a variation of the encounter angle of up to 50° from head sea. Just the peak shifts slightly due to the shift in the encounter frequency. Consequently the increase of the added resistance due to waves at high speeds makes a main engine overload even more probable.

Regarding the transfer functions for the relative motion at the bow and accordingly the slamming probability, here also a clear speed dependency can be found. For a wave encounter angle of 180°, these transfer functions show a pronounced peak that matches the peak of the rough weather spectra. This suggests that at rough seas in particular fast routes are affected.
The transfer functions for the vertical motion on the bridge rather show an inverse speed dependency, i.e. the slower ship is affected more. Furthermore there are no pronounced peaks. The humps at $\omega = 0.6$, corresponding to a wave length of approximately 170m, are caused by the pitch motion characteristic of the vessel. This conclusion regarding the motions also holds for vertical accelerations. Finally the shapes of the transfer functions support the observation derived from the optimization results and from the recalculation.

Considering Fig. 57 the PARETO frontier applying the JONSWAP spectrum ends with a steep increase in fuel consumption for the fastest routes. This could be validated by local optimizations in this area. Thus the solution space offers the opportunity to take routes of longer distances at higher speed and accordingly higher fuel consumption, whereas the improvement in *ETA* is negligible (fastest design: *ETA* = 144.6h *FUEL* = 623t *DIST* = 2820nm, followed by: *ETA* = 144.9h *FUEL* = 574t *DIST* = 2812nm). Because of the considerable fuel savings, a route decision would take the second PARETO design into account.

To conclude, two time minimum routes are compared in Fig. 60. The one of the optimization applying PIERSON-MOSKOWITZ spectrum takes 143h, the one for the JONSWAP spectrum 145h respectively.

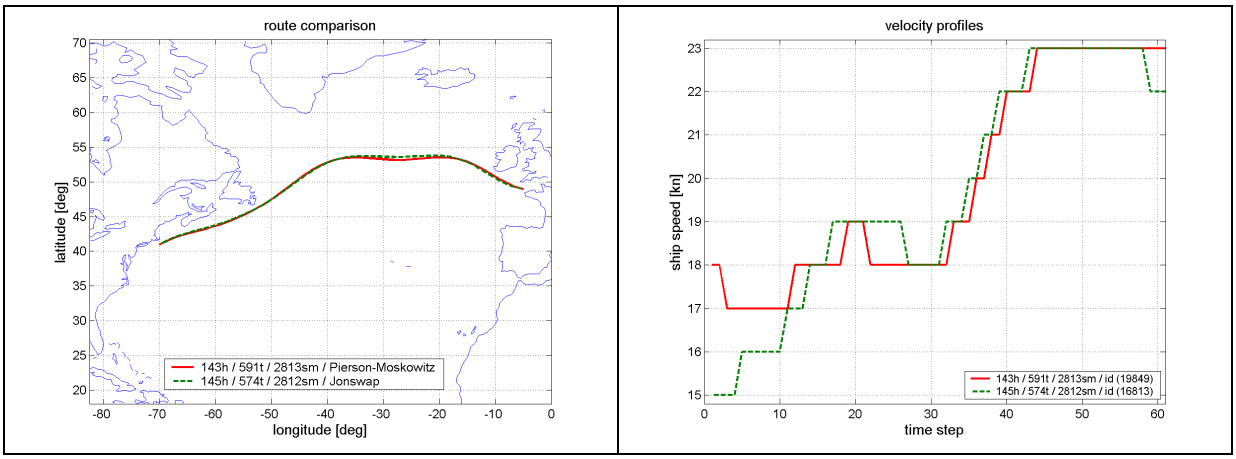

Fig. 60: Time minimum routes for the PIERSON-MOSKOWITZ and the JONSWAP spectrum

Both optimizations found more or less the same geographical shape for the time minimum route. The velocity profiles differ in particular at the beginning of the journey. Around midway these differences are balanced and finally the difference in *ETA* becomes relatively small. At least the basic trend of the velocity profiles is the same. Regarding the

investigations represented in the following sections, it can be said that taking a PIERSON-MOSKOWITZ spectrum instead of the more accurate 1-D spectra causes a negligible error. However with a view to reduce all involved sources of defect, a more accurate representation of the sea condition is desirable. For the time being the application of a PIERSON-MOSKOWITZ spectrum is absolutely sufficient to investigate this novel set-up of a routing approach.

6.3 Modified hull shape

A frequent question in connection with route optimization regards the required knowledge of the particular hull form and load condition. At least draft and trim are deciding for the determination of transfer functions, whereas the metacentric height GM_T and the radii of inertia for pitch and roll can be changed in remarkable magnitude, SEAROUTES (2003). Here the focus is put on the hull shape. To accomplish a hull form variation, two container ships with a hull topology similar to the one of HANNOVER EXPRESS are taken from the SEAWAY/OCTOPUS hull form database. They are called JOURNÈE.044, also known as S175, and VERSLUIS.051. Both ships are scaled to the main dimensions of CMS HANNOVER EXPRESS. To solely regard the influence of the hull form variation due to waves, the calm water resistance and propulsion characteristics of the HANNOVER EXPRESS are applied to both scaled ships. However, it is not the aim to conduct a systematic variation on hull form parameters that are crucial for the seakeeping behavior of a ship, but:

- to give a rough assessment on the desirable accuracy of a hull description,
- and as the applied seakeeping method for the determination of transfer functions is based on strip theory, the hull form variations also provide an insight into the sensitivity of strip theory.

Tab. 12 shows the hull properties of CMS HANNOVER EXPRESS, scaled VERSLUIS.051, and JOURNÈE.044. The lines plans available within the Seaway hull form editor are given in Fig. 61. The differences in the frame spacing between HANNOVER EXPRESS and both other ships visible in the bow and stern region in Fig. 61 do not affect the numerical result.
From the viewpoint of main dimensions they are similar ships. Nevertheless, there are distinct differences in the displacement, the centers of buoyancy, and the centers of the water-plane area. For VERSLUIS.051 and HANNOVER EXPRESS also block- and water-plane area coefficient are similar or actually the same. In this way it is possible to compare three similar ships.

Tab. 12: Hull properties of compared ships

hull parameter	Versluis.051 scaled	CMS Hannover Express	Journée.044 (S175) scaled
***LWL* / *B* / *T* (trim by stern) [m]**	293.4 / 32.25 / 11.79 (0.14)	293.4 / 32.25 / 11.79 (0.14)	293.4 / 32.25 / 11.79 (0.14)
displacement [t]	77287	74474	62609
***CB* (*LWL*)**	0.68	0.65	0.55
***LCB* to *AP* [m]**	145.1	136.2	140.4
***CWP* (*LWL*)**	0.80	0.80	0.67
***LCF* to *AP* [m]**	140.8	129.1	134.4

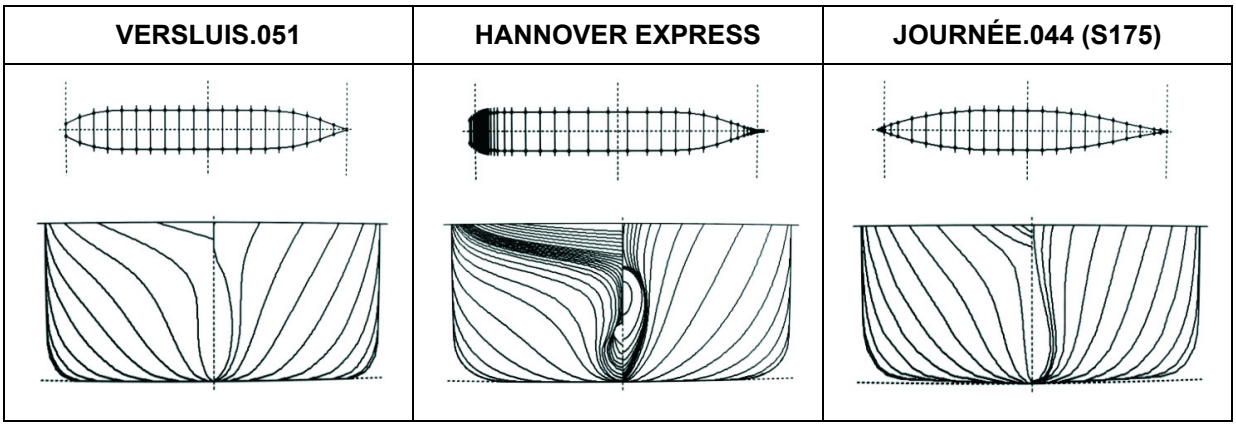

Fig. 61: Lines plans of VERSLUIS.051, CMS HANNOVER EXPRESS and JOURNÉE.044 (S175)

Fig. 62 shows diagrams for the added resistance due to heading waves at a ship speed of 23kn. Compared from left to right, only a slightly increasing resistance can be observed. Regarding the calm water resistance of 1900kN and a wave height of e.g. 6m at a peak period of 15s the total resistance would amount about 2400kN. Therefore the deviation of ±50kN would represent 2%, a small but remarkable amount.

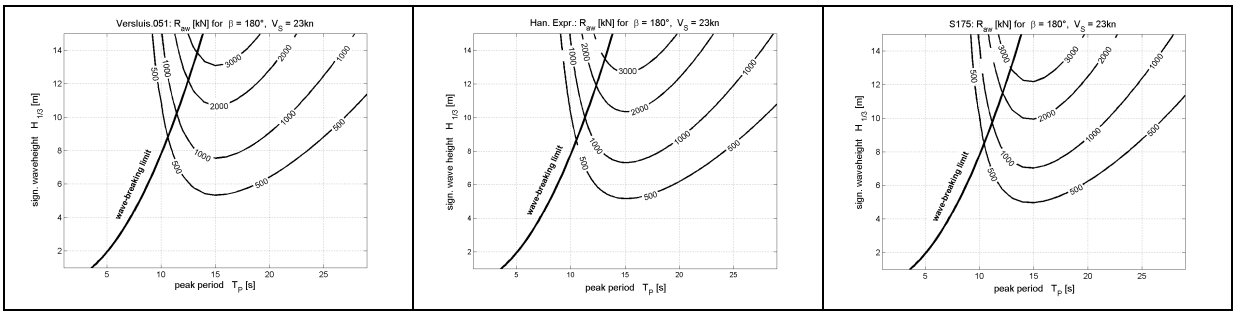

Fig. 62: Added resistances due to waves for different hull shapes

Fig. 63 shows the slamming probability in head waves at 23kn. It is the combination of all mentioned hull form parameter that impact on the heave and pitch motion and on their phase shift and consequently on the slamming probability. Therefore it is not possible to point out the deciding parameter here, but it can be seen that the probability of slamming is quite different for these three ships.

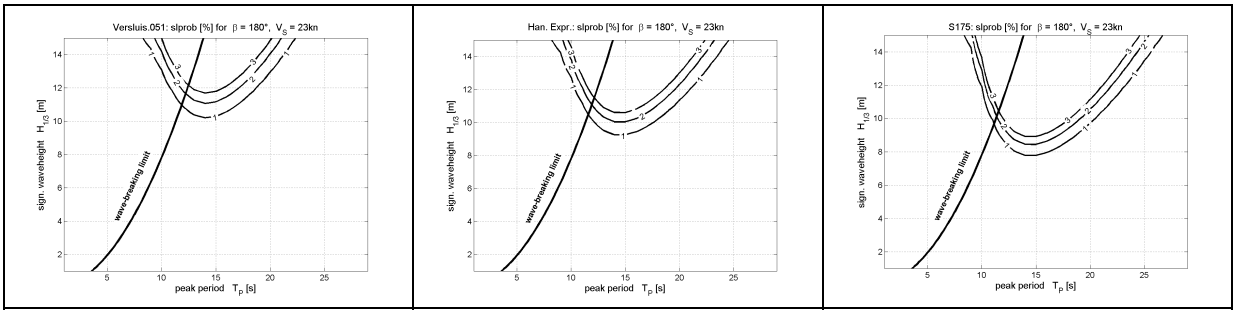

Fig. 63: Slamming probabilities for different hull shapes

Fig. 64 depicts the vertical acceleration on the bridge in head waves for a ship speed of 23kn. Here as well remarkable differences can be observed. S175 differs most distinctly from the others. For VERSLUIS.051 and HANNOVER EXPRESS the ship responses are more similar in smaller waves, but they become more different when wave heights increase.

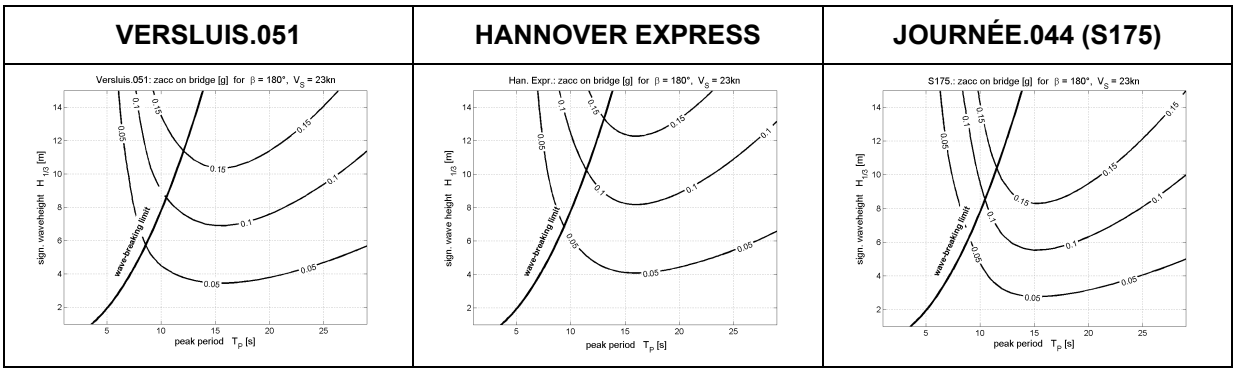

Fig. 64: Significant amplitudes of vertical accelerations on the bridge for different hull shapes

Fig. 65 shows optimization results and courses for the time minimum routes at rough sea conditions. On the left side, PARETO frontiers for *ETA* and fuel consumption, on the right side, the courses for time minimum routes are given. The differences of PARETO frontiers and courses are appreciable, compared to the influence of the weather situations, presented in section 6.1, they are quite small.

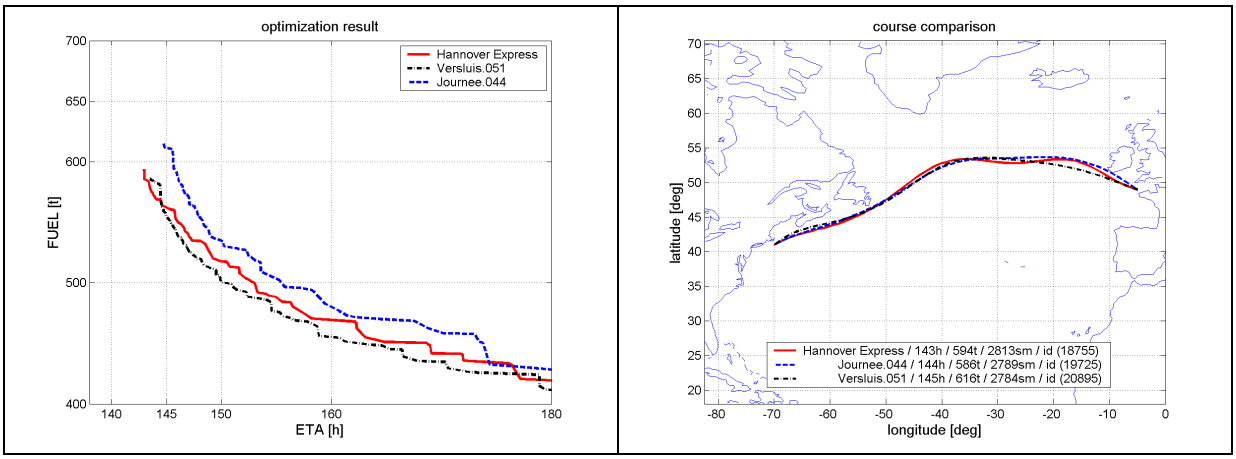

Fig. 65: PARETO frontiers and ETA_{min} routes for HANNOVER EXPRESS, scaled VERSLUIS.051 and JOURNÈE.044 (S175)

At least the velocity profiles of the ETA_{min} routes, presented in Fig. 66, show that there are clear differences between these optimum routes. In particular at the beginning of the journey CMS HANNOVER EXPRESS is able to sail faster than both other ships. In this period of the journey the ships already have to withstand a first storm region. Mainly due to the constraint posed for main engine load and vertical acceleration on the bridge, the ships have to reduce velocity. The ship with the lowest acceleration response, i.e. HANNOVER EXPRESS, is able to maintain the highest speed, and although the ship takes the longest route it arrives earlier than the others.

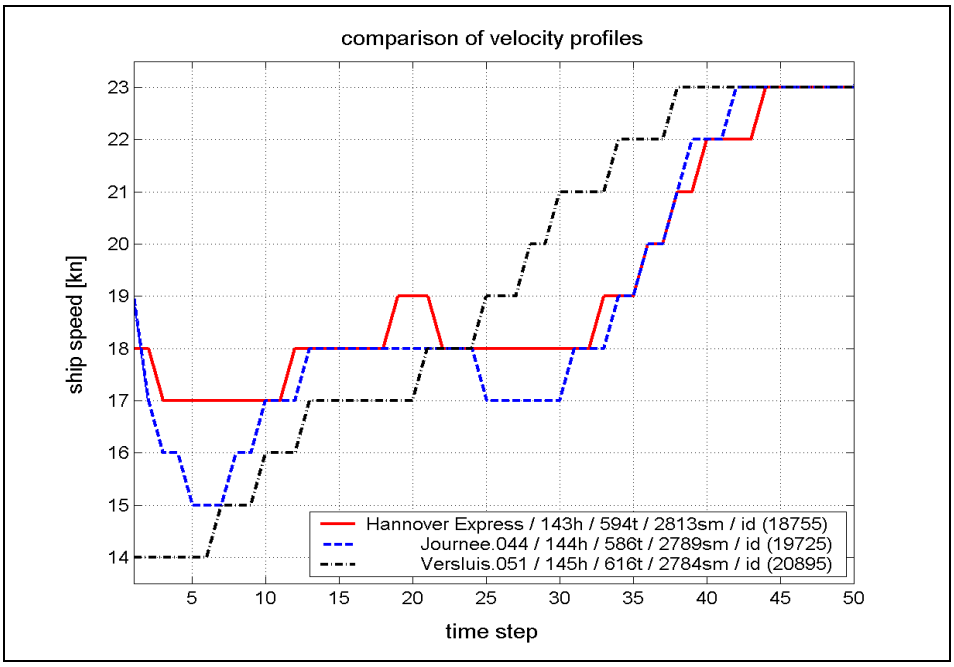

Fig. 66: Velocity profiles for ETA_{min} routes of HANNOVER EXPRESS, scaled VERSLUIS.051 and S175

Balancing the factors that are deciding for the accurateness of an optimization result suggests:

- There is no need to model the hull shape of the ship in waves with extreme accuracy while underlying conditions do not serve to maintain this accuracy. For example, balancing the effect of probable changes of the predicted weather development on the PARETO frontier (this topic will be addressed in section 6.6) and the effects of hull form variations on the seakeeping behavior (shown here) the ship behavior of a related ship may be sufficient for the modeling within route optimization. Furthermore, by applying strip theory, the hull shape above the calm water line is kept out of consideration although it affects a lot of the seakeeping ability of a vessel. Therefore neglecting the hull above the waterline may deteriorate improvements by regarding the individual hull shape and load condition.

- On the other hand, even if the differences in the PARETO frontiers and courses are relatively small, the differences of the proposed velocity profiles are remarkable. From this point of view, a proper hull description is recommended and at least a closely related hull should be used. The recommendation should be to minimize the over-all error by minimizing the partial error and therefore to use an accurate hull description whenever it is possible. In the case of rough weather conditions this becomes even more important as optimization results are governed by constraints. In this regard seakeeping prediction based on strip theory turns out to be a suited method. For the considered hull form variations it is sensitive enough to take an influence of the hull shape on the optimization result into account. It is decided to apply strip theory, as there is a need for a fast method for the assessment of ship responses in waves. Known disadvantages like in the prediction of roll motion or neglecting the upper hull have to be taken into account by empirical and semi-empirical methods, as far as possible.

6.4 Constraint and threshold variations

Three further aspects are identified during the investigations focusing the optimization at rough sea conditions (cp. Tab. 9 on page 71):

- The extreme number of infeasible routes due to active constraints for the vertical acceleration on the bridge indicates that this constraint may be set too harsh.
- The constraint for the slamming probability is only active in cases of machine overload and therefore it probably can be left out of consideration at least for the full load or the design load case.
- The constraints for lateral acceleration *C_xacc* and *C_yacc* do not influence the optimization at all. Independent of any admissible threshold variations, they only became active when *C_zacc* distinctly exceeded its threshold. For this reason these constraints are left out in the following.

To step forward in the matters addressed by the first two bullet points, the threshold values for the maximum slamming probability and maximum vertical acceleration on the bridge are varied separately. The influence on the optimization result is observed. If advisable, modifications to the constraints are realized and investigated afterwards.
Regarding the last bullet point, roll motions substantially contribute to the transverse acceleration on the bridge. Furthermore roll motion is surely an important parameter in the operation of ships and in particular in the operation of container ships. As explained in chapter 4 resonant rolling is not included to this first approach yet. The fact that in the following neither roll motion nor transverse acceleration is further regarded does not imply that these parameters are of subordinate importance. They can be the deciding parameter for other routes, other load cases, or other weather conditions. As regards parametric rolling, it is known that strip theory is not able to account for it. An approach to overcome this and at least to identify situations that are suspicious for parametric rolling is presented in section 4.9, first results are given in section 6.5

6.4.1 Variation of the threshold for the vertical acceleration on the bridge

Fig. 67 shows PARETO designs for an investigation considering the constraint for vertical acceleration on the bridge, *C_zacc*. The threshold is varied from 0.10 to 0.20*g*. Expectedly a tightening of this constraint increases the attainable *ETA*. For a particular time of arrival, it produces higher fuel consumption mainly caused by longer distances. Whereas the PARETO frontiers for 0.10, 0.13, and 0.15*g* (0.17*g* is very close to 0.15*g* and therefore left out in the diagram) are relatively close to each other, the frontier for 0.20*g* clearly separates. Here *ETA* can be reduced significantly but this necessitates more fuel due to higher ship speed. In view of operational costs, for fuel consumption comparable to routes at tightened constraints, an earlier arrival is possible. Actually there is only a small difference between the PARETO frontier for a threshold value of 0.20*g* and the frontier when this constraint is deactivated. In the second case the optimization result is completely governed by another constraint, namely the one for machine overload.

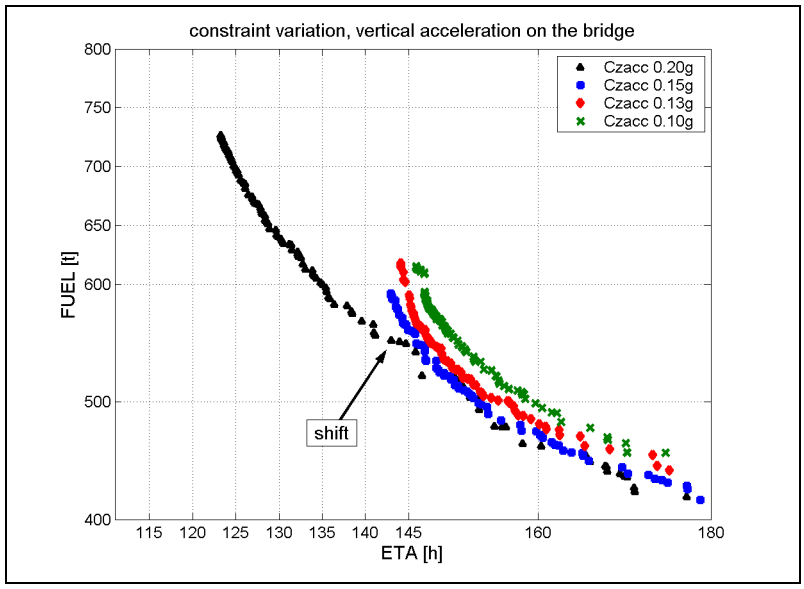

Fig. 67: Variation of the threshold for vertical acceleration on the bridge *C_zacc*

Fig. 68 illustrates the main reason for the reaction of the optimization result to the variation of *C_zacc*. It is the reduced distance and the increase of the ship speed, made possible by relaxing the constraint. The shift of the 0.20*g*-PARETO frontier towards faster route designs at approximately *ETA* = 145h, visible in Fig. 67, results from finding a shorter, still feasible, and faster route during the optimization.

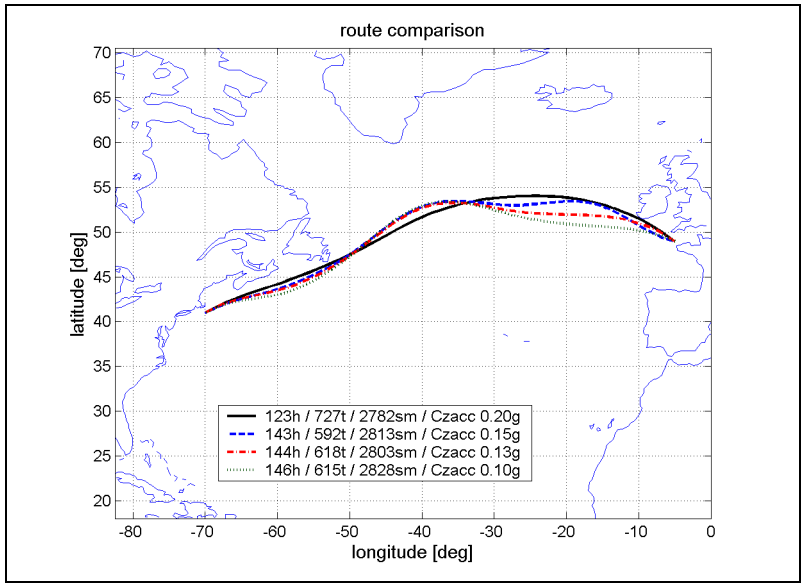

Fig. 68: Time minimum routes for varied *C_zacc*

At the end of the journey depicted in Fig. 68 the same characteristic can be found as already addressed in section 6.1. The routes do not follow the shortest track. This is the mentioned disadvantage of the genetic algorithm.
However, another rather strange result of these investigations should be mentioned. It is illustrated in Fig. 69.

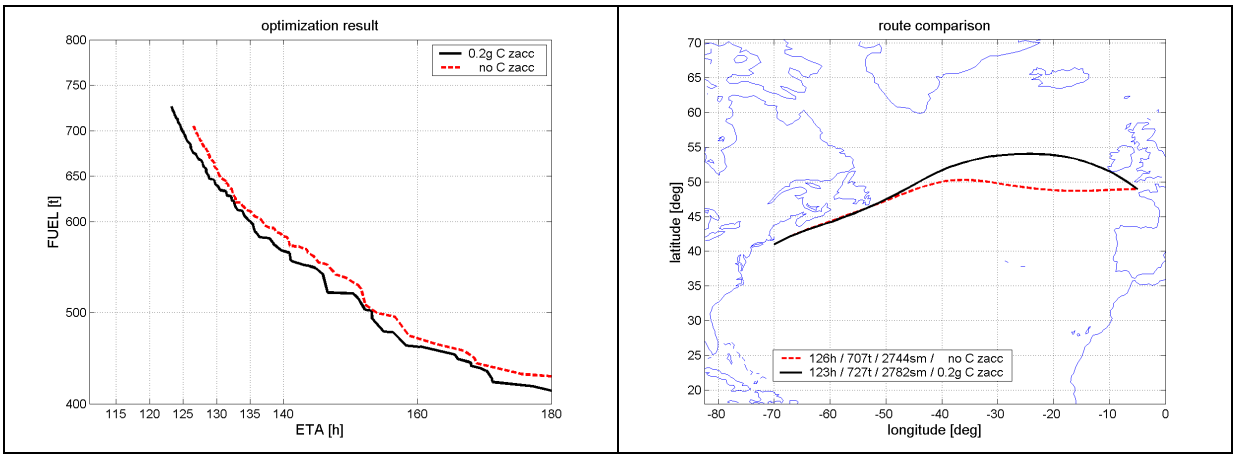

Fig. 69: Optimization result for deactivated and enabled *C_zacc*

Two optimization results are shown. One has got a threshold for *C_zacc* of 0.2*g* and the other one a deactivated constraint for vertical acceleration. The optimization with enabled constraint shows PARETO designs at decreased *FUEL* and *ETA* (left part of Fig. 69). Naturally these remain feasible when *C_zacc* is deactivated, i.e. enabling the constraint improves the optimization result. On the right hand side of the figure the time minimum routes of both optimizations are shown. The routes differ significantly. Within a range of *ETA* from 123 to 145h all PARETO results are more or less variations of the respective time minimum routes shown in Fig. 69. At *ETA* = 145h both optimizations identify PARETO designs of at least the same distance. These observations suggest that the unconstrained optimization identifies and finally sticks to a local optimum. Assuming that a stochastic method is always able to find the global maximum (what is obviously wrong) the optimization has to be ranked as incomplete. Furthermore, considering Fig. 50, it is reasonable to ask for the quality of an optimization result. A local optimum with high tolerance to variations of free variable and consequently a great potential to react on weather changing, may be preferred to a global optimum that doesn't allow any changes. On the other hand, the shape of the ship response, as presented in Fig. 28, qualifies this position. The flat characteristic of this response function denotes that changes in $H_{1/3}$ or T_p cause relative small changes in the ship response. For this reason the violation of a constraint may be small as well and tolerable. This matter is certainly an important point within route optimization and should be addressed in continuative research.

6.4.2 Variation of the threshold for the slamming probability

The second threshold variation considers the constraint for the slamming probability *C_slprob*. During the investigations at rough sea conditions, it turned out that the threshold for the tolerable slamming probability has to be reduced from 3% to less than 0.5% to get a remarkable influence of this constraint on the optimization result. Otherwise the constraint posed for the operability of the main engine *C_spef* becomes active long before *C_slprob* approaches its threshold value. But without doubt, Panmax container vessels are able to slam in such a way that this causes damage to the ship and to the cargo.

Various aspects may be considered to step forward in this matter:

- The assumption of a statistical independence of bow emergence and velocity of the re-entry in the calculation of the slamming probability (equation 4.25) does not hold. Therefore the probability is underestimated.
- The influence of horizontal velocity components is neglected, although they contribute to the local pressure impact.
- The applied methods are not suited or may need a revision to adapt them to modern ship hull forms and ship constructions.

The first two bullet points address themes that are beyond the scope of this study, however the latter one should be addressed as far as applied methods are affected.
The applied definition of slamming follows OCHI (1964) and is conducted according to the recommendations of JOURNÉE (2000). OCHI investigated ships with a TAYLOR[15] bulb. That is why it may be reasonable to shift the slamming point an amount towards the forward perpendicular *FP* when ships with a pronounced bulbous bow are considered. Here the bulb reaches out 2%*LPP* in front of *FP*. Therefore the slamming point may be put at 8% behind *FP* instead of 10%. Furthermore, according to OCHI the critical velocity is 4.88m/s. JOURNÉE represents a second method considering a critical velocity calculation based on a critical pressure. This method is set up by CONOLLY (1974) and is based on experiments with cones and wedges. With a deadrise angle of approximately 25° at 10% behind *FP* for the vessel considered here, the pressure coefficient within this calculation amounts to C_p = 10. Following JOURNÉE the critical pressure is given by:

$$p_{cr} = 0.05 \cdot \rho \cdot g \cdot L_{PP} \quad = 150\ kN/m^2\ , \tag{6.1}$$

this results to a critical velocity of:

$$\dot{s}_{cr} = \sqrt{\frac{2 \cdot p_{cr}}{\rho \cdot C_p}} \quad = 5.4\ m/s\ . \tag{6.2}$$

These considerations show that it is possible to vary the velocity threshold and the location of the slamming point in a reasonable range. Fig. 70 illustrates SEAWAY results for a variation of the slamming point and the threshold for the relative velocity, i.e. a variation of the two characteristic parameter used by OCHI where one is varied, whereas the other one is held constant.

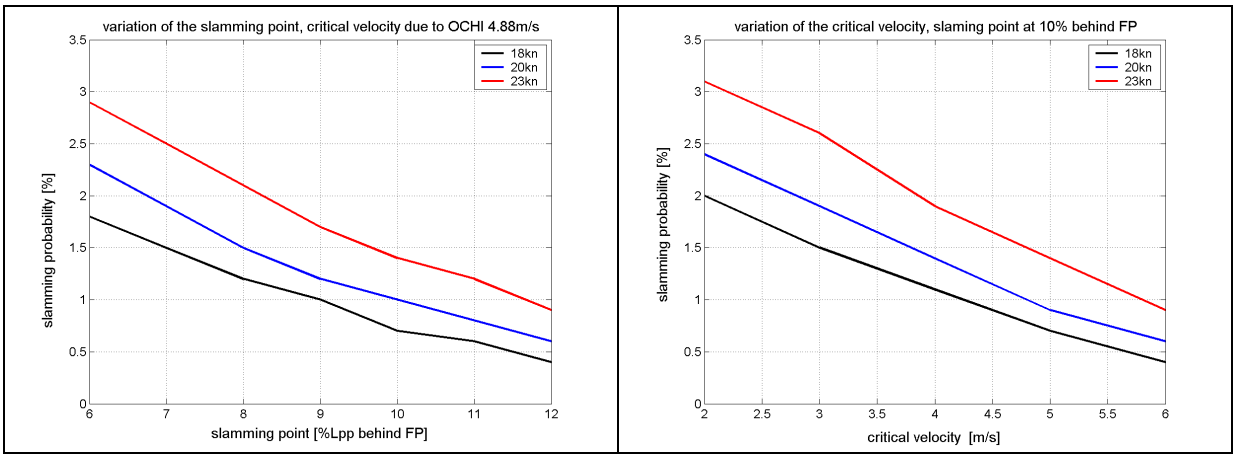

Fig. 70: Parameter variations influencing the slamming probability

[15] David Watson Taylor, naval architect and engineer, rear admiral of the US Navy, 1864-1940, USA

The slamming probability for three ship velocities is calculated at a wave encounter angle of 180° and for $H_{1/3}$ = 10m and T_p = 15s, a very extreme sea condition where the wave length approximately matches the ship length. Although slamming should be quite probable in such extreme waves, the calculated slamming probabilities do not exceed the 3% level, neither at reduced velocity threshold nor by shifting the slamming point towards the bow. However, a clear dependency on the addressed parameters is obvious and the re-consideration of these parameters and of the threshold for the slamming probability may be the most available way to come to a contemporary and appropriate method to define slamming.
The considerations above regard the CMS HANNOVER EXPRESS at design draft of 12m. Reducing the draft to ballast load condition of 9m the slamming probability would increase to 6.2%, i.e. 30 slams per hour (at $H_{1/3}$ = 10m, T_p = 15s, 23kn ship velocity, 180° wave encounter angle, and no trim).
In this context "no active constraint for slamming" is also a result of the optimization, this constraint may become active for other load conditions. Nevertheless, a reduction of the threshold value for the slamming probability seems to be recommended. This, inter alia, will be addressed in the following section.

6.4.3 Comparison to thresholds posed by NORDFORSK

So far the threshold values posed within SEAROUTES are applied here. These threshold values refer to maximum tolerable significant amplitudes of accelerations or probabilities of occurrence in case of the slamming probability. Other and more classified thresholds are established during the Nordic Cooperative Project, NORDFORSK (1987). Tab. 13 and Tab. 14 show threshold values posed within this project. Herein the threshold values are given as root mean square values, *RMS*.

Tab. 13: NORDFORSK, general operability criteria (JOURNÉE, 2001)

General Operability-Limiting Criteria for Ships [NORDFORSK, 1987]			
Phenomena	Merchant Ships	Naval Vessels	Fast Small Craft
RMS of vertical accelerations at F.P.P.	0.275 *g* (L_{pp} < 100 m) 0.050 *g* (L_{pp} > 330 m)	0.275 *g*	0.650 g
RMS of vertical accelerations at bridge	0.150 *g*	0.200 *g*	0.275 g
RMS of lateral accelerations at bridge	0.120 *g*	0.100 *g*	0.100 *g*
RMS of roll motions	6.0 deg	4.0 deg	4.0 deg
Probability on slamming	0.03 (L_{pp} < 100 m) 0.01 (L_{pp} > 300 m)	0.03	0.03
Probability on deck wetness	0.05	0.05	0.05

Following equation (4.44) the relation between *RMS* and the significant amplitude of an irregular motion follows from:

$$s_{a1/3} = 2 \cdot \sqrt{m_0} = 2 \cdot \sqrt{\frac{1}{T}\int_0^T a^2 dt} = 2 \cdot RMS \,. \qquad (6.3)$$

A detailed explanation regarding the conversion of significant and root mean square values is given in Appendix 3.

With regard to the slamming probability, JOURNÉE (2001) recommends a linear interpolation of the threshold values according to the ship length. This suggests a reduction of the threshold for *C_slprob* to 1%. Even if this does not affect the PARETO frontier of the rough weather optimization, it may affect the optimization procedure.

Tab. 14: NORDFORSK, operability criteria for various types of work (JOURNÉE, 2001)

Operability-Limiting Criteria for Accelerations and Roll Motions for Various Type of Work and for Passenger Comfort [NORDFORSK, 1987]			
Phenomena	*RMS* of Vertical Accelerations	*RMS* of Lateral Accelerations	*RMS* of Roll Motions
Light manual work	0.20 *g*	0.10 *g*	6.0 deg
Heavy manual work	0.15 *g*	0.07 *g*	4.0 deg
Intellectual work	0.10 *g*	0.05 *g*	3.0 deg
Transit passengers	0.05 *g*	0.04 *g*	2.5 deg
Cruise liner	0.02 *g*	0.03 *g*	2.0 deg

Regarding the threshold for the vertical acceleration on the bridge, the threshold for intellectual work as given in Tab. 14 should be applied to ensure situation awareness in dangerous situations. This would result in a threshold of 0.2*g* for maximum allowable significant amplitude of vertical acceleration, i.e. a considerable lowering of the constraint. To summarize the above made considerations:

- The threshold value for the slamming probability may be tightened to 1%.
- Additional the slamming point can be shifted to 8% behind *LPP*.
- Following Tab. 14 the threshold for the significant amplitude of vertical acceleration may be put up to 0.2*g*. According to Tab. 13 it is even 0.3*g*.

Results of the optimizations with adjusted constraints and thresholds are presented in section 6.4.5. But before, a further method considering vertical acceleration, the motion sickness incidence *MSI*, should be discussed. This is to reassure that a lowering of the constraint for acceleration on the bridge is admissible.

6.4.4 Comparison of the motion sickness incidence *MSI* and significant values for vertical acceleration

According to Tab. 13 and Tab. 14, a *RMS* of 0.1*g* to 0.15*g* of vertical acceleration on the bridge seems acceptable. This would result in 0.2*g* to 0.3*g* of significant amplitude of vertical acceleration. Thus the constraint for vertical acceleration *C_zacc* applying a threshold of 0.15*g* seems to be set too harsh. On the other hand, the duration of the exposure to the motion and the frequency of excitation, both important parameters to analyze kinetosis, are neglected. Therefore the *MSI* producing an optimization result comparable to a threshold of 0.15*g* for *C_zacc* is identified. By getting a further indicator for the load on the crew, it should be possible to get a comprehensive view on this matter.

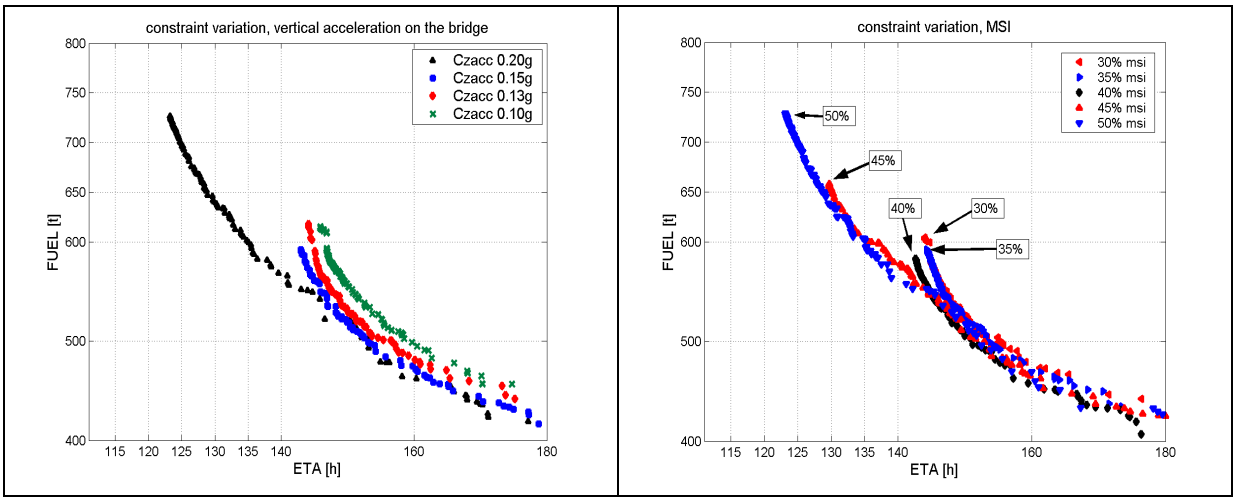

Fig. 71: PARETO frontiers applying different thresholds for the vertical acceleration

Fig. 71 shows both, the PARETO frontiers of Fig. 67 produced by optimizations applying different thresholds for significant amplitudes of vertical acceleration and the results for various thresholds applying *MSI*. Posing 0.2*g* for maximum significant vertical acceleration would require an admissible *MSI* of approximately 50%, an extremely high value. But also the *MSI* related to 0.15*g* lying at about 40% *MSI* is still enormous. It has to be said that the applied concept to calculate *MSI* does not integrate the exposure to accelerations of consecutive time steps of a ship route. That is why the load on the crew is rather underestimated by the *MSI* given here. In this regard, a lowering of the constraint for the vertical acceleration as suggested by the NORDFORSK data is refused. So far it seems recommended to keep the threshold for vertical acceleration on the bridge at 0.15*g* for significant amplitudes or at an *MSI* of 40% respectively.

6.4.5 Optimizations with modified constraints

Closing this matter, the following four optimizations with modified constraints will be compared, i.e. moderate variations of the constraints for the slamming probability and the acceleration on the bridge as applied so far. This investigation serves to gain insight to the functioning and to the interaction of applied constraints and the optimization method. The threshold value combinations and resulting PARETO frontiers, given in Fig. 72, are:

- *slprob* of 1% at 8% *LPP* behind *FP* and a *MSI*= 40% → Curve 1,
- *slprob* of 1% at 8% *LPP* behind *FP* and a *MSI*= 30% → Curve 2,
- *slprob* of 1% at 8% *LPP* behind *FP* and *C_zacc* = 0.15*g* → Curve 3,
- *slprob* of 3% at 10% *LPP* behind *FP* and *C_zacc* = 0.15*g* → Curve 4.

To enhance the overview, the PARETO designs of Fig. 72 are connected by lines and not depicted as dots. Dashed lines mark the position of PARETO designs applying *MSI*, solid ones represent the acceleration threshold counterpart.

Curve 4 depicts the PARETO frontier applying the previous constraints (*zacc* = 0.15*g*, *slprob* = 3%). It is enveloped by the frontiers applying 30% and 40% *MSI*. Curve 3 represents the PARETO frontier preserving the acceleration threshold of 0.15*g* but reducing the one for the slamming probability to 1% at 8% behind *LPP*. Even if differences in the PARETO frontiers are relatively small, less than 1% *ETA* and 3% *FUEL* for the fastest designs, there are differences caused by the interaction of the applied constraints as well as by the applied optimization method.

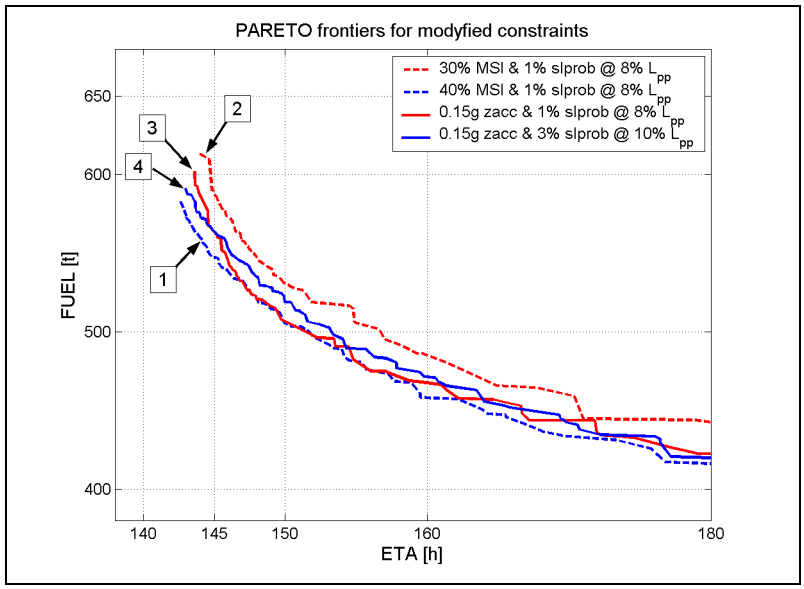

Fig. 72: Optimization results for modified constraints

Fig. 73 illustrates the achieved distances of the PARETO designs represented in Fig. 72. It can be seen that referring to the distance, in the low *ETA* region the PARETO designs clearly separate.

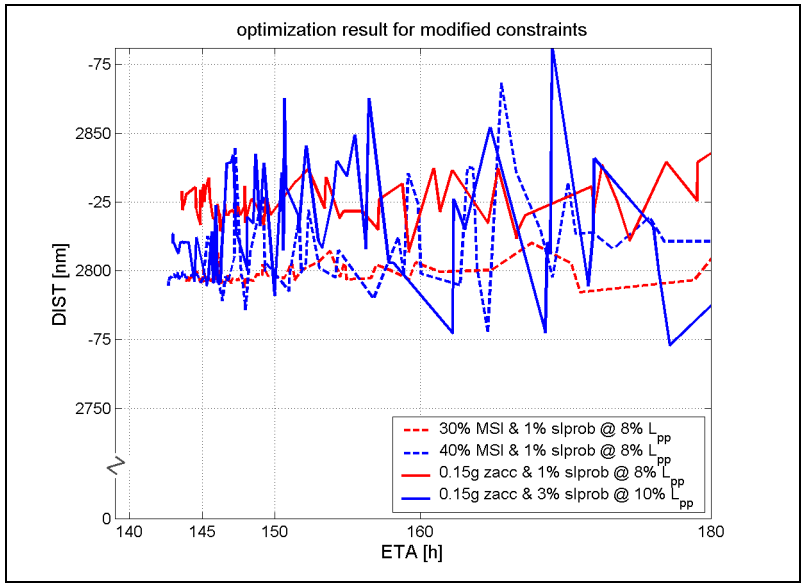

Fig. 73: Distance over *ETA* for modified constraints

Fig. 74 illustrates the courses of the fastest route from each of the optimizations, the ETA_{min} routes of curve 1 – 4.

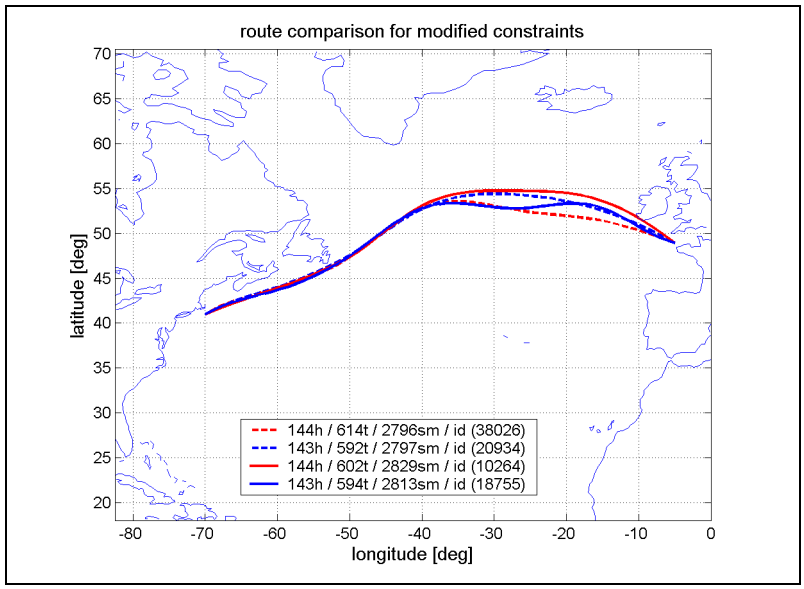

Fig. 74: Fastest routes for modified constraints

Four conclusions are supported by these optimizations:

- In no case, the PARETO frontier is directly affected by the constraint for the slamming probability, i.e. filtering the designs following to the optimization by enabling or disabling this constraint does not change the shape of the PARETO frontier or changes the attribute of a PARETO member from feasible to infeasible. But in contrast to the former threshold (3% at 10% *LPP* behind *FP*), the optimization applying the tightened threshold (1% at 8% *LPP* behind *FP*) produces about 5% infeasible designs that are infeasible due to this constraint exclusively. This shows that a reasonable variation of this constraint as discussed above makes it affecting at least the optimization procedure. Therefore it seems recommended to maintain this constraint for a route optimization, anyhow.
- Comparing the optimization results for the threshold of 0.15*g* maximum significant amplitude of vertical acceleration (curves 1 + 2), the PARETO frontiers do not clearly separate. Nevertheless, even if PARETO frontiers are quite close to each other, the shape of the fastest routes clearly differs, as can be seen in Fig. 74. Furthermore Fig. 73 shows that these routes take tracks of a bit more distance, compared to the routes where *MSI* is applied. Cross calculations, i.e. evaluating the optimization result of one optimization with the constraints of another optimization, suggest that this again may be the weak point of the MOGA mentioned above. The designs of both PARETO frontiers remain feasible when replacing the appropriate slamming constraint. Either the MOGA sticks to a local optimum or it doesn't proceed due to the insignificance of the achievable improvement. However, a further adaptation of the MOGA or any other suited multi objective optimization algorithm is necessary.
- In the range of *ETA* = 147h - 155h the PARETO frontiers for 40% *MSI* and 0.15g *zacc* (cures 1 + 3) mostly overlap. At low speed, above *ETA* = 155h the frontiers separate. This is caused by different start designs in the first generation of the optimizations. By contrast, the separation of the frontiers below *ETA* = 147h is caused by the different constraints referring to vertical acceleration. In this region the PARETO designs

achieving a threshold of 0.15*g* in significant amplitude of vertical acceleration show a *MSI* above 40%. Finally both methods, applying thresholds for *MSI* or for significant amplitudes of vertical acceleration, are useful to pose a constraint. It is a matter of taste to put the focus on the duration of an exposure or on maximum values or on both.

- All routes in Fig. 74 differ only in the first half of the journey. Considering Fig. 48 on page 61 shows that it is the circumnavigation of the first storm (upper right part of Fig. 48). Here the differences in the constraint for the vertical acceleration cause the differences of these route designs. Besides differences in the velocity profiles, which are not shown here, a remarkable lateral displacement is obvious. Although the routes show a lateral shift of approximately 3° (180nm = 333km) their difference in *ETA* is only 1h. Compared to the medium- and calm weather optimizations the difference in fuel consumption of 3% is relatively small, too. So far it seems that sizeable variations of the constraints influence, but not dramatically distort, an optimization result. In other words, there may be a considerable range of admissible route variations without deteriorating the qualities marked by the PARETO designs. This characteristic may rapidly change when further constraints are applied and of course, these assumptions deserve further study.

6.5 Parametric rolling

Parametric rolling is one of the main reasons for cargo losses in seaborne container transportation. According to the importance of this topic it is worth to investigate how often sea states that are suspicious for parametric rolling occur during the route optimization. Since most mathematical models, e.g. strip theory, account only for a coupling of surge, pitch and heave or sway, roll and yaw respectively, they are not able to predict this motion sequence. Nevertheless, the module established in section 4.9 may serve to answer the question, if parametric rolling should be included to route optimization or not. Even if it is not able to predict, it may help to avoid this kind of extreme roll motions.
To investigate in this matter the constraints developed in section 4.9 are added to the previously applied constraints. Thresholds considering the absolute and the relative wave height are checked for plausibility. The effect of these constraints to optimization results is evaluated.

6.5.1 Initial investigations

In the following the approach for parametric rolling and its two variants, applying a threshold (i) for the encountering wave height and (ii) for the relative wave elevation at *FP*, *COG*, and *AP* are investigated. Tab. 15 summarizes the constraints as posed for these investigations. Besides general constraints controlling machine overload, geographic feasibility, and the maximum acceptable duration of the journey also the constraints for slamming probability and motion sickness incidence are used. These are set to thresholds identified in the previous sections. All parameters used within the assessment of parametric rolling account for the **n**umber of times **p**er **h**our a situation occurs that may excite this motion. Therefore the threshold names start with *nph* and the ending indicates if the criterions for *FP*, *COG*, *AP*, or the critical wave height are faced (*nph4h*$_{crit}$, to be read as *nph* for h_{crit}, and *nph@ap* as *nph* at *AP*).
Threshold values are set to <1>, i.e. maximal one exceeding per hour of the thresholds posed in section 4.9 is tolerated.

Tab. 15: Applied constraints for the investigation of parametric rolling

parametric rolling investigation	constrained parameter	content	threshold
basic constraints	*slprob*	slamming probability at 8% *LPP* behind *FP*	1%
	MSI	motion sickness incidence	40%
constraints for the relative wave elevation	*nph@fp*	times per hour a threshold value for the relative motion between ship and water surface is exceeded	1time x 6m
	nph@cog		1 time x 5m
	nph@ap		1 time x 4m
constraints for the absolute wave height	*nph4hcrit*	times per hour a threshold value for the wave height is exceeded	1 time x 10m

Fig. 75 shows four PARETO frontiers. The right diagram of the figure is a cutout of the low *ETA* region from the left diagram.

- The solid black line represents the optimization result where no constraints for parametric rolling are posed.
- The blue-dashed line represents the result when constraints for the wave elevation relative to the ship are set.
- Blue dots are related to constraints for the absolute wave height.
- The red-dash-dotted line represents the optimization result where both types of constraints are used. It is congruent to the line representing the PARETO frontier for the enabled constraint that observes the relative wave elevation.

Surprisingly the application of an additional constraint serves to improve the optimization result. For the same *ETA*, routes of slightly lowered fuel consumption are found and *ETA* itself could be reduced by 1h. In particular the constraints for the relative wave elevation seem to serve in this regard. As a matter of course, the improved PARETO frontier stays feasible when all parametric rolling constraints are deactivated. That means there is no obvious reason that it was not found before, without applied parametric rolling constraints.

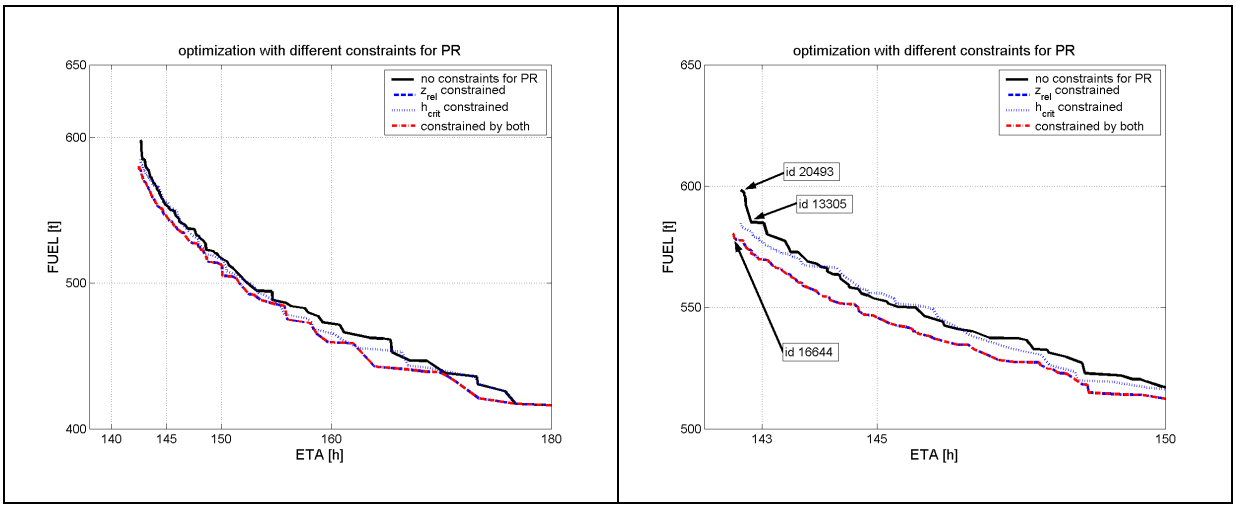

Fig. 75: PARETO frontiers for optimizations considering parametric rolling

In the right part of Fig. 75 three time minimum route designs are marked. Because of the steep ascent of the PARETO frontier, two routes of the optimization without, and one time

minimum route for the run applying both types of parametric rolling constraints are chosen for further comparison. Fig. 76 shows these three routes.
Those routes where no parametric rolling constraints are applied take nearly the same course. The one where all parametric rolling constraints are applied takes a shorter course, which is more northern in the beginning of the journey. Assumedly this again relates to the characteristics of the genetic algorithm as observed in section 6.1, i.e. not completely converging if achievable improvements are small.
A recalculation of fast routes taken from the optimization result with deactivated parametric rolling constraints shows that several of these routes would be infeasible if these constraints are enabled. Applying parametric rolling constraints serves to deplete the population in the low *ETA* region. In this way selective pressure increases and the chances for alternative solutions to become dominant improve. Although this is an unintended effect, it is beneficial for the convergence of the optimization procedure.

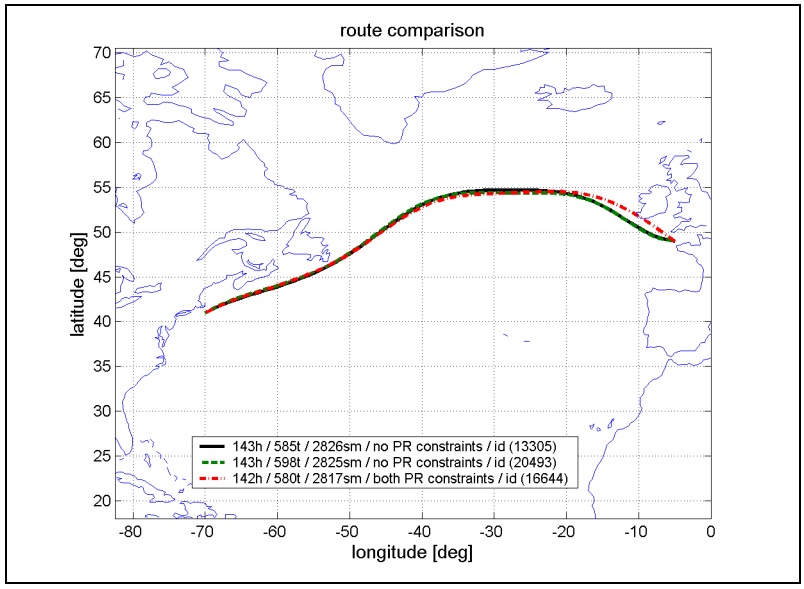

Fig. 76: Routes of minimum *ETA*

In conclusion the attainable *ETA* and the fuel consumption do not vary greatly, and in this regard the results of the optimizations remain nearly the same: An arrival on schedule is impossible and the earliest possible arrival is around 143h. In contrast to the constraints for *MSI* and accelerations that are very active on the shape of the PARETO frontier, the constraints for parametric rolling are less dominant, i.e. there are only a few routes that are ranked infeasible exclusively by these constraints and they are spread over the whole solution space. Therefore the focus should be put on each of the applied parametric rolling parameter.

6.5.2 Assessment of the sensitivity for the parametric rolling parameter

It is obvious that the considered parametric rolling constraints influence the optimization result, even if the effect on the PARETO frontier is relatively small. In the following step they are focused in detail to assess their sensitivity and to get insight into their operating behavior. For this purpose the result of the optimization applying all parametric rolling constraints is evaluated more in detail. The number of feasible and infeasible routes for this optimization is given in Tab. 16.

Tab. 16: Optimization applying all parametric rolling constraints

number of all designs	20.000
twofold generated designs	2.206
feasible designs	5.618
infeasible designs	12.176
thereof infeasible due to parametric rolling	3.276

All routes are evaluated at a number of discrete points. Regarding parametric rolling, for each route point the number of threshold exceedings is calculated and the maximum value is given back to the optimizer to decide whether a route is feasible or not. Except from about 30 routes, i.e. 1% of the infeasible routes due to parametric rolling, the most suspicious route points according to the criterion that accounts for the absolute wave height are also the most suspicious points that are identified by the constraints considering the relative wave elevation at *FP*, *COG*, and *AP*. All the variants of the constraints posed for parametric rolling provide almost the same ranking of route points regarding the constraint violations. However the magnitude of the violation, i.e. the number of times the threshold is exceeded, is different. Fig. 77 shows histogram plots for the designs that are infeasible due to parametric rolling given in Tab. 16. The abscissa depicts the maximum number of exceedings for a particular route. The height of the bars shows the number of routes with this maximum value. The exceedings are grouped in bins from 1-5, 5-10, …, and 245-250. The most left bar represents the route designs with 1-5 exceedings, those that are hardly infeasible. The ordinates are cut off at number 400. Higher bars are described by giving the numeric value.

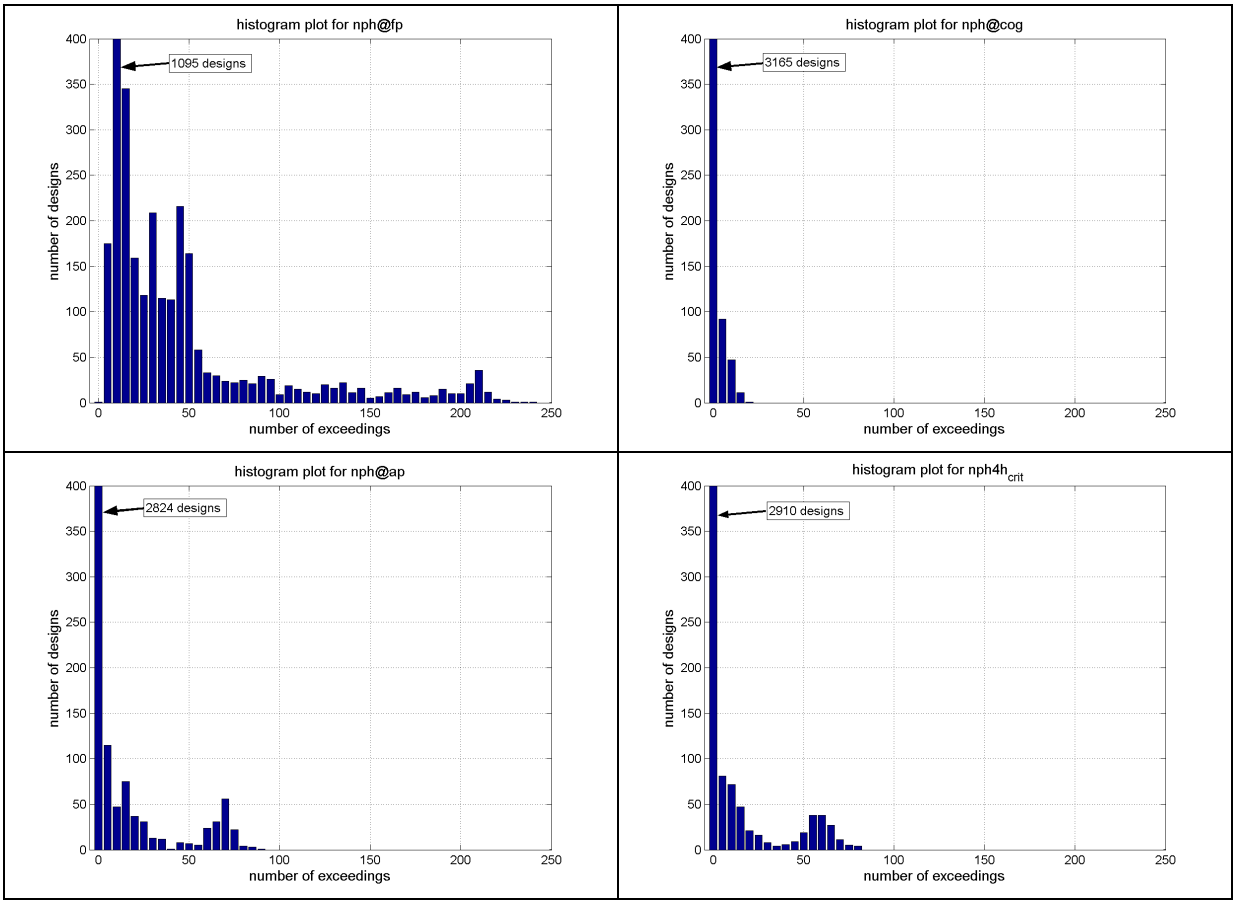

Fig. 77: Histogram plots for parametric rolling criteria

The histograms at the bottom (considering *nph@ap* and *nph4h*$_{crit}$) show a similar characteristic. Most route designs are in the 1-5 bin and only a few show a higher number of exceedings. The characteristic for *COG* is related too even if the number of routes in the 1-5 bin increases a little (*nph@cog*, upper right side). However, the histogram plot for the relative wave elevation at *FP* (*nph@fp*, upper left side) is different from all others. The maximum bar is at the 10-15 bin and also other bars nearby are relatively large. Further more there are some routes that show up to 240 exceedings of the threshold per hour. It is interesting to observe that the 1-5 bin is absolutely empty. Obviously the parameter that assesses the exceedings of the relative wave height at the bow reacts much more sensitive. This could imply that the threshold is set too harsh, on the other hand it is self-evident as in head seas like here, the relative wave elevation at the bow is much larger than at other parts of the ship, because encountering waves coincide with large vertical motions by pitching. Therefore high values regarding the relative motion at the bow appear plausible. To step forward in this matter, model tests or further simulations would be needed. Here the functioning of the parametric rolling constraints will be illustrated by a further example and a resultant parameter variation regarding the admissible relative wave height at the bow.
Fig. 78 compares the course of the feasible time minimum route from Fig. 76, the optimization with all parametric rolling constraints, to an infeasible route due to at least one active parametric rolling constraint close to this one, i.e. with a similar *ETA* and fuel consumption.

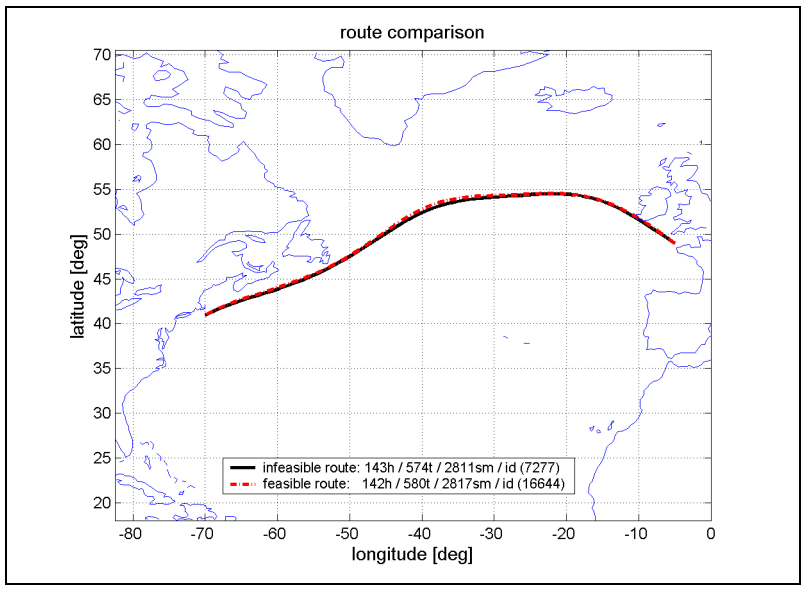

Fig. 78: Feasible and infeasible route

Both routes take nearly the same course. Certainly, there is no information about the position of the ship at a particular time, as no velocity profiles of the ships are given. For this reason both routes are evaluated again step by step. The result is illustrated in Tab. 17. The route point that caused the infeasibility of route *id* (7277) is identified. It is at 3d:3h:49min (75.8h) after departure. Then, the closest route point in time of route *id* (16644), the feasible one, is identified. It is at 3d:3h:21min (75.4h), half an hour earlier. At least both routes bring the ship at the same time to the same sea area. As can be seen in Tab. 17 the wave conditions have not changed except from the wave encounter angle. The latter one is the reason that the parametric rolling parameter of the infeasible route have been evaluated according to equations (4.55) and (4.56), whereas they are set to zero for the feasible one because the encounter angle criterion is only active from 175 – 180°.

Tab. 17: Parametric rolling parameter for compared routes

route data	feasible route *id*(16644)	infeasible route *id*(7277)
at time stamp [d:h:min]	3:3:21	3:3:49
$H_{1/3}$ [m]	4.3	4.3
T_P [s]	14.8	14.9
enc. angle [deg.]	167	177
V_s [kn]	17	18
nph@fp [1/h]	0	11.35
nph@cog [1/h]	0	0
nph@ap [1/h]	0	0.01
nph4hcrit [1/h]	0	0.01

Fig. 79 shows both routes at the time given in Tab. 17, displayed in the wave field interpolated for a time at 3d:4h. The figure serves to illustrate that both designs share the same sea area at the same time and that both ships do not encounter extraordinary high waves.

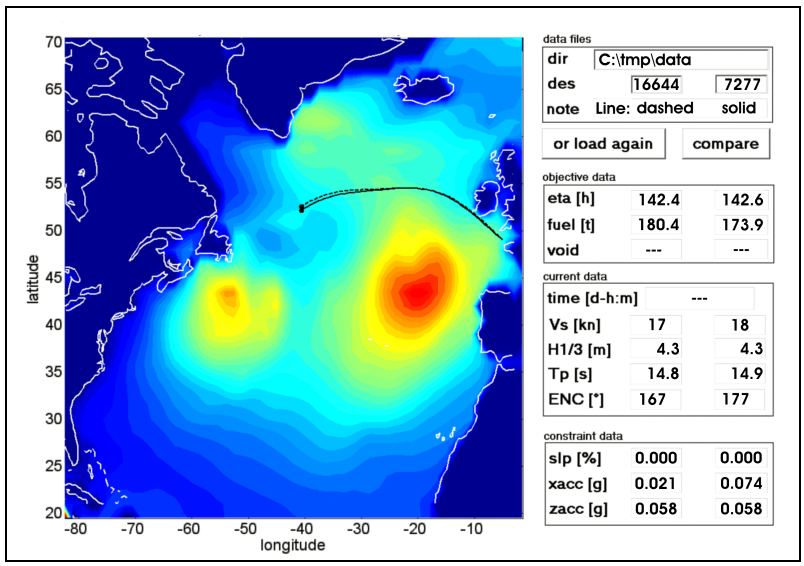

Fig. 79: Parametric rolling, route comparison

Again the conclusion is that (i) either the constraint for the relative wave elevation at the forward perpendicular is set too harsh or (ii) a harmless appearing situation may bear a risk of parametric rolling. However, also both conclusions can turn out to be true. The first conclusion has to be addressed in route optimization, whereas the second one relates to operational aspects.

Regarding route optimization, section 6.5.3 presents results for variations of the threshold value for the relative wave elevation at the forward perpendicular.

Regarding operational aspects, it is known that parametric rolling can cause abruptly increasing roll angles and -accelerations. This motion behavior often occurs unexpected but needs to be identified immediately to induce suited countermeasures. Analytical methods like e.g. developed during the research project SinSee – evaluation of ship safety in severe seas, cp. CLAUSS and HENNIG (2004), and finally implemented in several on-board monitoring systems help to increase situation awareness and support in save navigation. In general polar plots are employed to display hazardous operating conditions depending on wave height, wave encounter angle, and ship speed. Fig. 80 gives two examples for these approaches.

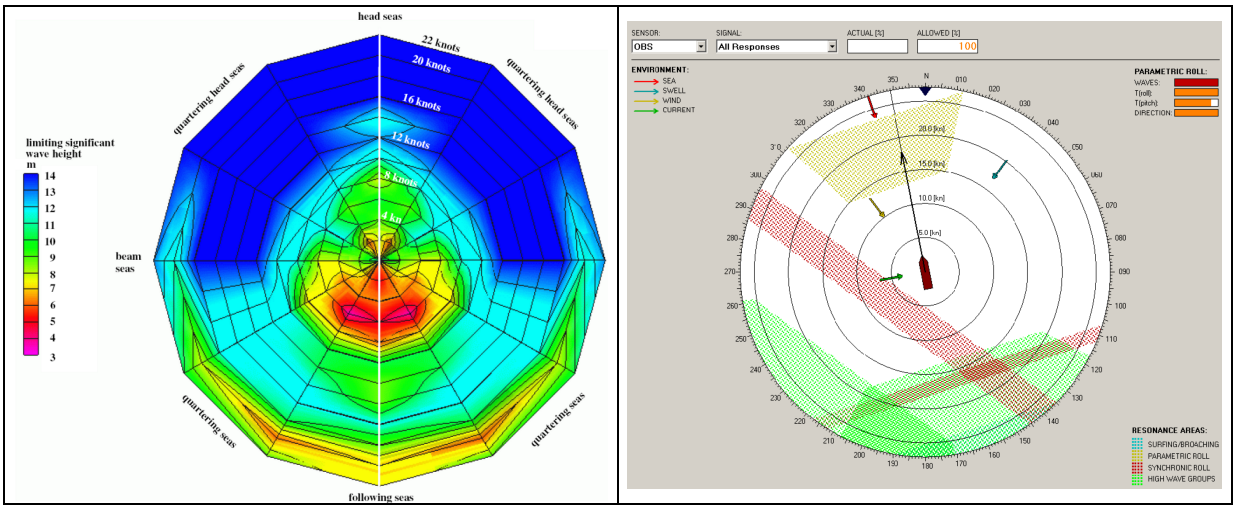

Fig. 80: Polar plots, left side: limiting significant wave heights depending on ship speed and encounter angle, right side: screen shot from OCTOPUS RESONANCE
(left side CLAUSS (2008), right side http://www.amarcon.com)

6.5.3 Increasing of the threshold value for the forward perpendicular

To take a step further in this matter, the threshold for the relative wave height at *FP* is increased to 7m and 8m, respectively. For route *id* (7277) of Tab. 17 this would cause a *nph@fp* of 3.2 respectively 0.74 exceedings per hour, i.e. for a threshold of 8m the route becomes feasible. The histogram plots in Fig. 81 illustrate the effects on all routes that are infeasible due to parametric rolling during the optimization. Already when increasing the threshold to 7m, the 1-5 bin becomes the maximum one. Expectedly the number of routes in the lower bins further increases, when the threshold is set to 8m. But in all cases, the histograms for forward perpendicular *FP* show more routes with a high number of exceedings than the histograms for *COG* and *AP* or those for the critical wave height.

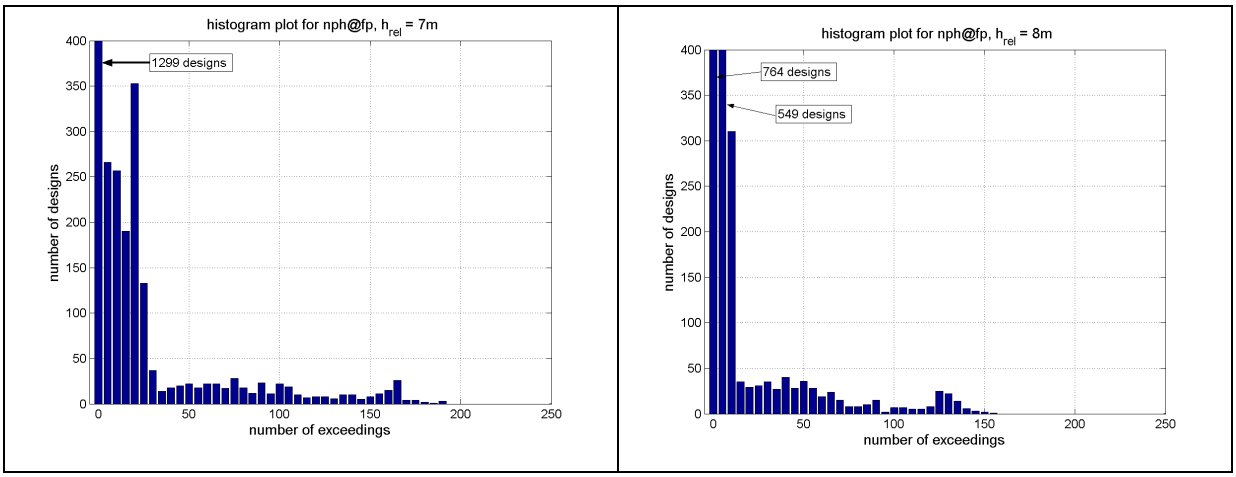

Fig. 81: Histogram plots for a threshold for h_{rel} of 7m and 8m

It has to be borne in mind that the used thresholds for the relative wave elevation are roughly estimated. Anyhow, the constraint considering the relative motion at *FP* behaves different from the other ones. Whereas a threshold of 6m produces a lot of infeasible designs a threshold of 8m seems to be a quite risky and high value compared to Fig. 44.

On the other hand a threshold of 8m produces a similar histogram plot like the threshold for the critical significant wave height and for this reason it seems permissible. Finally it would be interesting to extend the focus on the relative motion within further investigations, i.e. simulations and model tests.
Definitely, the proposed method is only a first step to establish a parameter that allows to handle the risk of parametric rolling and to avoid hazardous situations. Considering the assessment of threshold exceedings per hour it works and behaves suitable being used as constraint. It serves to identify critical situations, and regarding the wave height it behaves moderate, i.e. there are no jumps in the constraint functions. However, referring to encounter angle, wave length, as well as encounter and pitch period, the proposed constraint functions work like a switch, a behavior that is unfavorable to constraints. General in optimization it is preferable to use constraint- and objective functions that show only minor changes of the function value at minor changes in the design phenotype. To overcome this behavior, it is possible to use e.g. a ramp instead of a jump function to pose a weight, related to the distance of the current operating point to a range that is considered as critical. In this way a fuzzy transition from feasible to infeasible can be realized.
In addition these constraints may become somewhat like the master's choice. Based on the numerical investigations the minimum safety requirements for a particular ship are posed. Additional the master extends these requirements according to his/her experience.

6.6 Robust optimization

So far, analyzed weather data are applied as deterministic forecast. This will be continued in the following, as no real deterministic forecast is available yet. The comparisons of optimization results for deterministic-, mean- and ensemble forecasts still use and also call the analyzed weather as deterministic forecast. This has no influence on the argument and on the conclusions regarding the benefit of robust optimization. Nevertheless this circumstance will be adjusted in section 6.6.4.

Robustness in optimization denotes the ability of an optimized design to stay optimal even if essential parameters of the considered system are modified. In this consideration, a local optimum with a great capacity to withstand parameter changes may be favorable compared to a global optimum that loses its advantages if some system parameters deflect. Besides numerical accuracy and the decision to consider some and neglect other system parameter, the differences between the forecasted and real trend of weather are the most influencing parameter for the robustness of a route optimization result. Therefore the focus in section 6.6 is put on the influence of probable weather changes on route optimization.

The assessment of robustness against weather changes uses ensemble forecasts, the set of 50 forecasts with an equal probability of occurrence. Here robustness will be used as:

- Constraint, i.e. a route has to stay feasible in a given number of ensemble forecasts.
- Objective, i.e. the number of ensemble forecasts where a route stays feasible is to be maximized.

Besides, all other constraints and objectives stay active. Just like in the previous sections only the rough sea condition at 20. – 30.1.2002 is considered.

To make the discussion of results more comprehensive and easier to read, the following abbreviations are introduced:

- *DF*, *MF*, *EF* refers to **D**eterministic- **M**ean-, and **E**nsemble **F**orecast, used within the legends of figures.
- *EF N* refers to ensemble forecast number ***N***, with $N = (1\ldots50)$.
- *EF-id*(*M*) refers to a route optimized by applying an ensemble forecast, the route is identified by the ***ID*** number ***M***, the number is assigned by the optimizer.
- ETA_{min}-*DF* refers to the time minimum route identified by an optimization applying the **D**eterministic **F**orecast.
- ETA_{min}-*MF* refers to the time minimum route identified by an optimization applying the **M**ean ensemble **F**orecast instead of the appropriate deterministic forecast.
- ETA_{min}-*EF N* refers to the time minimum route identified by an optimization applying ensemble forecast number *N* instead of the appropriate deterministic forecast.

6.6.1 Deterministic, mean- and ensemble forecast

To step into this topic, the optimization result using the deterministic forecast is compared to results produced by utilizing other forecasts types for the rough weather condition in January 2002. Fig. 82 shows the PARETO frontiers of the optimization applying the deterministic- and simply the corresponding mean ensemble forecast. Nearly all constraints mentioned in chapter 6 are posed, i.e. 1% slamming probability, maximum 1 event per hour that is suspicious for parametric rolling and operability of the main engine. For the acceleration on the bridge a threshold of 40% *MSI* is put. Here too, the constraints considering accelerations, posed for *MSI*, and for main engine operability are the most active and deciding ones.

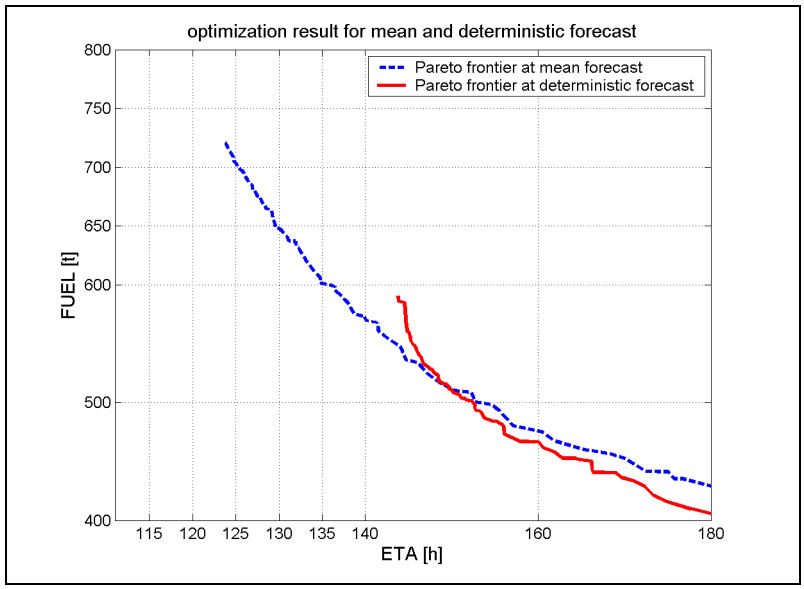

Fig. 82: PARETO optimum routes for deterministic and mean forecast

The optimization result firstly looks marvelous. A much faster journey than predicted by the deterministic forecast seems possible, or with the same fuel consumption it is possible to arrive 6 h earlier. Still *ETA*s like achieved in the medium or calm weather condition (114h, 117h) are not reached. But an *ETA* of 124h seems to be reachable and consequently an arrival on schedule would be possible. As mentioned in section 3.3, caution is recommended because the computation of a mean forecast implies the danger of damping extreme values. Therefore it may roughly underestimate the coming weather situation. Fig. 83 shows the time minimum routes of the optimizations applying the deterministic and the mean forecast. For comparison, the shortest course is depicted as well. The right part of the figure shows the velocity profiles for both routes. It can be seen that within the deterministic forecast a much lower speed level is required. Fig. 84 depicts the occurring significant wave heights as predicted by the deterministic-, mean-, and ensemble forecasts. On the left side the wave heights for the ETA_{min}-*MF* route are shown, on the right the wave heights for ETA_{min}-*DF* respectively.

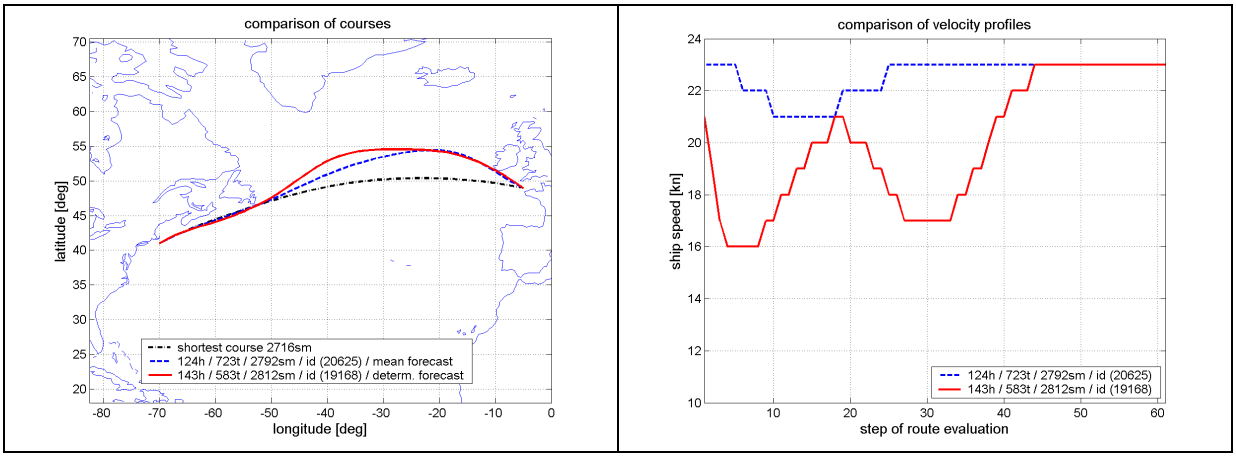

Fig. 83: Time minimum routes for mean- and deterministic forecast

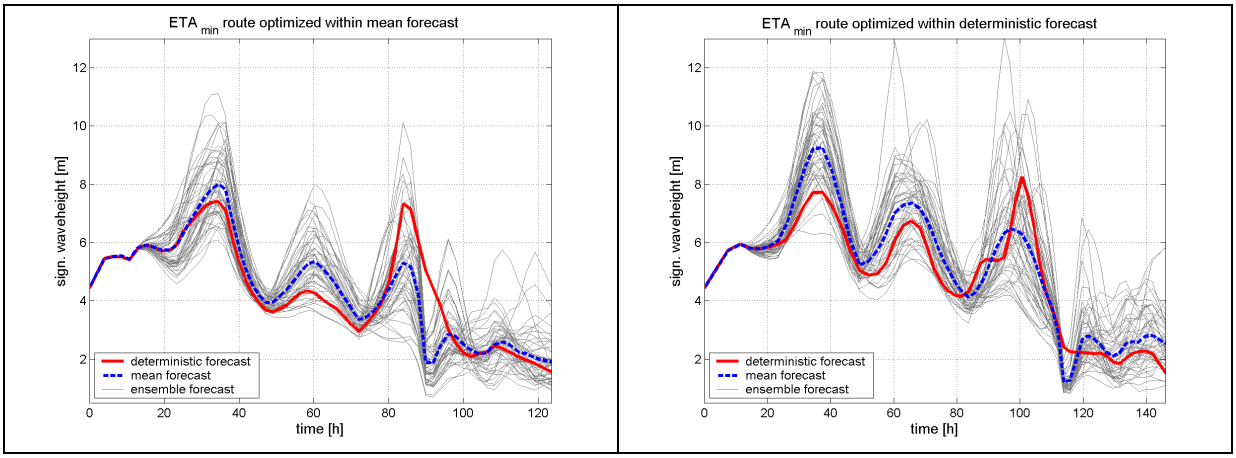

Fig. 84: Significant wave heights for minimum *ETA* routes in mean- and deterministic forecast

Both routes are only feasible within the corresponding forecast. As shown in Fig. 84 both routes cross three areas of rough weather. ETA_{min}-*MF* gets infeasible in the third wave field of the deterministic forecast (left diagram of Fig. 84). On the other hand, ETA_{min} -*DF* already gets infeasible within the first rough weather area of the mean forecast (right diagram of Fig. 84).

The comparison of both routes, i.e. courses, velocity-profiles, and predicted waves, nicely illustrates that a reduction of the ship speed does not only follow from current sea conditions but serves also as a tactical maneuver to let strong wave fields pass. In this way it becomes possible to save fuel, when faster variants would get infeasible due to wave conditions at a later time of the journey. This at least gives an impression of the complexity of a routing decision.

For example the route recommended within the deterministic forecast reduces speed at the beginning of the journey to let the first storm field pass, Fig. 83 and Fig. 48. Later on it takes a course more northerly and in addition it reduces speed again before crossing the tip of Newfoundland. This is to reduce the impact of a third area of adverse weather.
Considered apart, both optimization results are plausible. To decide if the improvements indicated by the mean ensemble forecast are trustable or not, the time minimum routes of both optimizations are evaluated within the 50 corresponding ensemble forecasts.
The result is shown in Fig. 85. The diagrams of the left column belong to the ETA_{min}-*MF* route, the right column depicts the results for the ETA_{min}-*DF* route, respectively. The three most active constraints are considered. The diagrams in the upper line represent those for the motion sickness incidence *MSI*, below those for the slamming probability, and at the bottom line is the indicator for the main engine operability. Gray, horizontal lines represent thresholds. Red-solid and blue-dashed, horizontal lines represent the values resulting from the mean- and the deterministic forecast. Black dots represent the result for a particular ensemble forecast. On the abscissa the ensemble number is given, on the ordinate the appropriate value of the constraint.

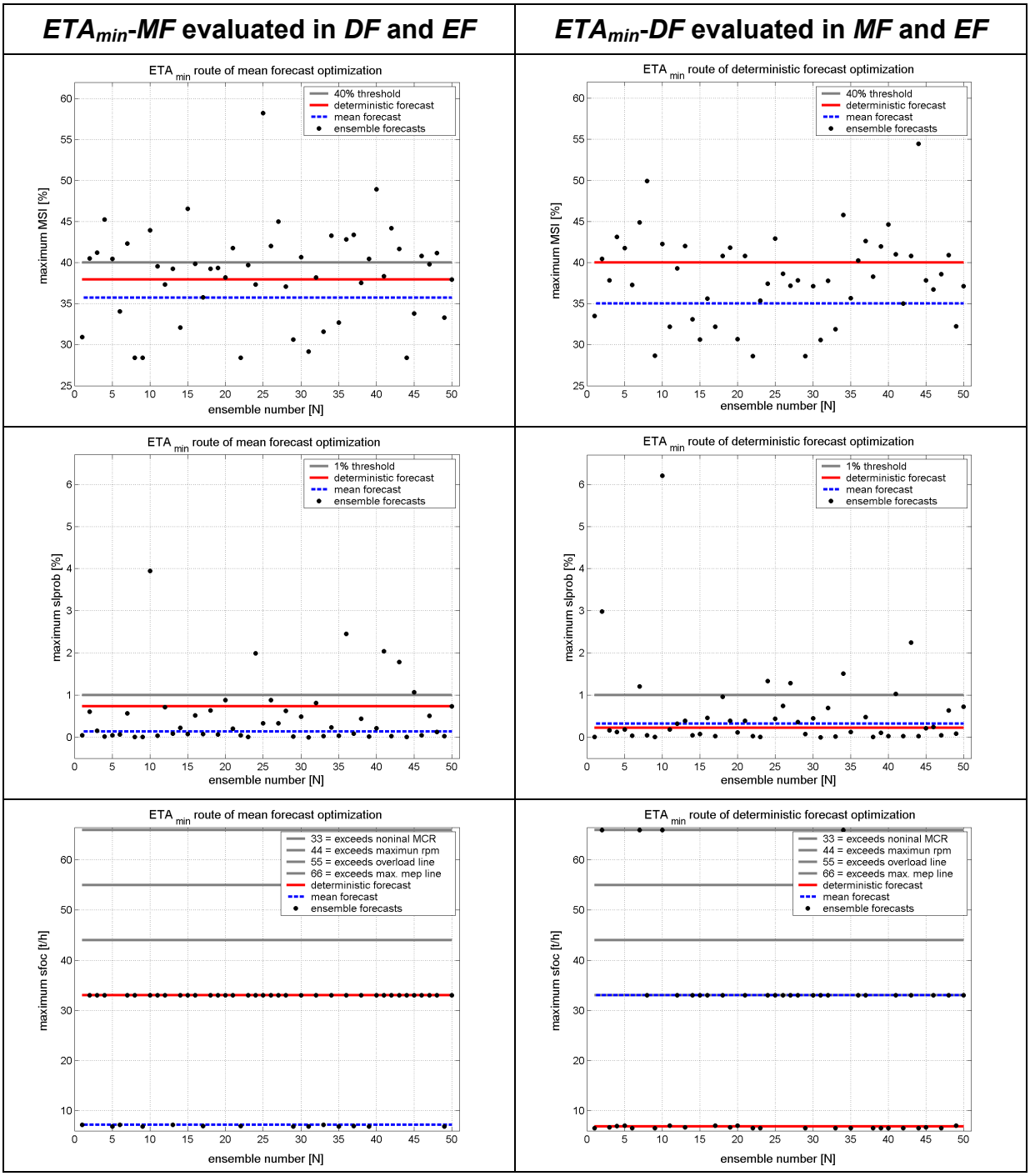

Fig. 85: Assessment of constraints in different forecasts

Regarding motion sickness incidence *MSI* and slamming probability *splrob*, even if *ETA$_{min}$-DF* reaches the 40% *MSI* limit, both routes are feasible within both, the deterministic and the mean forecast. In this case the main engine operability, represented by the specific fuel oil consumption *sfoc*, is the crucial parameter. The deterministic forecast causes a machine overload for the *ETA$_{min}$-MF* route and vice versa. Tab. 18 gives the numeric results of this investigation.

Tab. 18: Optimized routes evaluated in ensemble forecasts

number of *EF*, rating a route as infeasible	ETA_{min}-*MF*	ETA_{min}-*DF*
due to *MSI*	21 / 50	20 / 50
due to slamming	6 / 50	9 / 50
due to engine overload	36 / 50	24 / 50
due to all constraints	39 / 50	33 / 50

Finally 39 ensemble forecasts rate the ETA_{min}-*MF* route as infeasible and 33 the time minimum route of the deterministic forecast. Admittedly the difference between both routes is lower than expected and against all skepticism, the optimization utilizing the mean forecast brings a remarkable result. At least, the mean forecast seems capable to assess if improvements are possible, to be faster or less fast than the optimization result predicted within the deterministic forecast. As long as the shift in time of maximum values of the ensemble forecasts is small, this assumption may hold. Nevertheless, the spread in peak periods and encounter angles is neglected from this point of view, although it is important for the prediction of ship response.

Completing this first application of ensemble forecasts, two further optimizations are run. As observed from Fig. 85, both time minimum routes of the optimizations above are feasible in *EF35* and infeasible in *EF25*. In a way these two forecasts represent edge cases of probable weather development, both have the same probability of occurrence like the deterministic forecast. Therefore these two ensemble forecasts are taken as forecast for a route optimization. Fig. 86 shows the resulting PARETO frontiers and the appropriate time minimum routes ETA_{min}-*DF*, ETA_{min}-*MF*, ETA_{min}-*EF25* and ETA_{min}-*EF35*.

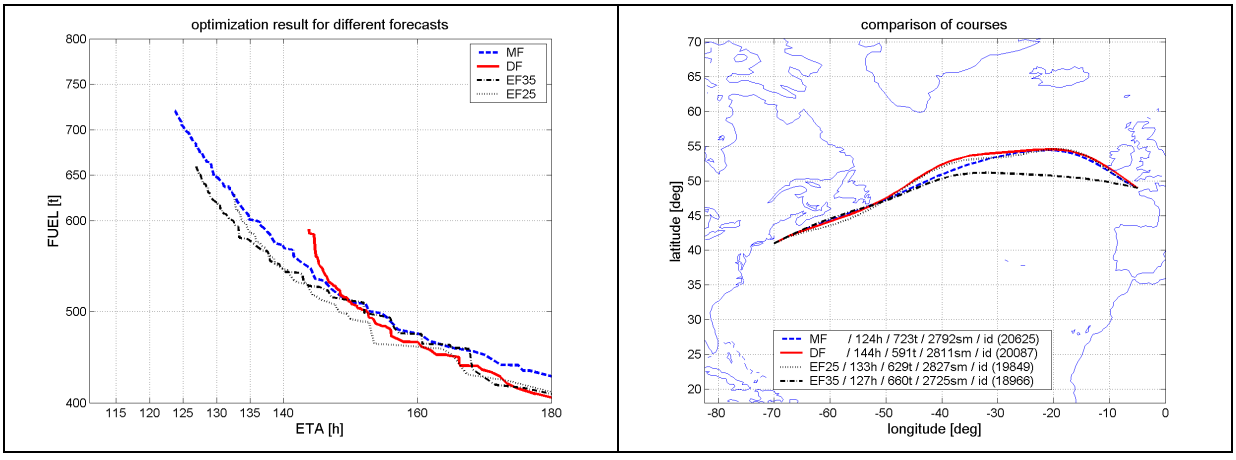

Fig. 86: PARETO frontiers and optimum routes in different forecasts

Both ensemble forecasts show an improvement of the PARETO frontier. Although ETA_{min}-*MF* is feasible in ensemble *EF35*, the PARETO frontier of the optimization applying *EF35* does not match this design. A first hint for the reason is given by comparing the courses in Fig. 86. The course of ETA_{min}-*EF35* clearly differs from all other courses. Here the genetic algorithm converges in a local optimum and it is not able to jump out of this suboptimal region. A comprehensible matter as the probability to find a favorable design decreases the more the phenotype has to change.

Further on, the course of ETA_{min}-*EF25* is quite close to ETA_{min}-*DF*, nevertheless it requires 11 hours less. Accidentally ETA_{min}-*DF* is infeasible in *EF25* although it lies in the region of probable feasible solutions. This is no reason for concern, during an optimization most infeasible designs are inside the area of feasible solutions, i.e. lying above and to the right side of the PARETO frontier does not automatically include being feasible. On the other hand, all designs below and left from a time minimum design are infeasible. Regarding the PARETO frontier of the optimization within *EF25*, all PARETO designs of the optimizations applying *MF* and *EF35* that lie below or at the left are infeasible. However, as aforementioned, there is no proof for a convergence.
Definitely the robustness of an optimization strongly depends on the quality of the weather forecast. Fig. 86 clearly shows the diversity of possible solutions. In this case, the deterministic forecast optimization seems to overvalue the achievable *ETA*. It is a common strategy to repair this weak spot by re-optimizing from the current waypoint of a journey using updates of the weather forecast. Preferably there are measurement devices on-board the ship to recognize the difference between the present wave field and the forecasted one. Thinking of an intelligent ship management system it would be possible:

- In the case of deteriorated weather, to demand for suited countermeasures, e.g. reduce the ship speed, consequently falling behind the aimed route point, assess a reachable route point, and optimize again with an updated forecast.
- In the case of more convenient weather, it is surely possible to reach the aimed waypoint and furthermore it can be possible to step beyond. Admittedly, as long as optimizations applying a genetic algorithm are time consumptive, a faster algorithm is favorable as it is necessary to quickly optimize from the achieved waypoint applying an updated forecast. Certainly the convergence characteristic should be regarded, too.

En-route optimizations with updated forecasts will remain necessary as long as the weather pattern deviates from the forecasted weather. Here the benefit of the ensemble forecast system should be focused more in detail in order to assess its capability to give the most comprehensive insight for a route decision prior to the departure.

6.6.2 Robustness as constraint

Even by applying route optimization with updated forecasts, the actual achievable *ETA* is not known until the end of a journey. Using ensemble instead of deterministic forecasts may serve to get more comprehensive insight to the future and to assess achievable *ETA*s right at the beginning. Therefore a further constraint is posed that covers all constraints considered within the route optimization, called *C_nef* (**C**onstraint observing the threshold posed for the **n**umber of **e**nsemble **f**orecasts where a route has to stay feasible). This constraint counts in how many of the 50 ensemble forecasts a particular route stays feasible. It becomes active when the number of ensemble forecasts where the considered route stays feasible falls below a threshold value. Tab. 19 shows the constraints posed for the following optimizations. The number of ensemble forecasts where a route should stay feasible is varied.

Tab. 19: Constraint for robust route optimization

constraint name	criteria	threshold
C_slprob	slamming probability	1% at 8% *LPP* behind *FP*
C_MSI	motion sickness incidence	40%
C_spef	main engine operability	accordance with main engine
C_nef	number of ensemble forecasts where a route stay feasible due to C_slprob, C_MSI and C_spef	20, 25, 30, 35, 40 or 45

Differences in the weather conditions of the ensemble forecasts and resulting different additional resistances due to waves for a given velocity and course angle cause a spread in the fuel consumption of a considered route. For this reason the objective function uses a mean fuel consumption instead of the fuel consumption. It is the mean value of fuel consumptions taken from the ensemble forecast evaluations where a considered route stays feasible. Infeasible results are left out of consideration. The objective function regarding the mean fuel consumption is built by simply replacing the fuel consumption in equation (5.2) by the mean fuel consumption.
Fig. 87 compares the PARETO frontier of *ETA* and fuel consumption of the optimization applying the deterministic forecast with a frontier for *ETA* and mean fuel consumption for the same routes.

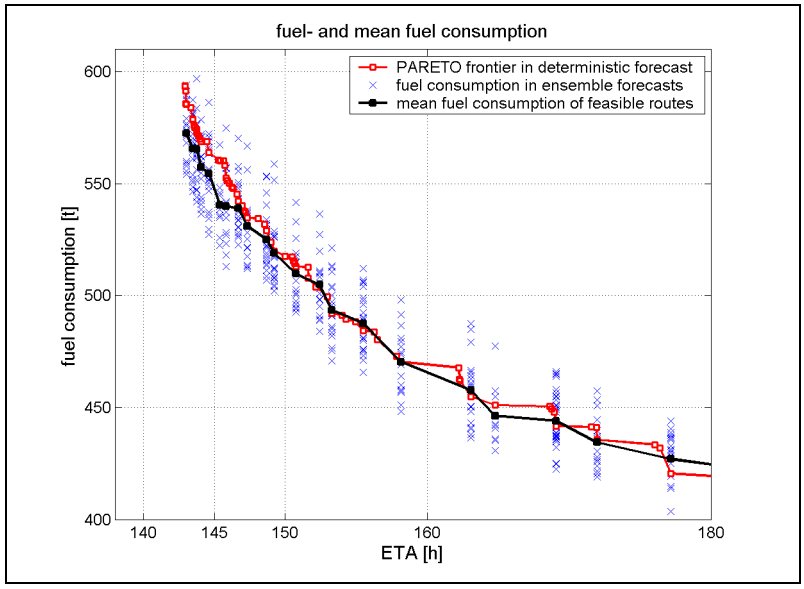

Fig. 87: Fuel consumption and mean fuel consumption

A PARETO design is represented by a red square, a black square in vertical direction represents the corresponding mean fuel consumption. Furthermore the figure contains information about the robustness of the optimized routes against weather changes. The number of blue crosses in the vertical direction relates to the number of ensemble forecasts where this route stays feasible. If there are no markers vertically to a PARETO design, it is infeasible in all ensemble forecasts. The spread in the fuel consumption may be utilized as well to value robustness, however, this is not done here to keep things simple. All in all the mean fuel consumption deviates not much from the fuel consumption, whereas the spread, i.e. possible differences in the fuel consumption, is remarkable. Here 10% of the overall fuel consumption simply depends on the weather development!

Fig. 88 shows PARETO frontiers for route optimizations in ensemble forecasts applying different thresholds considering the number of ensemble forecasts where a route stays feasible. In addition the PARETO designs of the deterministic forecast, evaluated for mean fuel consumption, taken from Fig. 87, are shown. The right part of the figure shows an enlarged sector of the left part. Minimum attainable *ETA*s are pointed out. Contrary to expectations the PARETO frontier for routes feasible in 25 ensemble forecasts lies above the frontier for routes that are feasible in 30 ensemble forecasts. This for sure is not plausible but with regard to the PARETO frontiers depicted in the left part of Fig. 88 this defect is small. It may be due to a limited capability of the optimization method, and therefore it should be resolvable by further adjustments of the optimization method to the routing problem.

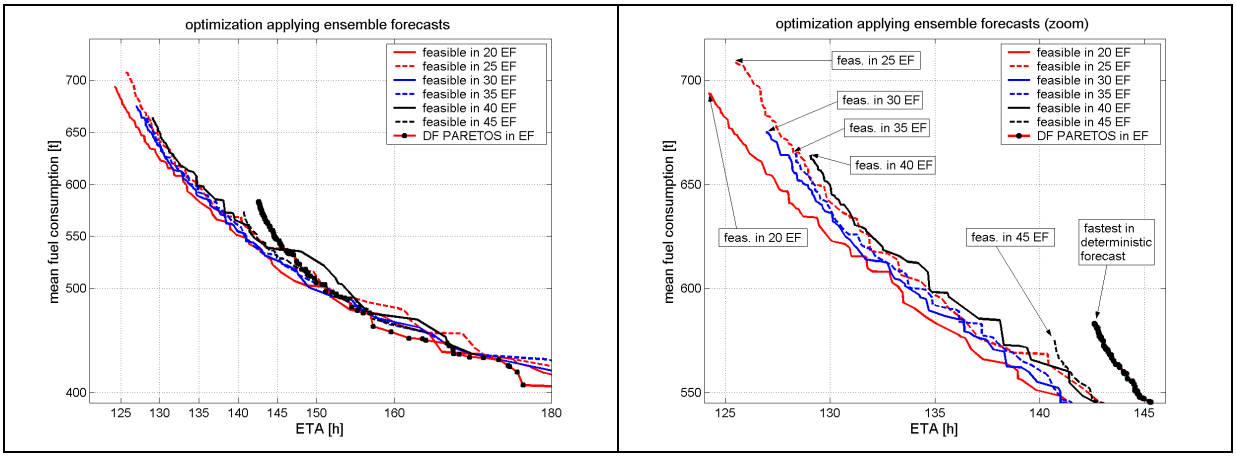

Fig. 88: PARETO frontiers for optimizations in a deterministic and an ensemble forecast

As already discovered in section 6.6.1, the optimization within the deterministic forecast seems to roughly overvalue the attainable *ETA*. Increasing the threshold of *C_nef* from 20 to 40 surprisingly increases ETA_{min} just from 124h to 129h. Only a further increase of the threshold leads to remarkable increases in ETA_{min}. The PARETO frontiers for all thresholds lie close together. Obviously, for a particular *ETA* the differences in the mean fuel consumption are clearly lower than the total spread due to the ensemble forecasts, as given in Fig. 87.

Compared to the optimization result of the deterministic forecast, even the time minimum route that is feasible in 45 ensemble members arrives two hours earlier than the one of the optimization within the deterministic one, feasible in only 17 ensemble members, cp. Tab. 18. Furthermore, considering the fastest routes of the deterministic forecast optimization, the predicted fuel consumption within the ensemble forecasts is much lower. Fig. 89 illustrates the optimization results by plots of the courses and velocity profiles for the fastest routes from the optimizations with different thresholds for *C_nef* (20, 30, and 40) and from the deterministic forecast optimization.

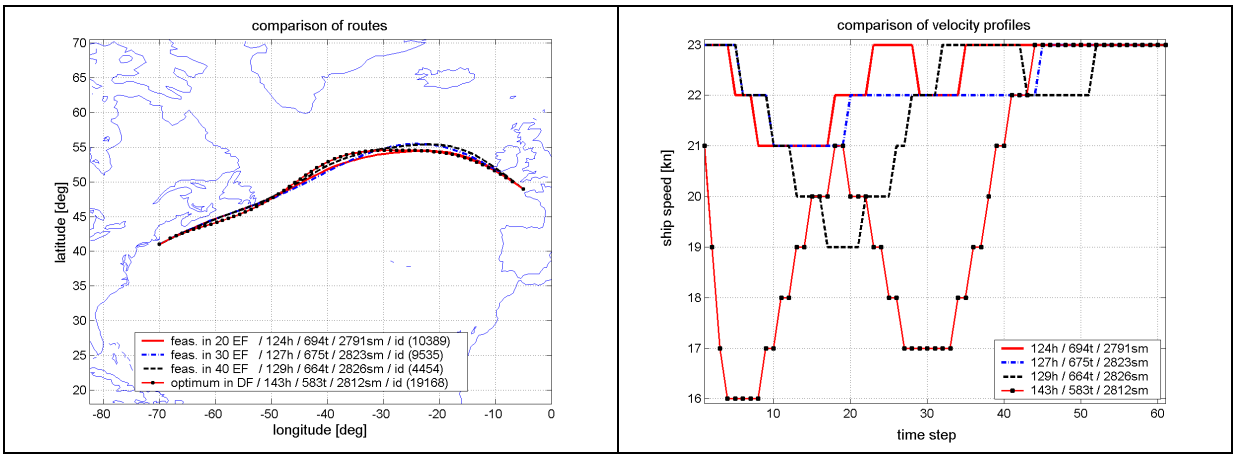

Fig. 89: Courses and velocity profiles of routes optimized in a deterministic and an ensemble forecast

Even if the courses seem to stay close together, there are deviations of about 100nm, a remarkable distance considering that extreme wave fields are circumnavigated here. Regarding the velocity profiles, in particular the difference between the deterministic and ensemble forecast optimization results become obvious. Within the deterministic forecast the ship speed has to be reduced much more to avoid heavy weather. Considering the ensemble forecast, the differences of the velocity profiles appear plausible, e.g. maximum speed reductions can be found at highest threshold values of the robustness constraint.
Finally all optimized routes clearly deviate from the shortest possible journey, the great circle route. So maybe a master who utilizes the deterministic optimization result can sail faster due to the current weather conditions. Finally he/she enters port with a comparable *ETA* as predicted in the ensemble forecast optimization. But taking the shortest track would clearly not succeed.

6.6.3 Robustness as objective

During the optimizations regarding robustness as a further constraint, all in all 126.000 routes are evaluated (threshold of *C_nef* varied from 20 to 45, i.e. 6 optimizations and in each case 300 generations with 70 members). Applying robustness as an objective, this reduces from six to one optimization. Here 500 generations each with 100 individuals are run, all together 50.000 routes are evaluated. Although this setup saves a lot of computational effort, the prime reason for this investigation is to support the observations made above. Similar to the usage as constraint, simply the number of ensemble forecast members where a route stays feasible is applied as objective, called *O_nef*. To produce a value for this objective comparable to the magnitude of the both others, the one for mean fuel consumption and *ETA*, it is set up as:

$$Objective\ NEF = \left(\sum_{i=1}^{50} n_i \right)^2 , \qquad (6.4)$$

where $n_i = 1$, if a route is feasible in the respective ensemble forecast and 0 otherwise.
Fig. 90 illustrates the result of an optimization utilizing robustness as objective of the optimization. The left part of the figure shows the mean fuel consumption versus *ETA*, the right part provides information on attainable *ETA*s relating to robustness against weather changes.

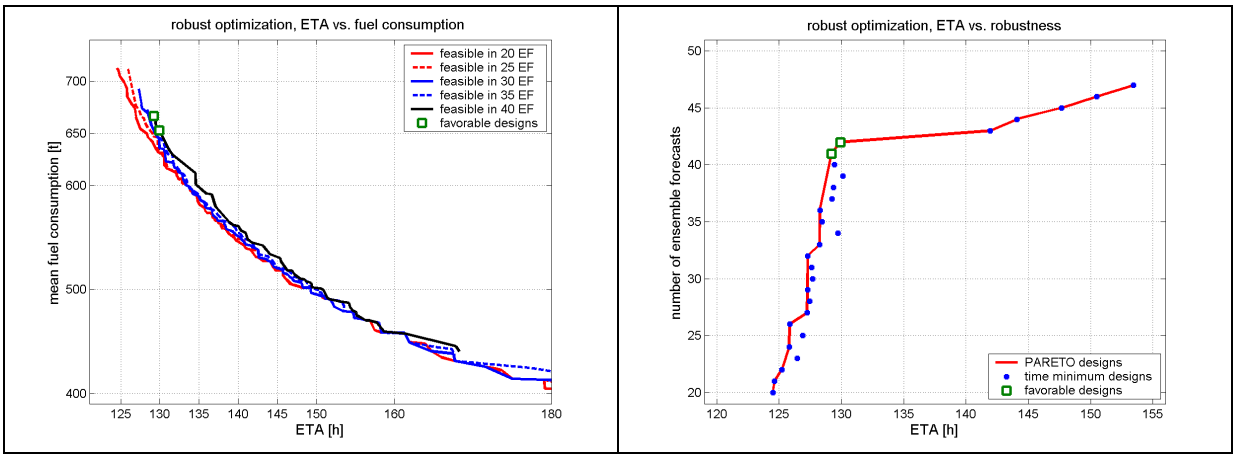

Fig. 90: PARETO frontiers of the ensemble forecast optimization

Regarding the PARETO frontiers on the left side of the figure, the mean fuel consumption is similar to the fuel consumption found when using robustness as constraint, as shown in Fig. 88. Here the PARETO frontiers for different threshold values are produced by filtering all evaluated route designs following to the optimization. The right part of the figure depicts the diagram for the objectives *O_nef* and *ETA*. Blue dots represent the time minimum routes for a particular number of ensemble forecasts *nef* that rank these routes as feasible. PARETO optimum designs regarding these two objectives are connected with a red line, i.e. for these designs an increasing robustness deteriorates the time of arrival. Two route designs are emphasized by green squares. Both are quite fast combined with reasonable fuel consumption, as they are located closest to the PARETO frontier for *ETA* and the mean fuel consumption. They would match the schedule, and furthermore they possess a high robustness against weather changes. As can be seen in Fig. 90, decreasing *ETA* would rapidly decrease the robustness, increasing robustness would strongly increase *ETA*. In a sense these two route designs represent "over all optimum routes."

Fig. 91 depicts courses and velocity profiles of these two routes. To compare, the ETA_{min} routes of the deterministic and the one of the mean ensemble forecast are shown, too.

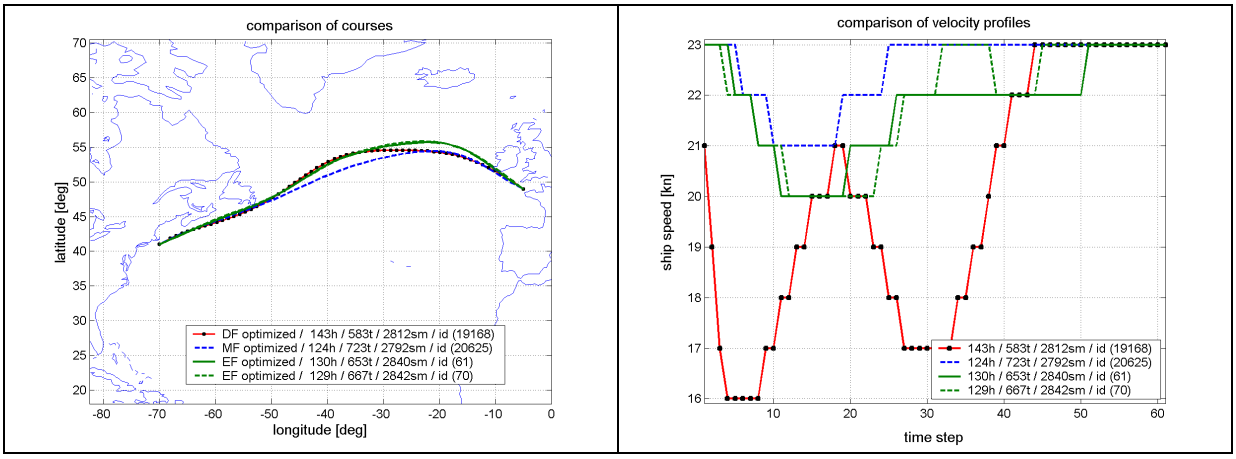

Fig. 91: Courses and velocity profiles of routes with different robustness

Except from ETA_{min}-*DF*, all of them are PARETO optimum regarding *ETA* and fuel consumption. Even if the ETA_{min}-*DF* is quite slow and ETA_{min}-*MF* is the fastest one here, both are less persuasive regarding the robustness against weather changes; the *DF*-optimized route

is feasible in 17, the *MF*-optimized in 11 ensemble forecasts, respectively. This clearly shows the advantages of including robustness into a route optimization. Applying a mean forecast does not automatically produce routes that are feasible in 50% of the ensemble forecasts; slower routes are not automatically more robust.

It finally proves true what is indicated by the mean ensemble forecast optimization, compared to the optimization in the deterministic forecast it is possible to decrease the duration of the journey. Furthermore it is possible to simultaneously increase the robustness against weather changes and reduce *ETA*. The required fuel consumption of the routes selected from the ensemble forecast optimization (favorable designs in Fig. 90) is in between the fuel consumption of ETA_{min}-*DF* and ETA_{min}-*MF*. Nevertheless, except from ETA_{min}-*DF*, they all represent an optimum regarding the fuel consumption as they are close to the PARETO frontier (Actually the PARETO frontier given in Fig. 90 is a PARETO surface now. It represents a 3-dimensional border of the solutions space for three objectives, *O_eta*, *O_fuel*, and *O_nef* where an improvement in one objective deteriorates or at most preserves the other objectives).
Both optimum routes of the ensemble forecast, presented in Fig. 91, distinguish clearly in course and velocity profile from their deterministic- and mean forecast counterpart. Regarding further research, it would be interesting to see if a route optimization applying updates of a deterministic forecast would lead to a comparable result.

6.6.4 Rectification for using analyzed weather as deterministic forecast

Unfortunately, there is no real deterministic forecast available yet and therefore the re-analysis is used instead. This in fact is no mistake, as the re-analysis surely could have been the real deterministic forecast. Consequently all conclusions made above are valid.

Fortunately, these weather data are much more than a forecast, they represent the best available description of the real weather condition during the considered period.

Now, the optimization results for this forecast / re-analysis should be taken as what they are, the re-calculation on routes that are possible at the best.

Regarding the PARETO frontiers of Fig. 86 and Fig. 90 it is obvious that the ETA_{min}-*MF* and the two favorable routes selected from the ensemble forecast optimization are not feasible in the weather condition that existed according to the re-analysis. For all of them one or more constraints that disapprove these routes would become active. This implies that most likely, suited countermeasures like course or speed changes would have become necessary. Consequently the ship leaves the planned route and the aspired *ETA* cannot be kept. In this case, a re-optimization from the current waypoint to the port of destination serves, e.g. to find the fastest track at maximum fuel savings. In doing so it is not possible to get comprehensive insight to an attainable *ETA* at the beginning of the journey. However, this is favorable e.g. for a conscious disposition of cargo. To step forward in this matter, Fig. 92 serves to evaluate the optimization results of the *MF*- and the *EF*-optimization. The figure shows the velocity profile and constraints for ETA_{min}-*MF* and for both routes selected from the ensemble forecast result *EF-id*(61) and *EF-id*(70) at re-analyzed weather conditions. Since the constraints for parametric rolling did not become active, they are left out of consideration. The appropriate courses can be seen in Fig. 91.

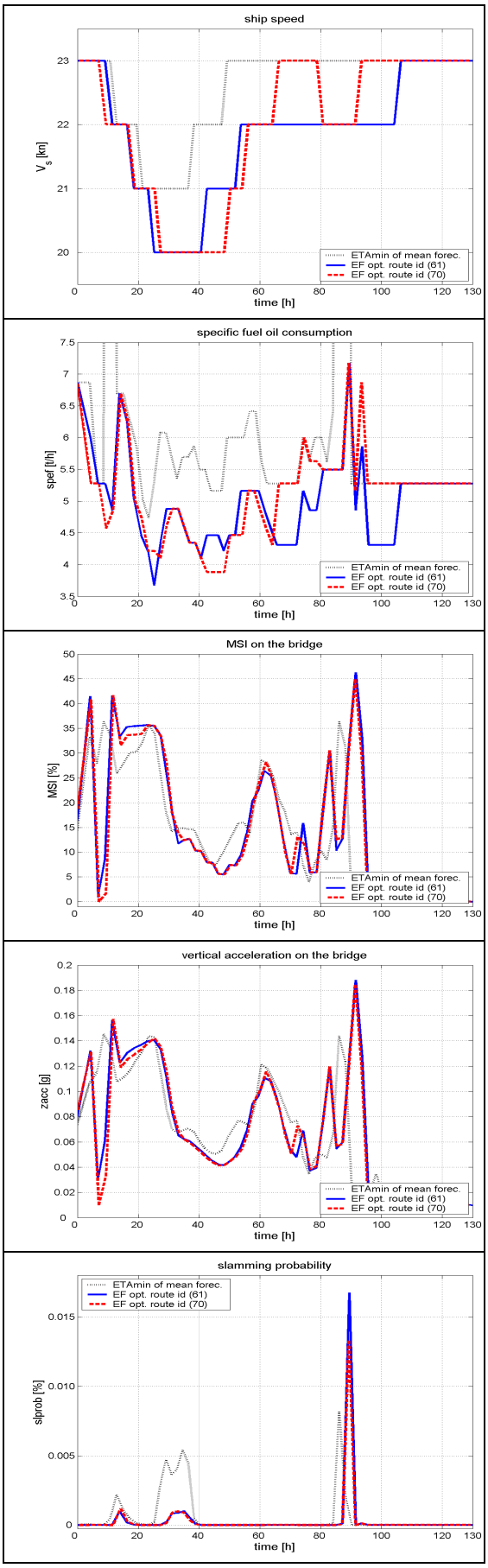

Fig. 92: Ensemble results in analyzed weather

Since ETA_{min}-*MF* takes a shorter track at higher ship speed, it is able to arrive 6h earlier than *EF-id*(70). Consequently the fuel consumption is higher but the route is anyway close to the attainable PARETO frontier.

Regarding the specific fuel oil consumption *spef*, both *EF*-routes stay feasible within the analyzed weather. ETA_{min}-*MF* becomes infeasible due to main engine overload. During the first and the fourth day *spef* of ETA_{min}-*MF* exceeds the upper level of the diagram. In these cases the load to the main engine exceeds the nominal *MCR*. In this regard ETA_{min}-*MF* becomes infeasible without any doubt.

Concerning the motion sickness incidence *MSI* and significant amplitudes of vertical accelerations on the bridge, the ETA_{min}-*MF* route does not violate any constraints. Here both routes taken from the ensemble forecast optimization produce active constraints. Three times the threshold for *MSI* and two times the one for significant amplitudes of vertical acceleration is exceeded. However, these violations are small and limited to a short period. Therefore they may be tolerated. Admittedly, the graphs for *zacc* and *MSI* look very similar. This becomes clear as steps of the route evaluation are arranged more or less equal in time by the routine for the route perturbation. Regarding the acceleration around $t = 20$h, a period of high accelerations spanning a longer time can be observed. This certainly produces a much higher *MSI* like reckoned here, and an integration of time steps for the assessment of *MSI* appears recommended.
Related to the slamming probability there seems to be no risk for none of the routes to be affected by slamming.

Altogether the optimization result produced by means of the ensemble forecast is the more reliable one. It is possible to execute the journey according to the optimization result when slightly higher accelerations are tolerated. Admittedly, this is just one example applying one weather scenario and it is necessary to extend these investigations to more weather cases, to see if the drawn conclusions hold. On the other hand, the computational effort for an ensemble optimization is more than fifty times higher than an optimization applying a single forecast. Notwithstanding all thinkable improvements to accelerate the optimization procedure, an application of the current set-up for the ensemble route optimization on-board a ship seems not possible, as it is too time-consuming. Nevertheless, regarding the explanatory power, the approach to employ ensemble forecasts should be continued. Up to now it turned out to be a reasonable attempt to look out for the future and to predict the unpredictable.

7 Summary and outlook

7.1 Initiation of a new approach

As shown by the operators of the Dutch Ship Performance Optimization System SPOS, it is possible to achieve a significant reduction of time operating in bad weather by applying a weather routing system. Weather routing and route optimization are meaningful methods to improve the safety on-board a ship regarding threads by adverse weather. Dependent on the set-up of objectives for a route optimization, it is furthermore possible to save operational costs, mainly fuel- and lubrication oil, in order to find the fastest track or to save fuel for an arrival on schedule. Inspired by the work of SEAROUTES the set-up of a new route optimization approach is decided. This approach is able to handle multiple objectives separately, as including opposing objectives into a single objective function becomes difficult to comprehend. Already traveling time and operating costs, major objectives of any route optimization and here represented by the estimated time of arrival *ETA* and the fuel consumption of the main engine, depict opposing targets, as improving one normally deteriorates the other. This suggests an optimization that is able to identify PARETO optimum routes. As long as an arrival on schedule is possible the optimization has to identify routes that comply with the schedule at minimum operational costs. When weather worsens and an arrival on schedule becomes impossible, the optimization should depict routes of minimum operational costs for achievable *ETA*s. That is why the knowledge about feasible PARETO optimum routes, as depicted in Fig. 93, supports a conscious decision making in terms of safer ship operation, reducing operational costs and the ability to rearrange the sailing list if necessary.

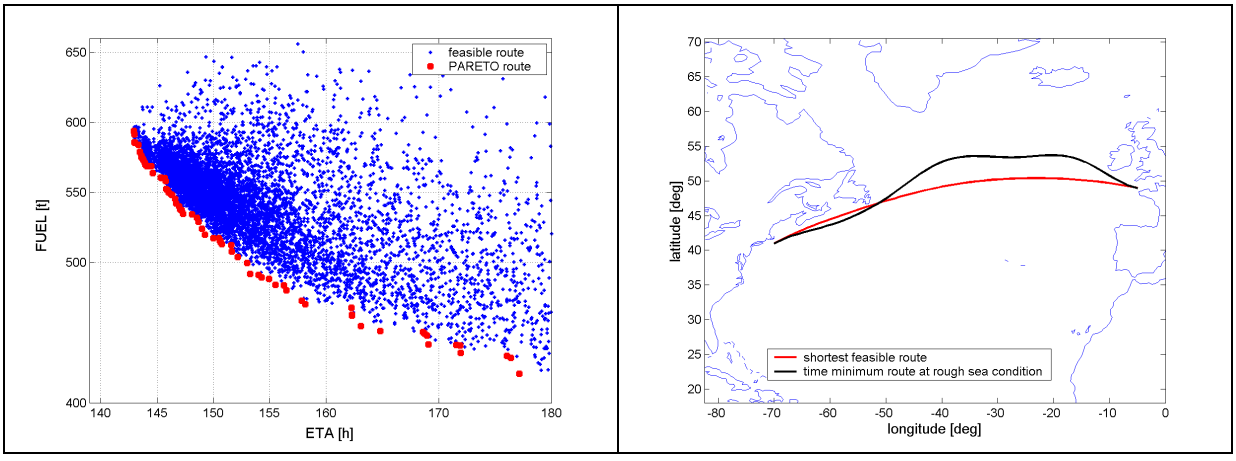

Fig. 93: PARETO frontier and time minimum route at rough seas

Expectedly, at calm weather the shortest route is the optimum one. When weather worsens it is mostly possible to maintain the optimum track by retaining the shortest route and reducing speed if necessary. In a rough weather situation the routing decision becomes more complex, as the shortest route is not necessarily the best one anymore. The optimum becomes a trade-off between (i) additional fuel consumption due to a longer course and (ii) fuel saving by reducing the additional resistance due to waves by means of circumnavigation of strong wave fields. For the rough weather scenario, considered within this study, it turns out that applying optimization serves to reduce the fuel consumption up to 15 %. Regarding the demands for the optimization process, it is expected that objective functions show humps and hollows or at

least become quasi-multimodal when optimization results are governed by constraints. Therefore the optimizer should be able to overcome local optima. Generally stochastic methods serve for this purpose. Here a multi-objective genetic algorithm, available within the generic optimization environment modeFRONTIER, is applied.
As a rule of thumb, it turned out that a stochastic method requires the tenfold number of designs compared to their deterministic counterpart. Approximately half of the evaluated designs are necessary to be sure that a global optimum is detected. Anyhow there is no proof.
A frequent requirement during the set-up of an optimization procedure is the reduction of computational effort, generally to accelerate the procedure. In the case of genetic algorithms the number of designs within one generation depends on the number of free variables and the number of objectives. Furthermore, each route design has to be evaluated at a number of points that are tight enough to recognize the weather pattern. Altogether, a fast method to assess the ship behavior in waves is necessary. Therein the modeling of ship routes should require as few free variables as possible. For this purpose the mathematical description of a route design and its evaluation base on:

- a B-spline technique to model course and velocity profile of a route,
- standard spectra to describe the seaway,
- the theory of linear superposition to assess ship responses.

The applied B-spline modeling technique provides a small set of free variables that enables a smart modeling of the course and the velocity profile. It is possible to extend the method to a finer spatial and temporal resolution or to cut-off areas that do not allow passages, like land or islands. In this way the perturbation for the maximum northern shift in Fig. 13 is controlled.

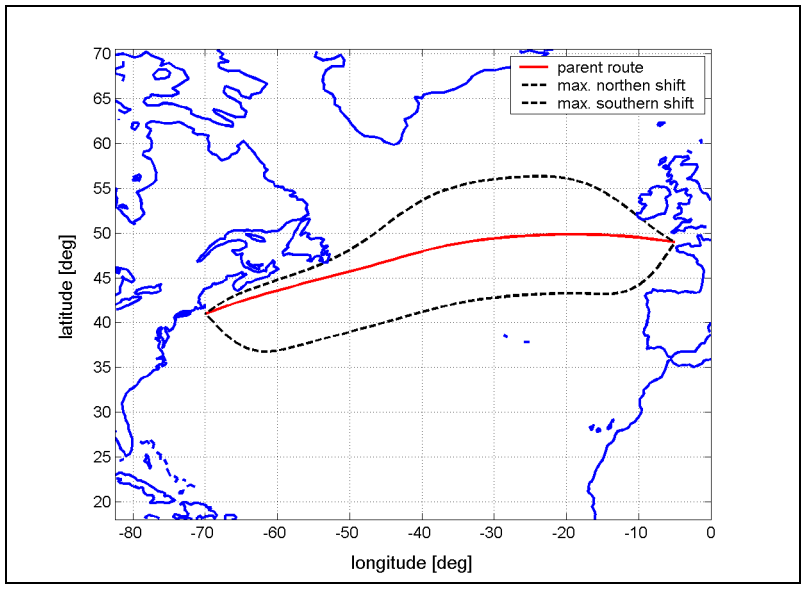

Fig. 13: Parent route and maximum perturbations

To describe predicted wave conditions, deterministic- and ensemble forecast data from the European Centre for Medium-Range Weather Forecasts ECMWF are used. In both cases they consist of significant data that are used in combination with standard spectra. A PIERSON-MOSKOWITZ spectrum provides good results.

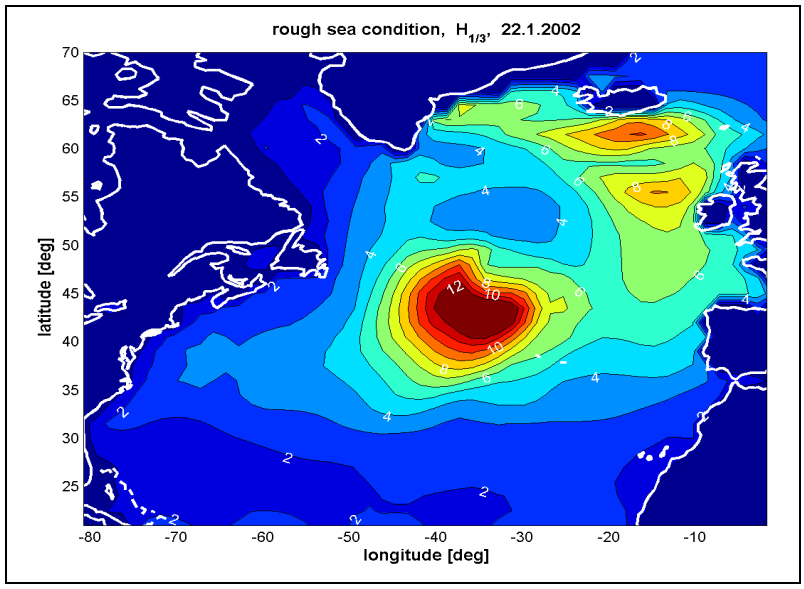

Fig. 94: Significant wave heights of a severe winter storm in North Atlantic, 22. January, 2002

For the assessment of ship responses in waves, transfer functions for the ship motion and response functions for the added resistance due to waves are applied. They are calculated by means of the well-established strip theory code SEAWAY that is based on potential theory, JOURNÉE (2001). Response functions for the added resistance due to waves are calculated according to the integrated pressure method of BOESE (1970). Together with the calm water resistance according to HOLTROP and MENNEN (1984), a characteristic of a similar propeller provided by YASAKI (1962), and the main engine characteristic, MAN B&W (2000), the fuel consumption for particular service conditions in a seaway is assessed.

Transfer functions are used for the set-up of constraints within the optimization. They are calculated for various points on-board the ship and serve to assess absolute motions like the acceleration on the bridge and motions relative to the water surface, e.g. applied to a constraint for the slamming probability.

Inspired by the current discussion on parametric rolling, an additional module is established to detect situations that are suspicious for such events. The proposed model is not straightforward strip theory, but a combination of strip theory and results from sophisticated capsize simulations, provided by KRUEGER et al. (2006). In this way it becomes possible to identify hazardous situations with reasonable computational effort.

It has to be pointed out that the applied constraints represent an arbitrary selection used to demonstrate the feasibility of a new approach for route optimization. A sophisticated decision support system should include all available features to assess the behavior of a ship in waves, otherwise a route recommendation would become delusive by pretending a safety that does not exist. In this regard it is a trade-off between numerical accuracy and computational time, e.g. between the achievable accuracy of employed methods, the accuracy of underlying data, and the computational effort to predict the ship behavior on a particular route.

Regarding the accuracy of underlying data, one of the most important topics in ship route optimization is the forecast uncertainty, i.e. the increasing deviation of the upcoming from the forecasted weather, the more the forecast reaches into the future. Deterministic medium range forecasts are considered to be reliable for three days. The rough weather example applied in this study implies that, under severe conditions, this assumption may not hold. Normally en-route countermeasures are necessary to avoid danger to the crew or damage to the ship and the cargo.

For conscious route planning and disposition of cargo it is favorable to get the most comprehensive insight to the upcoming weather as soon as possible. To step forward in this matter, the robustness of optimized routes to weather changes is assessed by means of ensemble forecasts. Finally a definition of robustness against weather changes is established. It is used to extend the optimization approach by applying robustness as further constraint or objective. In this way it becomes possible to identify PARETO optimal routes that, in contrast to the optimizations applying the deterministic forecast, comply with the schedule for a reasonable violation of constraints, cp. Fig. 95.

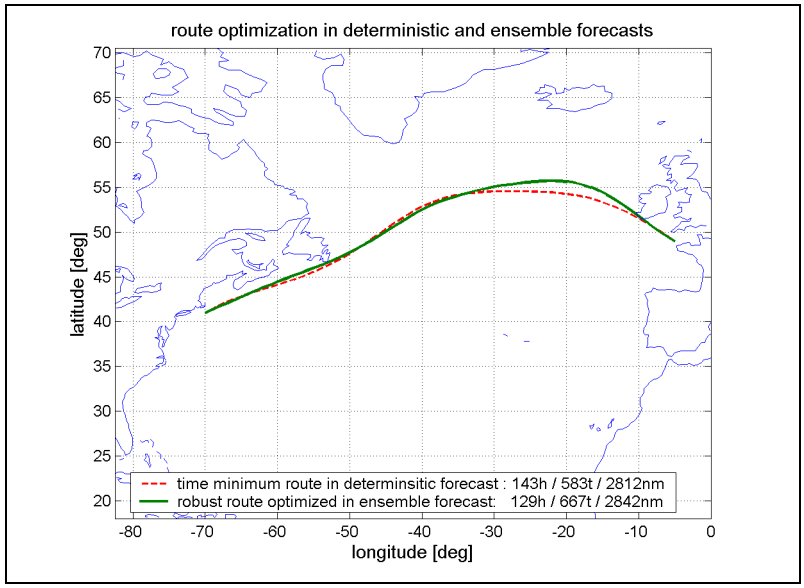

Fig. 95: Rough weather route optimization for deterministic and ensemble forecasts

7.2 Discussion on the performance

Various sensitivity analyses serve to assess the capability and the reliability of the route optimization approach. Therein, the following aspects are addressed:

- Considering different weather conditions serves as a first plausibility check for the optimization setup.
- Applying different spectra, namely a PIERSON-MOSKOWITZ and a JONSWAP spectrum, is used to assess the error induced by the approximate description of swell.
- The required accurateness for the representation of the hull shape, within strip theory based motion prediction, is addressed by hull form modifications.
- Threshold levels and constraints are evaluated by variations of thresholds and by enabling and disabling constraints while the remaining parameters of the optimization are held constant. In some cases reasonable modifications are installed, e.g. for the assessment of the slamming probability.
- Benefits and performance of two add-ons, addressing parametric rolling and robustness against weather changes, are evaluated by threshold variations.
- Besides all these investigations it is possible to assess the performance and usability of strip theory and of the genetic algorithm within route optimization.

Regarding the variation of the weather condition, the optimizations show plausible results. As sea conditions worsen the fuel consumption increases for a given *ETA*. At the same time the minimum attainable *ETA* increases as well. Actually this is just an initial test for a qualitative assessment of the optimization result. However, regarding the fuel consumption the results fit very well to data measured during the SEAROUTES project. Therefore the resistance prediction by means of the method provided by HOLTROP and MENNEN yields good results for the design draft. Furthermore the usage of a similar propeller is admissible. At minor draft load condition, e.g. ballast load condition, the calm water resistance is assessed too low.

Regarding the modeling of the sea state, a method considering simply swell is sufficient as long as the inaccuracies of other applied methods dominate the quality of the optimization result, e.g. the uncertainty of the forecast is the much more influencing parameter. Surely, applying 1-D or even 2-D spectra can improve the accuracy of the calculated ship responses. But it has to be borne in mind that resulting little additional time requirements during the evaluation would summarize to significant amounts when computed repeatedly. Therefore simply significant data together with a PIERSON-MOSKOWITZ spectrum are preferred here. A suited compromise, to improve the modeling of swell and to keep the amount of data in a reasonable magnitude, could be the usage of parameters for scaling the peak width similar to those applied in a JONSWAP spectrum. In that way significant wave data would consist of data fields for wave heights, -periods, and -direction and additional three to four parameters that serve to scale the spectrum, given on the same grid as the other ones. Finally, as long as wind forces and currents are neglected, the application of a PIERSON-MOSKOWITZ spectrum can be regarded as satisfactory.

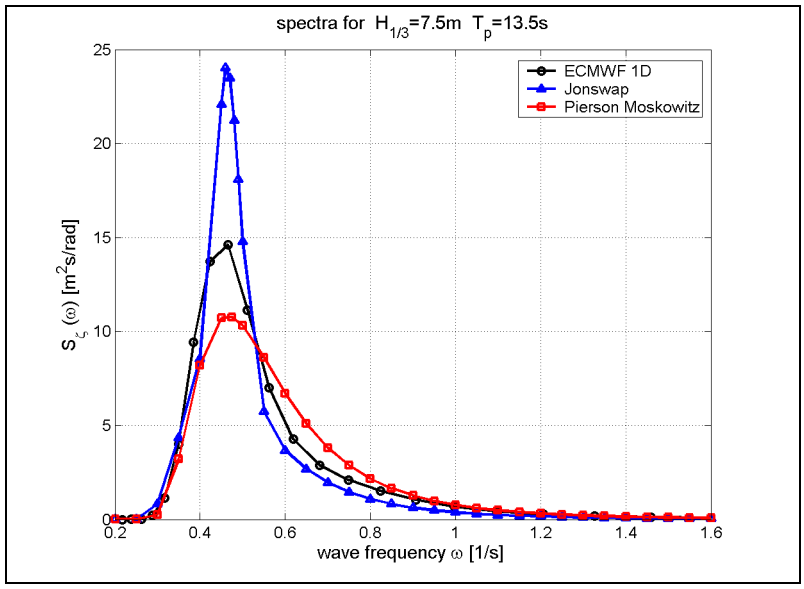

Fig. 56: Typical storm spectra for the North Atlantic, PIERSON-MOSKOWITZ, JONSWAP and ECMWF-1D spectrum

During an optimization about 20,000 routes at 60 route points are investigated. This amounts to 1.2 million calculations of ship responses in a particular sea state. Obviously a fast method for the assessment of ship responses is needed. This implies that the method of linear superposition is recommended, applying wave spectra, transfer functions, and their statistical evaluation. Here transfer functions for a particular load condition calculated by means of strip-theory are used. It turned out that there is no need to consider the changes regarding departure and arrival condition, i.e. to consider fuel consumption during the journey. The usage of an intermediate load condition is absolutely sufficient.
Even if strip theory does not take the hull form above the water line into consideration, a proper hull description is recommended, as is shown by hull form variation studies. However, the upper hull shape has a clear impact on the seakeeping behavior of a ship. In some cases the upper hull has to be included, e.g. by methods like the proposed parametric rolling module that is a combination of strip theory with results from more sophisticated numerical investigations. To include more of the ship behavior that is definitely not covered by the numerical representation, it is still possible to employ the master's knowledge and experience to build constraints that represent so to speak *master's choice.* This is performed for example in the SPOS routing system.

The initial setup uses constraints for the load to the main engine, the vertical acceleration on the bridge and for the slamming probability. For the latter two, thresholds comply with the thresholds posed in the European project SEAROUTES (2003). It turns out during the sensitivity analysis that the constraint posed for vertical acceleration on the bridge is the most deciding one for the optimization and for the shape of the resulting PARETO frontier. Comparisons to thresholds posed by NORDFORSK (1987) indicate that the applied threshold might be too low. For this reason the model is extended by applying a constraint for the acceleration on the bridge that is based on *MSI*. Including amplitude, frequency, and duration of the exposure, the *MSI* provides a more comprehensive evaluation. In that way, a second indicator for the load on the crew by means of accelerations is provided for a more differentiated assessment. Following investigations show that the load on the crew in an adverse weather situation can be enormous and with regard to maintain situation awareness, the thresholds for vertical acceleration on the bridge are kept tight.

Considering the threshold for the slamming probability, no influence on the shape of the PARETO frontier is recognized, even if this constraint is tightened significantly. Here the study shows that commonly applied methods to assess slamming could need revision. It is known that Panmax container vessel slam, but this is ignored by the initially applied procedure, based on the method of OCHI. It turns out that the method could be improved by permitted tuning of thresholds and parameters. But still the influence of this constraint to the shape of the PARETO frontier is small, at least it affects the optimization process. Obviously the concept of slamming probability deserves further investigation. It is the question whether modern structures in ship design withstand the criteria that formerly were posed for slamming or not.

The constraint for the load to the main engine is not changed, as the operating point has to comply with the characteristic of the main engine. However, this constraint has a high impact on the optimization result, similar to the one for vertical acceleration.

Regarding parametric rolling, first sensitivity analysis show that it is possible to establish and adjust thresholds applying the absolute wave height and thresholds for relative wave height in a reliable way. Furthermore wave length, encounter angle, and the period of encountering waves, related to the pitch period of the ship, are applied to successfully identify situations that are suspicious for parametric rolling. Similar to the constraint for the slamming probability the constraints for parametric rolling show only minor influences to the shape of the PARETO frontier. So far the operating behavior of the constraints posed for parametric rolling are plausible, surely the reliability is to be proved comprehensively before the application to a decision support system can be recommended.

Considering the robustness of optimized routes against probable weather changes, the usability of a mean-ensemble- and an ensemble forecast is investigated. Achieved optimization results are compared to results of optimizations utilizing the deterministic forecast. For the weather case considered here, applying a mean-ensemble forecast indicates that a considerable reduction of the duration of the journey is possible. Still these optimizations yield no information whether optimized routes improve in terms of robustness. For this purpose the ensemble forecast is applied and robustness is included as constraint as well as objective to the optimization. In this way, routes that are PARETO optimum regarding *ETA*, fuel consumption, and robustness against weather changes can be identified. Two superior routes are taken for further investigations. Regarding the high number of ensemble forecasts (84%) that rank these faster routes as feasible it seems reasonable to say that even if there is a probability of 16% that constraints are violated, the severity of violation will be small as its probability is reasonably low. Observations of constraints along optimized routes in analyzed weather supported this assumption. Anyhow, this aspect needs to be proved by further investigation. So far, employing ensemble forecasts appears to be a reliable method for a conscious decision support. The major obstacle that has to be solved for a practical application is reducing the required computational time.

For this first approach it is absolutely sufficient that constraints simply control the maximum values of an investigated route. More sophisticated constraints that also account for the duration of an incidence can be included quite simple. This is shown by the concept of *MSI*. However, it is an important matter of the set-up to find reasonable threshold values. For vertical acceleration on the bridge it turns out to be meaningful to account for the duration of the exposure. Regarding e.g. the slamming probability, there is no need to account for durations as the constraint already includes a time dependency.

The applied generic optimizer, here a genetic algorithm, produces reasonable results even if it is not at all adapted to the route optimization problem. If merit functions are shaped relatively flat, the genetic algorithm shows problems to identify an optimum. This is because the probability of a design to be considered for producing the next generation is coupled to the fitness relative to other designs and not to its absolute fitness. Up to certain limits, this can be overcome by applying objective functions instead of the objectives themselves. Nevertheless, an adaptation of the applied stochastic method is recommended to accelerate the code and to yield convergence improvements. It turns out that even if constraints do not directly affect the PARETO frontier, they are able to influence the optimization. In the case of *MSI* or slamming, the enabled constraint helps to improve the optimization process, local optima are overcome a lot easier, and consequently the procedure converges faster to the desired PARETO designs. Even if the number of infeasible designs during a rough weather optimization is already high, additional constraints can stabilize the optimization. In this regard, improvements of the optimization result are observed when parametric rolling is included. Applying this constraint, serves to deplete the population in the low *ETA* region. Consequently selective pressure increases, i.e. making an achieved optimum less comfortable. This serves to keep the genetic pool diversified and the chances for alternative solutions to survive become more probable. As the probability to produce different route variants during the recombination increases, it becomes easier for the optimization to overcome local optima. Although this is an unmeant effect, it is beneficial for the optimization.

In the present, provisional setup the investigation of one route takes 2.5s, i.e. the whole optimization would take nearly 14h. Fortunately, repeated designs are investigated only once, this reduces the computational time to approximately 10h. This is still too time consuming for an application on-board. However, there has been no runtime optimization in terms of integrating the whole process into one program. Currently separate programs perform the perturbation, the evaluation, and the optimization of a route and the data transfer takes a lot of computation time. There is definitely a high potential to accelerate the procedure. However, if the computational speed of workstations increases like it has done in last years, an application of the proposed optimization method should be possible within the near future. On the other hand, it is not necessary to apply a genetic algorithm. Other stochastic methods, e.g. particle swarm optimization that is known for its high adaptability and speed, may serve better. This for sure, is an important topic to be addressed in further research, in particular when an integration of the routing system on-board a ship is desired.

7.3 Conclusions

Within this study the set-up of a new ship route optimization approach is documented. Benefits and obstacles of the method are pointed out and discussed. The introduction of further constraints and features, like e.g. wind resistance, current, and wind waves, is straightforward. Regarding the method itself, enhancement of the numerical performance is the most important topic for further improvements. To be competitive to other methods, a considerable reduction of computation time is needed. As a matter of fact, a genetic algorithm based method will never reach the computational speed of a deterministic or graph theory based method. This disadvantage is compensated by some clear advantages. Instead of one optimum route design, the result consists of a number of PARETO optimum routes.
As the optimization method is able to handle more than one objective, new objectives can be easily introduced. For a merchant ship *ETA* and fuel consumption are major aspects for a route decision. Cruise liner may prefer *ETA* and *MSI* as objectives to stay on schedule and assure the well-being of passengers. By employing ensemble forecasts, also robustness

against weather changes can be used as further objective. By means of the PARETO ranking it is possible to come to a more conscious decision. The master is provided with a complete overview on what is feasible for which price or risk.
The topic of computational effort is closely connected to the discussion on where to situate a decision support system. Requirements on computational power suggest a positioning ashore. On the other hand, this is far away from the ship in operation, and a feedback of the master or other related devices becomes difficult. Following the current development in ship operation, integrated monitoring and decision support systems will clearly take place on-board. With regard to uncertainties of a weather forecast, there are good reasons to integrate the route optimization functionality into an integrated monitoring and decision support framework. Forecasted and nowcasted weather provided by meteorologists and direct wave measurements of a ship monitoring system give the officer a comprehensive view on current and upcoming weather conditions. Route optimization supports to find the optimum course during the route planning. At sea, deviations of the forecasted weather to on-site wave measurements indicate if forecast updates and recalculations for optimum routes are necessary. Wave monitoring and real-time seakeeping simulation serve to identify hazardous situations shortly before they arise and enable instantaneous countermeasures. In this way monitoring and routing will merge to support a prudent seamanship.

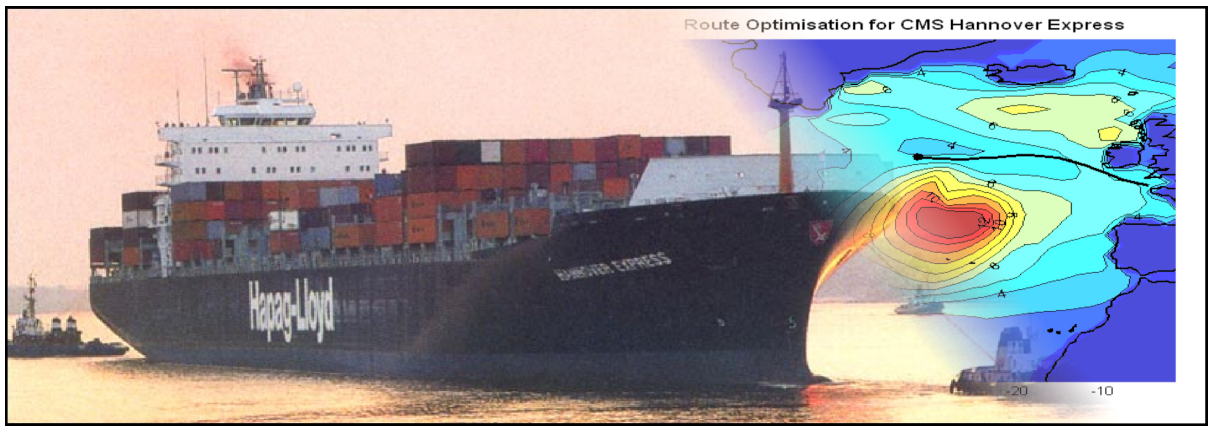

GODSPEED !

8 References

ADOPT (2005), Advanced Decision Support System For Ship Design, Operation And Training, EU 6th Framework Program, April 2005 – Sept. 2008, http://adopt.rtdproject.net

BENFORD, H. (1965), *Fundamentals of Ship Design Economics*, The University of Michigan, Department of Naval Architecture an Marine Engineering, Ann Arbor, Michigan

BIDLOT, J.-R.; HERSBACH, H.; RICHARDSON, D.; SAETRA, Ø. (2002), *Effects of observation errors on the statistics for ensemble spread and reliability*, Technical Memorandum 393, Research Department of the ECMWF, Reading, UK

BIRK, L.; CLAUSS, G.F. (2001), *Automated Hull Optimization of Offshore Structures based on Rational Seakeeping Criteria*, Proceedings of the 11th International Offshore and Polar Engineering Conference, Stavanger, Norway, ISBN 1-880653-51-6

BIRK, L.; HARRIES, S. (2003), *OPTIMISTIC – Optimization in Marine Design*, 39th WEGEMT Summer School, Mensch & Buch Verlag, ISBN 3-89820-514-2

BOESE, P. (1970), *Eine einfache Methode zur Berechnung der Widerstandserhöhung eines Schiffes im Seegang*, IFS-Bericht Nr. 258, Institut für Schiffbau der Universität Hamburg, Germany

BRETSCHNEIDER, C.L. (1957), *Review of Practical Methods for Observing and Forecasting Ocean Waves by Means of Wave Spectra and Statistics*, Trans. American Geophysical Union, Vol. 38, No. 2, U.S. Navy Hydrographic Office, Publ. 603

CHRISTIANSEN, M.; FAGERHOLT, K.; RONEN, D. (2004), *Ship Routing and Scheduling: Status and Perspectives*, Transportation Science, Vol. 38, pp. 1-18, ISSN 0041-1655

CLAUSS, G.; LEHMANN, E.; ÖSTERGARD, C. (1988), *Meerestechnische Konstruktionen*, Springer-Verlag, ISBN 3-540-18964-5, ISBN 0-387-18964-5

CLAUSS, G.; LEHMANN, E.; ÖSTERGARD, C. (1994), *Offshore Structures, Strength and Safety for Structural Design*, Vol.II, Springer-Verlag, ISBN 3-540-19770-2

CLAUSS, G.; RIEKERT, T. (1999), *Stochastische Analyse meerestechnischer Systeme*, lecture notes, department for offshore technology, Technische Universität Berlin, Germany

CLAUSS, G.F.; HENNIG, J.; CRAMER, H.; KRUEGER, S. (2003), *Development of Safer Ships by Deterministic Analysis of Extreme Roll Motions in Harsh Seas*, 22nd international Conference on Offshore Mechanics and Arctic Engineering, Proceedings of OMAE'2003, Mexico

CLAUSS, G.F.; HENNIG, J. (2004), *Deterministic Analysis of Extreme Roll Motions and Subsequent Evaluation of Capsizing Risk*, International Shipbuilding Progress, Vol. 51, Issue 2/3, Stability

CLAUSS, G.F. (2008), *The Taming of the Shrew – Tailoring Freak Wave Sequences for Sea keeping Tests*, 29th Georg Weinblum Memorial Lecture, Journal of Ship Research, Society of Naval Architects and Marine Engineers, to be published in September 2008

CONOLLY, J.E. (1974), *Standards of Good Sea keeping for Destroyers and Frigates in Head Seas*, International Symposium on the Dynamics of Marine Vehicles and Structures in Waves, No. 8, London, UK

CRAMER, H.; REICHERT, K.; HESSNER, K.; HENNIG, J.; CLAUSS, G.F. (2004), *Seakeeping Simulations and Seaway Models and Parameters Supporting Ship Design and Operation*, 9th International Symposium on Practical Design of Ships and other Floating Structures, PRADS 2004, Germany

EMMECHE, C. (1994), *Garden in the Machine. The Emerging Science of Artificial Life*, Princeton University Press

ES.TEC.O s.r.l. (1999), *modeFRONTIER, Multi-Objective Design Environment, User Manual*, Engin Soft Tecnologie per l'Ottimizzazione, Italy

FARIN, G. (2001), *Curves and surfaces for CAGD, a practical guide*, Morgan Kaufmann Publishers Inc., ISBN 1-55860-737-4, USA

FRANK, W. (1967), *Oscillation of Cylinders in or below the Free Surface of Deep Fluids*, Naval Ship Research and Development Center, Technical Report 2375,Washington DC, USA

GERMANISCHER LLOYD (2002), annual report, Hamburg, http://www.gl-group.com/magazines/ann_02/cover02.pdf

GERRITSMA, J.; BEUKELMAN, W. (1972), *Analysis of the resistance increase in waves of a fast cargo ship*, International Shipbuilding Progress, Vol. 19, No. 217

HAGIWARA, H.; FUKUDA, H.; SUGAI, K.; KUSAKA, Y. (1999), *A Study on Weather Routing of High Speed Ships*, FAST´99, 5th International Conference on Fast Sea Transportation, Seattle

HAGIWARA, H.; SPAANS, J.A. (1987), *Computation of Optimum Routes for Ship Weather Routing*, International Symposium on Weather Routing, Tokyo

HAPEL, K.-H. (1990), *Festigkeitsanalyse dynamisch beanspruchter Offshore-Konstruktionen*, Vieweg & Sohn Verlagsgesellschaft mbH, Technische Universität Berlin, Germany

HARRIES, S. (1998), *Parametric Design and Hydrodynamic Optimization off Ship Hull Forms*, Dissertation at TUB, Institut für Schiffs- und Meerestechnik, ISBN 3-933346-24-X

HASSELMANN, K.; ROSS, D.B.; MÜLLER, P.; SELL, W. (1975), *A Parametric Wave Prediction Model*, Journal of Physical Oceanography, Volume 6

HINNENTHAL, J.; SAETRA, Ø. (2005), *Robust Pareto – Optimal Routing of Ships utilizing Ensemble Weather Forecasts*, Proceedings of the 4th International Conference on Computer and IT Applications in the Maritime Industries, COMPIT'05, Hamburg, Germany, ISBN 3-00-014981-3

HOFFSCHILDT, M.; BIDLOT, J-R.; HANSEN, B.; JANSSEN, P.A.E.M. (1999), *Potential benefit of ensemble forecast for ship routing*, ECMWF Techn. Memo. 287, Internal Report, ECMWF, Reading/UK

HOLLAND, J. (1975), Adaptation in natural and artificial systems, University of Michigan Press, reprinted in 1992 by MIT Press. Cambridge

HOLTROP, J. (1978), *Statistical Data for the Extrapolation of Model Performance Tests*, International Shipbuilding Progress, Vol. 25, Rotterdam

HOLTROP, J.; MENNEN, G.G.J. (1984), *An approximate power prediction method*, International Shipbuilding Progress, Vol. 31

IMO (1988), *Code on Intact Stability for All Types of Ships*, A.749(18), amended by resolution MSC.75(69)

IMO (1995), *Guidance to the Master for Avoiding Dangerous Situations in Following and Quartering Seas*, MSC/Circ.707

IMO (2000 and 2003), *Casualty Statistics and Investigations*, International Maritime Organization, Ref. T1/2.02, FSI3/Circ.3 and 6, UK

IMO (2007), *Revised Guidance to the Master for Avoiding Dangerous Situations in Adverse Weather and Sea Conditions*, MSC/Circ.1228

ITTC (1978), *Performance prediction method for single screw ships*, 15th Int. Towing Tank Conf., The Hague

JOURNÉE, J.M.J. (2000), *Theoretical Manual of SEAWAY, Rel. 4.18*, Report 1216, Delft University of Technology, The Netherlands

JOURNÉE, J.M.J. (2001), *User Manual of SEAWAY, Rel. 4.19*, Report 1212a, Delft University of Technology, The Netherlands

JOURNÉE, J.M.J.; ADEGEEST, L.J.M. (2003), *Theoretical Manual of SEAWAY, "SEAWAY for Windows"*, Report 1370, Delft University of Technology and AMARCON Advanced Maritime Consulting, The Netherlands

JOURNÉE, J.M.J.; MASSIE, W.W. (2001), *Offshore Hydromechanics*, First Edition, Delft University of Technology, http://www.shipmotions.nl

JOURNÉE, J.M.J.; MEIJERS, J.H.C. (1980), *Ship Routing for Optimum Performance*, Conference on Operation of Ships in Rough Weather, Transactions IME, London

KRAPPINGER, O. (1983), *Beurteilung des Einflusses von Schiffsbewegungen auf die Besatzung*, Schiffstechnik Bd. 30, Hamburgische Schiffbau Versuchsanstalt

KRUEGER, S.; HINRICHS, R.; KLUVE, F.; BILLERBECK, H. (2006), *Towards the Development of Dynamic Stability Criteria*, TUHH 3-14, Hamburg, also available as *Proposal of a probabilistic intact stability criterion*, Revision of the Intact stability Code, IMO, SLF 49/5/2

LAGARIAS, J. C.; REEDS, J. A.; WRIGHT, M. H.; WRIGHT, P. E. (1998), *Convergence Properties of the Nelder-Mead Simplex Method in low Dimensions*, SIAM Journal on Optimization, Vol. 9, available at wikipedia.org

LASSE (2006 –2008), scientific project funded by the German Ministry, http://www.naoe.tu-berlin.de/MT/Forschung/forschung.html,

LEWIS, E.V. (Ed.) (1998), *Principles of Naval Architecture - Motions in Waves and Controllability*, Vol. III, SNAME, Jersey City

LLOYD, A.R.J.M. (Ed.) (1998), *Sea keeping, Ship Behavior in Rough Weather*, RPM Reprographics, Chichester, Sussex, United Kingdom, ISBN 0 9532634 0 1

MAN B&W (2000), *K90MC MK6 Project Guide Two-stroke Engines*, 5th Edition, www.manbw.dk

MATLAB (2002), version 6.5.0, release 13, http://www.mathworks.com/

NELDER, J.A.; MEAD, R.A. (1965), *A Simplex Method for Function Minimization*. Computer Journal Vol.7, Oxford University Press, UK

NORDFORSK (1987), *Assessment of Ship Performance in a Seaway*, Results of a Nordic Co-Operative Project on Seakeeping Performance of Ships, Denmark, ISBN 87-982637-1-4

NOWACKI, H.; BRUSIS, F.; SWIFT, P. (1970), *Tanker preliminary design – An optimization problem with constraints*, Transactions Vol. 78, SNAME

NOWACKI, H.; LESSENICH, J. (1976), *Synthesis models for preliminary ship design*, Jahrbuch der Schiffbautechnischen Gesellschaft STG, Vol. 70

OCHI, M.K. (1964), *Extreme Behavior of Ship in Rough Seas – Slamming and Shipping of Green Water*, Transactions Volume 72, The Society of Naval Architects and Marine Engineers, New York

PAPANIKOLAOU, A. (1977), *Zum nichtlinearen Problem eines vertikal schwingenden zylindrischen Körpers beliebiger Form*, Techische Universität Berlin, Doctoral Thesis, D83

PAPANIKOLAOU, A. (1982), *Über Analytische und Numerische Methoden zur Behandlung des Irregularitätenproblems bei der Anwendung von Integralgleichungsmethoden*, Technische Universität Berlin, TUB/ISM Bericht Nr.82/10

PAPANIKOLAOU, A.; GRATSOS, G.; BOULOUGOURIS, E.; ELIOPOULOU, E. (2000), *Operational Measures for Avoiding Dangerous Situations in Extreme Weather Conditions*, 7th International Conference on the Stability of Ships and Ocean Vehicles STAB 2000, Australia

PIERSON, W.J.; MOSKOWITZ, L. (1964), *A Proposed Spectral Form for Fully Developed Wind Seas Based on the Similarity Theory of S.A. Kitaigorodskii*, Journal of Geophysical Research, Vol. 69

PINGREE, B.J.W. (1988), *A review of human performance in a ship motion environment*, Warship Technology No. 4, Institute of Naval Medicine, Alverstoke Hampshire

RATHJE, H.; BEIERSDORF, C. (2004), *Decision support for Container Ships in Heavy Seas – Shipboard Routing Assistance*, International Symposium Information on Ships ISIS 2004, German Institute of Navigation DGON, Hamburg

RECHENBERG, I. (1973), *Evolutionsstrategie, Optimierung technischer Systeme nach Prinzipien der biologischen Evolution*, Reihe Problemata Vol. 15, Friedrich Frommann Verlag, Stuttgart

SAETRA, Ø. (2004), *Ensemble Shiprouting*, ECMWF Technical Memorandum 435, Reading/UK

SAMSUNG SHIPBUILDING & HEAVY INDUSTRIES (1991), *4,400 TEU Container Vessel, Trim and Stability Calc. (M/V Hannover Express)*, Koje Island, South Korea

SCHÖNEBURG, E.; HEINZMANN, F.; FEDDERSEN, S. (1994), *Genetische Algorithmen und Evolutionsstrategien – Eine Einführung in Theorie und Praxis der simulierten Evolution*, Addison-Wesley, ISBN 3-89319-493-2

SEAROUTES (2003), *Routing Parameters and Priorities*, Advanced Decision Support for Shiprouting based on Full-scale Ship-specific Responses as well as Improved Sea and Weather Forecasts Including Synoptic High Precision and Real-time Satellite Data, EU 5th Framework Program, Contract G3RD-CT-2000-00309

SHIN, Y.S.; BELENKY, V.L.; PAULLING, J.R.; WEEMS, K.M.; LIN, W.M. (2005), *Criteria for Parametric Roll of Large Containerships in Longitudinal Seas*, ABS, a contribution to the SNAME 13th ad-hoc panel parametric rolling

SPAANS, J.A.; STOTER, P. (2000), *Shipboard Weather Routing*, International Symposium Information on Ships ISIS 2000, German Institute of Navigation DGON, Wilhelmshaven

TREBY, A. (2002), *Optimal Weather Routing Using Ensemble Weather Forecasts*, 37th annual conference, Operational Research Society of New Zealand

TSUJIMOTO, M.; TANIZAWA, K. (2006), *Development of a Weather Adaptive Navigation System Considering Ship Performance In Actual Seas*, 25th International Conference on Offshore Mechanics and Arctic Engineering, Proceedings of OMAE 2006, Germany

YASAKI, A. (1962), *Design diagrams for modern four, five, six and seven-bladed propellers developed in Japan*, 4th Naval Hydrodynamics Symposium, Office of Naval Research

Appendix 1 Stochastic evaluation

The stochastic evaluation of the ship motion uses equations (4.9) and (4.10) to assess the 0th moments of the response spectra for velocity and acceleration:

$m_{0\dot{S}} = m_{2S}$ and $m_{0\ddot{S}} = m_{4S}$. (4.9) and (4.10)

In the following a derivation of these equations will be given in detail. For the time being, the random process of wave elevation of an irregular sea state $\zeta(t)$ is focused. However, it is shown that these considerations are valid for ship motions, too. The derivation bases on the WIENER-CHINTSCHIN[16]-relations. They describe the relation of a spectrum (autospectrum) and the appropriate autocorrelation function of a random stationary process:
the FOURIER transform of a the autocorrelation function gives the spectrum

$$S_{\zeta\zeta}(\omega) = \frac{1}{2\pi} \int_{-\infty}^{+\infty} R_{\zeta\zeta}(\tau) \cdot \exp(-i\omega\tau)\, d\tau \ , \qquad \text{(A1.1)}$$

the inverse FOURIER transform of a spectrum gives the autocorrelation function

$$R_{\zeta\zeta}(\tau) = \int_{-\infty}^{+\infty} S_{\zeta\zeta}(\omega) \cdot \exp(i\omega\tau)\, d\omega \ , \qquad \text{(A1.2)}$$

cp. CLAUSS and RIEKERT (1999).

The relation between autospectrum and the wave spectrum that is used for the statistical evaluation of ship motions is illustrated in Fig. 96 and given by equation (A1.3). The autospectrum occurs because negative frequencies are permitted within the FOURIER transform. In contrast to the mathematical evaluation, no negative frequencies exist from the physical point of view. For this reason the asymmetric representation of the spectrum is employed to assess e.g. wave elevation or ship motions. The transformation given by equation (A1.3) follows the requirement that the area m_0 under both curves has to be the same as it represents a measure for the energy of the considered process.

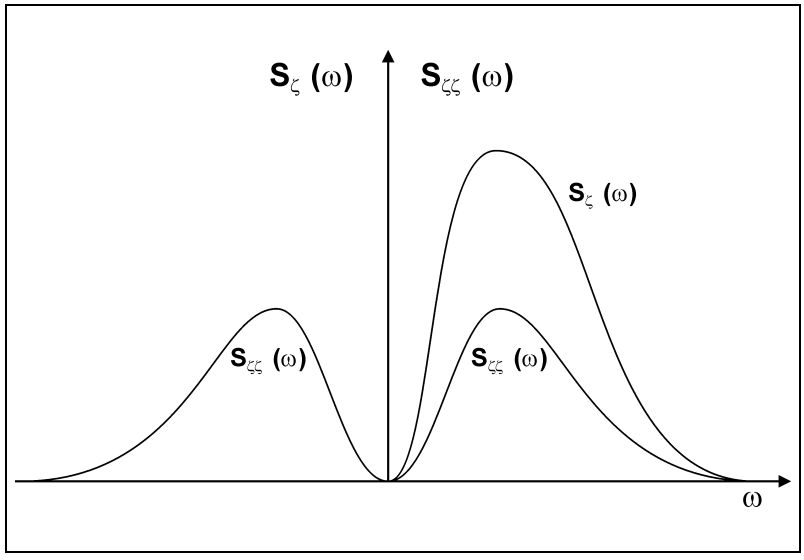

Fig. 96: Symmetric autospectrum and asymmetric spectrum of a random stationary process

[16] Alexander Jakowlewitsch Chintschin, mathematician, 1894 – 1959, Russia
Norbert Wiener, mathematician, 1894 – 1964, North America

$$S_{\zeta}(\omega) = 2\, S_{\zeta\zeta}(\omega) \qquad \text{for: } 0 < \omega < \infty \tag{A1.3}$$

Another definition of the autocorrelation function is given by:

$$R_{\zeta\zeta}(\tau) = \lim_{T\to\infty} \frac{1}{T} \int_{-T/2}^{+T/2} \zeta(t) \cdot \zeta(t+\tau)\, dt\,. \tag{A1.4}$$

Combining equations (A1.2) and (A1.4) result in equation (A1.5):

$$R_{\zeta\zeta}(\tau) = \lim_{T\to\infty} \frac{1}{T} \int_{-T/2}^{+T/2} \zeta(t) \cdot \zeta(t+\tau)\, dt = \int_{-\infty}^{+\infty} S_{\zeta\zeta}(\omega) \cdot \exp(i\omega\tau)\, d\omega\ . \tag{A1.5}$$

Just as the surface elevation of irregular waves ζ, surface velocities $\dot{\zeta}$ and accelerations $\ddot{\zeta}$ represent random distributed GAUSSian processes. Thus the relation of the autocorrelation function and the spectral density for the velocity of the process is given by:

$$R_{\dot{\zeta}\dot{\zeta}}(\tau) = \lim_{T\to\infty} \frac{1}{T} \int_{-T/2}^{+T/2} \dot{\zeta}(t) \cdot \dot{\zeta}(t+\tau)\, dt = \int_{-\infty}^{+\infty} S_{\dot{\zeta}\dot{\zeta}}(\omega) \cdot \exp(i\omega\tau)\, d\omega\ . \tag{A1.6}$$

Equations (A1.5) and (A1.6) are used by HAPEL (1990) to show the validity of equations (4.9) and (4.10). Building the derivative of $R_{\zeta\zeta}(\tau)$ with respect to τ leads to:

$$\frac{dR_{\zeta\zeta}}{d\tau} = \lim_{T\to\infty} \frac{1}{T} \int_{-T/2}^{+T/2} \zeta(t) \cdot \dot{\zeta}(t+\tau)\, dt = i \int_{-\infty}^{+\infty} \omega\, S_{\zeta\zeta}(\omega) \cdot \exp(i\omega\tau)\, d\omega\ . \tag{A1.7}$$

The substitution $t = t - \tau$ yields:

$$\frac{dR_{\zeta\zeta}}{d\tau} = \lim_{T\to\infty} \frac{1}{T} \int_{-T/2}^{+T/2} \zeta(t-\tau) \cdot \dot{\zeta}(t)\, dt = i \int_{-\infty}^{+\infty} \omega\, S_{\zeta\zeta}(\omega) \cdot \exp(i\omega\tau)\, d\omega\ . \tag{A1.8}$$

A further derivative of $R_{\zeta\zeta}(\tau)$ with respect to τ and the substitution $t = t + \tau$ leads to:

$$\frac{dR^2{}_{\zeta\zeta}}{d\tau^2} = -\lim_{T\to\infty} \frac{1}{T} \int_{-T/2}^{+T/2} \dot{\zeta}(t-\tau) \cdot \dot{\zeta}(t)\, dt = -\int_{-\infty}^{+\infty} \omega^2\, S_{\zeta\zeta}(\omega) \cdot \exp(i\omega\tau)\, d\omega \tag{A1.9}$$

and further to

$$\frac{dR^2{}_{\zeta\zeta}}{d\tau^2} = -\lim_{T\to\infty} \frac{1}{T} \int_{-T/2}^{+T/2} \dot{\zeta}(t) \cdot \dot{\zeta}(t+\tau)\, dt = -\int_{-\infty}^{+\infty} \omega^2\, S_{\zeta\zeta}(\omega) \cdot \exp(i\omega\tau)\, d\omega\ . \tag{A1.10}$$

A comparison of equations (A1.6) and (A1.10) shows that following equations are valid:

$$R_{\dot{\zeta}\dot{\zeta}}(\tau) = -\frac{dR^2{}_{\zeta\zeta}}{d\tau^2}\,, \tag{A1.11}$$

$$S_{\dot{\zeta}\dot{\zeta}}(\omega) = \omega^2\, S_{\zeta\zeta}(\omega)\,. \tag{A1.12}$$

Repeating the process above yields the respective equation for the acceleration of the wave elevation $\ddot{\zeta}$:

$$S_{\ddot{\zeta}\ddot{\zeta}}(\omega) = \omega^4\, S_{\zeta\zeta}(\omega)\,. \tag{A1.13}$$

Equations (A1.12) and (A1.13) are also valid for asymmetric spectra like employed in the study because the area under each spectrum, i.e. for motion, velocity, or acceleration, remains the same and the transformation (A1.3) produces no shift of the spectral density with regard to the absolute value of the frequency. For this reason the following equations are employed within practical application:

$$S_{\dot{\zeta}}(\omega) = \omega^2\, S_{\zeta}(\omega), \tag{A1.14}$$

$$S_{\ddot{\zeta}}(\omega) = \omega^4\, S_{\zeta}(\omega). \tag{A1.15}$$

Consequently the 2nd and the 4th moment of the spectrum describing the surface elevation ζ equal the 0th moments of the velocity- and acceleration spectrum:

$$m_{2\zeta} = \int_0^\infty \omega^2 \, S_\zeta(\omega)\, d\omega = \int_0^\infty S_{\dot{\zeta}}(\omega)\, d\omega = m_{0\dot{\zeta}} \tag{A1.16}$$

$$m_{4\zeta} = \int_0^\infty \omega^4 \, S_\zeta(\omega)\, d\omega = \int_0^\infty S_{\ddot{\zeta}}(\omega)\, d\omega = m_{0\ddot{\zeta}} \tag{A1.17}$$

CLAUSS et. al. (1994) show that linear functions of GAUSSian random variables like the surface elevation of waves are themselves GAUSSian random variables. This applies to the determination of ship responses by means of equation (4.1), i.e. the ship motion represents a GAUSSian random process too.

$$S_s(\omega) = \left| \frac{s_a}{\zeta_a} \right|^2 \cdot S_\zeta(\omega) \tag{4.1}$$

Therefore the considerations made above are valid for the motion spectra, too.
The 0th moments of the velocity- and the acceleration spectrum of the ship equal the 2nd and the 4th moment of the response spectrum for the ship motion:

$$m_{0\dot{S}} = \int_0^\infty S_{\dot{S}}(\omega)\, d\omega = \int_0^\infty \omega^2 \, S_S(\omega)\, d\omega = \int_0^\infty \omega^2 \left| \frac{s_a}{\zeta_a} \right|^2 \cdot S_\zeta(\omega)\, d\omega = m_{2S} \qquad \text{(A1.18) or (4.9)}$$

$$m_{0\ddot{S}} = \int_0^\infty S_{\ddot{S}}(\omega)\, d\omega = \int_0^\infty \omega^4 \, S_S(\omega)\, d\omega = \int_0^\infty \omega^4 \left| \frac{s_a}{\zeta_a} \right|^2 \cdot S_\zeta(\omega)\, d\omega = m_{4S} \qquad \text{(A1.19) or (4.10)}$$

Appendix 2 Irregular frequencies

In case of strip-theory methods applied to seakeeping problems, the determination of hydrodynamic forces and moments requires the solution of a series of 2D potential theory boundary value problems (BVP) for a number of cross-sections that are representative for the three-dimensional hull shape of the ship. The solution of these BVPs leads to the determination of the velocity potential and hence to hydrodynamic coefficients (added mass and damping coefficients) which are dependent on the shape of the relevant cross-section, the frequency of oscillation, and the direction of the considered motion, i.e. the sway-, heave-, or roll motion. Hydrodynamic forces and moments, acting on the cross-section, the 2D-strip, are derived by integration of hydrodynamic pressure deduced from the determined velocity potentials by application of Bernoulli's equation.

When solving the potential theory BVP by numerical solution for formulated integral equations (i) with a distribution of pulsating sources along the wetted part of a cross-section and (ii) for surface piercing cross-sections, numerical results are disturbed at particular frequencies, the so called irregular frequencies, cp. JOURNÉE and MASSIE (2001). Fig. 97 shows non-dimensionalized mass- and damping coefficients for the heave motion of the S175, presented in section 6.3. Mass- and damping coefficients are given with respect to the frequency of the vertical motion and the position of the cross-section, where x/L_{pp} = 1 represents the bow, 0 the stern, respectively. The unrealistic peak at a frequency of about 2.5rad/s, in particular visible in the diagram for the damping coefficient, is caused by the occurrence of an irregular frequency.

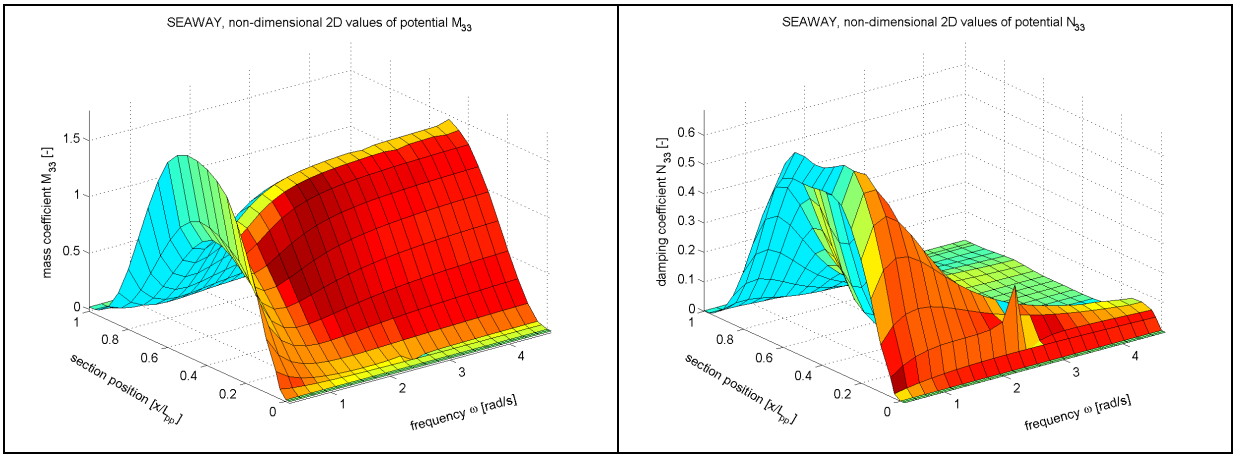

Fig. 97: 2D values for mass- M_{33} and damping N_{33} coefficients, S175

Fig. 98 depicts mass- and damping coefficients for the affected cross-section near the stern. It is evident that both the mass- and damping coefficients are disturbed.

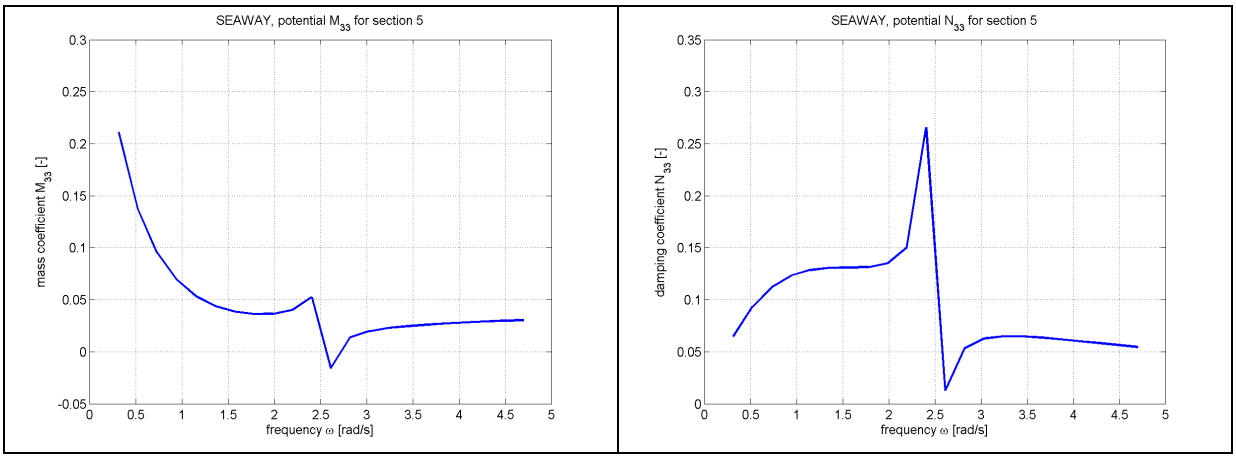

Fig. 98: 2D values for mass- M_{33} and damping N_{33} coefficients, section 5

As explained above, the determination of the hydrodynamic coefficients by means of potential theory presumes the solution of a boundary value problem that can be solved by different methods appropriate to the required accuracy. In case that a traditional conformal mapping method is not able to satisfactorily resemble a cross-section shape, which is often the case for realistic ship-like sections, it is useful to apply a 2D singularity distribution method for the solution of the relevant 2D BVP, e.g. FRANK's pulsating source method, see FRANK (1967). In this case the calculation of the flow field around the cross-section is based on the solution of a GREEN's function integral equation. Numerically the solution is provided by means of a discretized representation of the cross-section, i.e. the boundary conditions are fulfilled at a number of collocation points on the cross-section contour. For the appropriate discretized source distribution, given by a discretized representation of the GREEN's function integral, the unknown strengths of the pulsating sources have to be determined by solution of a linear algebraic set of equations.
The solution of this problem consists of an *internal* and *external* solution describing the flow field inside and outside the cross-section. The external solution is used for the determination of the fluid pressure around and along the cross-section, whose integration leads to the hydrodynamic coefficients. Dependent on the cross-sectional shape, the breadth/draught ratio B/T and the cross-sectional area coefficient A_m, the internal solution disposes eigenfrequencies corresponding to sloshing effects (resonances) of the imaginary internal flow. In this case no realistic solution for the unknown source strengths determining the external velocity potential exists and therefore the external solution is disturbed (because of the so-called *duality problem* of potential theory, see PAPANIKOLAOU (1977)). Definitely there is no physical reason for the sudden change of mass- and damping coefficients at particular frequencies, as visible in Fig. 98. Therefore the numerical results for the affected frequency band around the irregular frequencies cannot be used.

From the numerical point of view it can be shown that this problem is caused by a zero (or sudden decrease) of the determinant of the integral equation that has to be solved for the unknown source strengths. This also simply explains why mass- and damping coefficients determined by conformal mapping methods or for fully submerged cross-sections do not show a distortion by irregular frequencies. The former do not use the GREEN's function integral equation method and the latter always disposes a unique solution, as the internal fluid problem has no eigenfrequencies. Anyhow it is possible to avoid the occurrence of irregular frequencies or at least to shift them out of the considered practical frequency range, also for singularity panel methods.

PAPANIKOLAOU (1982) presents a series of different techniques to eliminate the disturbance by irregular frequencies regarding the 2D problem. They are divided into three classes:

- Analytical methods make use of a modified GREEN's function. Additional source terms in the GREEN's function modify the FREDHOLM's[17] determinant that finally serves to shift the eigenfrequencies, i.e. the frequencies where the determinant becomes zero are shifted to higher frequencies that are out of the practical range for the determination of ship motions.
- Analytic-numerical methods use a numerical lid-inside deck, i.e. a discretization of the free surface inside the cross-section contour. Alternative boundary conditions for the internal flow serve to control the internal solution and to eliminate eigenfrequencies in the practical range of frequencies. In a way this method forces the internal solution to behave like the one of a fully submerged cross-section. It finally results in a modification of the FREDHOLM's determinant, too.
- Numerical methods pre-assess the position of irregular frequencies by (i) identification of typical constellations of the breadth/draught ratio B/T and the cross-sectional area coefficient A_m or (ii) they observe the value of the FREDHOLM's determinant for this purpose. For the identified irregular frequencies the values of the flow potentials are interpolated, e.g. by a spline-interpolation using the surrounding values as interpolation values.

All three sets of methods have in common that they require access to the source code of the applied seakeeping program. In case of the code used within this thesis it was not possible to implement the above techniques and a simplified method to deal with this problem was adopted, as described in section 4.7.

[17] Erik Ivar Fredholm, mathematician, 1866 – 1927, Sweden

Appendix 3 Root mean square values

The abbreviation *RMS* represents the root mean square value of a stochastic process. Within the present study the root mean square values of two different but associated process factors are used:

- the *RMS* of the wave surface displacement or a ship motion,
- the *RMS* of the wave amplitude or a ship motion amplitude.

The following nomenclature is used to describe the relation between these terms and to avoid mistake:

symbol	name	unit
a	parameter of a harmonic or a random process	[dep.]
$\tilde{a}$	amplitude of a harmonic function	[dep.]
$a_{1/3}$	significant wave amplitude	[m]
a_{rms}	root mean square of the wave amplitude	[m]
$H_{1/3}$	significant wave height / double amplitude	[m]
H_{rms}	root mean square of the wave height	[m]
m_0	0^{th} order moment of a wave power spectrum	[m^2]
RMS	root mean square value	[dep.]
σ_a	standard deviation of the wave amplitude	[m]
σ_ζ	standard deviation of the wave surface displacement	[m]
T	time, time period of a wave record	[s]
$\zeta(t)$	wave surface displacement	[m]
ζ_{rms}	root mean square of the wave surface displacement	[m]

The equations (A3.1) to (A3.3) are used as starting point of this explanation:
Equation (A3.1) represents the relation of root mean square of the wave surface displacement of an irregular sea state, the standard deviation of the wave surface displacement, and the 0^{th} moment of the wave spectrum.

$$\zeta_{rms} = \sqrt{\frac{1}{T}\int_0^T \zeta^2(t)\,dt} = \sigma_\zeta = \sqrt{m_0} \qquad \text{(A3.1)}$$

Equation (A3.2) denotes the relation of significant wave height (significant double amplitude) and 0^{th} moment of the power spectrum.

$$H_{1/3} = 4 \cdot \sqrt{m_0} \qquad \text{(A3.2)}$$

Equation (A3.3) gives the relation of significant wave height and root mean square of the wave heights, in other words the relation of significant double amplitudes and root mean square of double amplitudes, respectively.

$$H_{1/3} = \sqrt{2} \cdot H_{rms} \qquad \text{(A3.3)}$$

The relation of root mean square of the wave height and 0th moment of the power spectrum is obtained from equating (A3.2) and (A3.3) with

$$H_{rms} = 2 \cdot \sqrt{2\, m_0}\ . \qquad \text{(A3.4)}$$

Equation (A3.1) shows the relation of standard deviation of the wave surface displacement and 0th moment of the power spectrum $\sigma_\zeta = \sqrt{m_0}$. In the same way equation (A3.4) can be used to obtain the relation of standard deviation of the wave amplitude and power spectrum

$$\sigma_a = \sqrt{2\, m_0}\ , \qquad \text{(A3.5)}$$

with:

$H_{rms} = 2 \cdot a_{rms} = 2 \cdot \sigma_a$,

the relation of root mean square of the wave height (double amplitude) and standard deviation (root mean square) of the wave amplitude.

Equating the 0th moments of the power spectrum from the equations (A3.1) and (A3.5) provides the relation of the standard deviations of wave amplitudes and wave surface displacement

$$\sigma_a = \sqrt{2} \cdot \sigma_\zeta\ , \qquad \text{(A3.6)}$$

or rather the relation of root mean square of the wave amplitudes and of the wave surface displacement

$$a_{rms} = \sqrt{2} \cdot \zeta_{rms}\ . \qquad \text{(A3.7)}$$

Setting up equation (A3.3) for amplitudes instead of double amplitudes provides

$$a_{1/3} = \sqrt{2} \cdot a_{rms}\ . \qquad \text{(A3.3a)}$$

The relation of significant wave amplitude and root mean square of the wave surface displacement is obtained from inserting equation (A3.7) in (A3.3a).

$$a_{1/3} = \sqrt{2} \cdot \sqrt{2} \cdot \zeta_{rms} = 2 \cdot \zeta_{rms} \qquad \text{(A3.8)}$$

These considerations regarding the wave surface displacement and wave amplitudes are transferable to the ship motions and amplitudes of motion obtained by linear theory. Regarding equation (6.3) the terms of this equation have to be interpreted as follows:

$$s_{a\frac{1}{3}} = 2 \cdot \sqrt{m_0} = 2 \cdot \sqrt{\frac{1}{T}\int_0^T a^2 dt} = 2 \cdot RMS\ , \qquad \text{(6.3)}$$

$s_{a\frac{1}{3}}$	significant amplitude of a motion,
$2 \cdot \sqrt{m_0}$	$\sqrt{2} \cdot \sqrt{2 \cdot m_0} = \sqrt{2} \cdot$ (root mean square of the motion amplitude),
$2 \cdot \sqrt{\frac{1}{T}\int_0^T a^2 dt}$	$2 \cdot$ (root mean square of the motion),
$2 \cdot RMS$	ditto.

The thresholds posed within NORDFORSK (1987) given in Tab. 13 and Tab. 14 represent root mean square values of vertical accelerations (not amplitudes of acceleration). Therefore the conversion from *RMS* to significant amplitudes has to follow equation (6.3).